DEPARTMENT OF PHYSICS & ASTRONOMY

UNIVERSITY OF WYOMING

MAGNETOSPHERIC MODULATION EFFECTS ON SOLAR COSMIC RAYS FROM SIMULTANEOUS OGO I AND III ION CHAMBER DATA IN 1968 AND 1969

D. J. Hofmann
Department of Physics and Astronomy
University of Wyoming

Final Report of Grant # NGR-51-001-033

Grant Period: 1/1/71 - 8/31/73

October 1973

TABLE OF CONTENTS

I. INTRODUCTION

In 1971 the University of Wyoming was awarded a grant to study existing cosmic ray data taken during 1968 and 1969 with ionization chambers aboard the satellites OGO I and III. The purpose of this study was to investigate the mechanism of entry of the charged solar particle radiation into the Earth's magnetosphere by comparing highly accurate data taken inside and outside of the magnetosphere. Previous work on earlier similar data by the principal investigator in collaboration with colleagues at the University of Minnesota, where the experiments were designed and constructed, formed a basis from which to work.

At the time the proposal was written, our information suggested that 12 months of simultaneous OGO I and III data existed (March-May 1968; Sept.-Nov. 1968; March-May 1969; Sept.-Nov. 1969). During this period more than 20 cosmic ray events occurred, which should have been a good statistical basis from which to work. In actuality, though the satellites were operating during this time, they were not always operating simultaneously. In fact, simultaneous data was available for a total time of less than one month of the 12-month period. Of this time, only about one week occurred during solar events. During these periods of simultaneous data, only portions of 6 solar events were covered. Thus our hope of a good statistical sample was not realized. However, from what data was obtained some interesting and useful results will be forthcoming. Although the data is now in its final form and will be presented here, the analysis is not yet complete and will follow, hopefully in published form, during the next year.

II. BACKGROUND AND OBJECTIVES OF THE RESEARCH PROGRAM

The Orbiting Geophysical Observatories (OGO) I and III have, in the past, offered an excellent opportunity to study certain phenomena inside and outside the Earth's magnetosphere simultaneously. Such studies can be especially significant when instruments having a high degree of comparable accuracy such as the University of Minnesota (J. R. Winckler, Principal Investigator) ion chambers (∿1% intercomparability) are employed. Thus Kane, Winckler and Hofmann (1968) [a reprint is attached and hereafter referred to as KWH], utilizing September 1966 solar flare proton streams as magnetospheric probes, were able to detect both minute and large-scale differences in ionization intensity in different regions of space within and without the magnetosphere. These differences were interpreted as a magnetospheric "screening" effect on the solar particles. The most startling case of magnetospheric screening occurred during a solar particle event on 7 May 1967 and is shown in Figure 16 of KWH. There is an apparent non-diffusive delay of 110 minutes for penetration of solar particles to the position of OGO III as compared to that of OGO I. Both satellites were in the magnetospheric cavity; however the delayed response was observed in the ion chamber nearest the center of the magnetospheric tail or neutral sheet. Thus it would appear that one would have to attribute this observation to a preferred connection of high latitude magnetic field lines to the interplanetary medium and complete disconnection of lower latitude field lines at this time rather than a diffusive entry process.

Following the original observation of the delayed access of solar protons to certain regions of the magnetosphere, numerous analogous

cases have been reported in the literature. Such data has suggested that both diffusion and direct access of particles into the tail of the magnetosphere must play an important role at times in order to explain the observations. It appears then that in order to contribute significantly to this study it is necessary to compile a large statistical sample of data under varying magnetospheric conditions. The ionization chambers aboard OGO I and III were well qualified for this task since they have a high degree of intercomparable accuracy and a low threshold of sensitivity. Their comparable accuracy is better than 1% and with an omnidirectional geometrical factor of about 1.2 m^2-ster, they have an ionization response of twice the normal galactic background for an average solar proton flux of 0.07 protons/cm^2-ster-sec above about 12 MeV energy. For example, the most interesting event of 7 May 1967 involved fluxes of the order of 0.5 protons/cm^2-ster-sec and probably went undetected or at least unnoticed by the usual small geometrical factor devices such as solid state detector arrays. In addition, the time resolution of the ionization chamber for such weak events is two seconds, while the smaller geometrical factor devices require considerably longer integration times for low flux events.

One would generally think the ion chamber a poor device to use when a spectrum of particle energies is present since the ionization rate varies with energy; however in depth analysis of the ion chamber response (see, for example, Figures 2 and 3 of KWH) has indicated otherwise--i.e., the chamber response peaks sharply around 15 MeV energy, with a wall cutoff at 12 MeV and a sharp drop in response above 15 MeV due to the steep solar particle energy spectrum and the reduction in specific

ionization with increasing energy. For further ion chamber characteristics and response to various particle energy spectrums, see KWH.

Thus the objective of this research program was to obtain as much simultaneous data from the two instruments as was available, scan these data for solar particle events and compile a statistically significant sample of simultaneous observations to obtain new information on the mode of particle entry into the near earth environment. Although the volume of such data was disappointing, the project can be considered worthwhile since some interesting data were obtained.

III. DISCUSSION

In this discussion we will refer to data plots in Section IV which are numbered in the upper right-hand corner from plot #1 to plot #96. These include both data plots and orbit plots. Salient features of the observations will be listed.

A. September 26, 1968 Event

1. Plot #2

Event: Apparent solar x-ray burst at 0030.

Comments: Probably identifies the energetic solar event (class 2B flare, E35) which resulted in the solar cosmic ray event observed to commence about 6½ hours later.

2. Plots #6 & #7

Event: Onset of solar cosmic rays at about 0700, probably accelerated by flare discussed in 1). Typical east quadrant flare--slow rise to maximum intensity, slow decay.

3. Plots #9 & #11

Event: Although this is probably an east quadrant event and is characterized by diffusive particle transport across interplanetary magnetic field lines, directional anisotropies in particle flux are evident in the OGO B 20 second average data. OGO B has a spin period of 95 seconds, OGO A only 12 seconds, thus the anisotropy can only be detected on A by looking at 1-2 second averages. This is currently being done. The anisotropy is observed because a portion of the spacecraft body blocks out the solar particle flow momentarily when such flow is directional (e.g., along interplanetary field lines). The OGO B spacecraft was situated outside and on the front side of the magnetosphere at this time (see plot #1), thus its position was probably accessible via interplanetary field lines. This observation then suggests that although the major mode of transport for this event was probably diffusive, guided transport played a role to some degree, at least in the vicinity of the Earth.

4. Plot #15

Event: There is evidence here that the anisotropy discussed in 3) was a transient feature, disappearing and then returning. This could be evidence for the spacecraft moving into small scale regions which are more accessible than others or that the actual anisotropy possessed a temporal variation.

B. October 29, 1968 Event

1. Plots #25 & #26

Event: Small increase at 0954 observed simultaneously on both satellites. A small flare (1N-2N) reached maximum around 0945-0947 and may have been the source of this increase (x-ray flare). This flare occurred in the same McMath Plage Region (9740) as the larger 2B flare which occurred at about 0900 and was probably the source of particles observed later.

2. Plots #27 & #28

Event: Another small increase observed simultaneously on both satellites at 1226. A 2B flare which began at 1209 and reached maximum at 1222, again in Region 9740, may be the source of this increase. OGO B was again outside the magnetosphere and OGO A inside. The timing of this event and that in 1) are so close that they are most probably x-ray events.

3. Plots #31 & #32

Event: Evidence for a small (~2 minute) delay in the particle structure occurring at 1730 inside the magnetosphere (OGO A) as compared to outside (OGO B).

4. Plots #35 & #36

Event: Apparent particle modulation effects outside the magnetosphere at the position of OGO B at about 2310 not observed inside at the position of OGO A.

C. November 1-2, 1968 Event

1. Plots #40 & 41

Event: The data begins with a large solar cosmic ray event in progress. The source of this event was probably in the same region (9740) as the October event and occurred with importance 2-3 between 0800 and 0930. A further increase is observed in plots 40 and 41 at about 2300. This increase is probably associated with an additional flare, classed 2B at about 2000-2015. The significance of this new event is that the particles were observed to arrive simultaneously at both spacecraft although OGO B was outside the magnetosphere and OGO A inside. Thus at this time, direct connection from within the magnetosphere to without existed.

2. Plots #44 & #45

Event: In contrast to the observation in 1), we now see 5-minute delays in features at about 0410 and 0450.

3. Plots #50 & #51

Event: At about 1030 and 1120 we see apparent large delays ($\sim$20 minutes) and flux suppression at the position of OGO A compared to OGO B.

4. Plots #52 & #53

Event: A classic example of about a 5-minute delay and a flux suppression at OGO A compared to OGO B at about 1250. Note the anisotropy at OGO B with a sudden removal of the anisotropy at about 1440 followed by an unusual constancy and isotropy in the flux for the ensuing 40 minutes.

D. November 18, 1968 Event

1. Plots #73 & #74

Event: Perhaps the best example obtained of the complicated nature of the magnetospheric entry problem. With OGO B outside the magnetosphere and OGO A in the skirt region moving into the magnetosphere, we see excellent agreement in the rapid onset of the solar event at 1027. A west limb flare of importance 1-2 began about 1017 (earliest report) and the prompt arrival (about 10 minutes later) and fast rise time would suggest essentially direct connection to the vicinity of the Earth. It is most probable that the flare started 10 or so minutes earlier than reported as transit times less than about 20 minutes are improbable for charged particles. About 30 minutes after onset, the flux at OGO A begins to become depressed below that at OGO B with a hint of a 5-10 minute delay in a feature at about 1055. The flux at OGO B is observed to become anisotropic at about 1130. Unfortunately, no more data was available after 1145.

IV. SIMULTANEOUS OGO I & III DATA OBTAINED

A. Time Intervals of Simultaneous Solar Event Data

Table 1 lists all the satellite data plotted for this report.

Table 2 lists probable solar flares associated with the data.

Figures 1 through 7 show the time intervals superimposed on Explorer Solar Proton Monitor data.

TABLE 1

DATE	TIME INTERVAL	PLOT TYPE	PLOT. NO.
9/25/68-9/26-68	2200,9/25-0000,9/27	(ORBIT A)	1
"	"	(ORBIT B)	1
9/25/68	2240-0110(9/26)	A	2
"	"	B	3
9/26/68	0110-0340	A	4
"	"	B	5
"	0630-0900	A	6
"	"	B	7
"	0900-1130	A	8
"	"	B	9
"	1130-1400	A	10
"	"	B	11
"	1400-1630	A	12
"	"	B	13
"	1630-1900	A	14
"	"	B	15
"	1900-2130	A	16
"	"	B	17
"	2130-0000(9/27)	A	18
"	"	B	19
10/29/68	0100-0000(10/30)	(ORBIT A)	20
"	"	(ORBIT B)	20
"	0130-0400	A	21
"	"	B	22
"	0400-0630	A	23
"	"	B	24
"	0900-1130	A	25
"	"	B	26
"	1130-1400	A	27
"	"	B	28
"	1400-1630	A	29
"	"	B	30
"	1630-1900	A	31
"	"	B	32
"	1900-2130	A	33
"	"	B	34
"	2130-0000(10/30)	A	35
"	"	B	36
11/1/68-11/2-68	0000,11/1-0000,11/3	ORBIT A	37a
"	"	ORBIT B	37b
11/1/68	0050-0320	A	38
"	"	B	39
"	2130-0000(11/2)	A	40
"	"	B	41
11/2/68	0000-0230	A	42
"	"	B	43
"	0230-0500	A	44
"	"	B	45

TABLE 1 (continued)

11/2/68	0500-0730	A	46
"	"	B	47
"	0730-1000	A	48
"	"	B	49
"	1000-1230	A	50
"	"	B	51
"	1230-1500	A	52
"	"	B	53
"	1500-1730	A	54
"	"	B	55
"	1730-2000	A	56
"	"	B	57
"	2000-2230	A	58
"	"	B	59
"	2230-0100(11/3	A	60
"	"	B	61
11/3/68	1500-2000	ORBIT A	62
"	"	ORBIT B	62
"	1530-1800	A	63
"	"	B	64
11/10/68-11/11/68	1700,11/10-0200,11/11	ORBIT A	65
"	"	ORBIT B	65
11/10/68	1800-2030	A	66
"	"	B	67
"	2300-0130(11/11	A	68
"	"	B	69
11/18/68	0700-1300	ORBIT A	70
"	"	ORBIT B	70
"	0730-1000	A	71
"	"	B	72
"	1000-1230	A	73
"	"	B	74
3/16/69	0600-1400	ORBIT A	75
"	"	ORBIT B	75
"	0600-0830	A	76
"	"	B	77
"	0830-1100	A	78
"	"	B	79
"	1100-1330	A	80
"	"	B	81
4/7/69	0500-1000	ORBIT A	82
"	"	ORBIT B	82
"	0500-0730	A	83
"	"	B	84
"	0730-1000	A	85
"	"	B	86

TABLE 1 (continued)

10/8/69	1100-1600	ORBIT A	87
"	"	ORBIT B	87
"	1100-1330	A	88
"	"	B	89
"	1330-1600	A	90
"	"	B	91
11/19/69-11/20/69	1900,11/19-0300,11/20	ORBIT A	92
"	"	ORBIT B	92
11/19/69	1900-2130	A	93
"	"	B	94
11/20/69	0030-0300	A	95
"	"	B	96

TABLE 2

DATE	PROBABLE TIME	POSITION	IMPORTANCE	McMath Plage Region
9/26/68	0026	N15,E25	2B	9687
"	0845	N14,E29	2N	9687
"	1121	N20,W60	2N	9688
10/29/68	0900	S14,W07	2B	9740
"	1115	S16,W12	2B	9740
11/2/68	0950	S14,W66	2B	9740
"	1026	S14,W69	2F	9740
"	1637	N21,E24	2B	9751
11/19/69	2011	N08,E22	2B	10432

SOLAR PROTONS BY SATELLITE
EXPLORER 34 (1967-51A)

SEPTEMBER 1968

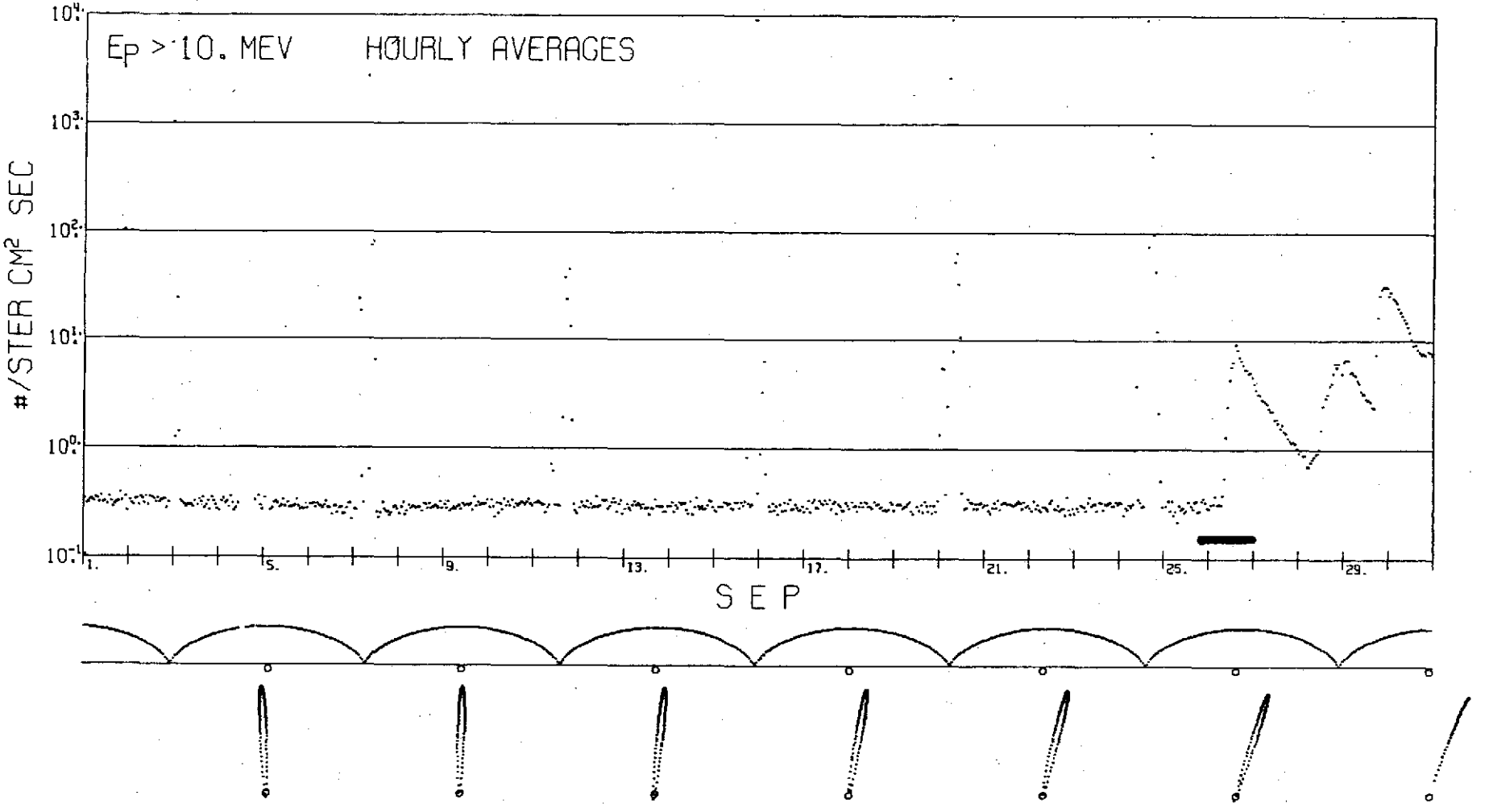

Plotted OGO A&B data

Figure 1

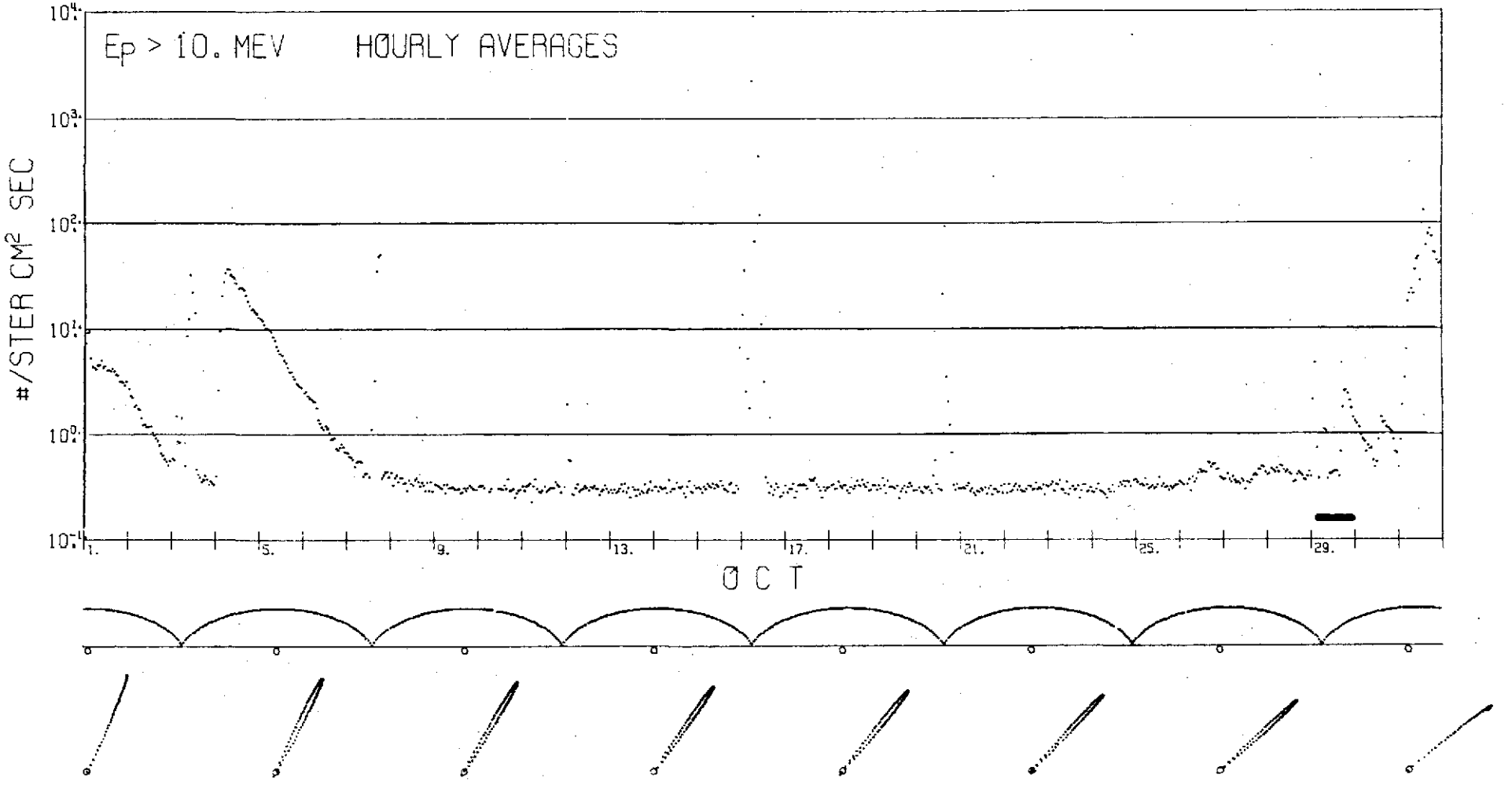
SOLAR PROTONS BY SATELLITE
EXPLORER 34 (1967-51A)
OCTOBER 1968
Ep > 10. MEV HOURLY AVERAGES
#/STER CM² SEC
10⁴
10³
10²
10¹
10⁰
10⁻¹
1.
5.
9.
13.
17.
21.
25.
29.
OCT
Plotted OGO A&B data

Figure 2

SOLAR PROTONS BY SATELLITE
EXPLORER 34 (1967-51A)

NOVEMBER 1968

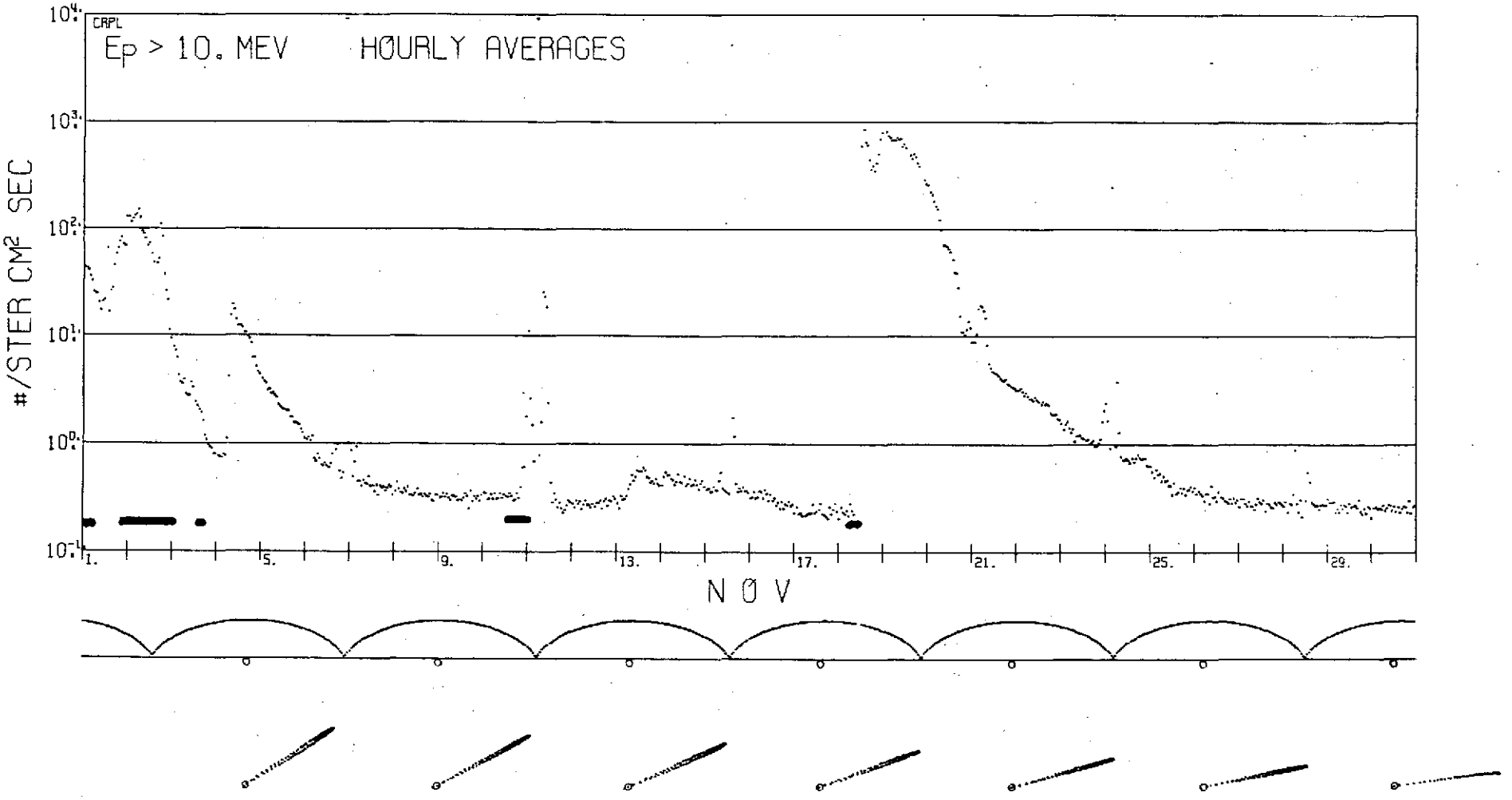

Plotted OGO A&B data

Figure 3

SOLAR PROTONS BY SATELLITE
EXPLORER 34 (1967-51A)

MARCH 1969

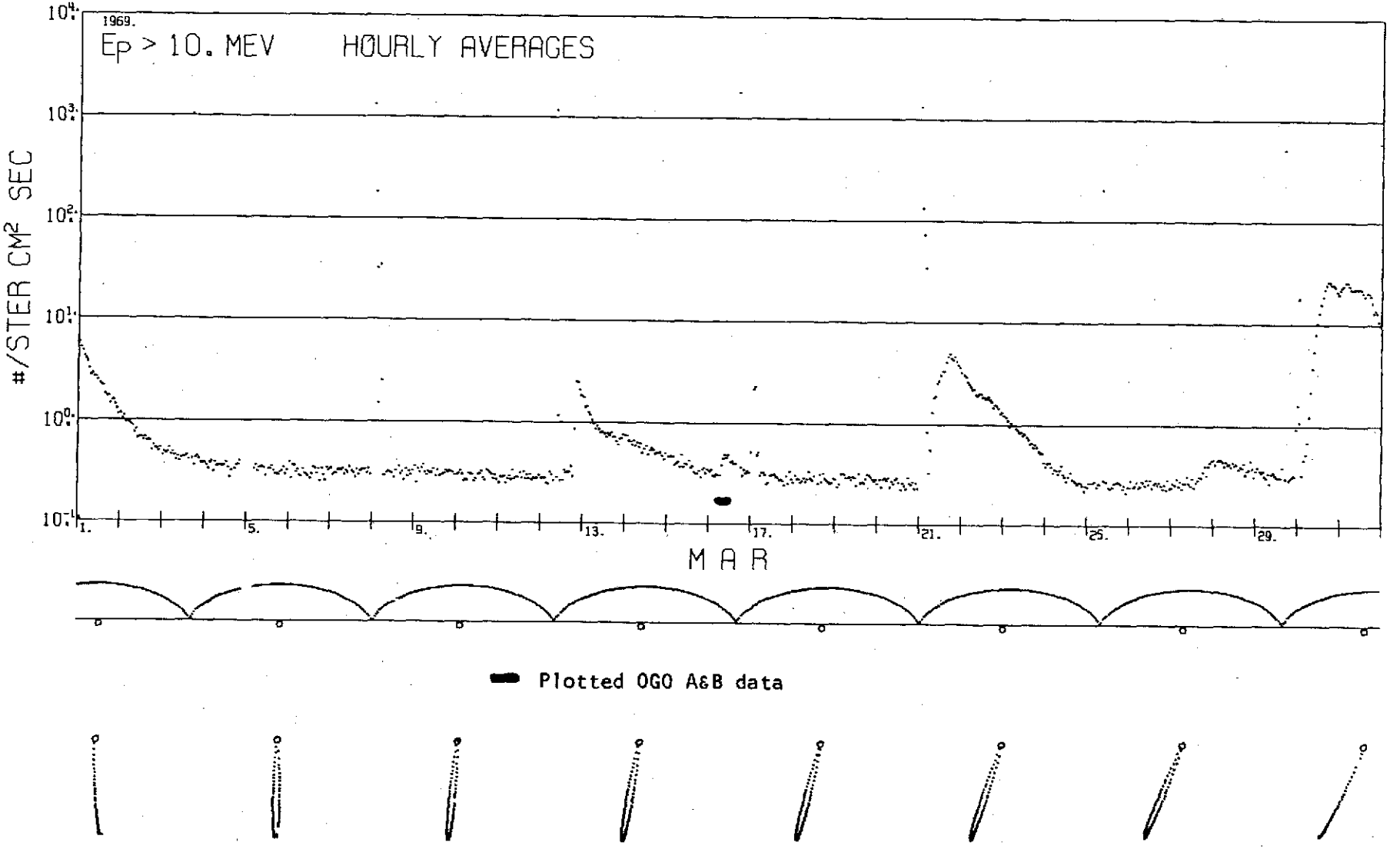

Figure 4

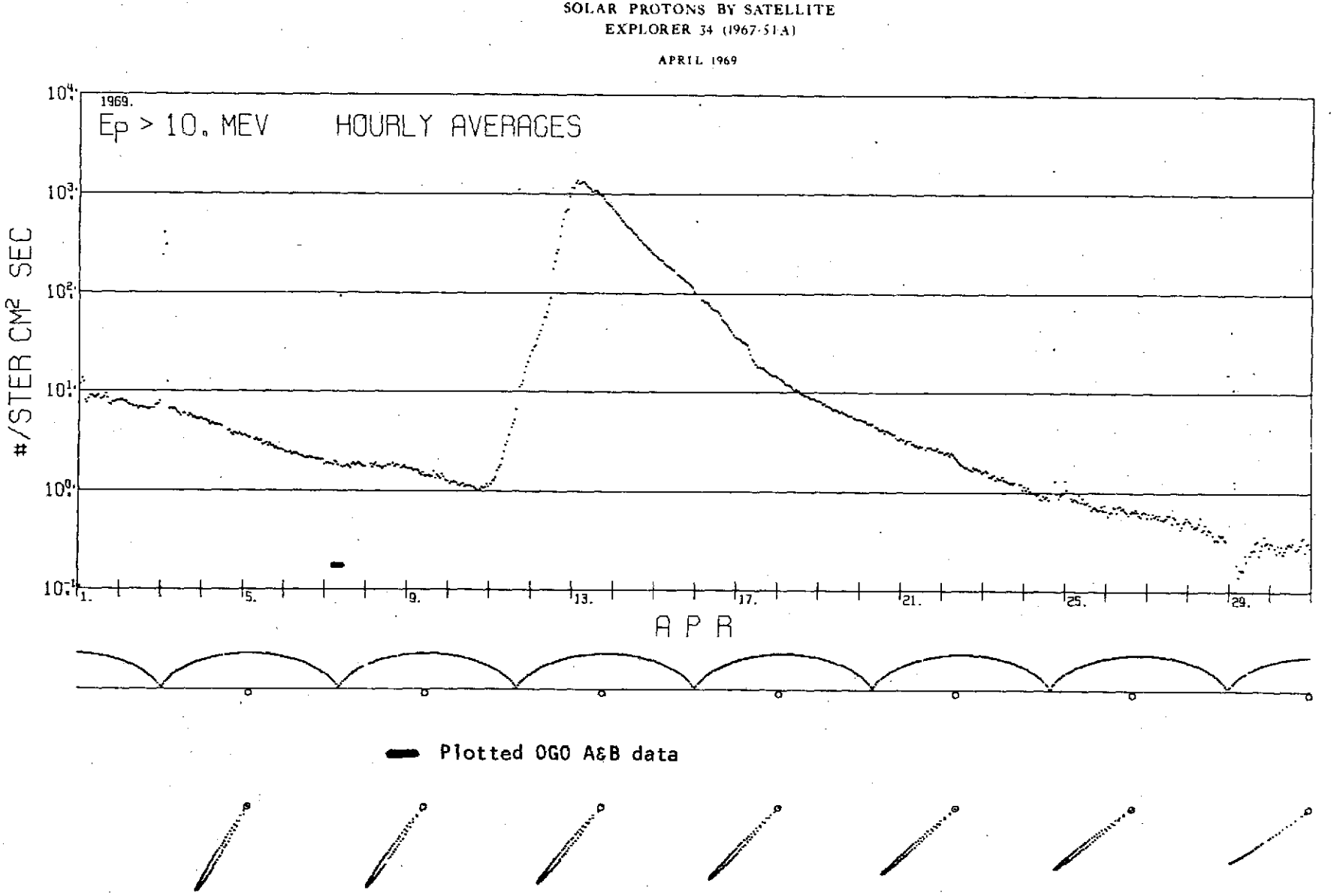
SOLAR PROTONS BY SATELLITE
EXPLORER 34 (1967-51A)
APRIL 1969
1969.
Ep > 10. MEV HOURLY AVERAGES
#/STER CM2 SEC
10^4
10^3
10^2
10^1
10^0
10^-1
1.
5.
9.
13.
17.
21.
25.
29.
APR
Plotted OGO A&B data

Figure 5

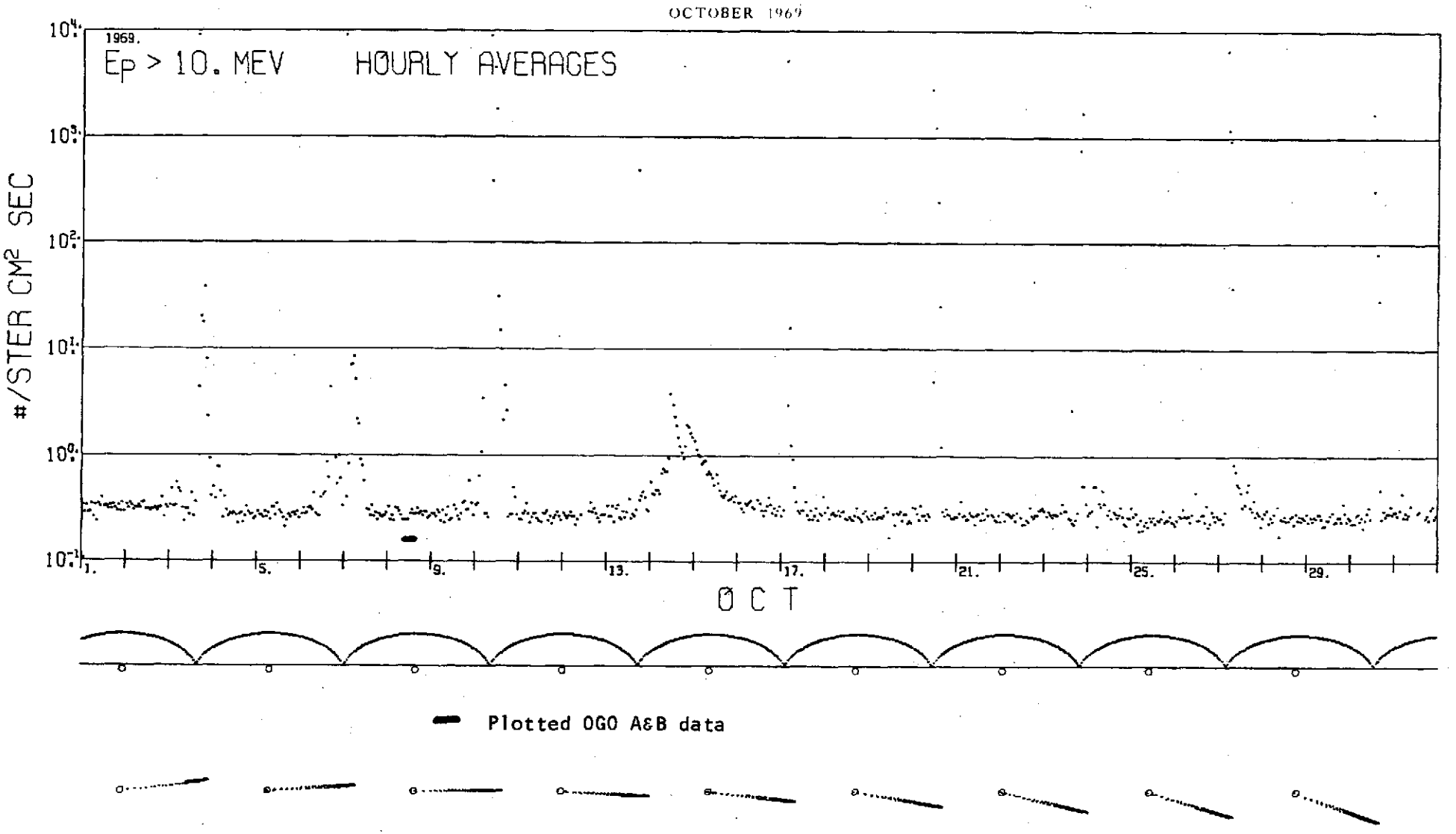
SOLAR PROTONS BY SATELLITE
EXPLORER 41 (1969-53A)
OCTOBER 1969
1969.
Ep > 10. MEV HOURLY AVERAGES
#/STER CM² SEC
10⁴
10³
10²
10¹
10⁰
10⁻¹
1.
5.
9.
13.
17.
21.
25.
29.
OCT
Plotted OGO A&B data

Figure 6

SOLAR PROTONS BY SATELLITE
EXPLORER 41 (1969-53A)

NOVEMBER 1969

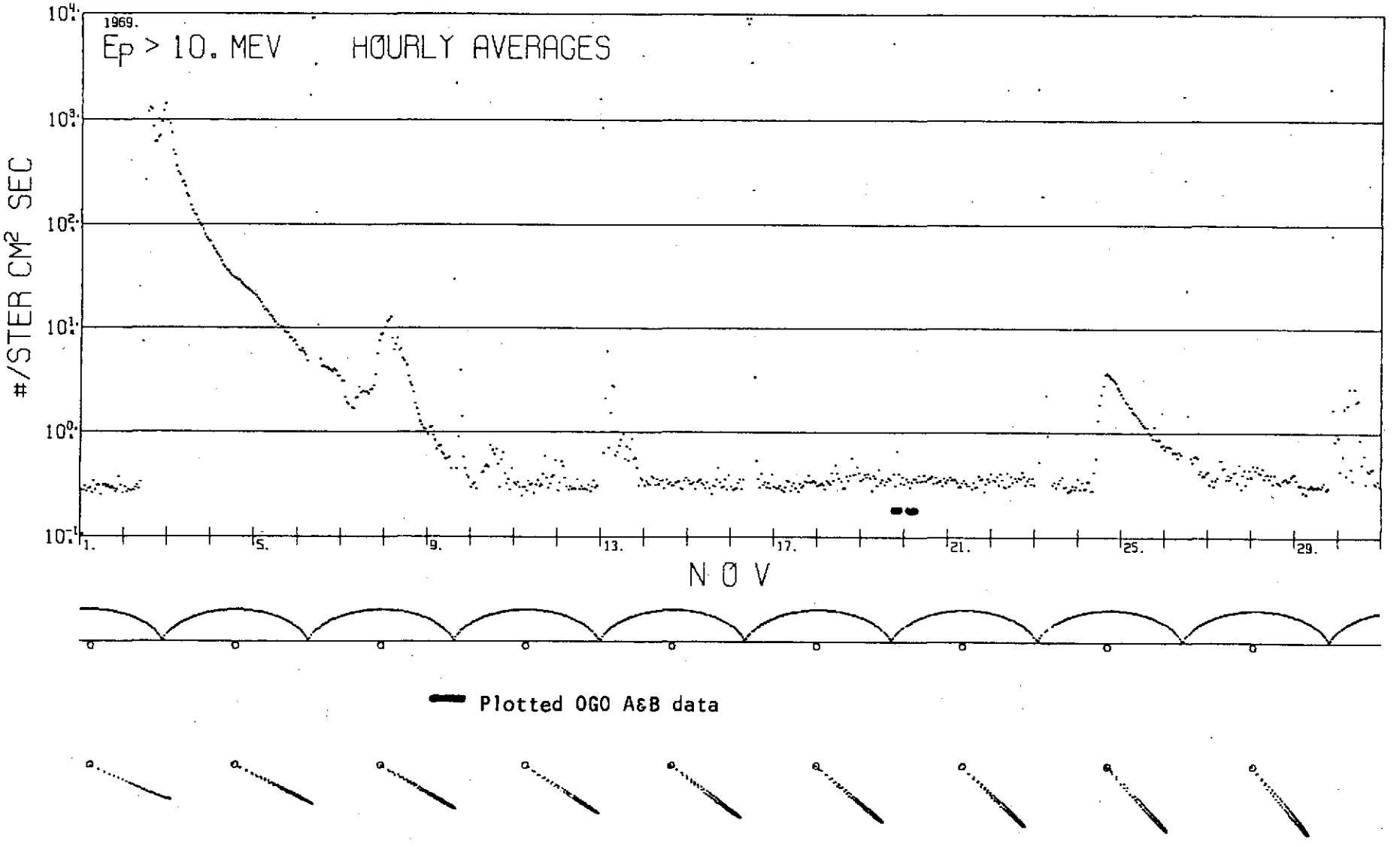

Figure 7

B. Data Format

The OGO I and OGO III satellite data are presented in the form of semi-log plots of ion chamber count rate versus time. Each point is a 20 second average of the count rate. For the OGO I satellite, this time interval is larger than the spin period of 12 seconds, while for the OGO III satellite, it is smaller than the period of 96 seconds. Thus, for OGO I the rates plotted are effectively spin-averaged while for OGO III they are not. This difference is only important when there is some sort of asymmetry in the solar proton flux in the region of space occupied by one of the satellites, and the asymmetry is directed in such a fashion that the satellite body blocks the solar proton beam from reaching the ion chamber out on its boom. Then the chamber rate for OGO III shows an oscillation with a period equal to the spin period. The rate for OGO I will not show this owing to the spin averaging of the plotted data. (It is possible to obtain finer structure for the OGO I data, down to a time resolution of one second.)

All plots are done in a uniform format. The ordinate is ion chamber rate, expressed in units of "normalized pulses per second X 10^3" (NPPS X 10^3), in conformity with earlier reports on OGO ion chamber data. (This unit derives from the calibrating process done before launch, in which a normalizing factor is found which produces a given count under a known radium source. For further information see attached reprint.) In each plot, the ordinate is a log scale varying from 10^1 to 10^6 (NPPS X 10^3). The abcissa is universal time, with each plot representing $2\frac{1}{2}$ hours, regardless of whether there is data for the full time interval. Each ordinate is a linear scale, with major divi-

sions every 10 minutes and every hour labeled.

Data presented in the plots is not always from the same source. In the information telemetered back to Earth from the satellites, there are actually three indications of the rate at which ion pairs are being produced inside the chamber. The shell of the chamber is connected to -380 volts, and the central collector rod is connected to the electrometer amplifier which has a condenser in the feed-back loop. The output of the electrometer against time is a ramp voltage which is automatically reset to zero by a shorting switch whenever the ramp reaches 5 volts. The number of such "ramp resets" occurring during telemetry intervals ($\sim$ 1 second) is one of the methods of calculating chamber rate.

The ramp voltage is also analyzed by a 16 level discriminator, leading to a chamber rate termed the "analog rate." Also the time taken by the ramp to go from the first to the sixteenth discriminator level is measured by counting the clock pulses available from the OGO spacecraft, leading to a chamber rate termed the "clock pulse rate."

Since one can calculate a chamber rate from the clock pulses and the ramp resets only after a reset has taken place--and at low rates the time averaging interval may be much less than the time taken for a ramp to occur--the analog calculation is the best indication of chamber rate at levels up to $\sim 10^3$ (NPPS X 10^3). Above this level the resets are taking place faster than the telemetry intervals occur and the analog rate becomes unreliable. For rates between 10^3 and 10^5 (NPPS X 10^3) the clock pulse rate is plotted. This rate gives a finer structure than the ramp resets, since in this interval the ramp calculation tends to show a certain degree of quantization. This is due to

the telemetry system. The number of ramp resets occurring in a telemetry interval is sent back in a 9-bit sequence, leading to a resolution of one part in 512, while the number of clock pulses accumulated during the ramp is sent back in a 13-bit sequence, leading to a resolution of one part in 8192.

In the highest decade plotted, $10^5 - 10^6$ (NPPS X 10^3), the rate is too fast for the clock pulse method and the ramp reset method is used. This rate is highly susceptible to noise, since a spurious bit may add 256, 128, etc. to the true number of ramp resets. This may be seen in a few of the plots (e.g., #49 and #51), where a layered structure can be seen, each layer corresponding to a different spurious bit multiplying the time rate by a constant factor.

Not all data available has been plotted. The selection criteria were:

1. Both satellites must be collecting data.
2. Periods when both satellites were measuring only cosmic ray background were eliminated.
3. Periods when one of the satellites was obviously in a radiation belt were rejected.

The first criterion was by far the most restrictive due to the standby or low-power status of both satellites for much of the period examined here.

Orbits for both satellites, for periods of plotted data, are included in the data presentation. The orbits are plotted in solar ecliptic coordinates in such a way as to show proximity to the magnetopause and bow shock. This is done by plotting

$$X_{SE} \text{ versus } R_{YZ} = \sqrt{Y_{SE}^2 + X_{SE}^2} \quad .$$

R_{YZ} is given the sign of Y_{SE}, thus showing whether the satellite was east or west of the sun-earth line. This treatment leads to discontinuities in the orbit, occurring whenever Y_{SE} passes through 0.

The bow shock and magnetopause depicted on the orbit plots comes from the work of Behannon.[1] The asymmetry about the sun-earth line of both structures leads to differing distances of the satellite from them, depending on which side of the sun-earth line the satellite is located on. To resolve this type of situation a plot in the X_{SE}-Z_{SE} is needed, but is not presented in this report.

[1] Behannon, K. V., J. Geophys. Res. 73, 907 (1968).

C. Data Plots

ACKNOWLEDGMENTS

The principal investigator in this project is indebted to Dan Carroll for the long hours spent in retrieving the data from the magnetic tapes, doing the computer plotting work, and aiding in the analysis. This work will form a part of his doctoral dissertation.

Bob Likes also aided in the data reduction and analysis and his contribution is appreciated.

Acknowledgment is also due Prof. John Winckler at the University of Minnesota, who was the principal investigator in the OGO experiments and who aided us in the initial stages of this analysis.

Planet. Space Sci. 1968, Vol. 16, pp. 1381 to 1404. Pergamon Press. Printed in Northern Ireland

OBSERVATIONS OF THE SCREENING OF SOLAR COSMIC RAYS BY THE OUTER MAGNETOSPHERE

S. R. KANE and J. R. WINCKLER
School of Physics and Astronomy, University of Minnesota, Minneapolis, Minnesota

and

D. J. HOFMANN
Department of Physics, University of Wyoming, Laramie, Wyoming

(*Received* 21 *June* 1968)

Abstract—Simultaneous observations by identical ionization chambers aboard the satellites OGO-I and OGO-III are utilized to investigate spatial variations in particle intensity near and inside the magnetosphere during the solar cosmic ray events of September 1966. The OGO ion chamber consists of a seven-inch diameter spherical shell of 0·035 in. thick aluminum filled with argon to a pressure of 50 lb/in² absolute. The minimum energy for wall penetration is 12 MeV for protons and ≃0·6 MeV for electrons. Cross-correlation of the absolute proton flux computed from the chamber rate during three solar particle events shows good agreement with the measurements by the IMP-F Solar Proton Monitor during the same events. The chamber has a dynamic range of over six orders of magnitude. Before launch it was calibrated in the laboratory with radiation dosages in the range 1 R/hr–6000 R/hr. The peak dosage measured during the September 1966 solar cosmic ray events varied from 4×10^{-4} R/hr–60 R/hr. The OGO-I and OGO-III chambers, which were normalized in the laboratory prior to the launch, are found to maintain their normalization within ≃1 per cent during their flight. The high sensitivity and absolute inter-comparability of the instruments allow small intensity differences to be detected and it is established that the observed differences can be explained by a magnetospheric 'screening' effect when an anisotropic beam of particles is present in space. Evidence is presented to show that the 'screening' is at times complete for a duration of as much as 110 min in the tail of the magnetosphere so that during this period the solar cosmic rays ($E \simeq 15$ MeV) have virtually no access to that region of the magnetosphere. Small intensity fluctuations of a temporal nature are observed and found to be subject to a damping effect inside the magnetosphere.

INTRODUCTION

Recent computations of geomagnetic cutoffs (Reid and Sauer, 1967; Gall *et al.*, 1968) indicate that at geocentric distances ≥10 Earth radii the cutoff energies for protons are in all probability much smaller than 12 MeV. Consequently, solar protons with energies >12 MeV presumably have free access to the outer magnetosphere. However, it is possible that because of the large anisotropy in the solar particle beam and the irregularities in the magnetospheric field, factors not considered in the usual computations, some constraints may be imposed on the propagation of these particles across the magnetopause and inside the magnetosphere. It is the purpose of this paper to investigate if there are any such magnetospheric effects on the energetic protons (>12 MeV). Simultaneous measurements with identical ionization chambers aboard OGO-I and OGO-III satellites presented later in this paper indicate that such magnetospheric effects are indeed observable and can at times be extremely large.

DESCRIPTION OF THE EXPERIMENT

The OGO ionization chamber experiment has been described in detail elsewhere (Kane *et al.*, 1966; Kane, 1967). The principal characteristics of the OGO chambers are summarized in Table 1. The ion chamber is a sphere 7 in. in diameter with 0·035 in. thick aluminum wall, filled with argon to an absolute pressure of 50 lb/in² in case of OGO-I

and 60 lb/in^2 in the case of OGO-III. In the laboratory, the rates of the two chambers are normalized to a standard pressure of argon. Therefore, in spite of the small difference in the argon pressure, the OGO-I and OGO-III chambers can be considered essentially identical.

TABLE 1. OGO ION CHAMBER CHARACTERISTICS

Diameter	17·8 cm
Wall thickness	0·085 cm Aluminum
Argon pressure	
OGO-I	50 lb/in^2 absolute
OGO-III	60 lb/in^2 absolute
Minimum energy for penetration by charged particles	
Protons	12 MeV
Electrons	0·6 MeV

The chamber is mounted on a boom which extends about 4 ft from the main body of the OGO spacecraft in a direction nearly perpendicular to its spin axis. The chamber is thus essentially in free space, except for about 0·2 steradians solid angle subtended at the location of the chamber by the main body of the spacecraft and the box containing electronic circuits.

Prior to launch the OGO-I and OGO-III ion chambers were calibrated and normalized with a γ-ray source. The rates are expressed in the units of 'normalized pulses sec^{-1} $\times$ 10^3' (NPPS $\times$ 10^3). During the actual flights of the OGO-I and OGO-III satellites the simultaneous pulsing rates of the two chambers are found to agree within 1 per cent whenever the two satellites are in similar regions of space. Some examples of this agreement can be seen in the measurements presented later.

A distinctive characteristic of an ionization chamber is its ability to measure the radiation dosage. The OGO ion chamber measures the radiation dosage behind its aluminium wall which is 0·22 g cm^{-2} thick. The chamber was calibrated with a wide range of radiation dosages at the University of Minnesota γ-ray facility. The results are shown in Fig. 1 where the chamber rate in NPPS $\times$ 10^3 is plotted against the radiation dosage in R/hr. The solid line is the expected relationship computed from the definition of the roentgen and the characteristics of the OGO chamber and gives the relation

$$\text{Dosage (R/hr)} = C \times \text{chamber rate (NPPS} \times 10^3)$$

where the conversion factor

$$C \simeq 2 \times 10^{-5}.$$

The OGO ion chamber has a dynamic range extending over six orders of magnitude. This entire range is often utilized in a single orbit of the OGO satellite during which the chamber rate varies from about 50 NPPS $\times$ 10^3 to 5 $\times$ 10^7 NPPS $\times$ 10^3, the former being the rate due to the galactic cosmic rays in free space and the latter due to the intense radiation in the Van Allen radiation belts. It can be seen from Fig. 1 that for radiation intensities producing pulsing rates less than 5 $\times$ 10^4 NPPS $\times$ 10^3, the chamber response is linearly proportional to the radiation intensity. However, at higher radiation intensities the response becomes non-linear, presumably because of the ion recombination losses in the chamber gas. The measurements presented later are corrected for this non-linearity of response. It is important to note that such a correction is significant only in relatively large solar cosmic ray events.

The minimum energy for penetrating the chamber wall is 12 MeV for protons and about 0·6 MeV for electrons. As far as the solar cosmic rays are concerned, the chamber rate is principally due to protons and α-particles, the response to bremsstrahlung produced by ≃40 KeV electrons being about six orders of magnitude less than that for penetrating protons. Figure 2 shows the basic response of the chamber to protons and α-particles.

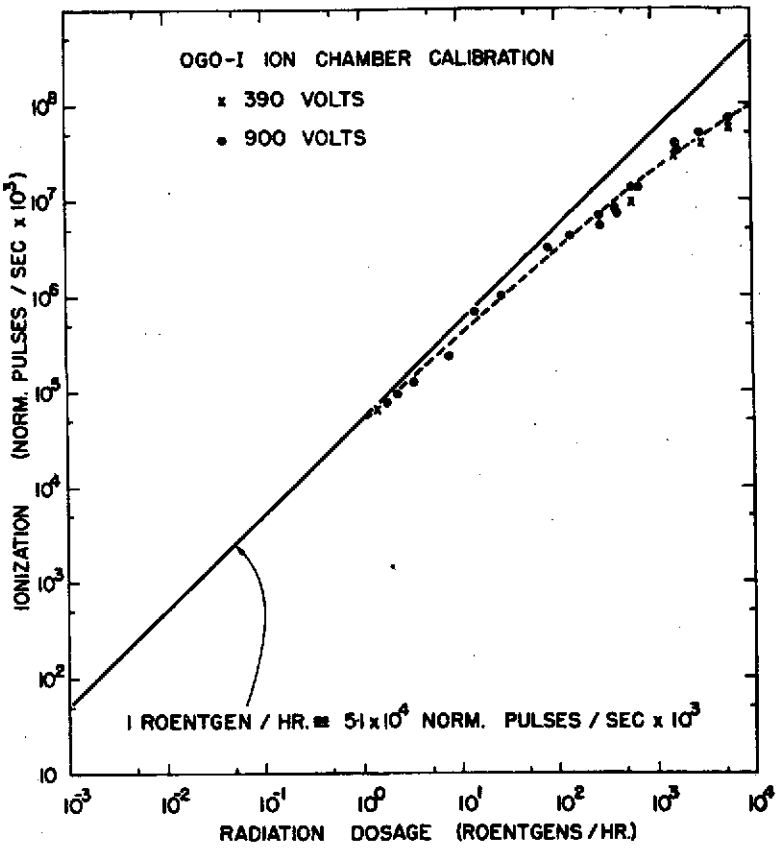

FIG. 1. VARIATION OF THE OGO ION CHAMBER RATE WITH RADIATION DOSAGE.
The solid line gives the computed relation. The two sets of points refer to two different voltages, viz. 390 and 900 Vs, across the chamber.

Here the ratio of the chamber rate $I_1(E)$ due to 1 particle cm^{-2} sec^{-1} of kinetic energy E MeV/nucleon and charge Ze to the rate $I_{\text{Min.}}$ due to the minimum ionizing particles of the same species is plotted against E. It can be seen that the response shown in Fig. 2 is strongly peaked at about 15 MeV/nucleon.

The total chamber rate depends on the energy spectrum of the solar protons and α-particles. From a study of the solar cosmic ray events before September 1961, Freier and Webber (1963) have shown that the proton and α-particle spectrums at energies ≥20 MeV/nucleon can be well represented by the differential rigidity spectrum

$$\frac{dJ_i}{dP}\ (P, t) = J_{0i}(t)e^{-P/P_0(t)}$$

where P is the rigidity of the particles, t is time and $i = 1, 2$ refer to protons and α-particles. The constant P_o is the same for both protons and α-particles although it varies during the course of an event and also from one event to another. For most of the events studied by Freier and Webber the values of P_o lie in the range 40–300 MV. The values of P_o for the events during the period September 1961–June 1965 are also found to lie in this range

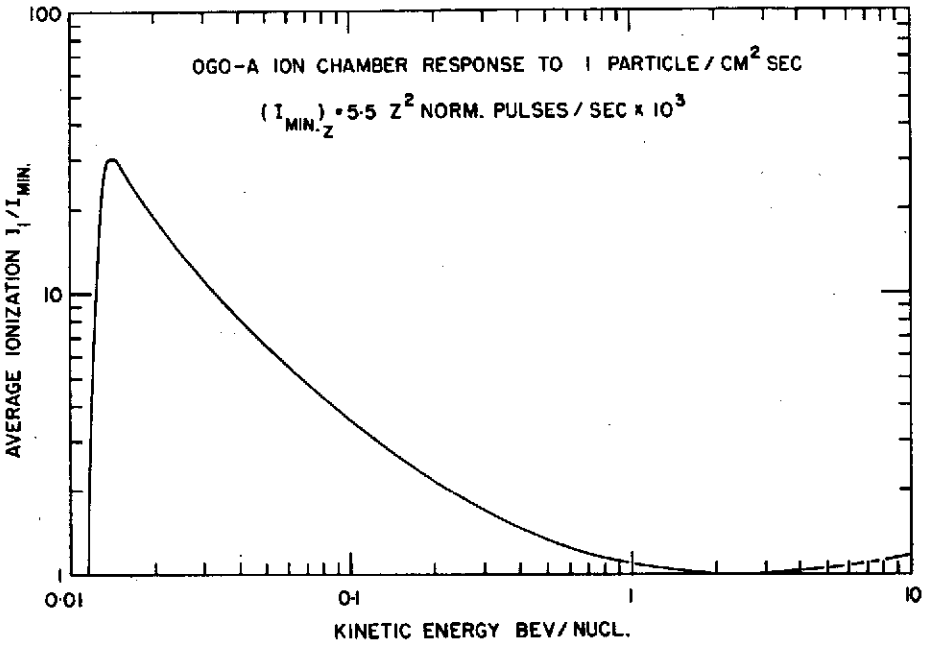

FIG. 2. RESPONSE OF THE OGO ION CHAMBER TO A FLUX OF 1 PARTICLE cm^{-2} sec^{-1} OF PROTONS AND α-PARTICLES AS A FUNCTION OF THEIR KINETIC ENERGY PER NUCLEON.

(Webber, 1966). The ratio of proton and α-particle intensitities

$$R_{p\alpha} = \frac{J_{01}}{J_{02}}$$

during these events was found to lie in the range 1–40. For the present discussion it will be assumed that these general characteristics of solar cosmic rays are valid for energies >10 MeV/nucleon. In order to estimate the variation of the OGO ion chamber rate with P_o and $R_{P\alpha}$ we first compute the differential response of the chamber,

$$\frac{dI_i'}{dP} = I_1(P)\frac{dJ_i}{dP}$$

where $I_1(P)$ is the response function derived from the basic response $I_1(E)$ shown in Fig. 2. Figure 3 shows the differential response of the chamber to solar protons and α-particles for two values of P_o viz. 50 and 300 MV, and $J_{01} = J_{02} = 1$ particle cm^{-2} sec^{-1} MV^{-1}. The total chamber rate

$$I = \sum_{i=1}^{2} \int_{150}^{\infty} \frac{dI_i'}{dP}\, dP$$

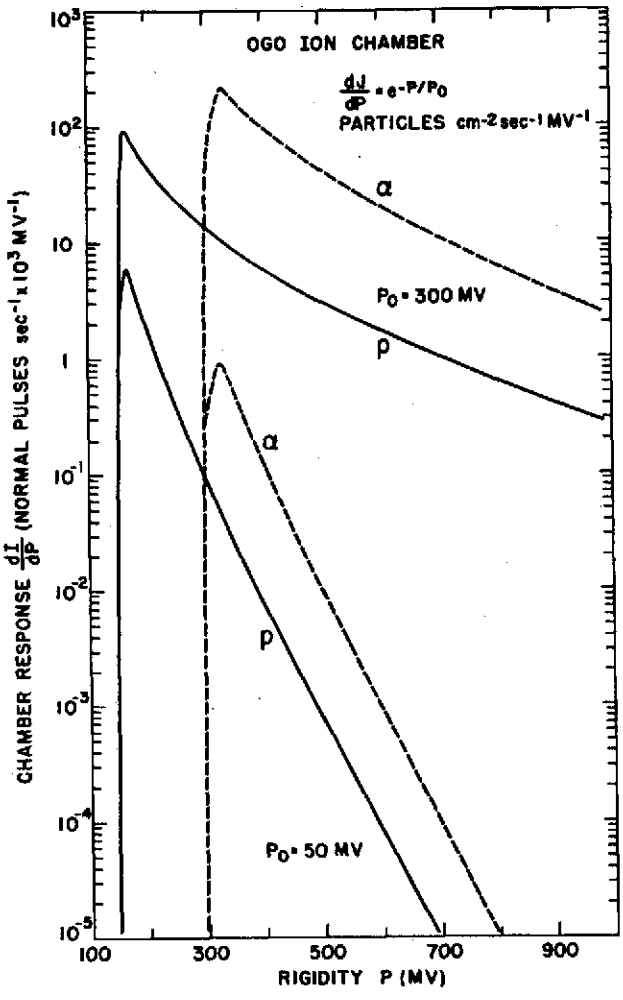

FIG. 3. DIFFERENTIAL RESPONSE OF THE OGO ION CHAMBER TO A DIFFERENTIAL RIGIDITY SPECTRUM OF SOLAR PROTONS (p) AND α-PARTICLES (α) AS A FUNCTION OF RIGIDITY.
Response is shown for a flat spectrum (P_o = 300 MeV) and a steep spectrum (P_o = 50 MeV).

for $J_{01} = \dfrac{1}{P_o} e^{150/P_o}$

and for a series of values of P_o and $R_{p\alpha}$ is shown in Fig. 4. It is important to note that in each case the spectrum is so normalized that the total number of protons above 150 MV

$$J(>150 \text{ MV}) = J_{01} P_o e^{-150/P_o} = 1 \text{ proton cm}^{-2} \text{ sec}^{-1}.$$

From the computed response shown in Figs. 3 and 4 it can be seen that for steep solar cosmic ray spectra the chamber response is principally due to protons >12 MeV even for $R_{p\alpha} = 1$. Moreover for $R_{p\alpha} > 4$ the total chamber rate varies at most by ± 50 per cent for a variation in P_o from 40 to 300 MV.

For an 'average' solar proton spectrum ($P_o = 175$ MV, $R_{p\alpha} = \infty$) one obtains the following relation from Fig. 4

$$1 \text{ proton cm}^{-2} \text{ sec}^{-1} (E > 12 \text{ MeV}) \equiv 58 \text{ NPPS} \times 10^3.$$

This is equivalent to

$$1 \text{ NPPS} \times 10^3 \equiv 1{\cdot}37 \times 10^{-3} \text{ protons cm}^{-2} \text{ sec}^{-1} \text{ ster}^{-1} (E > 12 \text{ MeV}).$$

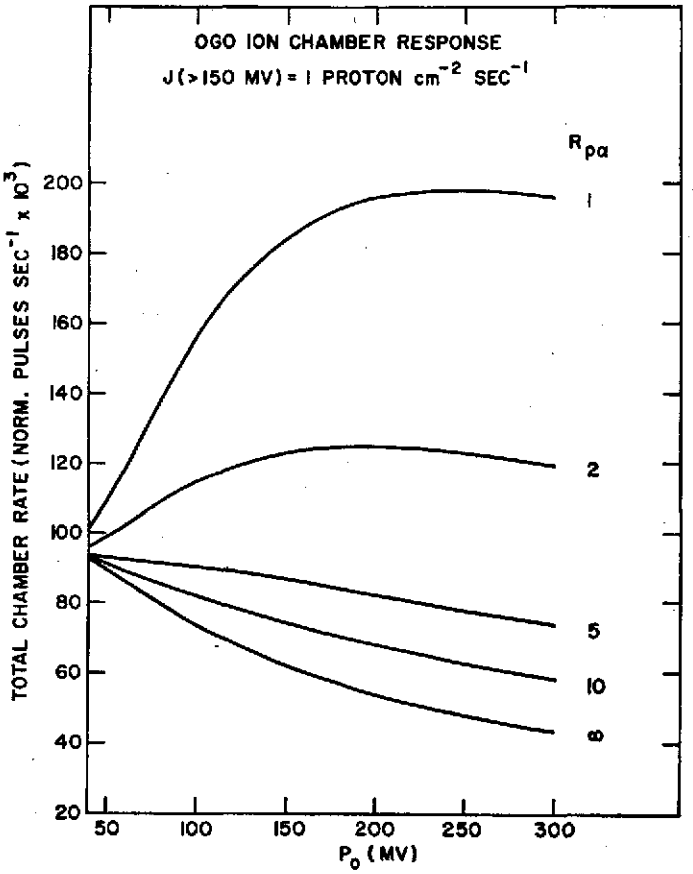

FIG. 4. TOTAL PULSING RATE OF THE OGO ION CHAMBER AS A FUNCTION OF THE EXPONENT P_0 IN THE EXPONENTIAL RIGIDITY SPECTRUM OF SOLAR COSMIC RAYS.
For each value of P_o the spectrum is so normalized that $J(>150 \text{ MV}) = 1$ proton cm^{-2} sec^{-1}. The different curves are obtained for different values of the proton to α-particle ratio $R_{p\alpha}$.

COMPARISON WITH OTHER SOLAR PROTON DETECTORS

The present study is concerned with the OGO ion chamber measurements outside the Earth's radiation belts during solar particle events. At times of low solar activity the ion chamber in this region of space records a nearly constant pulsing rate due to the galactic cosmic rays, with occasional spikes caused by transient magnetospheric radiation. At times of solar flares the chamber responds to the associated X-ray bursts and energetic particle events during which the chamber registers large increases above the galactic background (see, for example, Arnoldy *et al.*, 1968). An example of such events is shown in Fig. 5

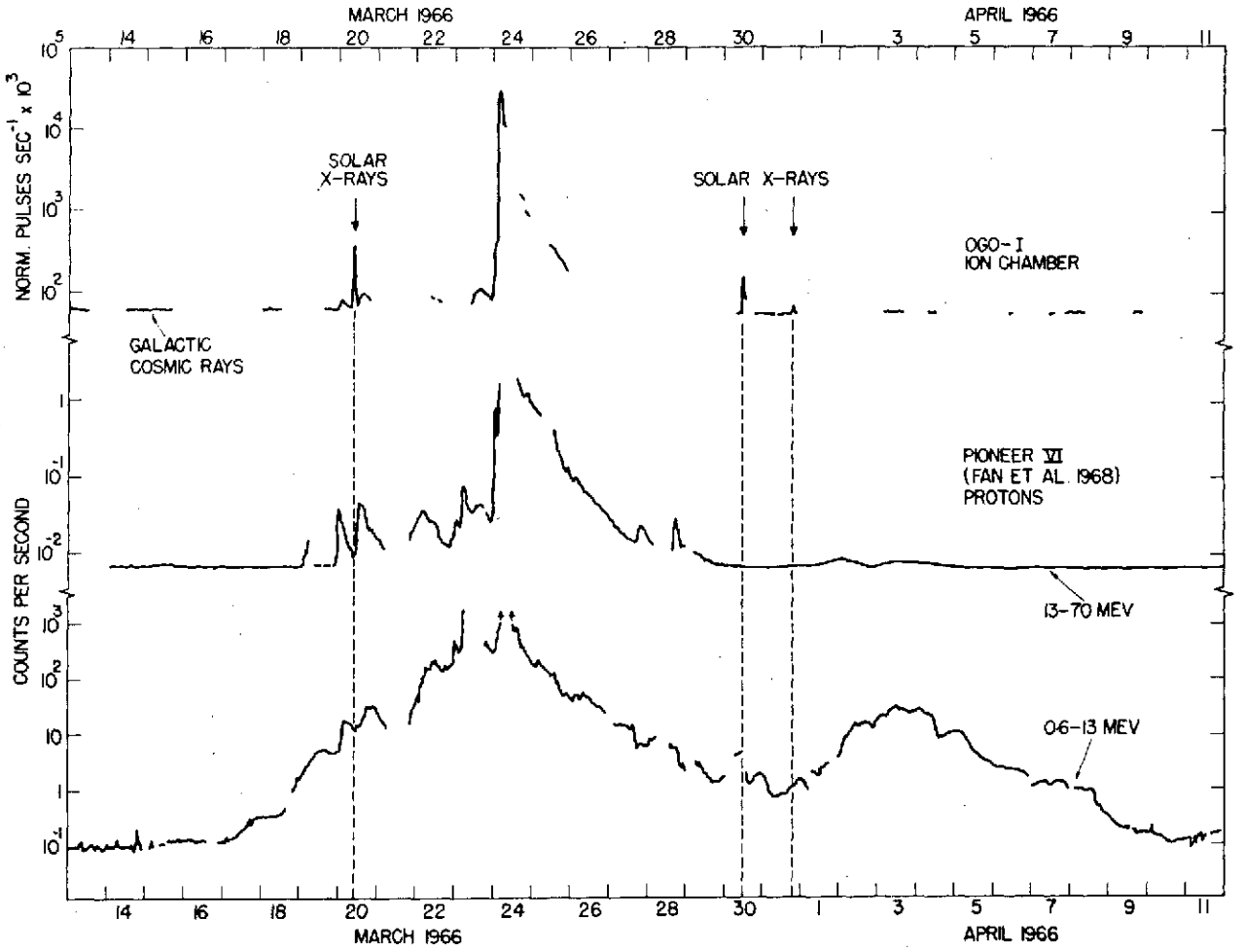

FIG. 5. HOURLY AVERAGE RATES OF THE OGO-I ION CHAMBER FROM 13 MARCH TO 11 APRIL 1966, A PERIOD DURING WHICH THREE LARGE SOLAR X-RAY BURSTS AND ONE LARGE SOLAR COSMIC RAY EVENT WERE OBSERVED.
For comparison the 0·6–13 MeV and 13–70 MeV proton measurements by Fan *et al.* (1968) made with University of Chicago detectors aboard Pioneer VI are also shown. Notice the good correlation of the OGO-I ion chamber with the 13–70 MeV protons and practically none with the 0·6–13 MeV protons.

where the hourly averages of the OGO-I ion chamber rates during the period 13 March–11 April, 1966 are plotted against time. Also, for comparison the measurements of protons in the energy ranges 0·6–13 MeV and 13–70 MeV made by Fan *et al.* (1968) with detectors aboard the Pioneer VI space probe are shown in Fig. 5. During this period the OGO ion chamber recorded three large X-ray bursts (20, 30 and 31 March, 1966) and a large solar particle event beginning on 24 March, 1966. It can be seen that, except for the three solar X-ray bursts which are not expected to be seen in the Pioneer VI data, there is an excellent correlation between the OGO ion chamber and the 13–70 MeV protons. Equally important is the fact that there is poor correlation between the OGO ion chamber and 0·6–13 MeV protons. This is consistent only with the chamber cutoff being 12 MeV for protons as deduced earlier. In fact, the proton flux above 12 MeV, computed from the peak OGO-I chamber rate during the solar particle event, agrees within 20 per cent with the simultaneous measurements of 13–70 MeV protons by Fan *et al.* in spite of the large spatial separation between the OGO-I and Pioneer VI spacecrafts.

Measurements of protons with energies >10 MeV made with the solar proton montitor aboard the IMP-F Earth satellite are available for the solar particle events during May and June, 1967 (Bostrom *et al.*, 1968b). During this period the OGO-III ion chamber was operating more or less continuously. However, the ion chamber is an omnidirectional detector while the proton monitor is a directional instrument. Moreover, these two spacecrafts are located in different regions of the magnetosphere. Therefore, comparison between the two detectors is possible only during the decay phase of a solar cosmic ray event when the directional anisotropy and spatial gradient in the particle intensity are believed to be small. Such a comparison is shown in Fig. 6 where the excess ion chamber rate above the galactic background is plotted against the corresponding rate of the proton monitor. The values for the galactic background taken in the two cases are 50 NPPS $\times 10^3$ and 0·35 particles-cm^{-2} sec^{-1} ster^{-1}, respectively. It may be noted that the background for the OGO chamber is $\ll$5 per cent and that for the IMP-F monitor $\ll$25 per cent for most of the points shown in Fig. 5. Consequently, the interpretation of this comparison is not critically dependent on the choice of the background. The horizontal bars represent the uncertainties in the IMP-F proton monitor data (Bostrom *et al.*, 1968a). The solid line $I/J = 6{\cdot}8 \times 10^2$ is the computed relation between the ion chamber rate I and the proton monitor rate J for an 'average' solar proton spectrum ($P_o = 175$ MV). J is computed by integrating the spectrum from 10 MeV to ∞. To compute I the same spectrum is integrated from 12 MeV to ∞ and the flux of protons >12 MeV thus obtained is then used to determine the chamber rate in NPPS $\times 10^3$ with the help of the relation deduced earlier. It can be seen that within the indicated errors most of the points do indeed lie close to the predicted solid line indicating a nearly linear relationship between the OGO ion chamber rate and protons above 10 MeV.

SIMULTANEOUS OBSERVATIONS BY OGO-I AND OGO-III

The OGO-I and OGO-III satellites were launched into highly eccentric orbits on 5 September 1964 and 7 June 1966, respectively. Both satellites are spin stabilized, the spin period being about 12 sec for OGO-I and 95 sec for OGO-III. Orbital parameters for the two satellites for the epoch 15 September 1966 are summarized in Table 2. Since their launch, OGO-I and OGO-III ion chambers have observed many energetic solar X-ray bursts and solar cosmic ray events. Observations of the X-ray bursts and their relationship

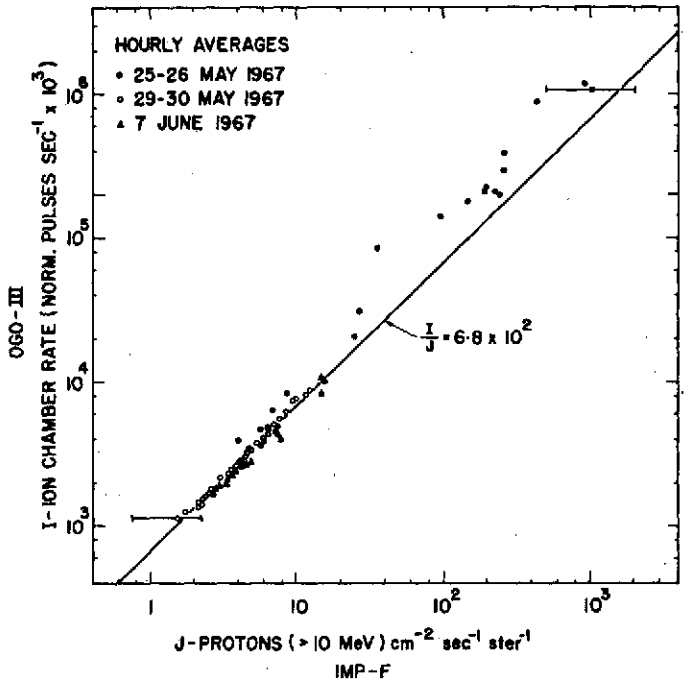

FIG. 6. COMPARISON OF OGO-III ION CHAMBER MEASUREMENTS WITH THE IMP-F MEASUREMENTS OF PROTONS >10 MeV DURING THE DECAY PHASE OF THREE SOLAR COSMIC RAY EVENTS. The straight line corresponds to a computed relation between the two measurements for the solar proton spectrum $dJ/dP = J_0 e^{-P/175}$ protons cm^{-2} sec^{-1} MV^{-1}.

with the radio and energetic particle emission have already been reported in earlier publications (Arnoldy *et al.*, 1967a, 1967b, 1968). In this report the simultaneous OGO-I and OGO-III observations of solar cosmic rays are presented.

The first opportunity to compare the simultaneous measurements with the two satellites occurred during the September 1966 solar cosmic ray events. Figure 7 shows the hourly averages of the excess ionization intensity (galactic background of about 50 NPPS $\times$ 10^3 has been subtracted) during the period 28 August–30 September 1966. A solar excess is observed throughout this period. The OGO-III data (lightline graph) is fairly complete, most of the breaks being due to the passage through the radiation zones. OGO-I data is obtained sporadically when the satellite was turned on, which occurred mainly during the latter half of September.

TABLE 2

	OGO-I	OGO-III
Perigee	3·55 R_E	1·09 R_E
Apogee	21·8 R_E	20·0 R_E
Inclination to equator	52°	34°
Local time at Apogee	2100 hr	1630 hr
Orbital period	64 hr	48·6 hr
Spin period	12 sec	95 sec
Spin orientation (Solar-ecliptic coordinates)	225°, −25°	224°, −39°

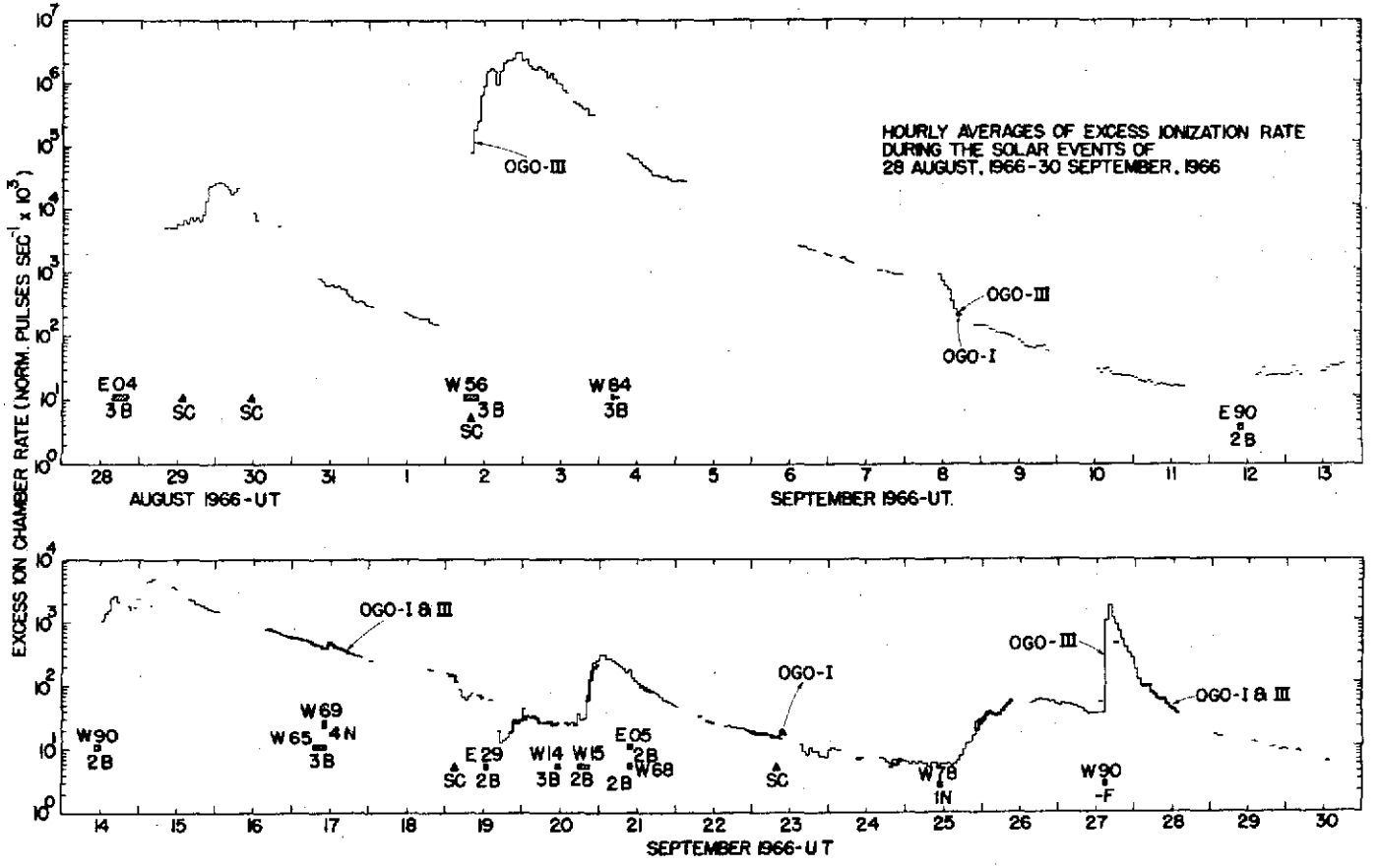

FIG. 7. HOURLY AVERAGE RATES OF THE OGO-I (THICK LINE) AND OGO-III (LIGHT LINE) ION CHAMBERS ABOVE THE GALACTIC BACKGROUND DURING THE PERIOD 28 AUGUST–30 SEPTEMBER, 1966 SHOWING SEVERAL SOLAR COSMIC RAY EVENTS DURING THAT PERIOD.

The sections of the OGO-I and OGO-III orbits projected perpendicularly on to the ecliptic plane are shown in Fig. 8 for time intervals in September 1966 when simultaneous data from the two satellites were available. For reference, the 'normal' location of the magnetopause and the shock front are also shown schematically. The OGO-III magnetometer measurements indicate that the satellite was outside the magnetosphere at these times (Smith and Holzer, private communication). No such magnetospheric boundary determination is available for the OGO-I satellite. On the basis of the 'known' topology of the magnetosphere, the OGO-I satellite is assumed to be inside the magnetosphere during the time intervals under consideration.

Table 3 lists the solar flares which are most probably associated with the ion chamber increases observed on OGO-III in space during this period. Also tabulated for each event are the peak ion chamber rate, the equivalent proton flux above 12 MeV obtained from the relation deduced earlier, the peak dosage rate in R/hr, and the number of hours of available OGO-I data. Most of these hours are accompanied by simultaneous data from OGO-III.

Figure 9 shows simultaneous data during the relatively small event of 17 September superimposed on the decay of a larger event which began on 14 September. Positions of the satellites at the intensity peak are depicted in the figure. These positions are obtained by rotating the position vector about the Sun–Earth line until it lies in the ecliptic plane. Actually, OGO-I was 45° above the ecliptic plane and OGO-III was 37° above the ecliptic plane. The main features to note here are that both before and after the peak of the event the two sets of data are in average agreement; however, fluctuations observed on OGO-III are somewhat damped at the position of OGO-I. At the peak of the event, the intensity at OGO-I is some 10 per cent lower than that at OGO-III. The roll period of OGO-III is about 95 sec and shows up on the 1 min averages as the ion chamber is blocked from the anisotropic beam by the satellite body. This roll modulation is shown in more detail in Fig. 10 before, during and after the peak of the event from 10 sec averages and appears to have a maximum of the order of 10 per cent during the intensity peak. This figure does not, however, indicate the true degree of anisotropy since one does not know what portion of the spacecraft is blocking the beam and thus to what degree the beam is actually being attenuated. Also, since the ion chamber is an omnidirectional instrument, the spacecraft body cannot be a very effective beam absorber and thus the true degree of anisotropy is probably considerably larger than that observed. The spin rate of OGO-I is considerably higher with a period of about 12 sec. This high spin rate requires a very high ionization intensity for accurate analysis; however, preliminary analysis of two second averages indicates that if any anisotropy existed at the position of OGO-I, it was certainly less than that at the position of OGO-III. As indicated in Fig. 10, shortly before the new event on 17 September and several hours after the peak in intensity, the roll modulation on OGO-III indicated an anisotropy of about 5 per cent. Thus, the increase phase is characterized by an increase in the degree of anisotropy at OGO-III and a lesser intensity at the position of OGO-I. It is our concensus that the lower intensity on OGO-I is due to its position with respect to the magnetosphere and the Archimedes spiral angle of the interplanetary magnetic field, i.e. during the initial phases of the new event, the anisotropy is field oriented and the magnetosphere acts as a 'screen' for OGO-I but not for OGO-III which is out in front of the magnetosphere. The smaller anisotropies observed before and after the intensity peak are probably of a non-field aligned nature as observed by Keath, Bukata and McCracken (1968) on Pioneer 8 and do not give rise to an intensity difference at the positions of the two spacecraft. The damping effect of the small fluctuations observed at OGO-I is probably

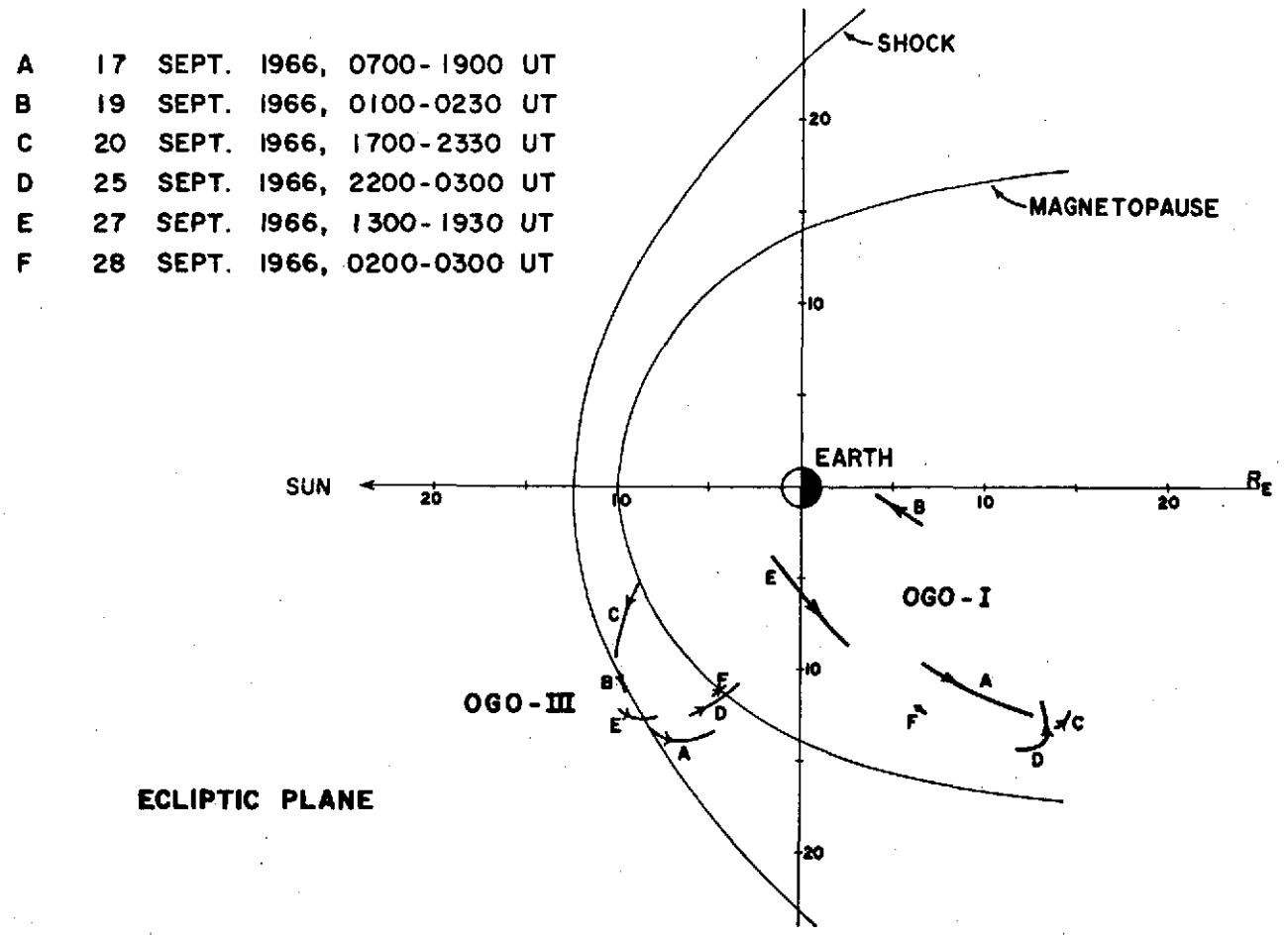

FIG. 8. PROJECTIONS IN THE ECLIPTIC PLANE OF SEGMENTS OF THE OGO-I AND OGO-III ORBITS FOR PERIODS DURING WHICH SIMULTANEOUS OGO-I AND OGO-III DATA (PRESENTED IN FIGS. 9, 11, 12, 13 AND 14) ARE AVAILABLE.

Table 3. SOLAR COSMIC RAY EVENTS 28 AUGUST–30 SEPTEMBER 1966

Date (1966)	Solar Flares: Probable time UT	Solar Flares: Position	Solar Flares: Importance	Solar Flares: McMath plage region	Peak OGO-III chamber rate (Norm. pulses $sec^{-1} \times 10^3$)	Equivalent flux of protons >12 MeV (Protons cm^{-2} $sec^{-1} \times ster^{-1}$)	Peak radiation dosage (R/hr)	Available OGO-I data during event (hr)
28 Aug.	1522	N23, E04	3B	8461	8×10^3	11·2	0·16	0
29 Aug.					$1{\cdot}9 \times 10^4$	26·6	0·38	0
2 Sept.	0542	N24, W56	3B	8461	3×10^4	4200	60	1
12 Sept.	0858	N15, E90	2B	8505	$\simeq 50$	$\simeq 0{\cdot}07$	$\simeq 10^{-3}$	0
14 Sept.	1014	S20, W90	2B	8484	5×10^3	7·0	0·10	16
17 Sept.	<0947	N24, W69	4N	8496	150	0·21	3×10^{-3}	13
19 Sept.	<1203	N23, E29	2B	8509	$\simeq 20$	$\simeq 0{\cdot}03$	$\simeq 4 \times 10^{-4}$	19
20 Sept.	<1738	N03, W15	2B	8505	275	0·39	$5{\cdot}5 \times 10^{-3}$	28
25 Sept.					50	0·07	10^{-3}	13
27 Sept.	1409	N19, W90	F,1	8509	$1{\cdot}7 \times 10^3$	2·38	$3{\cdot}4 \times 10^{-2}$	15

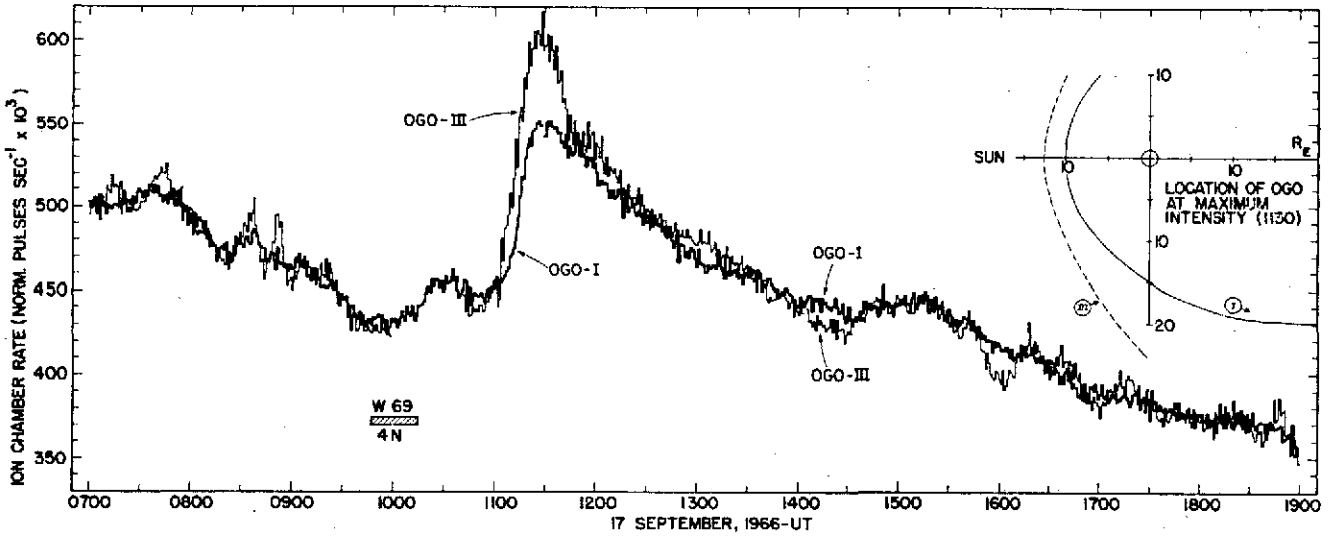

FIG. 9. ONE MINUTE AVERAGES FOR THE OGO-I AND OGO-III ION CHAMBERS FROM 0700 TO 1900 UT ON 17 SEPTEMBER 1966. The locations of the two spacecrafts at the time of the peak intensity (1130 UT) are shown in the inset and are obtained by rotating the radius vectors about the Sun–Earth line until they lie in the ecliptic plane.

due to the fact that OGO-I can be considered inside the magnetosphere while OGO-III is outside. A small amount of scattering near the magnetospheric boundary, giving rise to transit time differences for different particles, would then tend to smooth these small fluctuations. A portion of the decay of this event, while simultaneous data was available, is shown in Fig. 11. At this time OGO-I was in the tail of the magnetosphere near the midnight meridian. The excess intensity appears to be decaying smoothly outside the magnetosphere, while inside the magnetosphere, at the position of OGO-I, the intensity

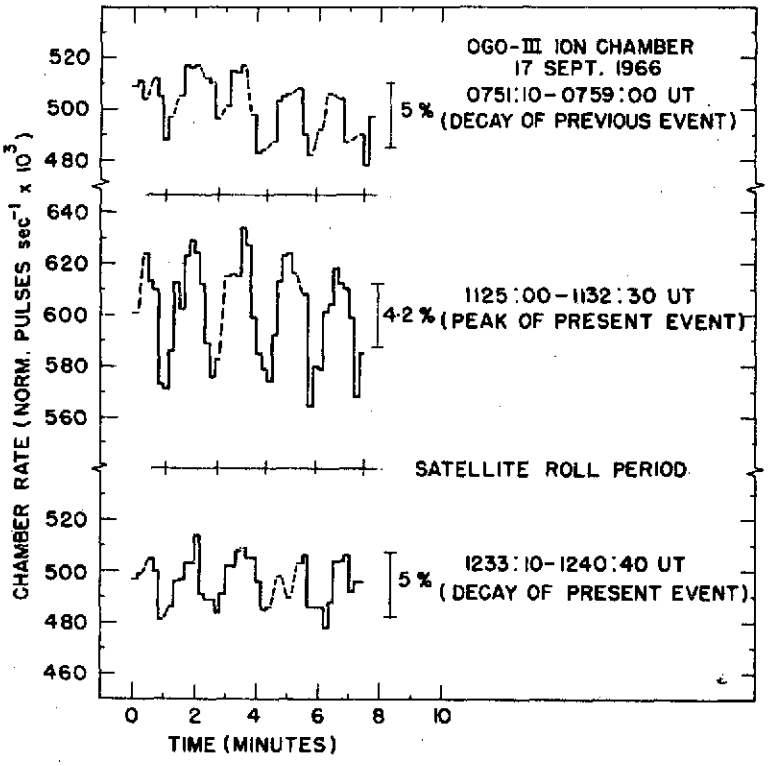

FIG. 10. TEN SECOND AVERAGES OF THE OGO-III ION CHAMBER SHOWING THE ROLL MODULATION DURING THREE TIME INTERVALS ON 17 SEPTEMBER 1966 (SEE FIG. 9).
The starting time (0 min) for each plot corresponds to the beginning time of the corresponding time interval.

appears to remain constant. The two measurements become equal at about 0230. This is probably not a geomagnetic cutoff effect since the satellite is some 7 Earth radii deep in the tail where the best estimates of the cutoff are considerably less than the ion chamber cutoff of 12 MeV (Reid and Sauer, 1967; Paulikas *et al.*, 1968). A plausible explanation is that during the time interval covered by Fig. 11 OGO-I is moving out towards the magnetopause where the 'screening' effect is smaller and is therefore beginning to sample a radiation equivalent to that observed by OGO-III outside the magnetosphere.

A solar flare X-ray event occurred on 20 September at about 1710 UT. This flare produced energetic particles as shown in Fig. 12. OGO-I was inside the magnetosphere and indicates several transient electron type increases superimposed on the solar event. Again

the difference in intensity in front of and inside the magnetosphere is evident, this time the 'screening' effect being some 20 per cent.

During the event of 25 September, which may be associated with a backside flare, simultaneous data from the two satellites outside the radiation zones was obtained for about five hours during the slow increase phase of the event. These data are shown in Fig. 13. The observed initial difference in intensity with a slow convergence could be of magnetospheric origin since OGO-III, which indicates initially a higher ionization intensity is

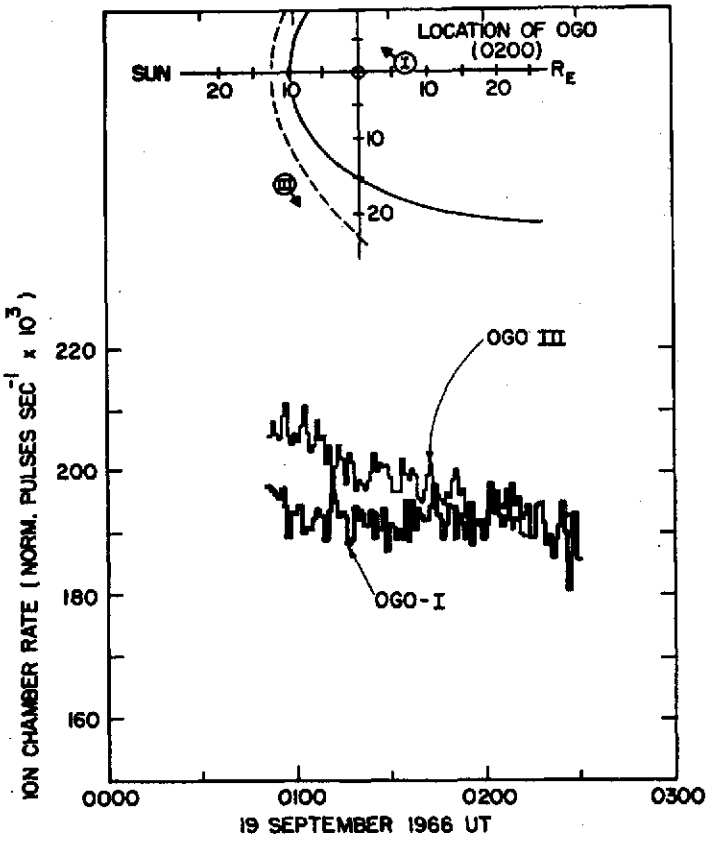

FIG. 11. ONE MINUTE AVERAGE RATES OF THE OGO-I AND OGO-III ION CHAMBERS FROM 0000 TO 0300 UT ON 19 SEPTEMBER 1966 DURING THE DECAY OF THE 17 SEPTEMBER EVENT.

moving toward the magnetopause. At about 0300 it encounters the trapped radiation inside the magnetosphere. If this phenomenon is indeed caused by a highly anisotropic beam impinging on the magnetosphere, it would indicate that even though the particle producing flare may have been on the backside of the Sun, an appreciable number of particles somehow found their way to interplanetary field lines which connect the Sun and the Earth. Such connection of eastern hemisphere events to western hemispheric field lines has been observed by Fan *et al.* (1968) and it appears that there is a region near the Sun which effectively funnels energetic particles onto field lines which allow easy access to the Earth.

Figure 14 shows the last of the events observed in September 1966. This event was probably associated with a small west limb flare at about 1410 UT, 27 September 1966.

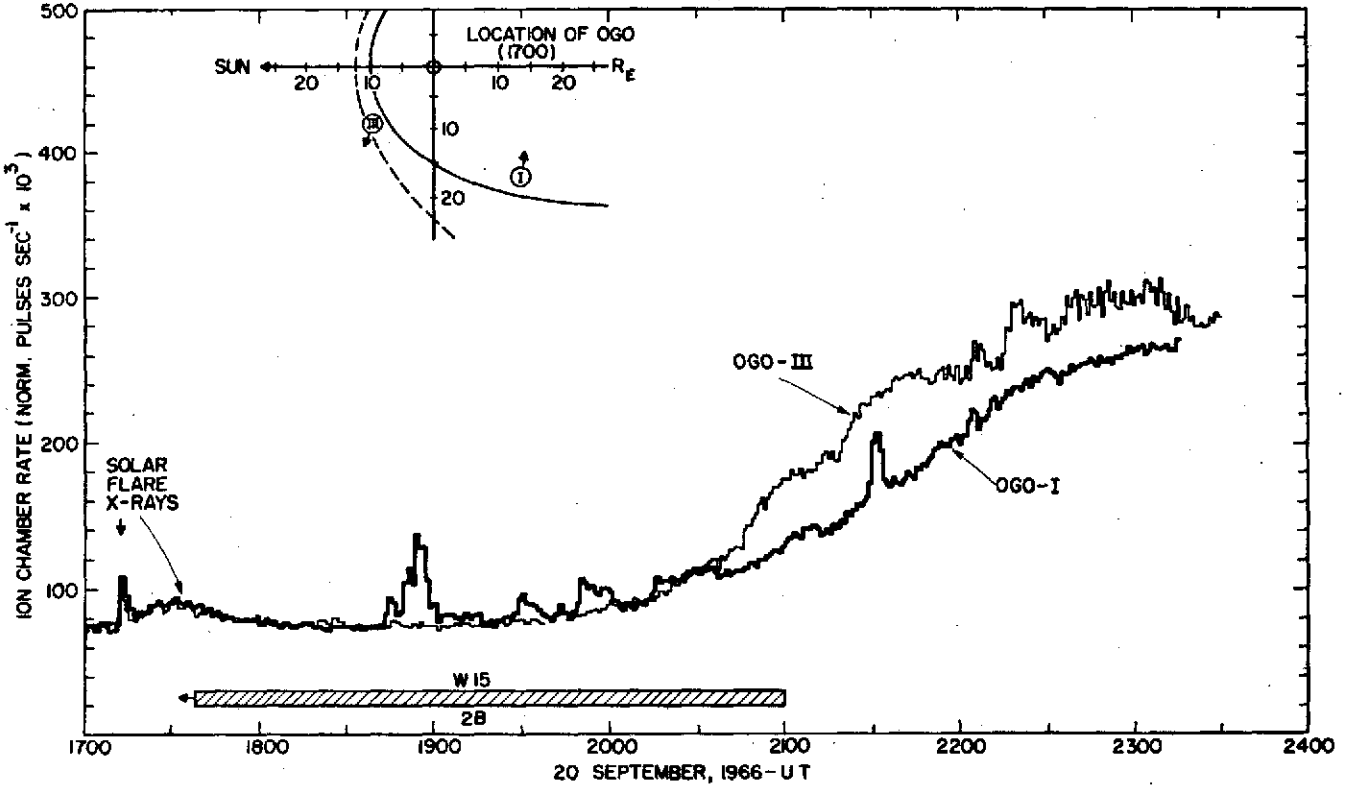

FIG. 12. ONE MINUTE AVERAGE RATE OF THE OGO-I AND OGO-III ION CHAMBERS FROM 1700 TO 2400 UT ON 20 SEPTEMBER 1966. Notice the solar X-ray burst observed simultaneously by the two chambers from 1710 to 1820 UT. The spikes in the OGO-I data) are presumably caused by the transient magnetospheric electrons.

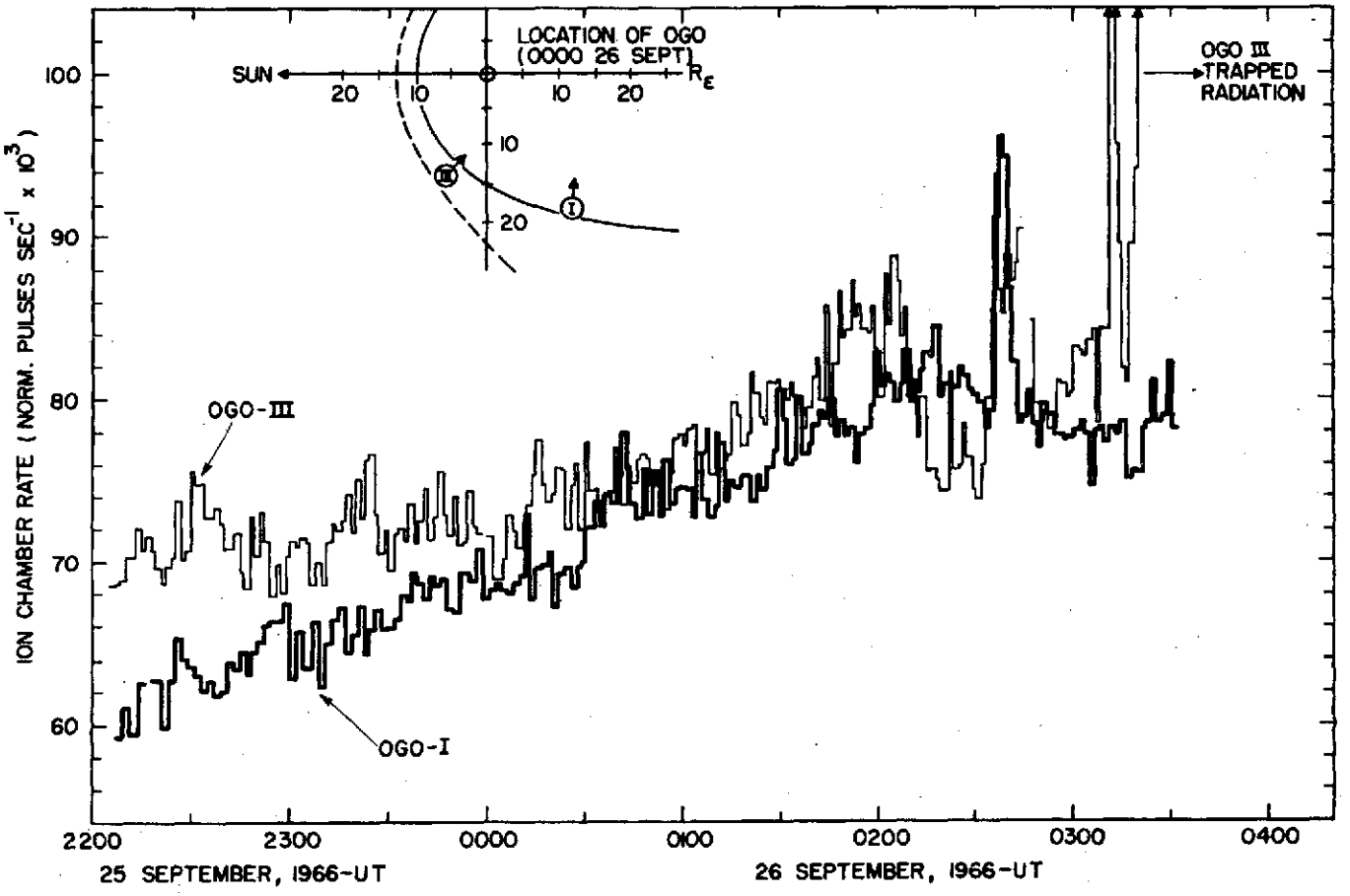

FIG. 13. ONE MINUTE AVERAGE RATES OF THE OGO-I AND OGO-III ION CHAMBERS FROM 2000 UT ON 25 SEPTEMBER TO 0430 UT ON 26 SEPTEMBER 1966.

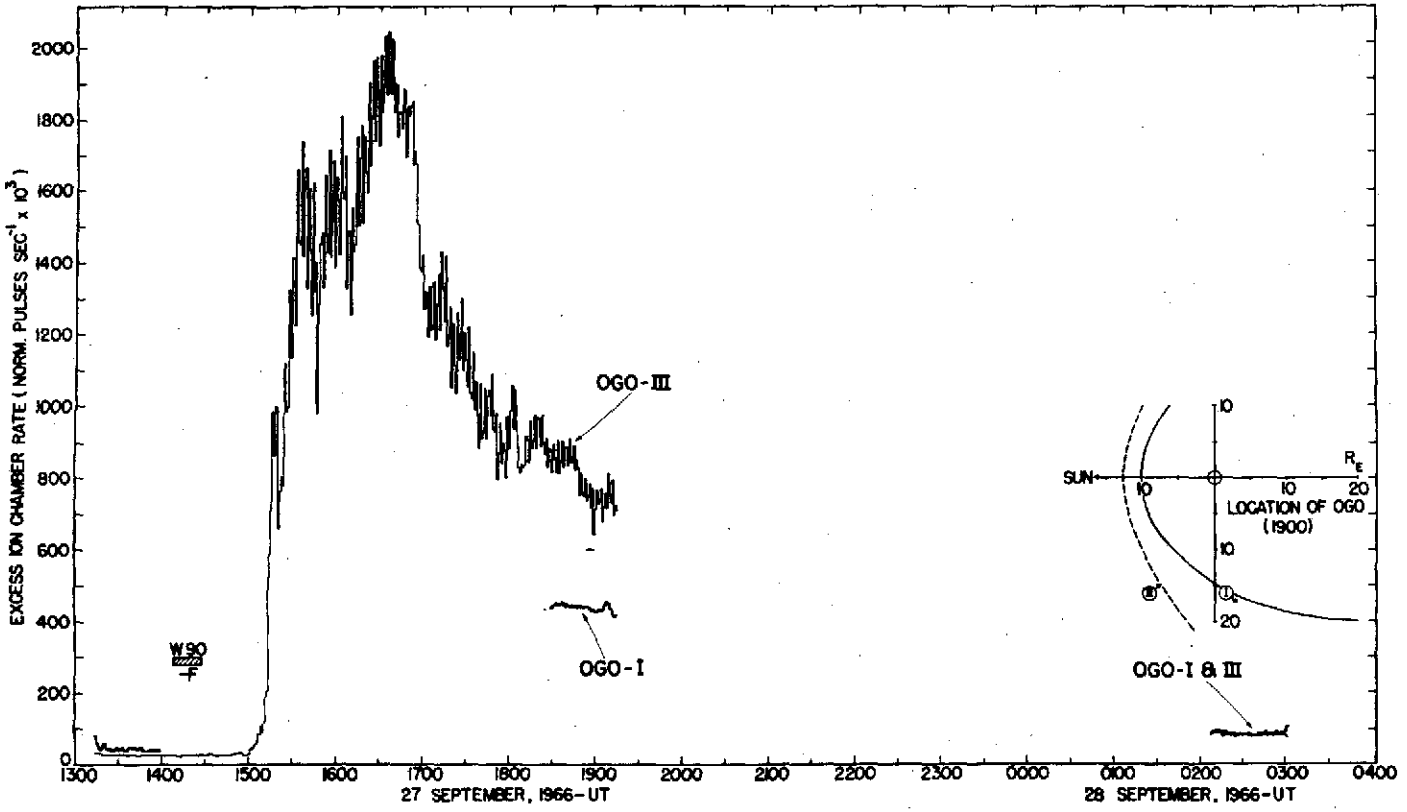

FIG. 14. ONE MINUTE AVERAGE RATES OF THE OGO-I AND OGO-III ION CHAMBERS FROM 1300 UT ON 27 SEPTEMBER TO 0400 UT ON 28 SEPTEMBER, 1966.

Notice that during the period 1830–1900 UT on 27 September the OGO-I rate is ≃50 per cent of the OGO-III rate although the two rates agree very well from 0210 to 0300 UT on 28 September.

The typical short transit time and fast intensity rise associated with a flare at this solar position is evident. Although no data was available from OGO-I during intensity maximum, a large difference of the order of 50 per cent was indicated during the early decay phase at about 1850 UT which essentially disappeared some seven hours later in the decay at ≃0230 UT on 28 September. An extreme anisotropy, visible even in the 1 min averages of the OGO-III ion chamber shown in Fig. 14, can be seen more clearly in Fig. 15 where 10 sec

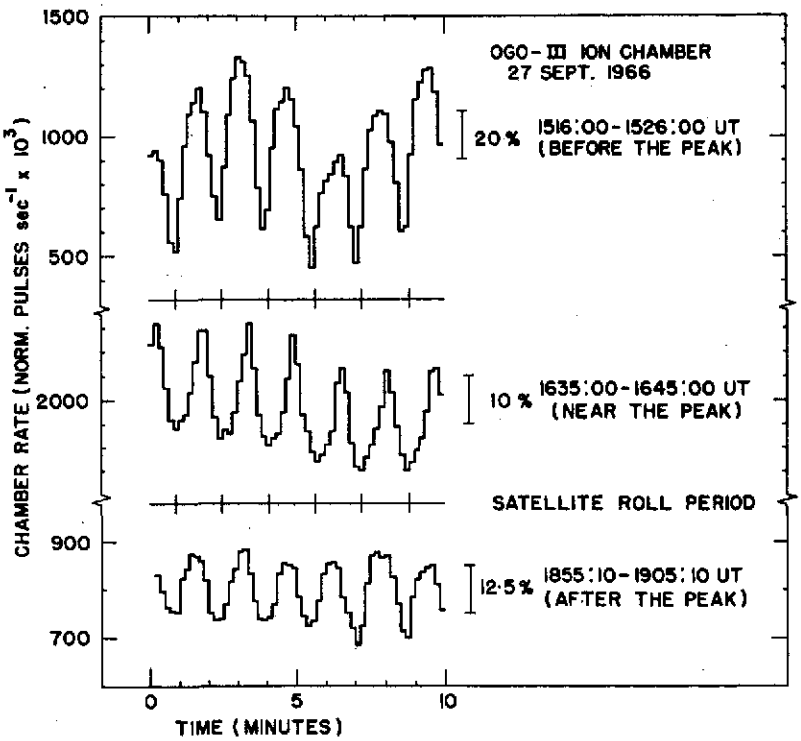

FIG. 15. TEN SECOND AVERAGE RATES OF THE OGO-III ION CHAMBER DURING THREE TIME INTERVALS ON 27 SEPTEMBER 1966 SHOWING THE LARGE ROLL MODULATION.

averages are plotted against time for three chosen time intervals during the event. During the time interval when simultaneous OGO-I and OGO-III data are available, the roll modulation is ~18 per cent for OGO-III. This high degree of anisotropy apparently enhances the 'screening' effect of the magnetosphere observed on OGO-I inside the magnetosphere and accounts for the large ionization intensity difference observed during this part of the decay phase. As in the case of earlier events the two ion chambers agree later in the event (0200–0300 UT, 28 September) presumably because the solar particle event has decayed considerably so that the particle intensity is very nearly isotropic, with any small existing anisotropies being of a non-field aligned nature.

An event quite distinct from the class of events described above was observed on 7 May 1967. A preliminary description of this event is presented here. Figure 16 shows the OGO-I and OGO-III observations for this event. During the period of interest (0300–1230 UT)

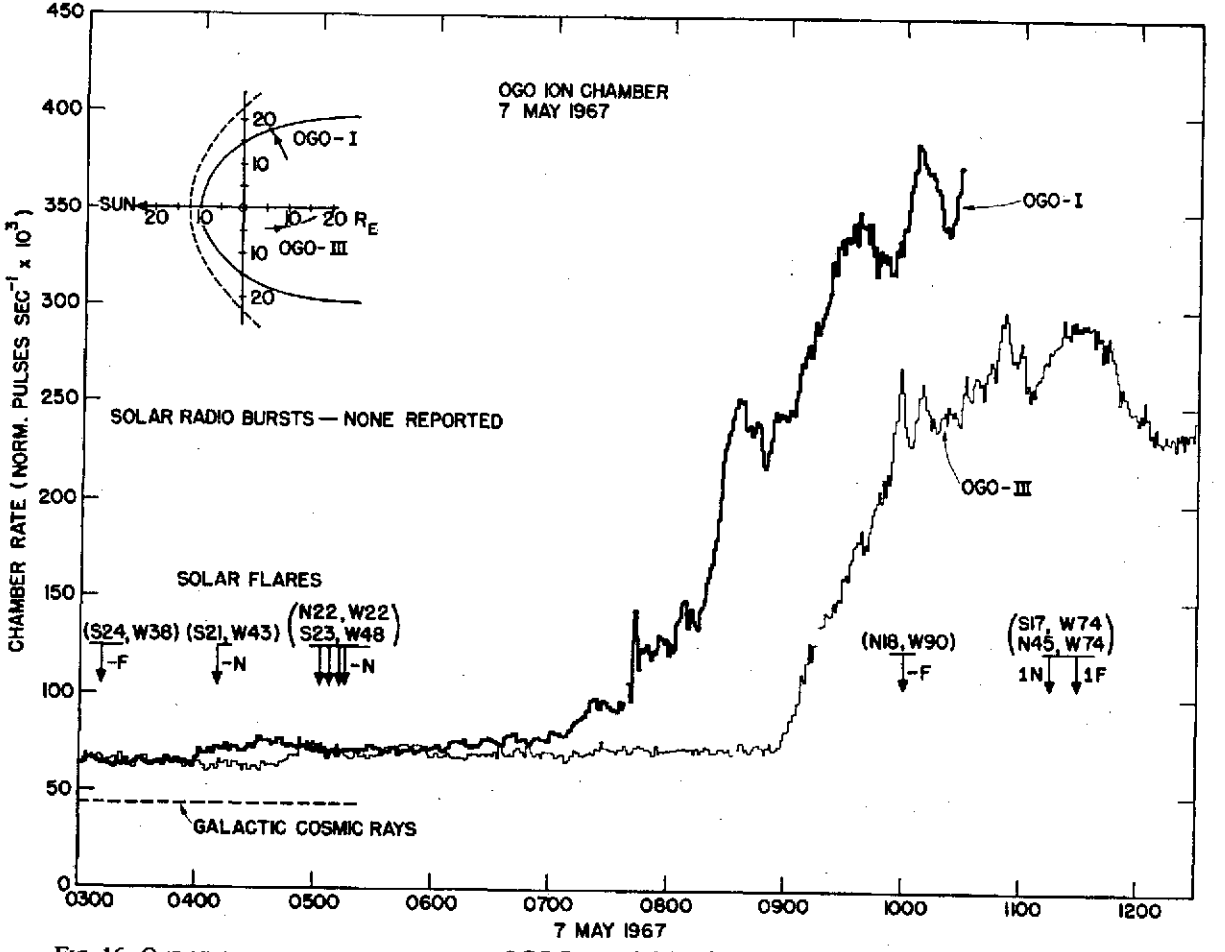

FIG. 16. ONE MINUTE AVERAGE RATES OF THE OGO-I AND OGO-III ION CHAMBERS DURING THE SOLAR COSMIC RAY EVENT ON 7 MAY 1967.

Notice the time lag of ≃110 min in the onset of the event, as seen by OGO-III and the similarity in the rise time of the events as seen by OGO-I and OGO-III.

OGO-I was presumably inside the magnetosphere and was moving towards the magnetopause. On the other hand OGO-III was close to the midnight portion of the magnetospheric tail and was moving away from the Earth. It may be noted that no measurements in free space are available for this event. At 0300 both OGO-I and OGO-III ion chambers were measuring a small excess above the galactic cosmic ray background ($\simeq$45 NPPS $\times$ 10^3) due to an earlier solar particle event. At this time the absolute rates of both OGO-I and OGO-III chambers were nearly equal ($\simeq$65 NPPS $\times$ 10^3). OGO-I observed a small increase beginning at $\simeq$0400 UT. After this increase the OGO-I rates remained approximately constant at a new level $\simeq$75 NPPS $\times$ 10^3 until about 0710 UT at which time a second larger increase started. The OGO-I data were apparently terminated before the peak intensity was reached. The highest pulsing rate recorded before the termination of the data was 385 NPPS $\times$ 10^3 at 1006 UT. The first increase was observed by OGO-III at $\simeq$0450 UT, nearly 50 min later than OGO-I. The second larger increase was seen by OGO-III at $\simeq$0900 UT, about 110 min later than OGO-I. However, in spite of this large delay, the rate of increase in intensity at the OGO-III location was at least as large as at OGO-I. Moreover, some of the structure in the time-intensity curve for OGO-I can also be seen in the OGO-III intensity curve. The peak pulsing rate observed by OGO-III was $\simeq$295 NPPS $\times$ 10^3 which is $\simeq$25 per cent less than the highest rate observed by OGO-I.

A careful time-check between the two satellites was made by cross-checking the spacecraft clocks against real time references, by the known occurrence time of an X-ray burst on the same record and by the time of observation of known radiation belt phenomena. The timing error is probably no more than 1 sec.

The solar flare responsible for the large increase on 7 May 1967 has not been identified. The relatively rapid increase in intensity indicates a west limb flare. Several flares were in fact observed on the western half of the solar disc, but they are probably of too small importance (−F, −N) to be able to produce energetic particles. The most important fact established by the 7 May 1967 event is that there are times when solar protons with energy >12 MeV have virtually no access to parts of the magnetospheric tail.

DISCUSSION

The observations presented above can be summarized as follows:

(1) For solar protons with energy >12 MeV the intensity inside the magnetosphere is less than or equal to the intensity outside the magnetosphere.

(2) The difference in the two intensities, when present, is larger during the initial phase of the solar particle increase and appears to be greater when the solar particles in the interplanetary space are more anisotropic.

(3) The time fluctuations in the particle intensity outside the magnetosphere are more or less reproduced inside the magnetosphere but with considerably smaller amplitudes.

(4) The onset of a solar particle event as seen in the tail of the magnetosphere in one case occurred $\simeq$110 min later then the onset of the same event observed near the 'dawn region of the magnetosphere without giving rise to appreciable differences in the rise-time of the event at the two locations.

(5) Spatial differences in the intensity of protons >12 MeV exist inside the magnetosphere. During the maximum phase of the 7 May 1967 event the intensity in the midnight region of the magnetospheric tail was $\simeq$25 per cent less than the intensity in the dawn region. Other events, being studied at present, indicate similar spatial differences in other regions of the magnetosphere.

The solar protons to which the OGO ion chamber is most sensitive have energies $\simeq$15 MeV. In the interplanetary magnetic field of $\sim$5 gamma these protons have cyclotron radii of $\simeq$18 Earth radii, a distance comparable to the radius of the magnetosphere. On crossing the magnetopause these particles encounter a field of $\simeq$50 gamma. Hence, inside the magnetopause the cyclotron radii of these particles are $\simeq$2 Earth radii which is much smaller than the dimensions of the magnetosphere. Spatial gradients in the intensity of these particles inside the magnetosphere are therefore possible whenever a large anisotropy exists in the particle intensity outside the magnetosphere. This effect may be enhanced by the spatial irregularities or fluctuations in the magnetospheric field. Thus in the outer magnetosphere, although no conventional geomagnetic cutoff may be operative for protons with energy $>$12 MeV, significant spatial variations in the intensity of these particles can exist. A comparison of the 'averaged' intensities inside and outside the magnetosphere may thus show a reduced intensity inside the magnetosphere as if the latter acted as a 'screen' for these particles. A deceleration mechanism could, in principle, cause such a reduction in particle intensity, but it is not clear how such a mechanism can be effective under the magnetospheric conditions.

Both the fast rise time and the large time delay ($\simeq$110 min) observed in the onset of the 7 May 1967 solar particle event at the OGO-III location can be explained if the $\simeq$15 MeV solar protons could not arrive at the OGO-III position in the magnetospheric tail unless they entered the tail region about 1 A.U. away from the Earth and then moved up the tail towards the OGO-III position. It is also possible that the observed effect was produced by the motion of the OGO-III spacecraft from a region of complete screening of the solar particles to a region of partial screening.

SUMMARY AND CONCLUSION

From simultaneous observations with identical ion chambers it has been shown that a magnetospheric 'screening' effect on the $\simeq$15 MeV solar protons is probably a common observation if one is capable of distinguishing absolute intensity differences as low as 10 per cent between two instruments. Less common perhaps are the cases of a large effect such as the 50 per cent difference observed on 27 September 1967 and the $\simeq$110 min delay in the onset observed on 7 May 1967. It is notable that these differences generally exist only during onset and early decay of an event when particles are streaming in an anisotropic fashion presumably along ordered interplanetary magnetic field lines at the Archimedes spiral angle. Later during the decay phase the 'screening' effect seems to disappear although a small degree of anisotropy may still exist. It is concluded that a combination of the high degree of anisotropy in the solar particle beam and the structure of the magnetic field in the outer magnetosphere produces the observed 'screening' effect of the magnetosphere.

Acknowledgements—Thanks are due to Dr. E. J. Smith, Jet Propulsion Laboratory, California Institute of Technology, Pasadena, California and Dr. R. E. Holzer, University of California, Los Angeles for supplying the unpublished OGO-III magnetospheric boundary crossings during September 1966. Thanks are also due to Mr. Karl Pfitzer for many helpful discussions and for a major effort on the OGO data reduction. We appreciate the helpful discussions with Professor J. A. Van Allen, University of Iowa regarding the 7 May 1967 solar particle event. This work was supported by the National Aeronautics and Space Administration under Contract No. NAS 5-2071.

REFERENCES

ARNOLDY, R. L., S. R. KANE and J. R. WINCKLER (1967). A study of energetic solar X-rays. *Solar Physics* 2, 171–178.

ARNOLDY, R. L., S. R. KANE and J. R. WINCKLER (1967). The observation of 10–50 Kev solar flare X-rays by the OGO satellites and their correlation with solar radio and energetic particle emission (Presented

at the *Int. Astr. Un. Symp.* No. 35 on *The Structure and Development of Solar Active Regions*, September 4–8, 1967, Budapest, Hungary), University of Minnesota Tech. Rep. No. CR-197.

ARNOLDY, R. L. S. R. KANE and J. R. WINCKLER (1968). Energetic solar flare X-rays observed by satellite and their correlation with solar radio and energetic particle emission. *Astrophys. J.* **151,** 711–736.

BOSTROM, C. O., D. J. WILLIAMS and J. F. ARENS, February (1968a). *Solar Geophysical Data*, Descriptive Text, pp. 61–66.

BOSTROM, C. O., D. J. WILLIAMS and J. F. ARENS, February (1968b). *Solar Geophysical Data*, No. 282, pp. 156–165.

FAN, C. Y., M. PICK, R. PYLE, J. A. SIMPSON and D. R. SMITH (1968). Protons associated with centers of solar activity and their propagation in interplanetary magnetic field regions corotating with the Sun. *J. geophys. Res.* **73,** 1555–1582.

FREIER, P. S. and W. R. WEBBER (1963). Exponential rigidity spectrums for solar flare cosmic rays. *J. geophys. Res.* **68,** 1605–1629.

GALL, R., J. JIMENEZ and L. CAMACHO (1968). Arrival of low-energy cosmic rays via the magnetospheric tail. *J. geophys. Res.* **73,** 1593–1605.

KANE, S. R., September (1967). Application of an integrating type ionization chamber to measurements of radiation in space, Ph.D. Thesis, School of Physics and Astronomy, University of Minnesota; available as University of Minnesota Techn. Rep. No. CR-106.

KANE, S. R., K. A. PFITZER and J. R. WINCKLER, September (1966). The construction, calibration and operation of the University of Minnesota experiments for OGO-I and OGO-III, University of Minnesota Tech. Rep. No. CR-87.

KEATH, E. P., R. P. BUKATA and K. G. MCCRACKEN, March (1968). Pioneer 8 observations of solar induced cosmic radiation in the energy range 3–70 MeV/nucleon. *Midwest Cosmic Ray Conf.*, Iowa City, Iowa.

PAULIKAS, G. A., J. B. BLAKE and S. C. FREDEN (1968). Low-energy solar-cosmic-ray cutoffs: diurnal variation and pitch angle distributions. *J. geophys. Res.* **73,** 87–95.

REID, G. C. and H. H. SAUER (1967). The influence of the geomagnetic tail on low-energy cosmic-ray cutoffs, *J. geophys. Res.* **72,** 197–208.

WEBBER, W. R. (1966). An evaluation of solar-cosmic-ray events during solar minimum. Space Sciences Group, Space Division, The Boeing Company, Seattle, Washington, Tech. Rep. No. D2-84274-1.

2200,9/25/68 - 0000,9/27/68 1

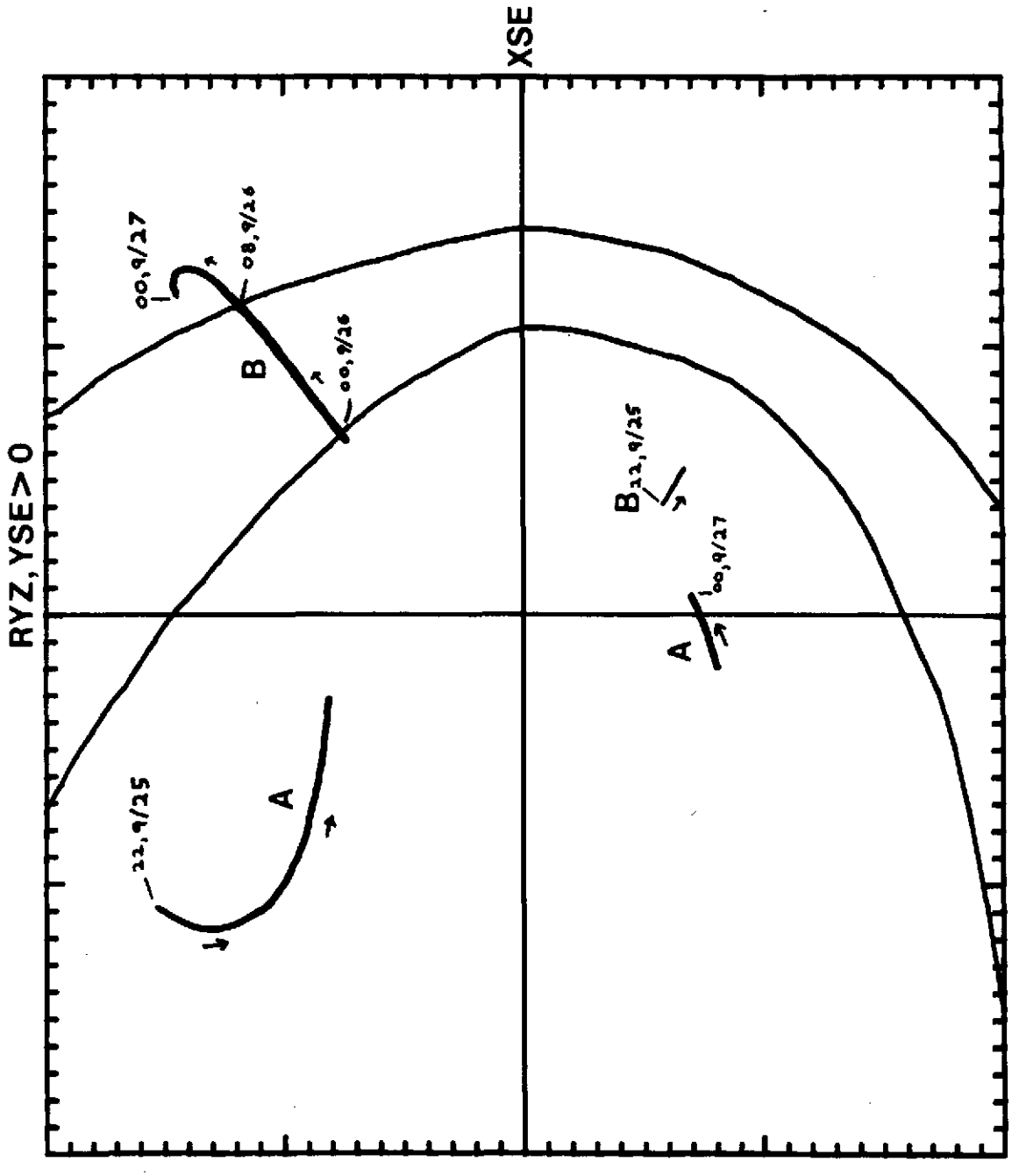

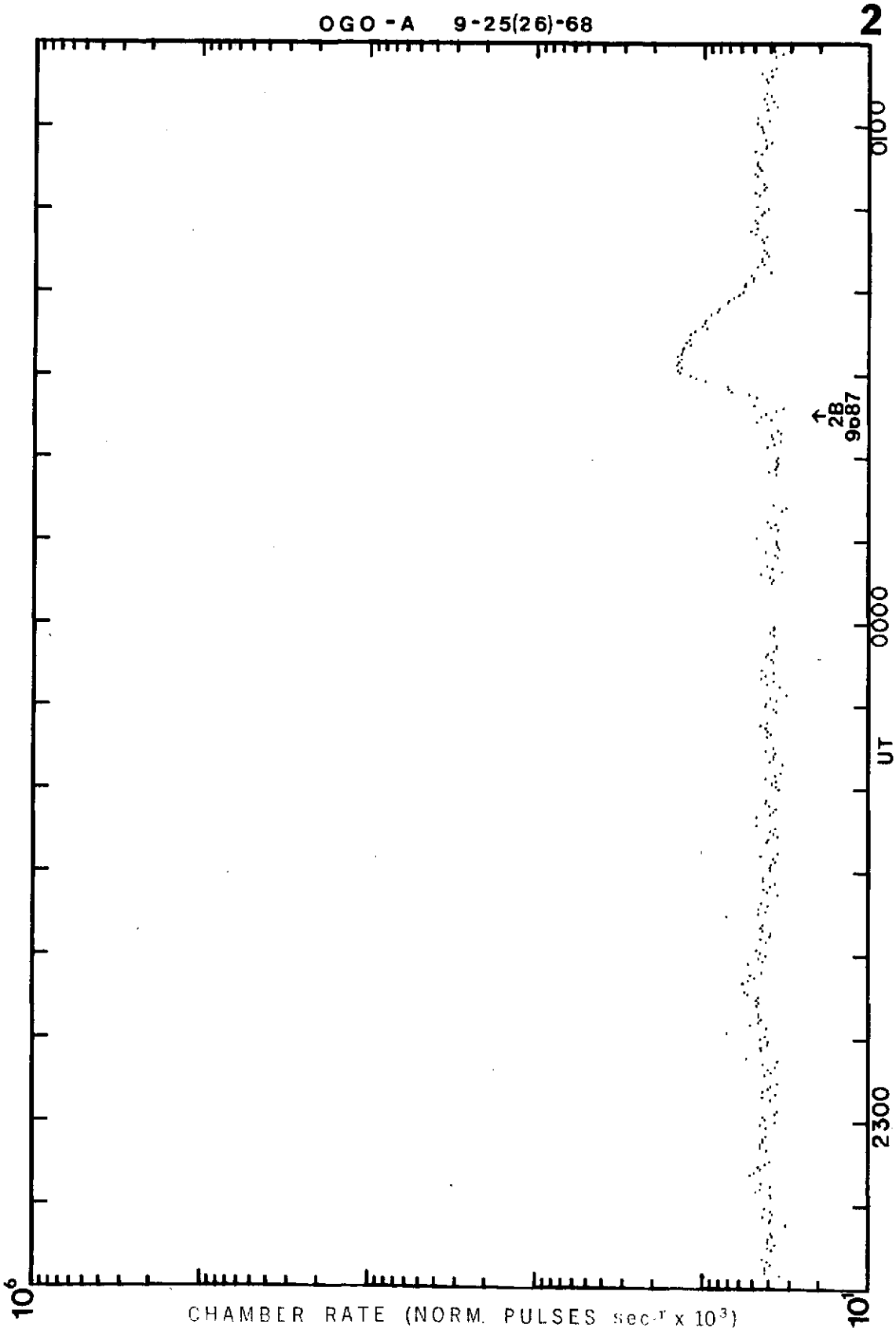
OGO - A 9-25(26)-68
2
0100
0000
2300
UT
28
9087
10^6
10^1
CHAMBER RATE (NORM. PULSES sec^{-1} x 10^3)

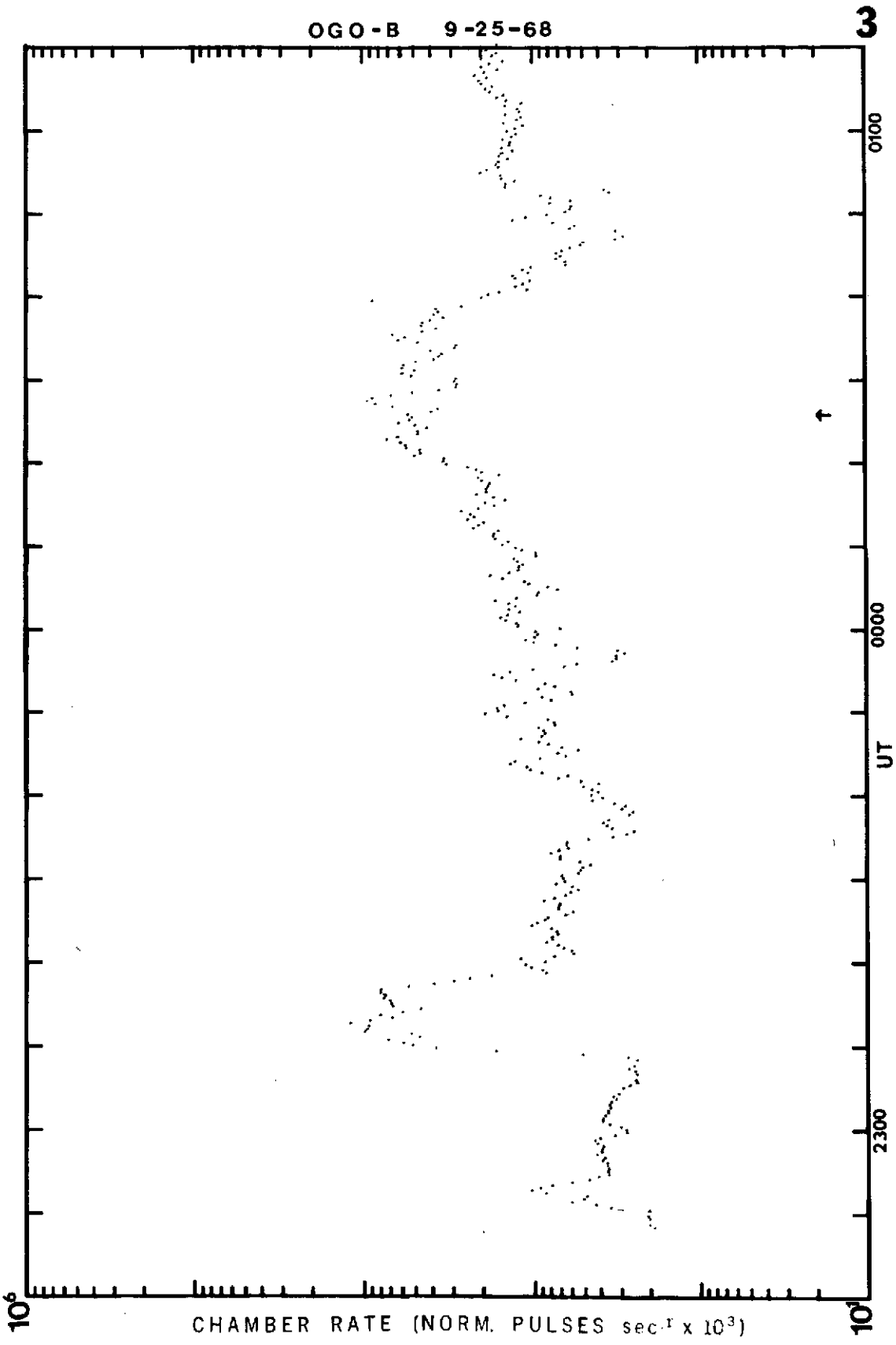
OGO-B 9-25-68
3
0100
0000
2300
UT
CHAMBER RATE (NORM. PULSES sec⁻¹ x 10³)
10⁶
10¹

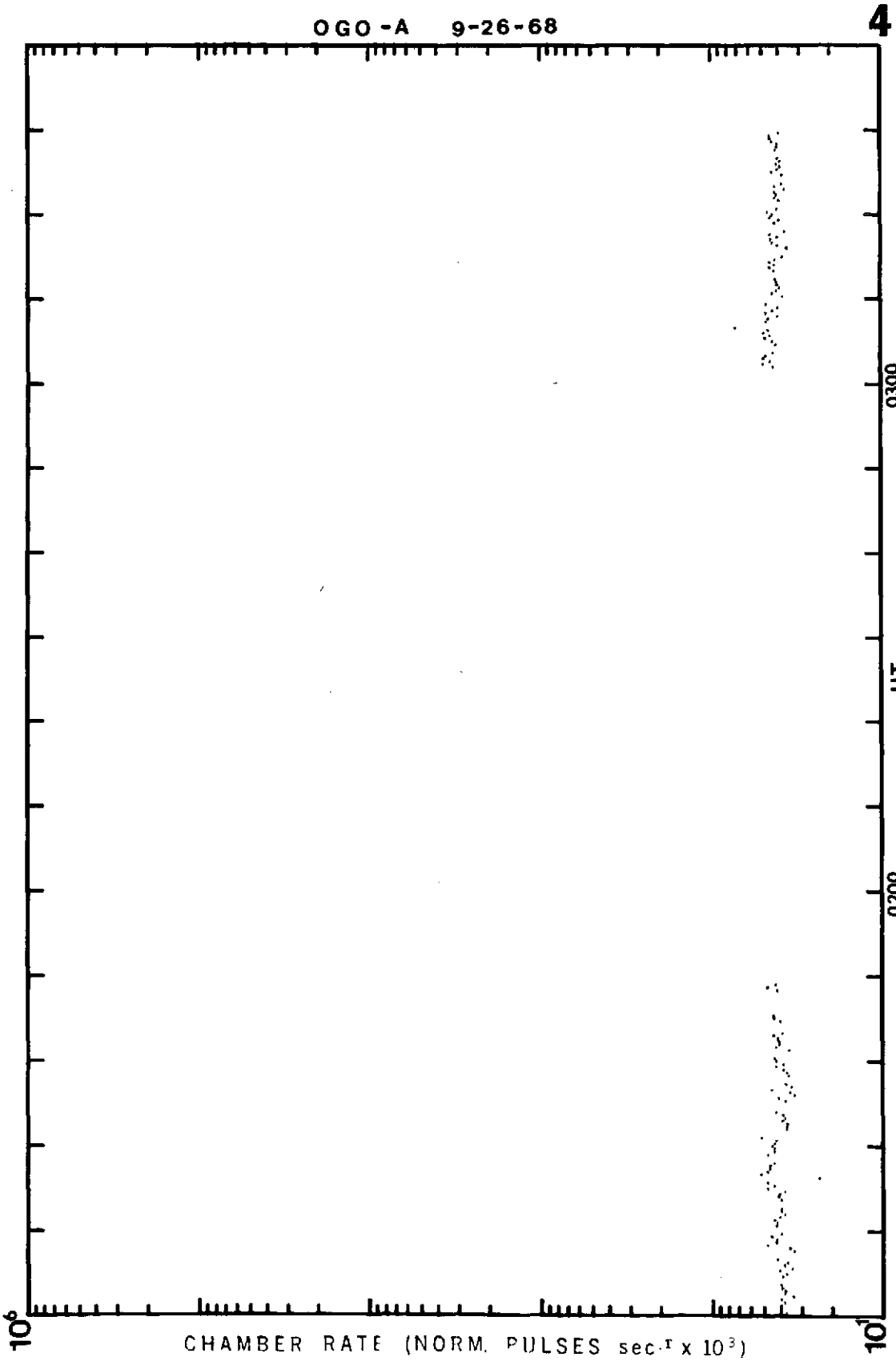
OGO-A 9-26-68
4
0300
UT
0200
10^0
CHAMBER RATE (NORM. PULSES $sec^{-1} \times 10^3$)
10^1

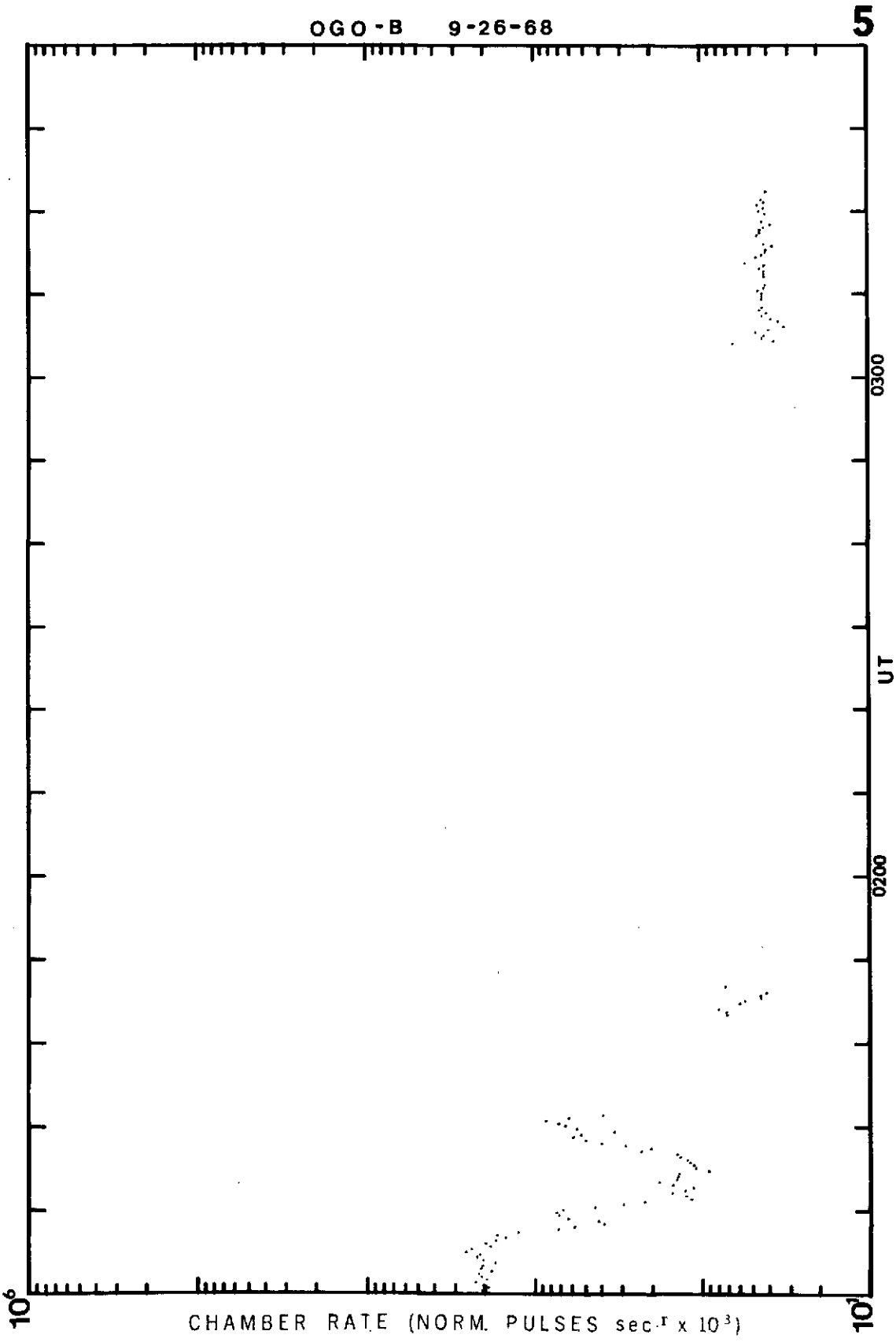
OGO-B 9-26-68
5
0300
UT
0200
10^6
CHAMBER RATE (NORM. PULSES $sec^{-1} \times 10^3$)
10^1

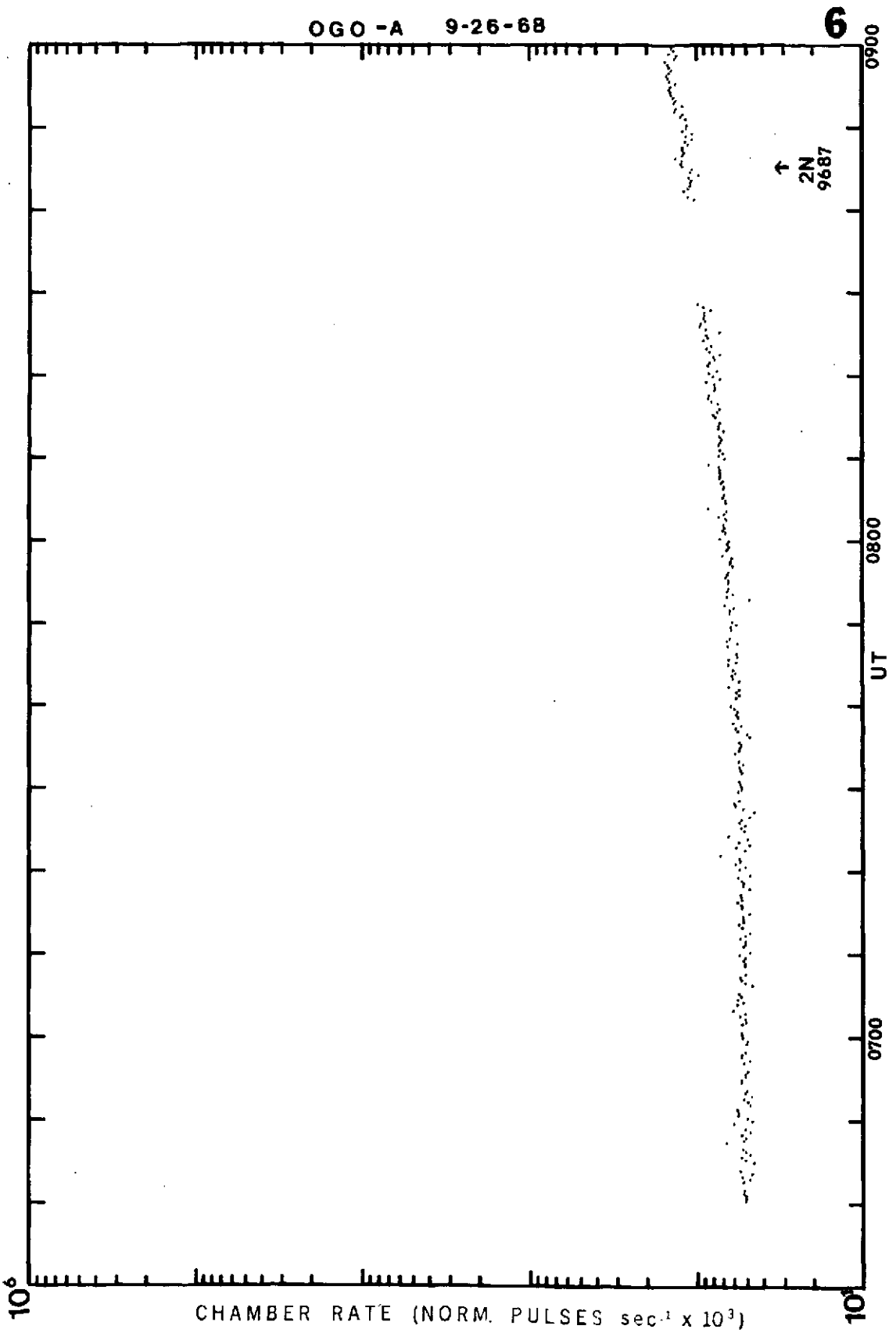
OGO -A 9-26-68
6
0900
0800
0700
UT
2N
9687
10^6
10^5
CHAMBER RATE (NORM. PULSES $sec^{-1} \times 10^3$)

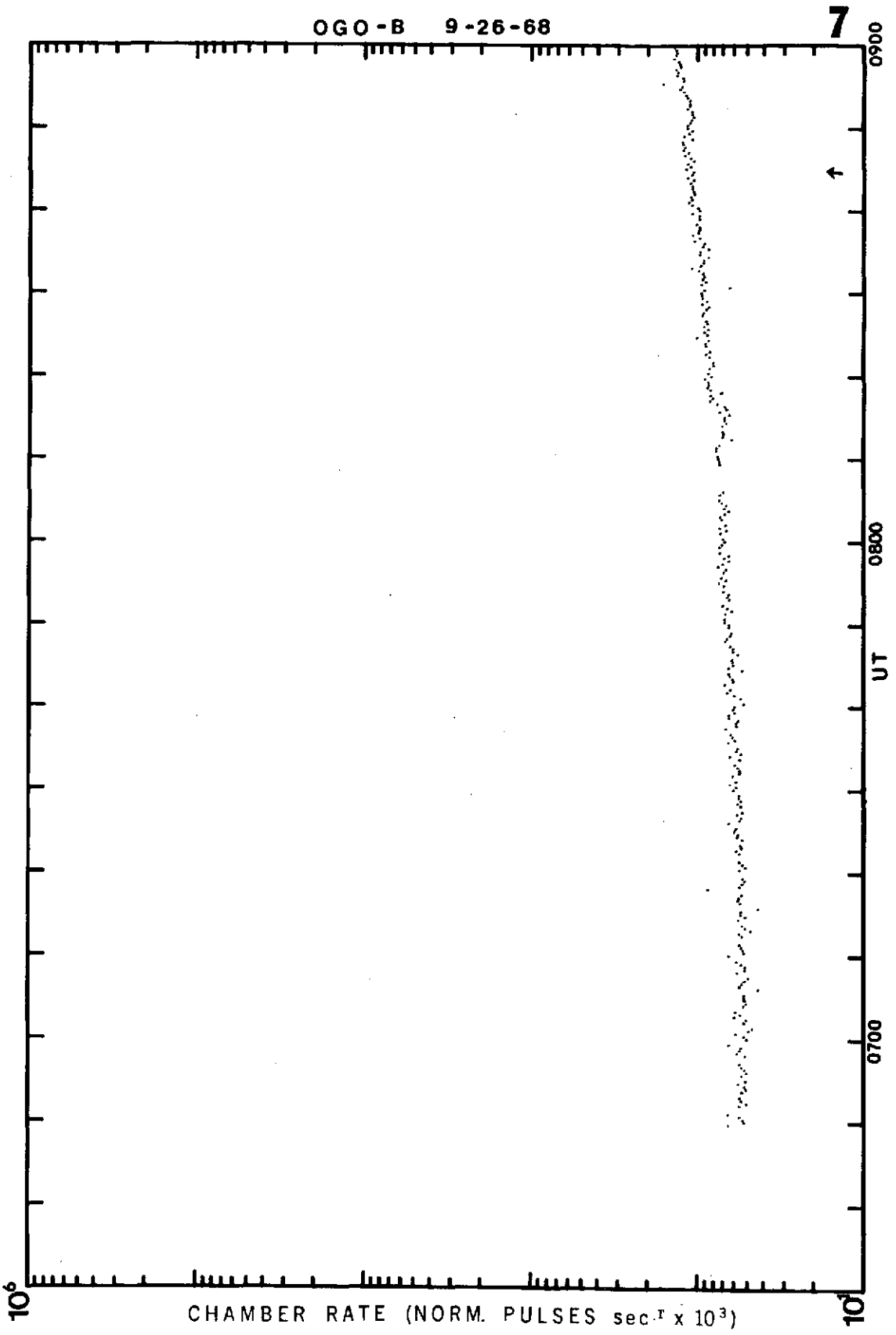
OGO-B 9-26-68
7
0900
0800
0700
UT
10^6
10^4
CHAMBER RATE (NORM. PULSES sec^{-1} x 10^3)

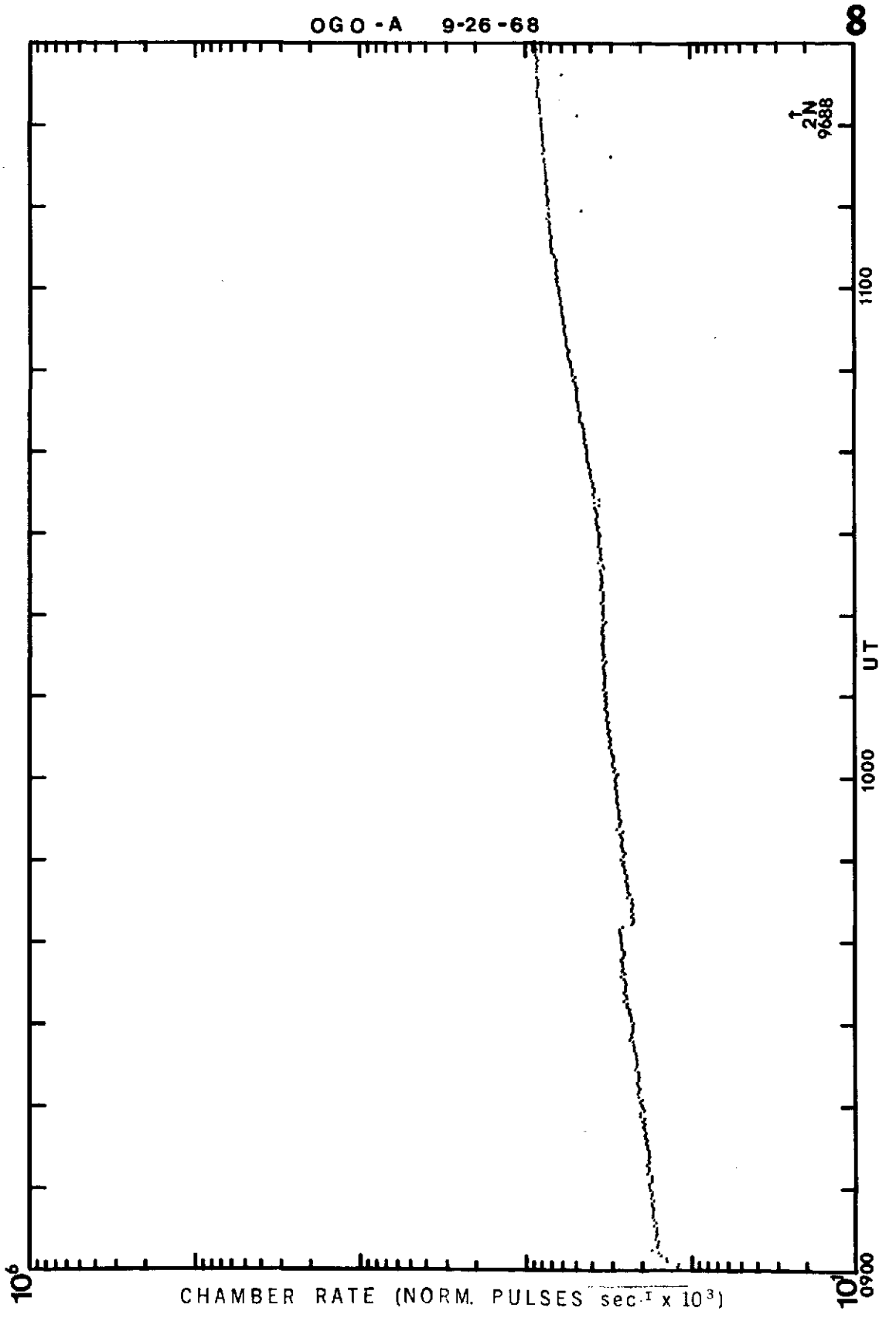
OGO - A 9-26-68
8
2N 9688
1100
1000
0900
UT
10^6
10^7
CHAMBER RATE (NORM. PULSES $sec^{-1} \times 10^3$)

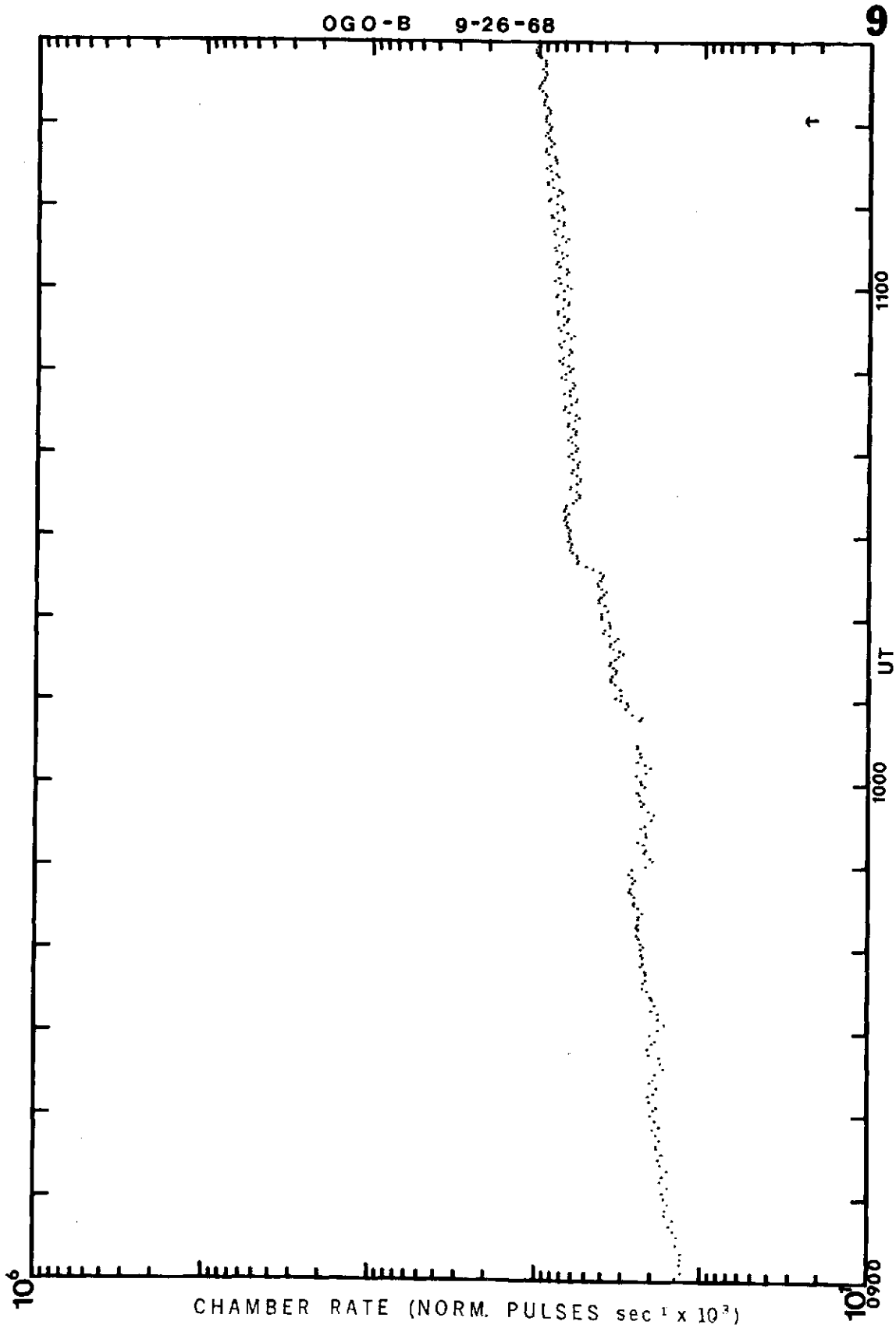
OGO-B 9-26-68
9
1100
1000
0900
UT
10^6
10^4
CHAMBER RATE (NORM. PULSES sec^{-1} x 10^3)

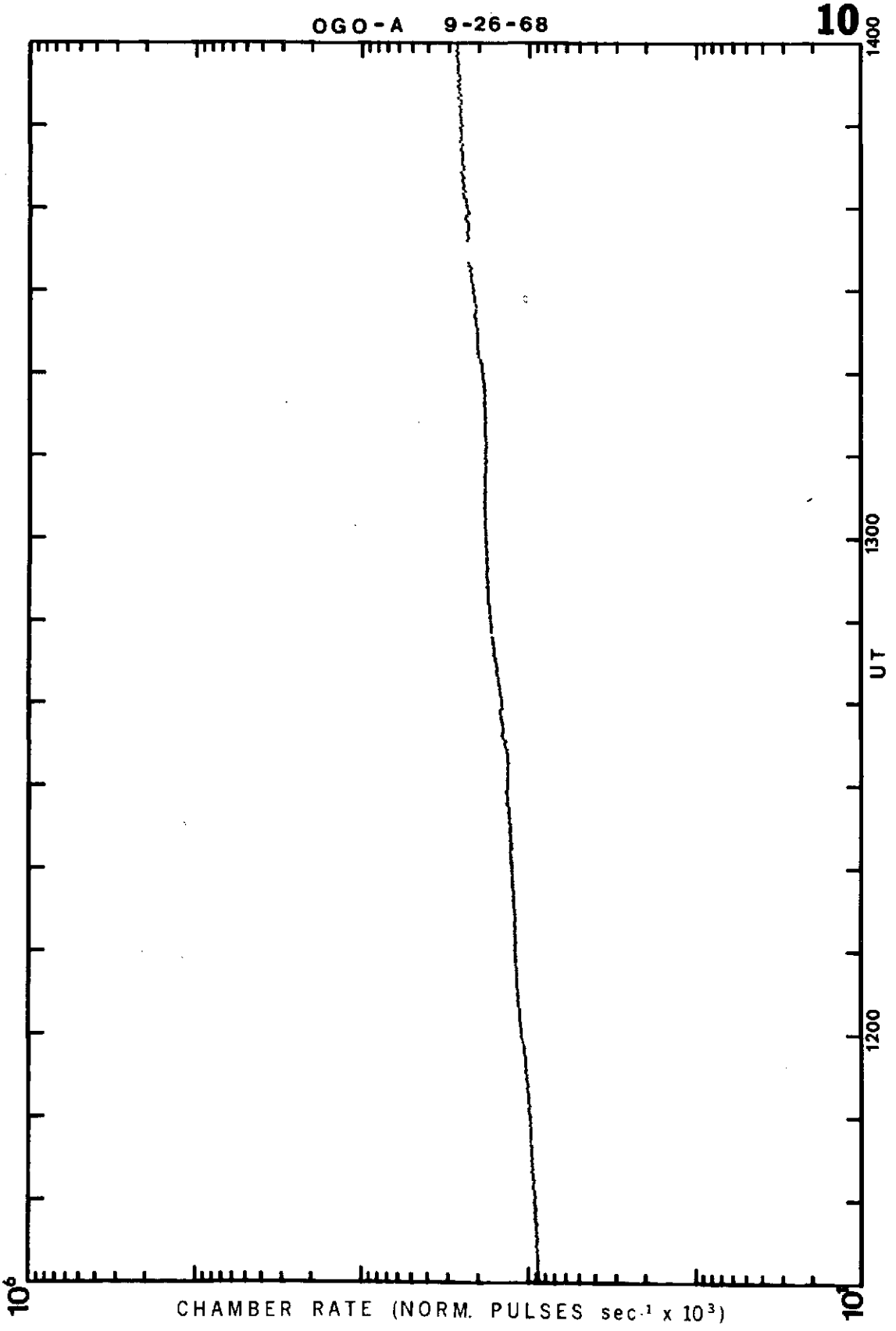
OGO-A 9-26-68
10
1400
1300
1200
UT
10^6
10^5
CHAMBER RATE (NORM. PULSES sec^{-1} x 10^3)

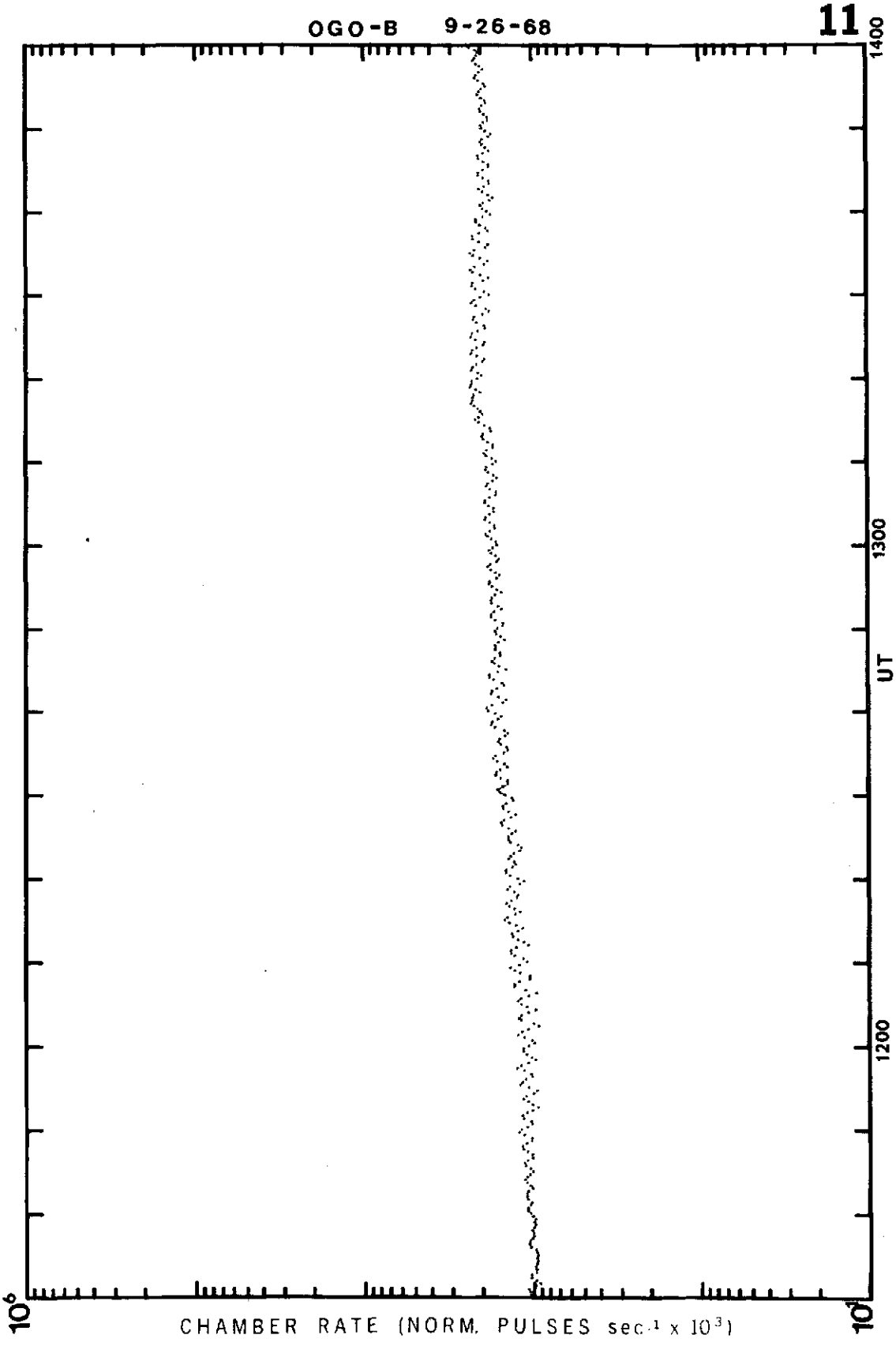
OGO-B 9-26-68
11
1400
1300
1200
UT
10^6
10^1
CHAMBER RATE (NORM. PULSES sec^{-1} x 10^3)

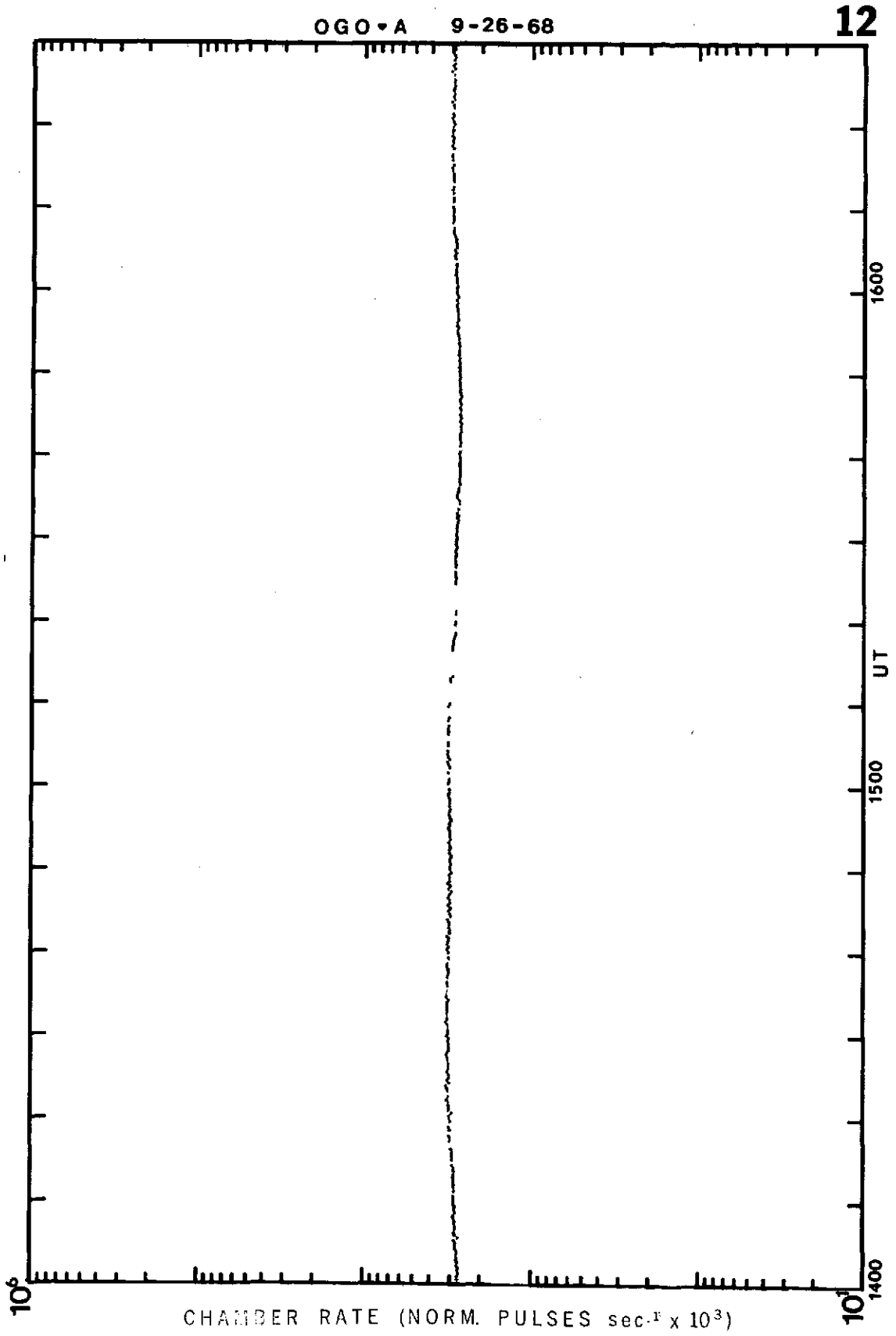
OGO • A 9-26-68
12
1600
1500
1400
UT
10^6
10^5
CHAMBER RATE (NORM. PULSES $sec^{-1} \times 10^3$)

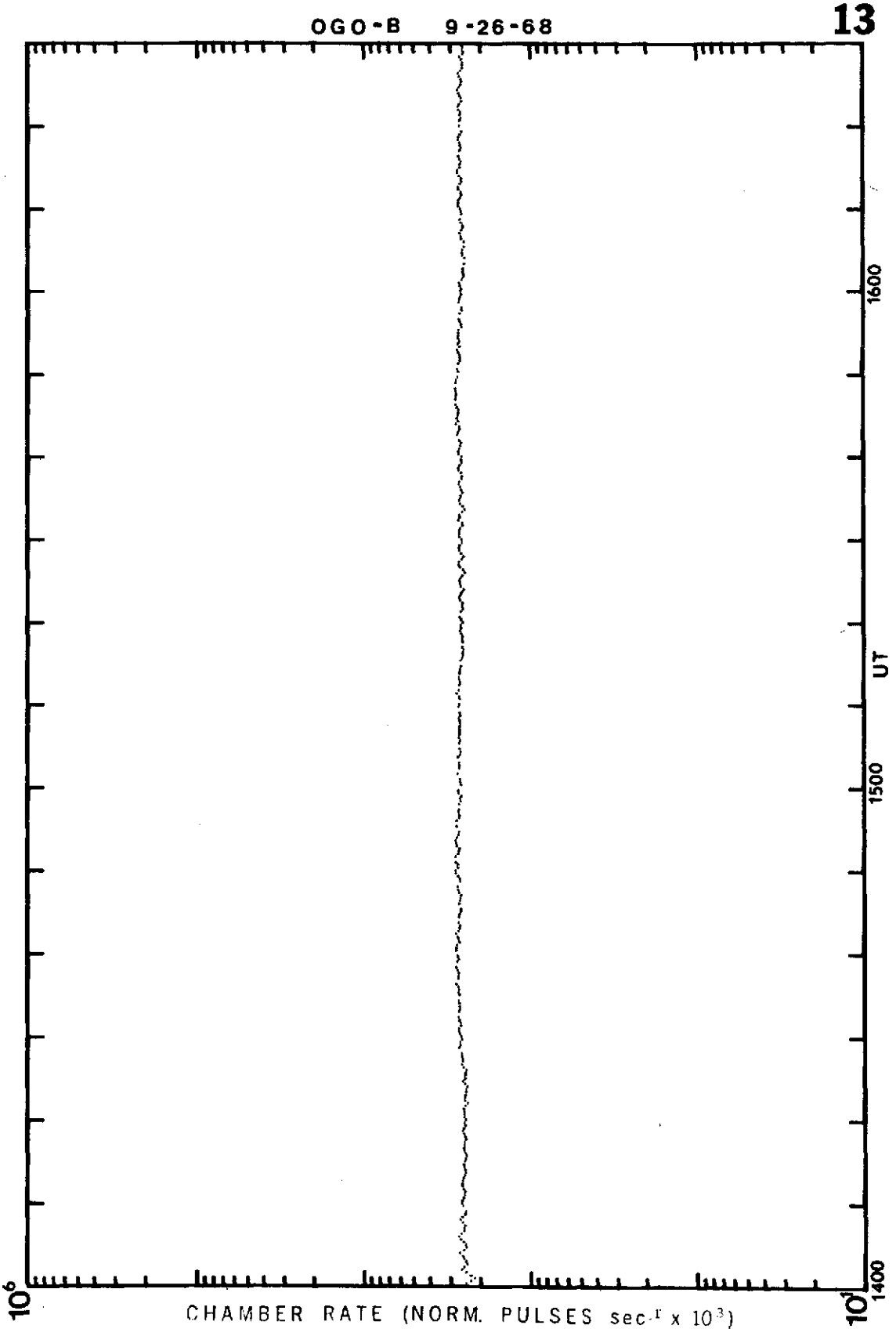
OGO-B 9-26-68
1600
1500
1400
UT
10^6
10^1
CHAMBER RATE (NORM. PULSES $sec^{-1} \times 10^3$)

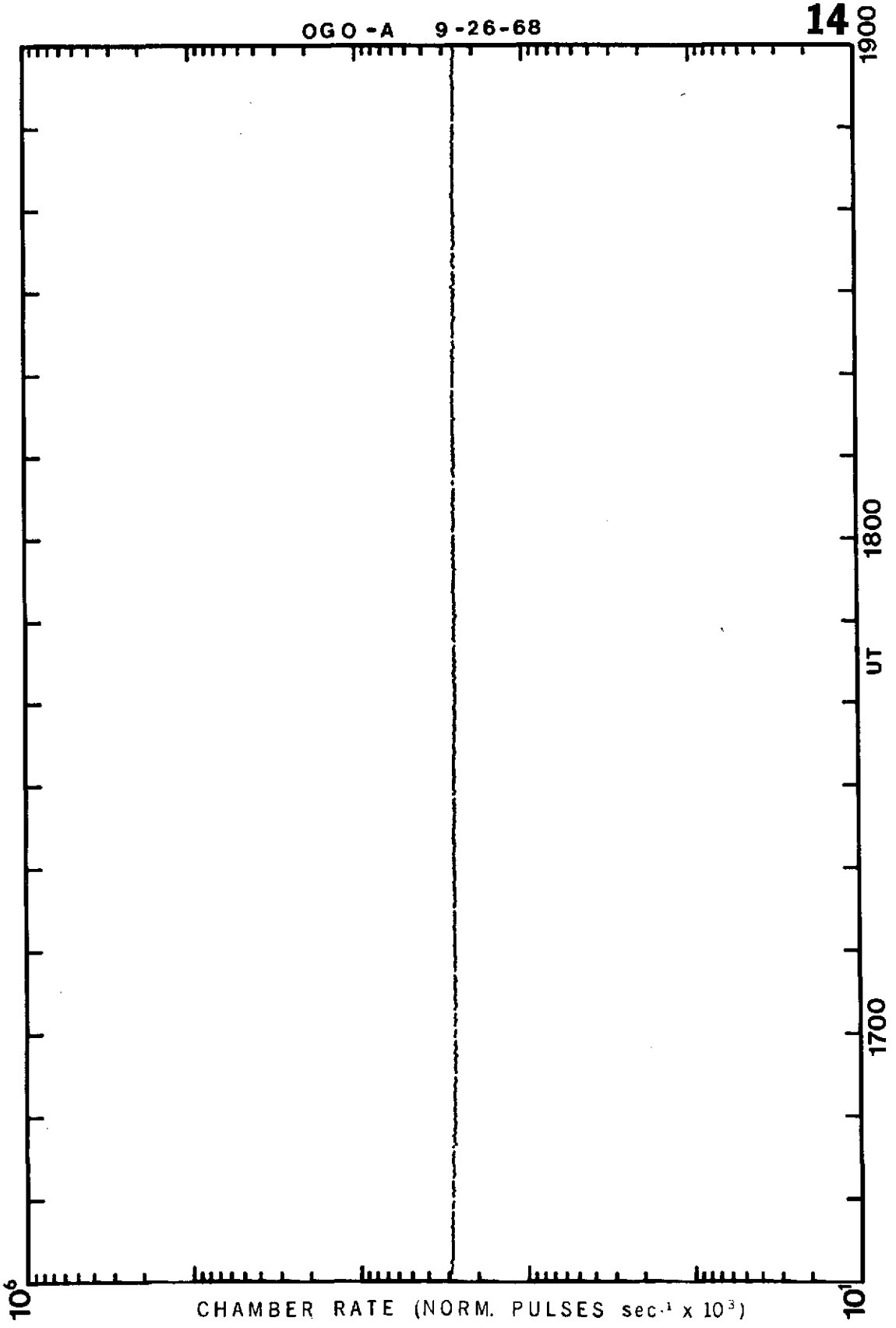
OGO-A 9-26-68
14
1900
1800
UT
1700
10^6
10^1
CHAMBER RATE (NORM. PULSES $sec^{-1} \times 10^3$)

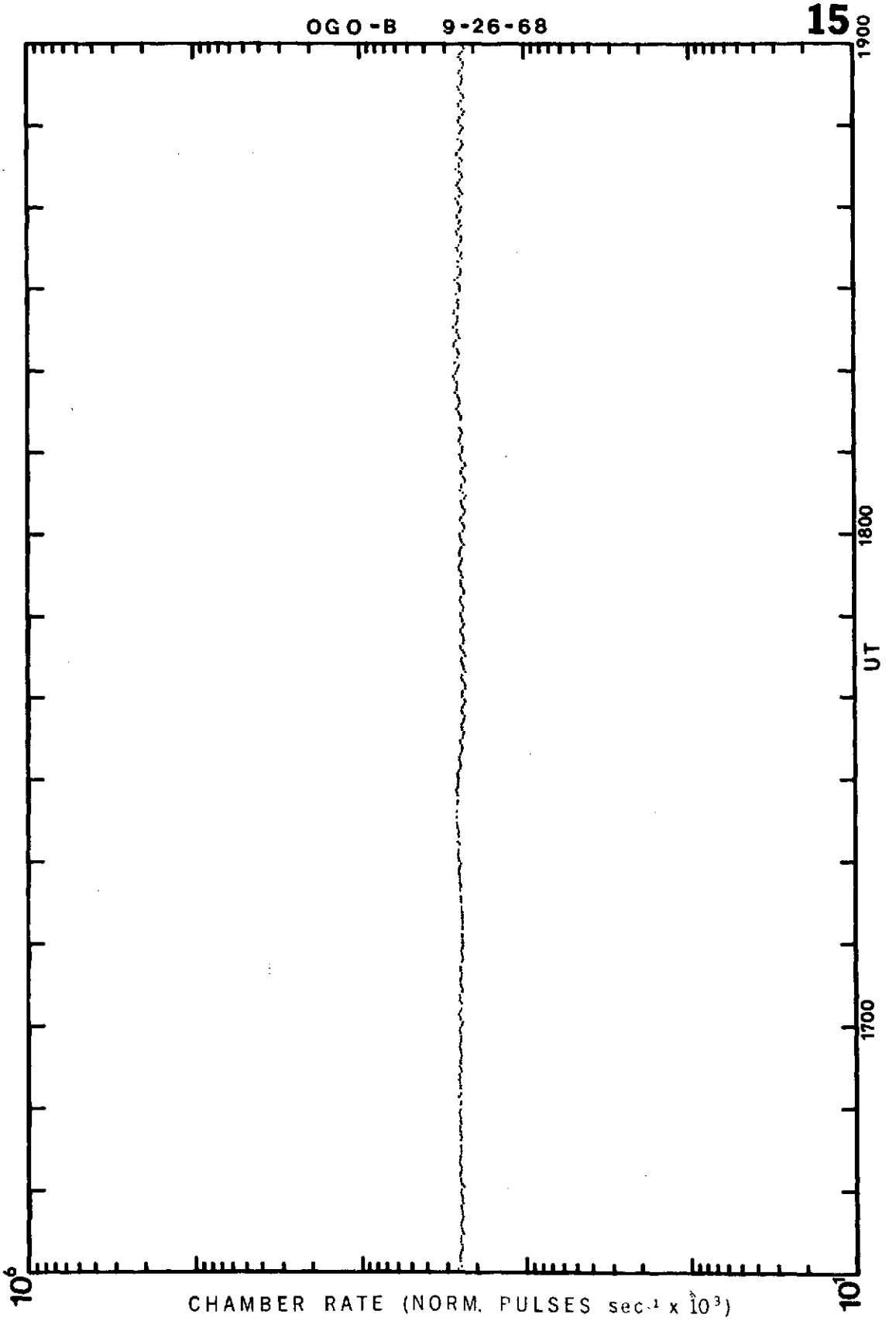
OGO-B 9-26-68
15
1900
1800
1700
UT
10^6
10^1
CHAMBER RATE (NORM. PULSES sec^{-1} x 10^3)

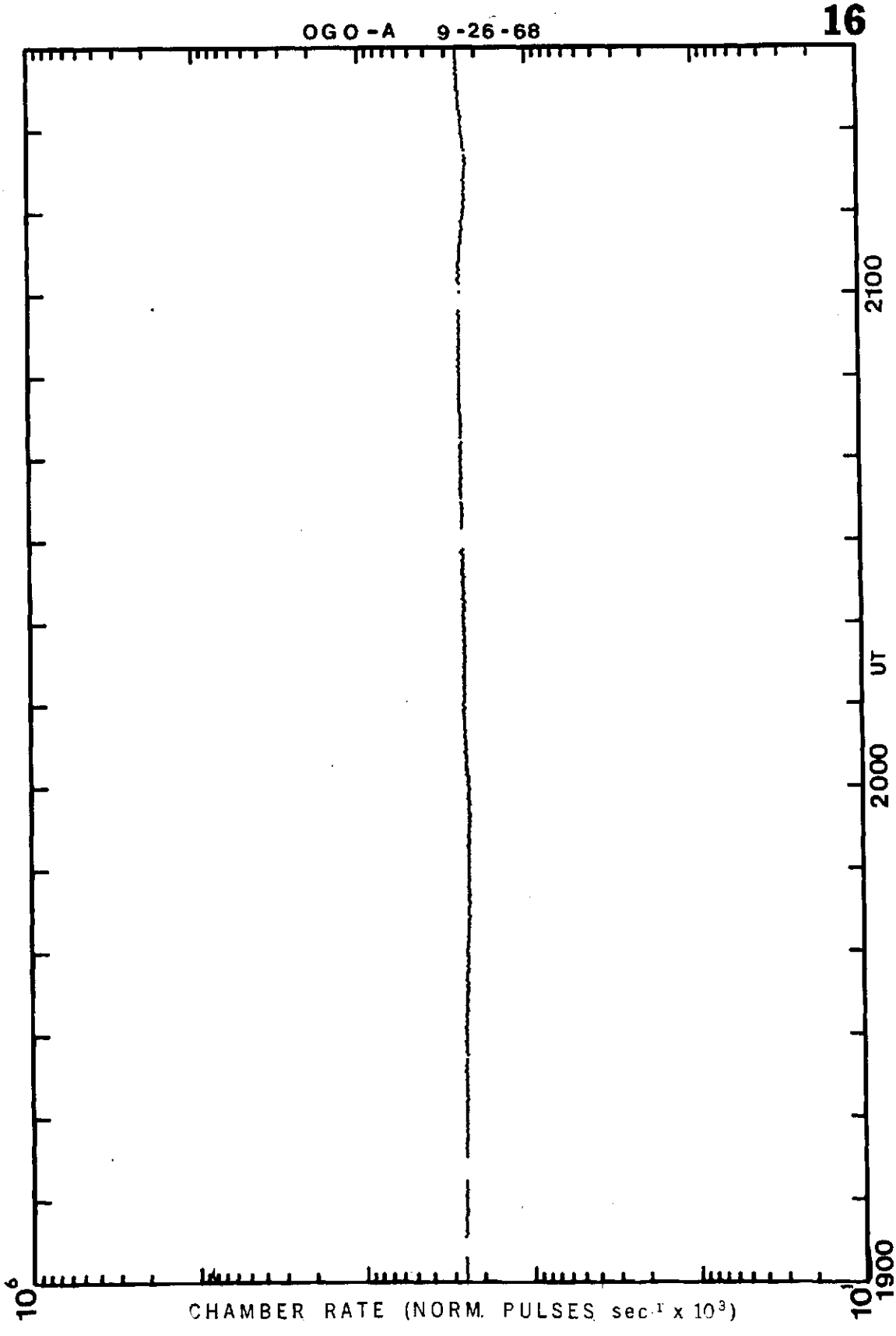
OGO-A 9-26-68
2100
2000
1900
UT
10^6
10^1
CHAMBER RATE (NORM. PULSES $sec^{-1} \times 10^3$)

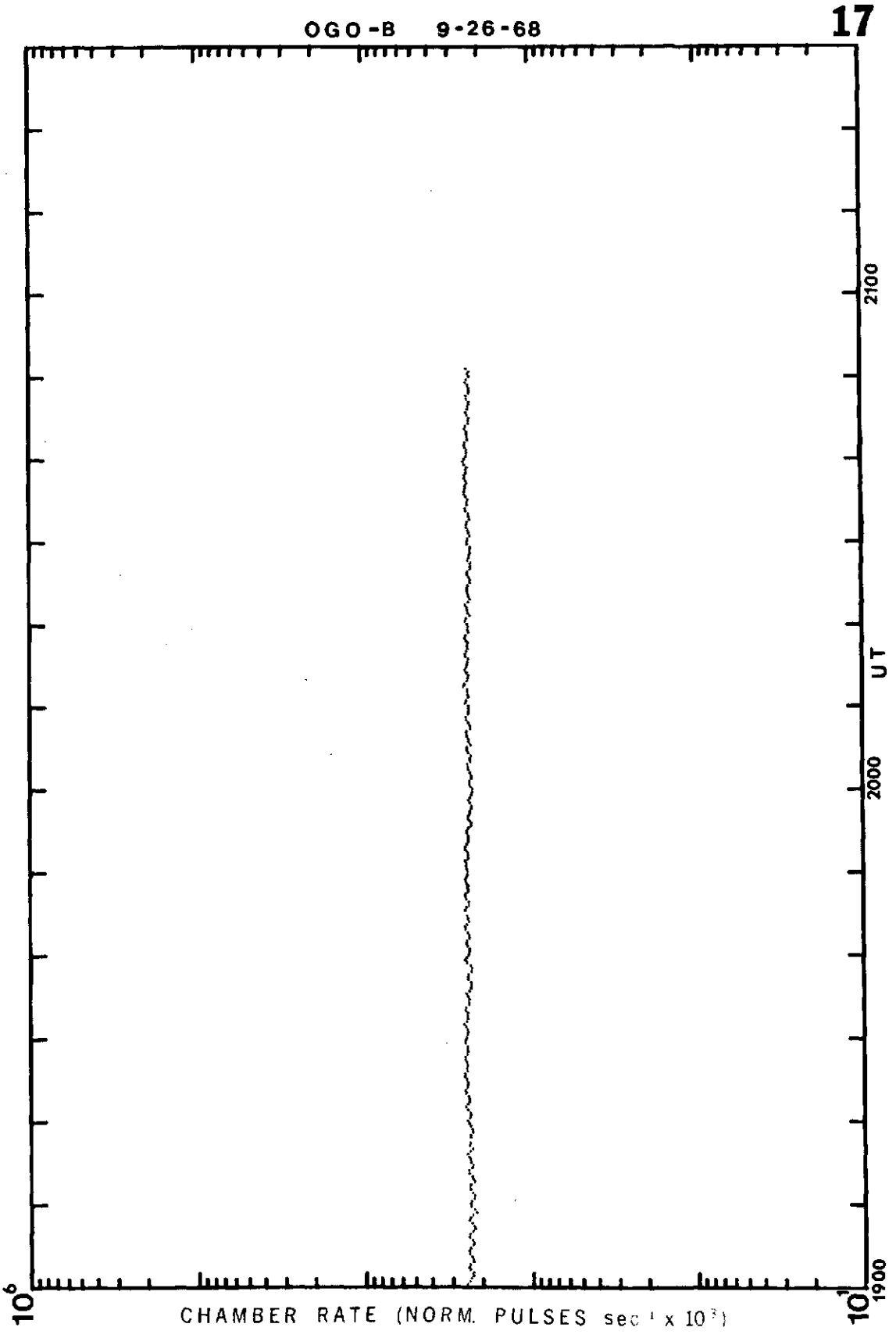
OGO-B 9-26-68
17
2100
2000
1900
UT
10^6
10^1
CHAMBER RATE (NORM. PULSES sec^{-1} x 10^3)

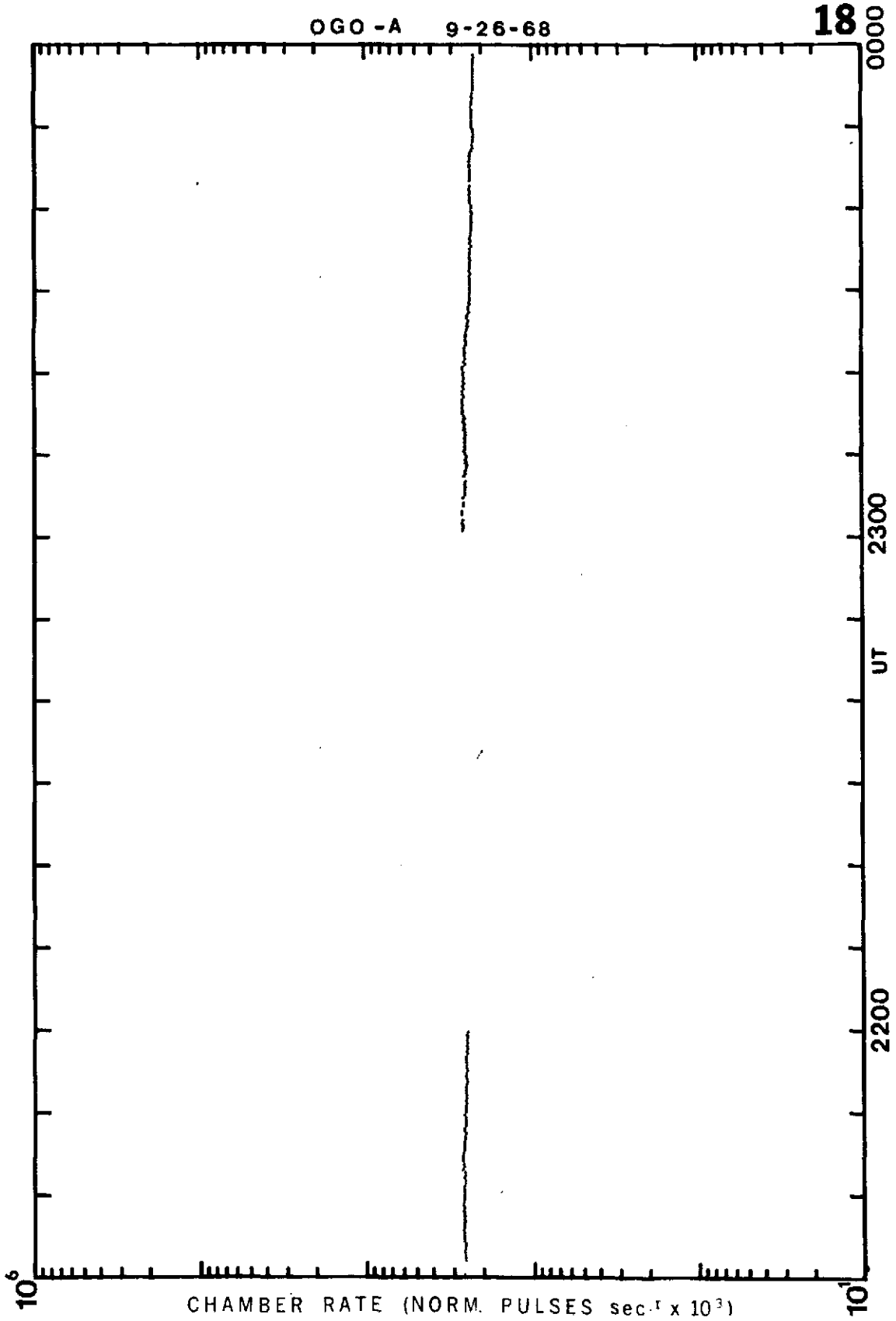
OGO -A 9-26-68
18
0000
2300
UT
2200
10^6
10^1
CHAMBER RATE (NORM. PULSES $sec^{-1} \times 10^3$)

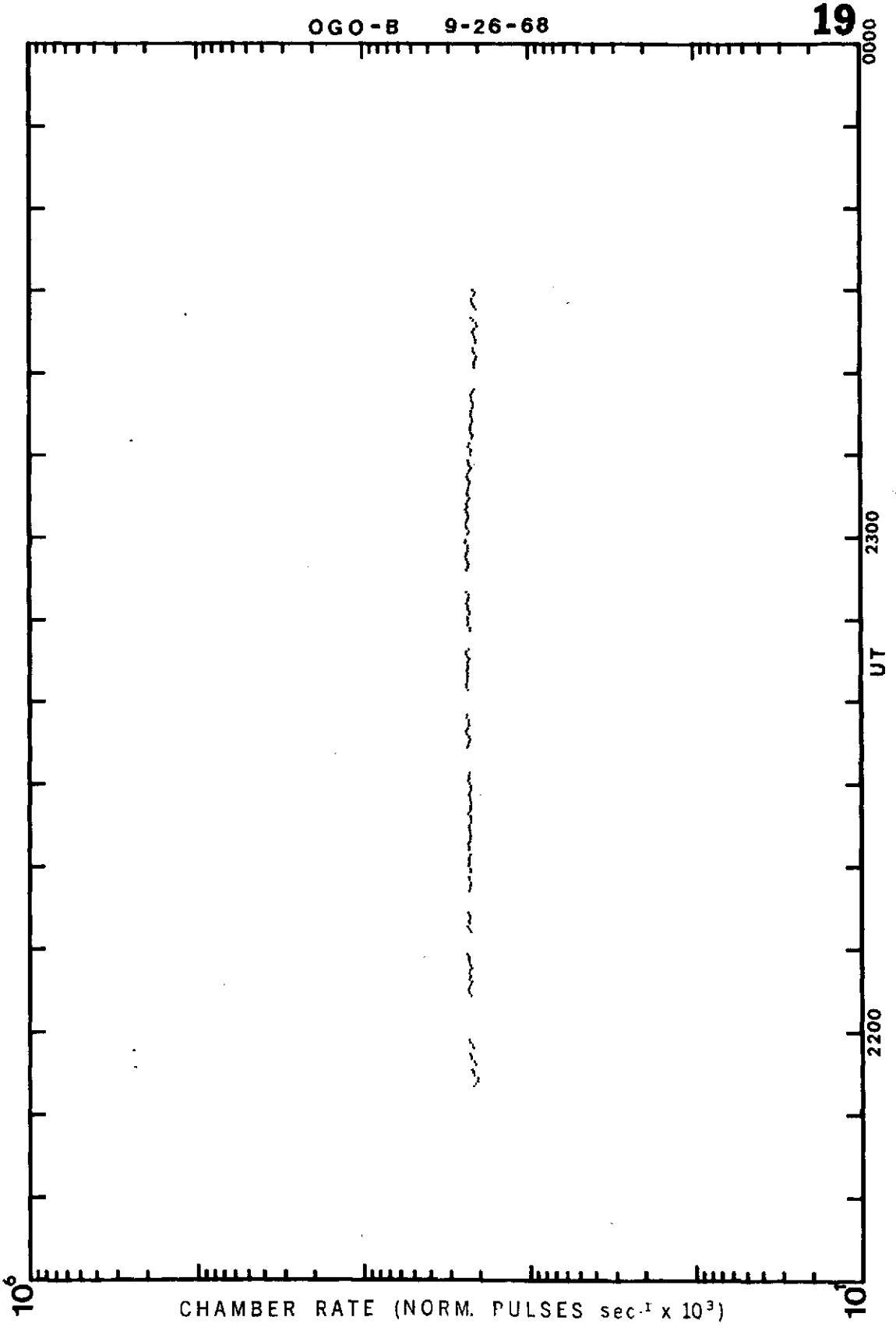
OGO-B 9-26-68
19
0000
2300
2200
UT
10^6
10^5
CHAMBER RATE (NORM. PULSES $sec^{-1} \times 10^3$)

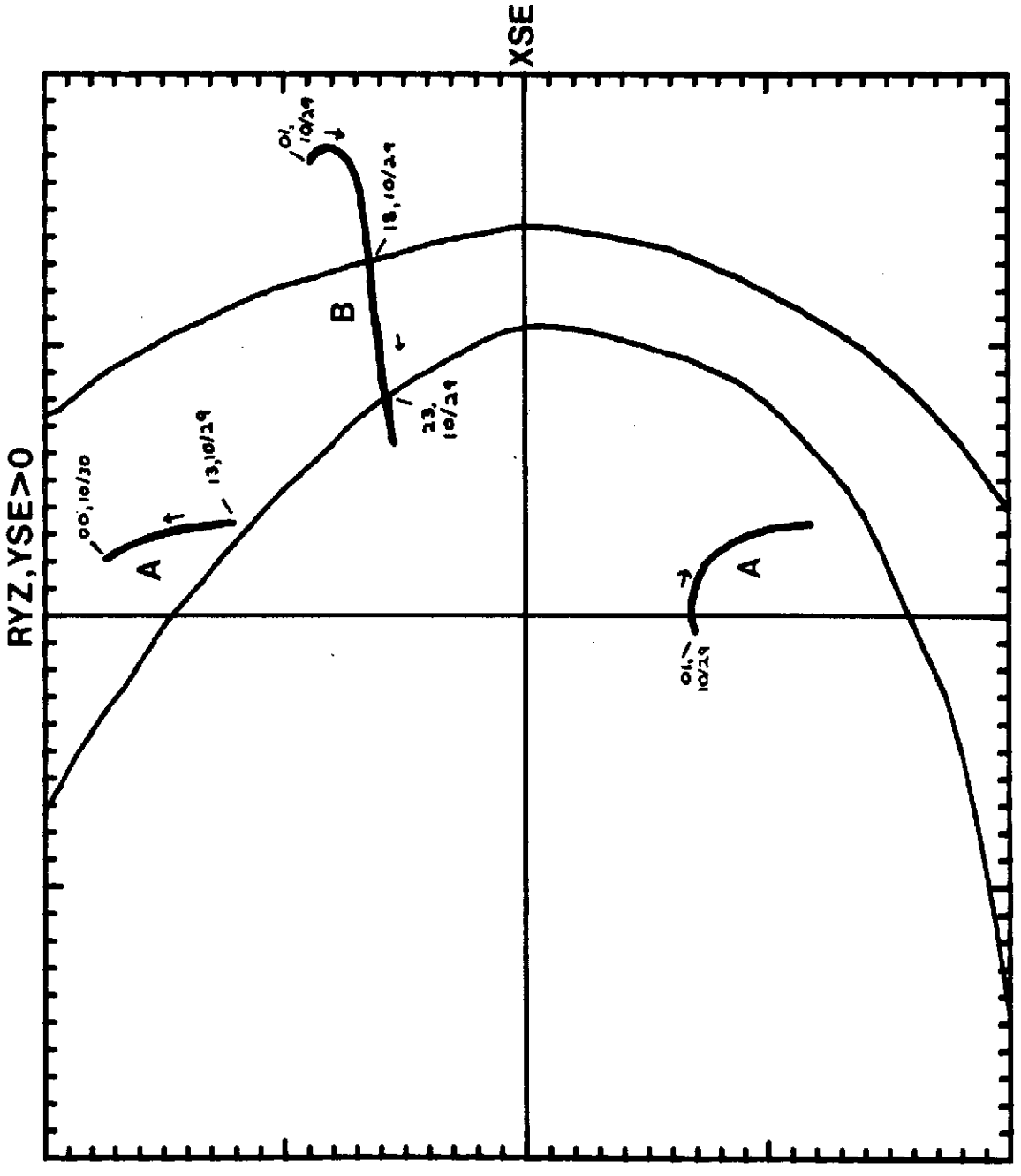
XSE
RYZ,YSE>0
01, 10/29
18, 10/29
B
23, 10/29
00, 10/30
13, 10/29
A
A
01, 10/29

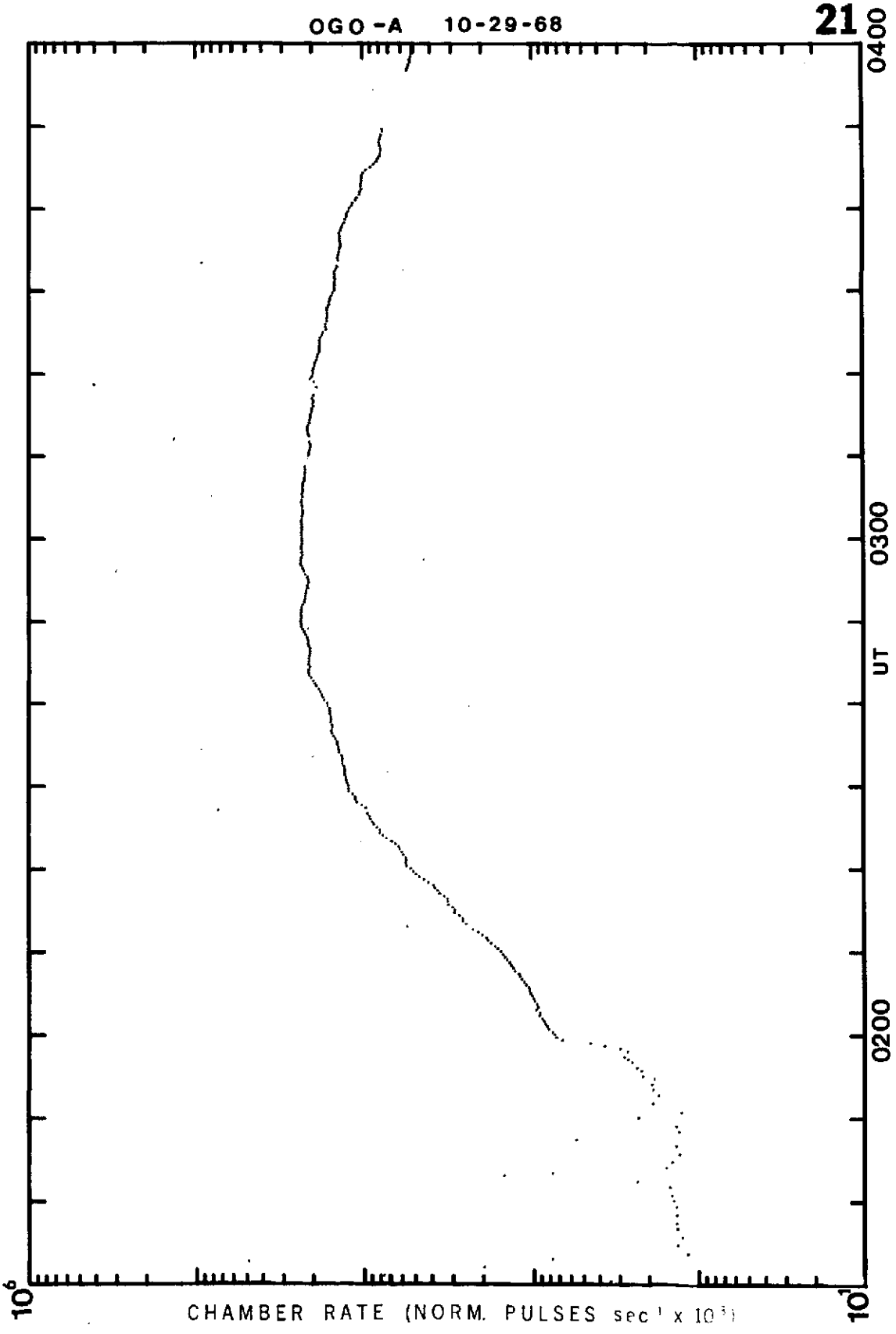
OGO-A 10-29-68
0400
0300
0200
UT
10^6
10^1
CHAMBER RATE (NORM. PULSES sec^{-1} x 10^3)

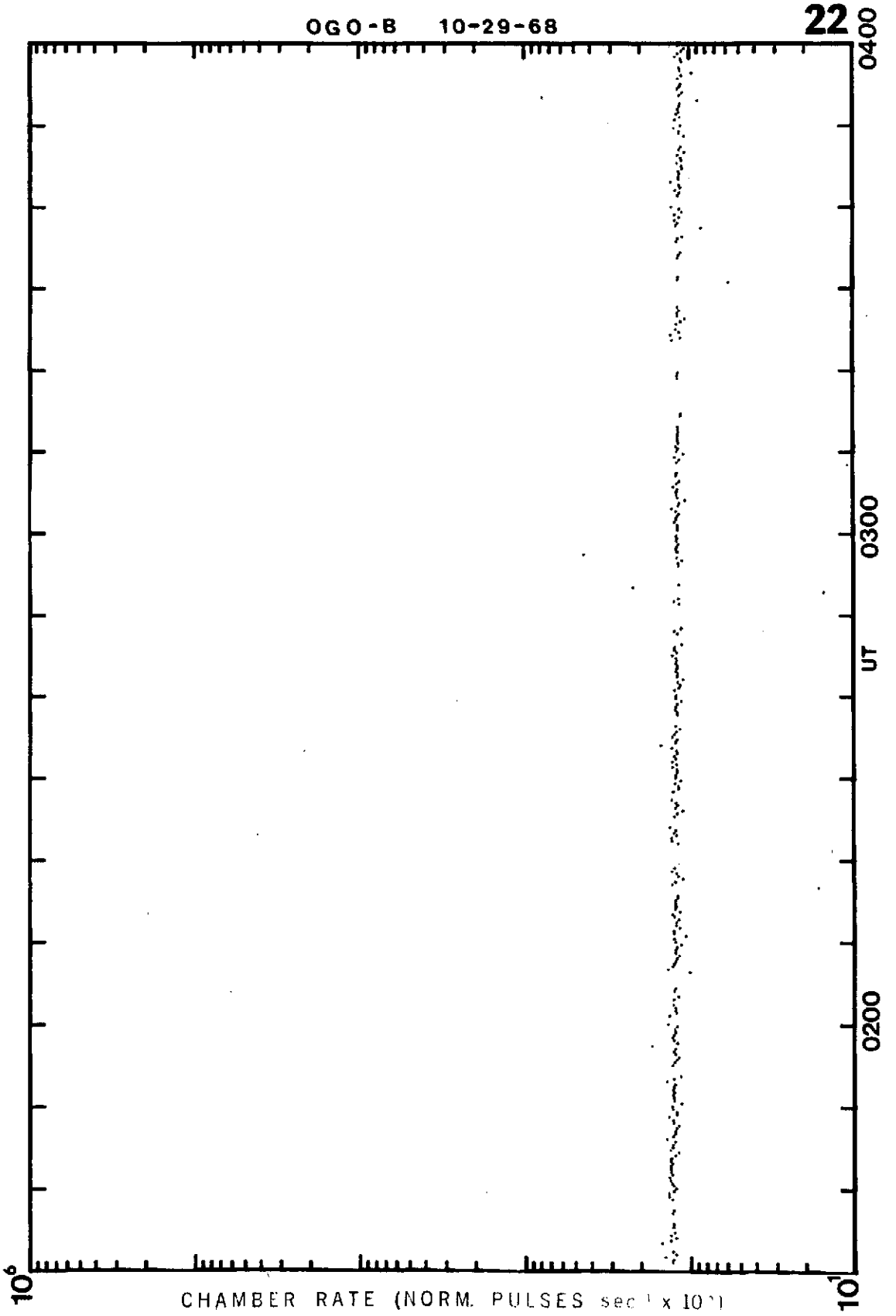
OGO-B 10-29-68
22
0400
0300
UT
0200
10^6
10^1
CHAMBER RATE (NORM. PULSES sec^{-1} x 10^{-1})

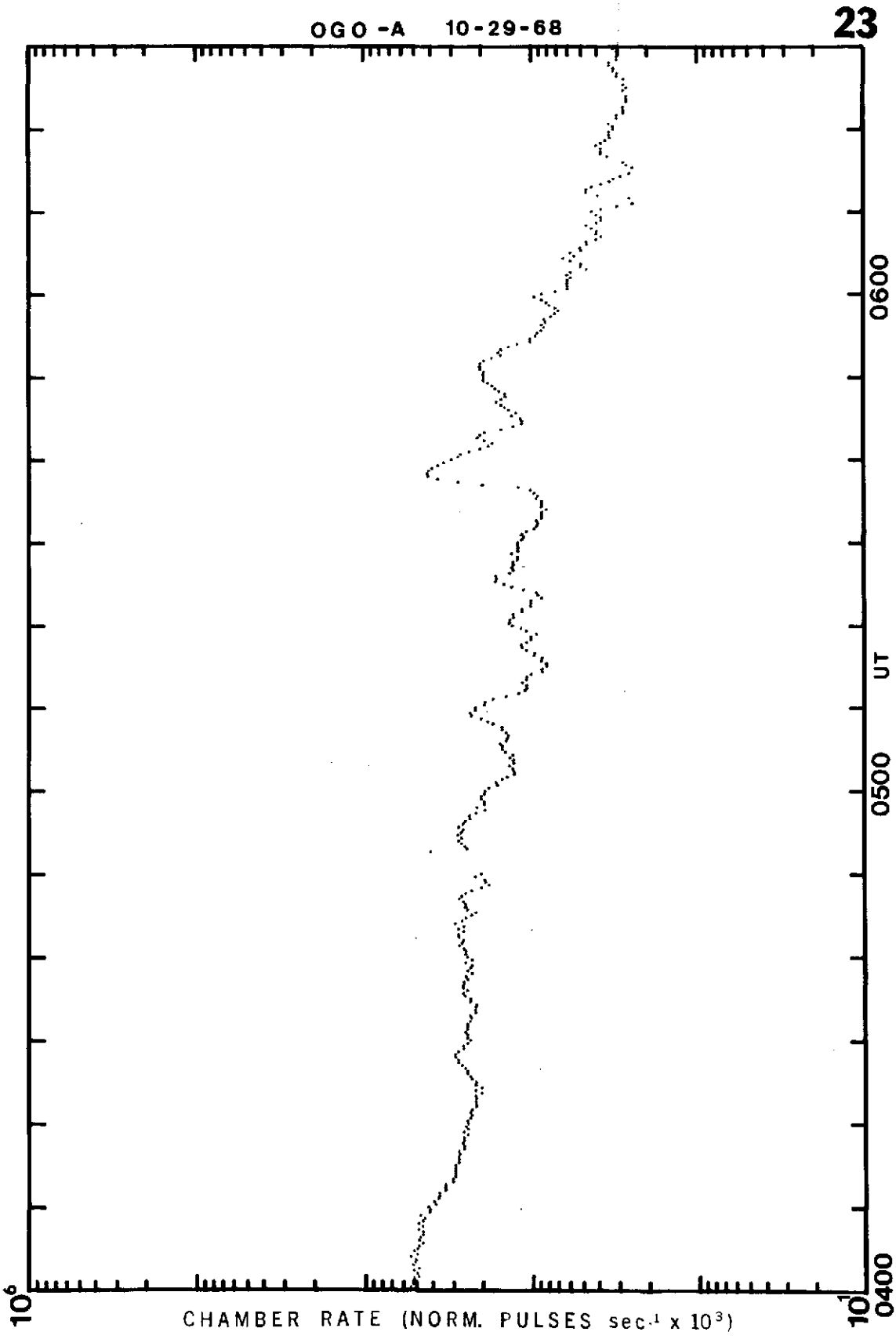
OGO -A 10-29-68
0400
0500
0600
UT
10^6
10^1
CHAMBER RATE (NORM. PULSES $sec^{-1} \times 10^3$)

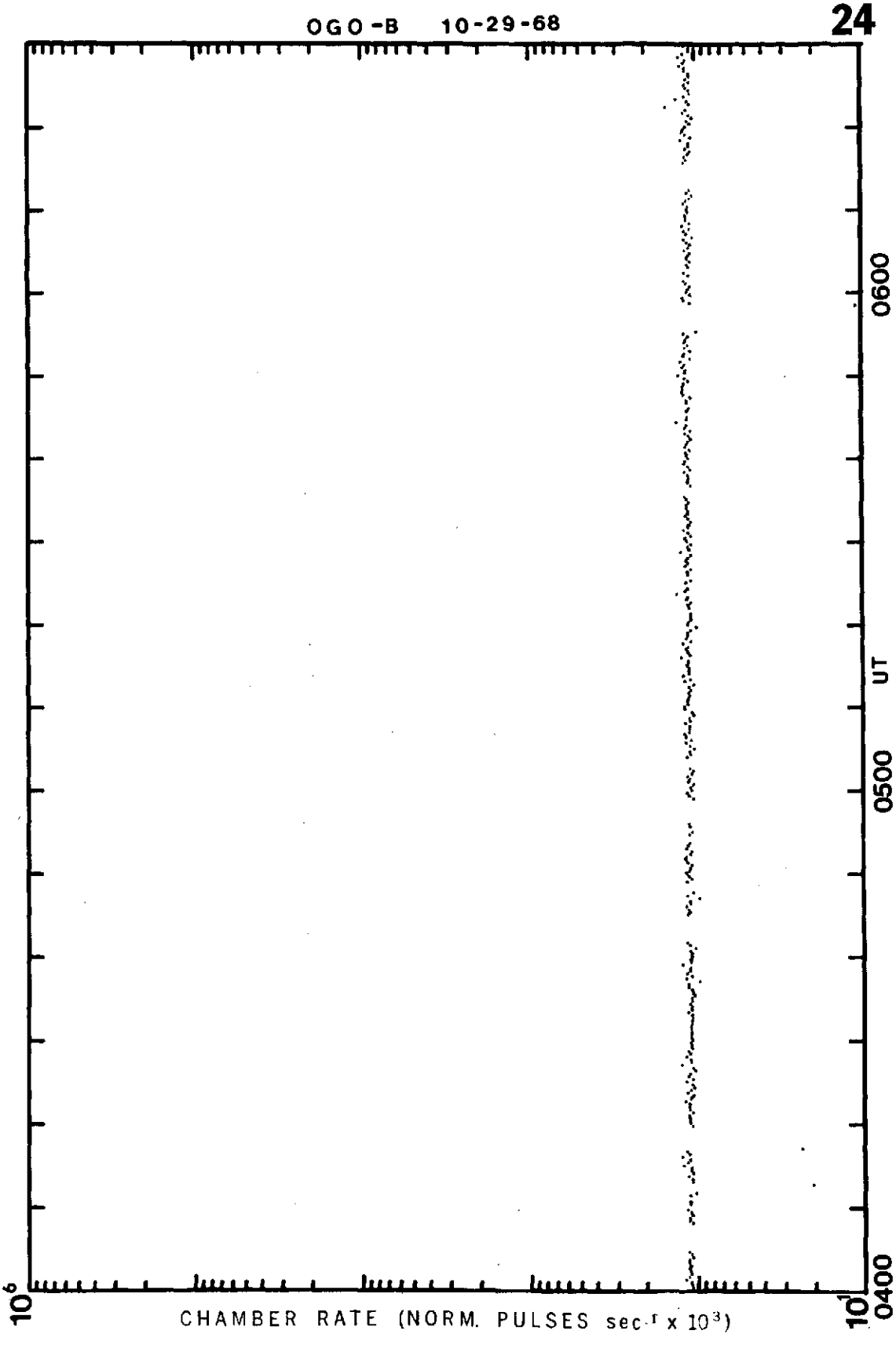
OGO-B 10-29-68
0600
0500
UT
0400
10^6
10^1
CHAMBER RATE (NORM. PULSES $sec^{-1} \times 10^3$)

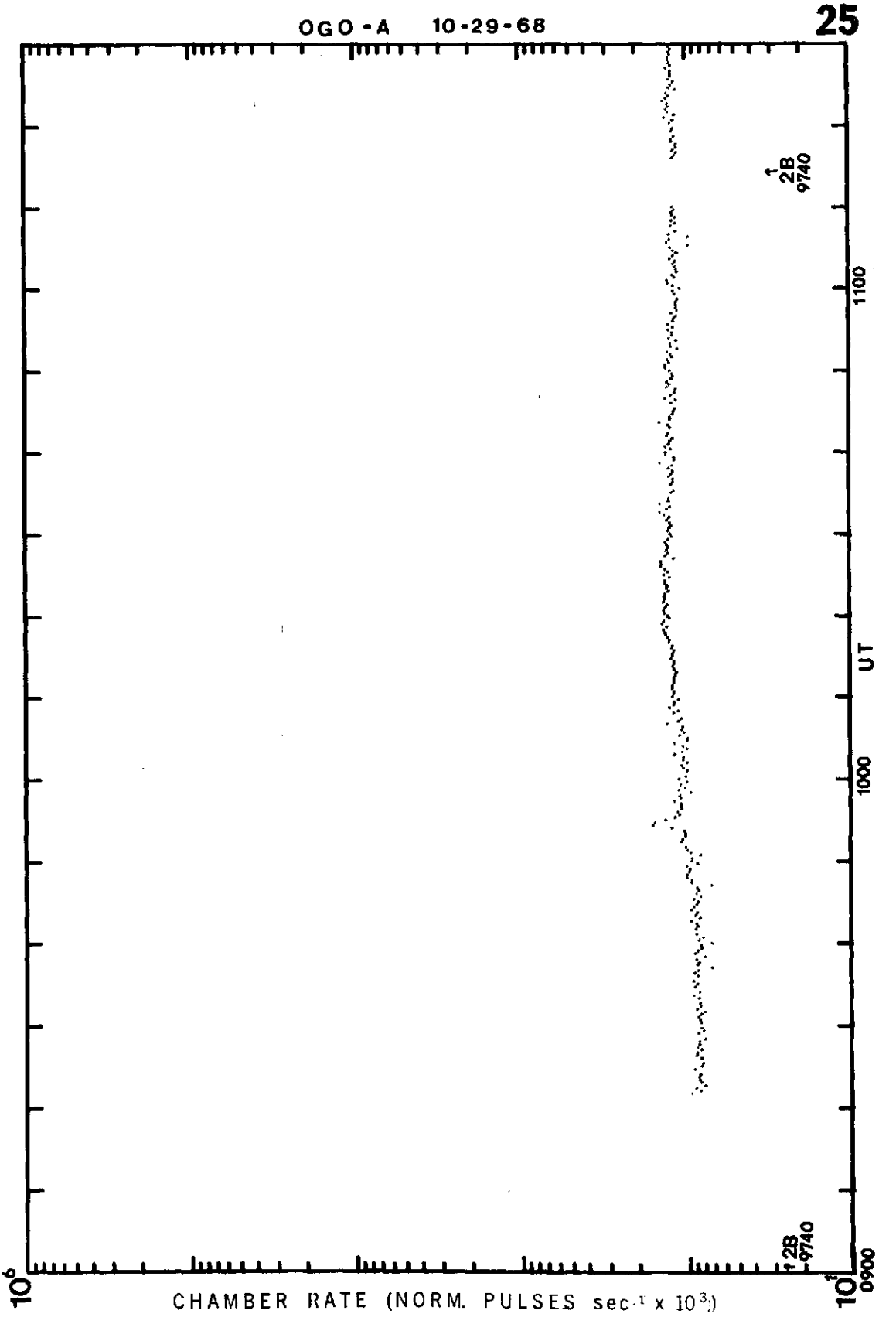
OGO-A 10-29-68
2B 9740
1100
1000
0900
UT
2B 9740
10^6
10^4
CHAMBER RATE (NORM. PULSES sec^{-1} x 10^3)

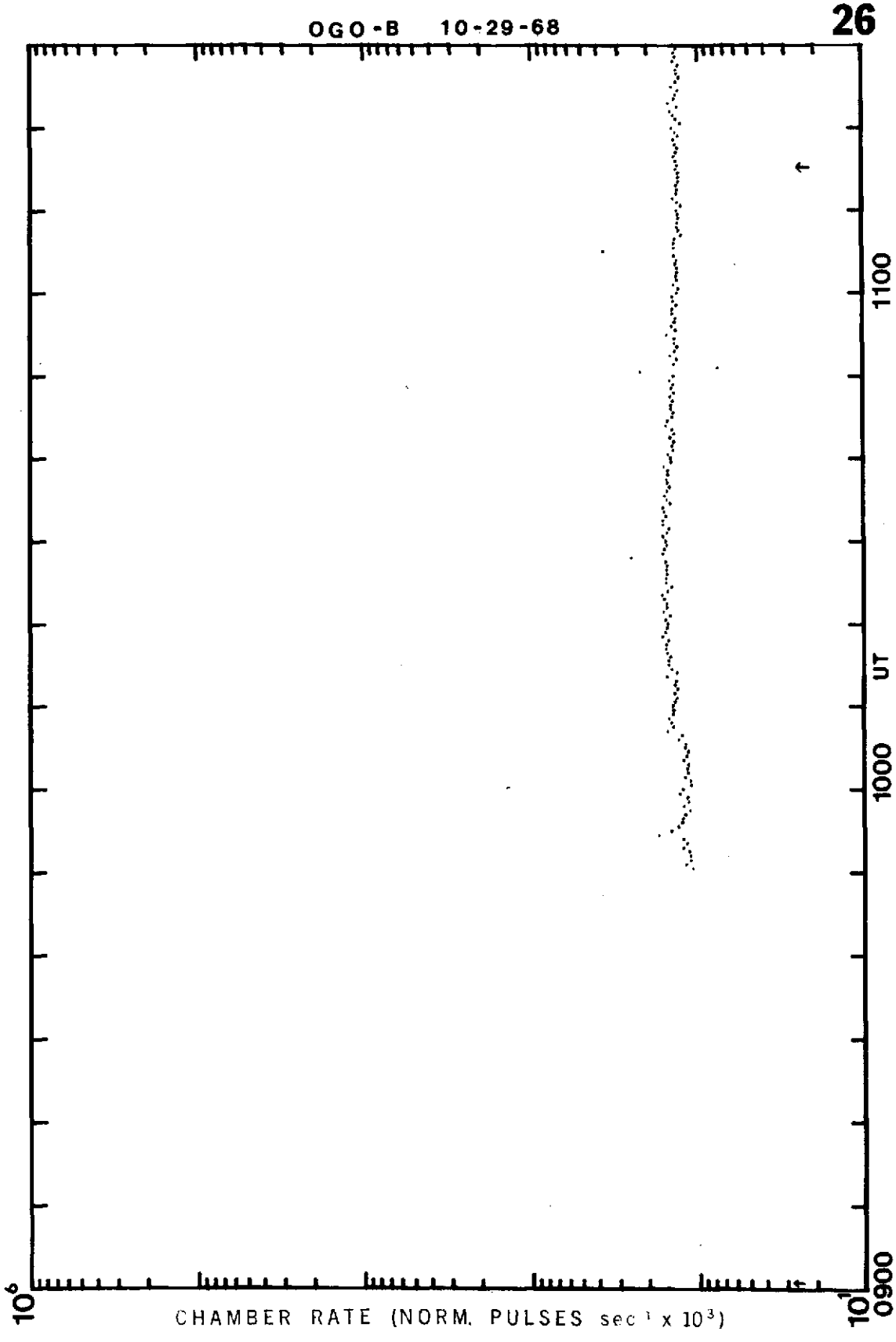
OGO-B 10-29-68
1100
1000
0900
UT
10^6
10^1
CHAMBER RATE (NORM. PULSES $sec^{-1} \times 10^3$)

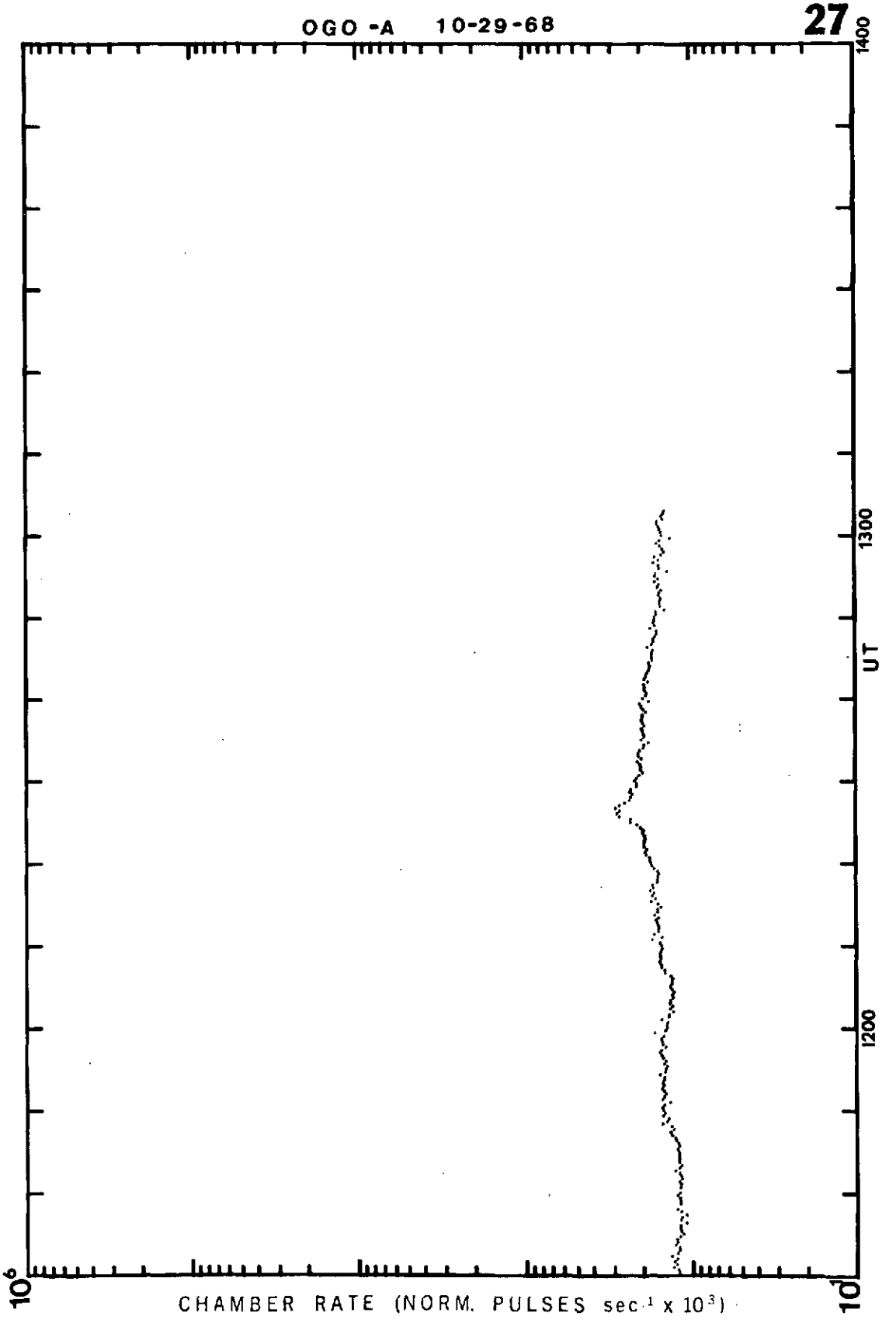
OGO -A 10-29-68
27
1400
1300
1200
UT
10^6
10^1
CHAMBER RATE (NORM. PULSES sec^{-1} x 10^3)

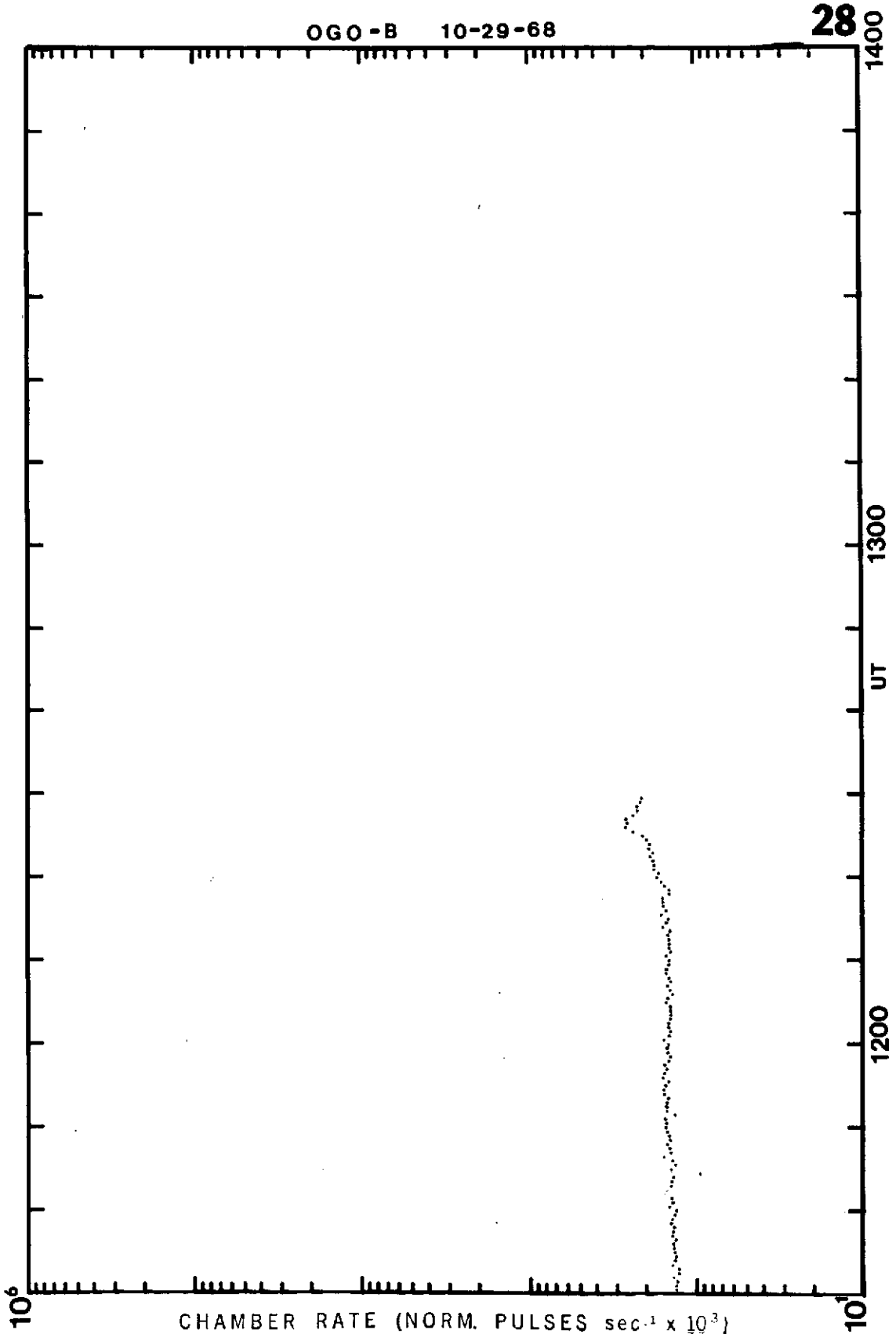
OGO-B 10-29-68
28
1400
1300
1200
UT
10^6
10^1
CHAMBER RATE (NORM. PULSES sec^{-1} x 10^{-3})

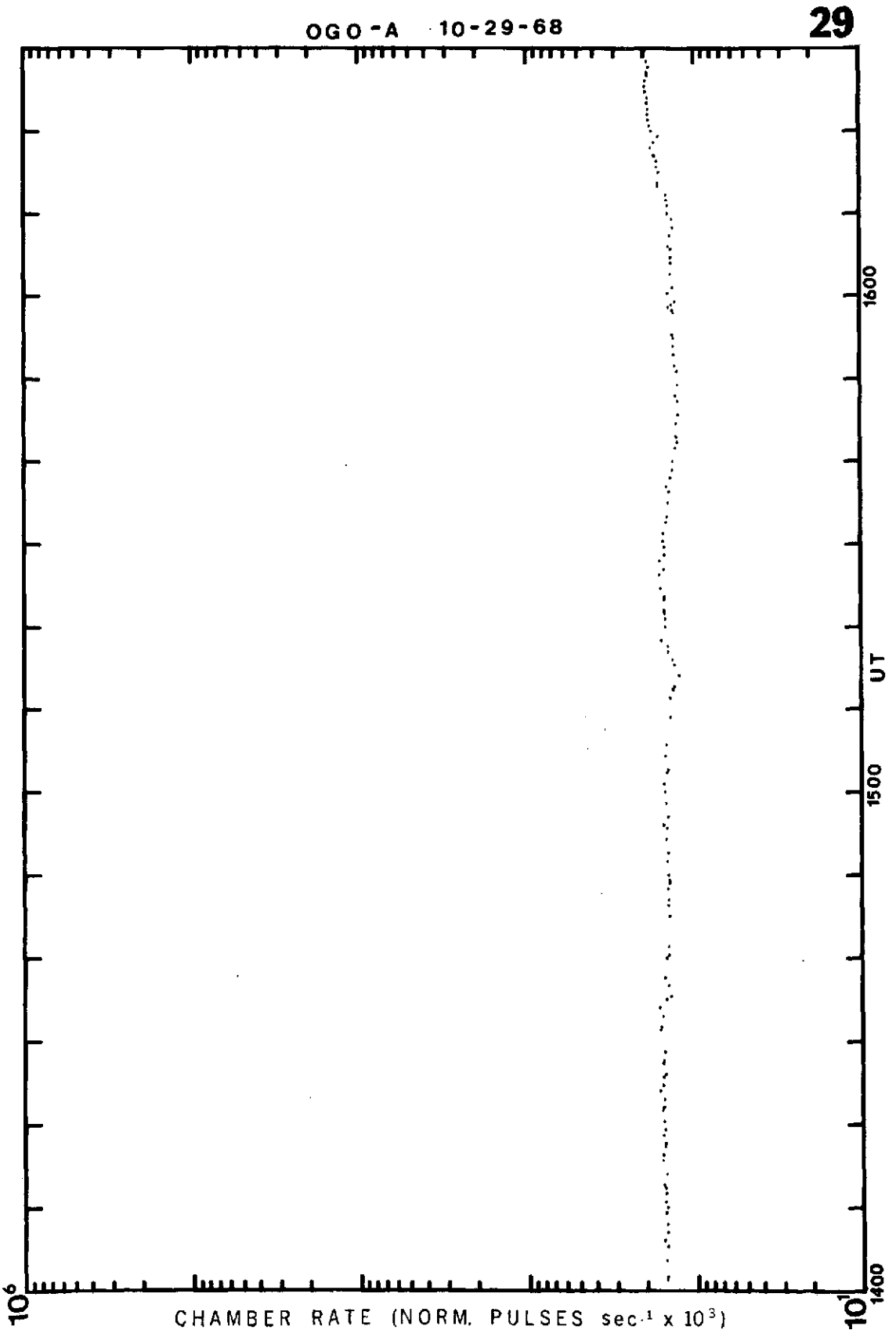
OGO-A 10-29-68
29
1600
1500
1400
UT
10^6
10^1
CHAMBER RATE (NORM. PULSES sec^{-1} x 10^3)

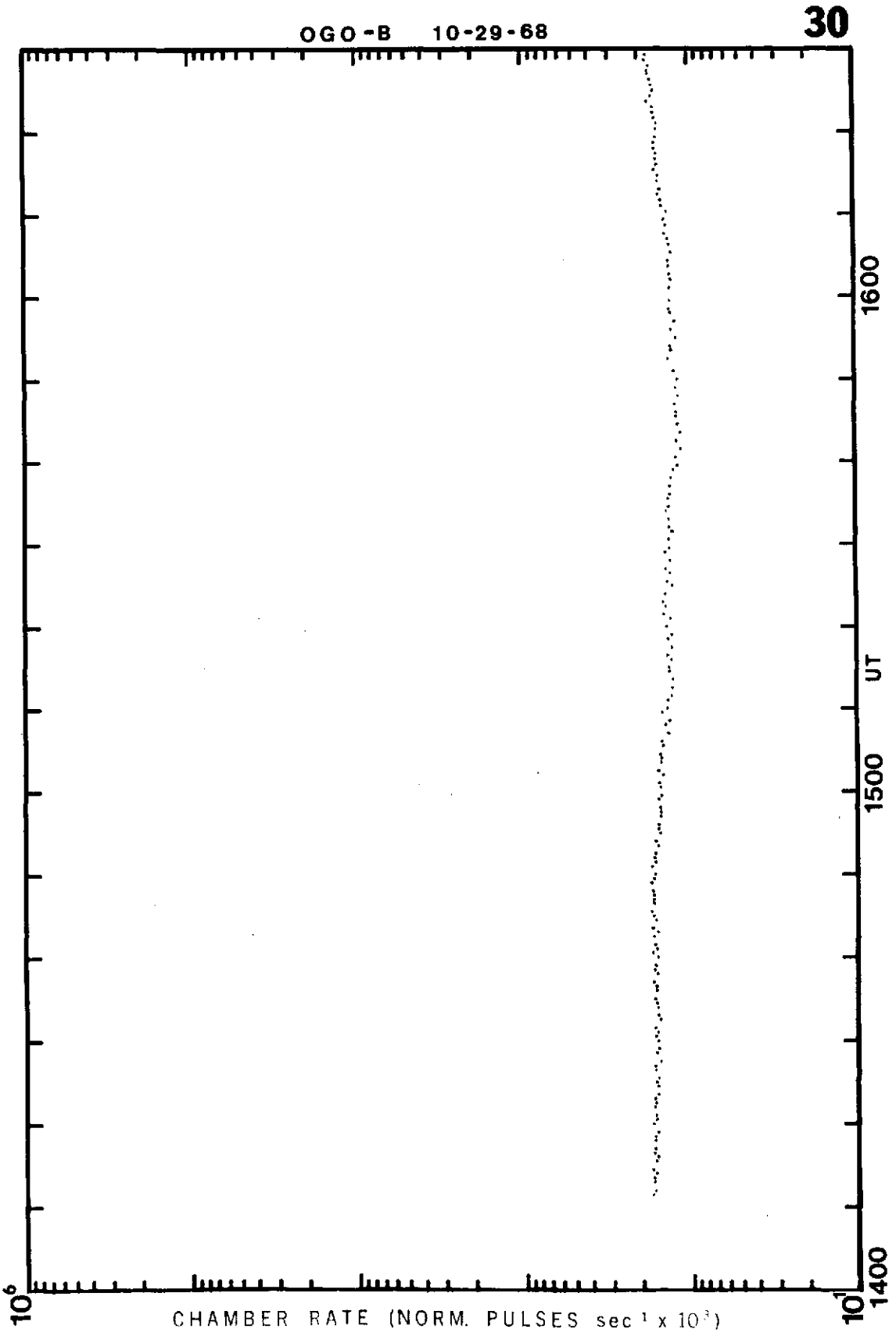
OGO-B 10-29-68
30
1600
1500
1400
UT
10^6
10^1
CHAMBER RATE (NORM. PULSES sec^{-1} x 10^3)

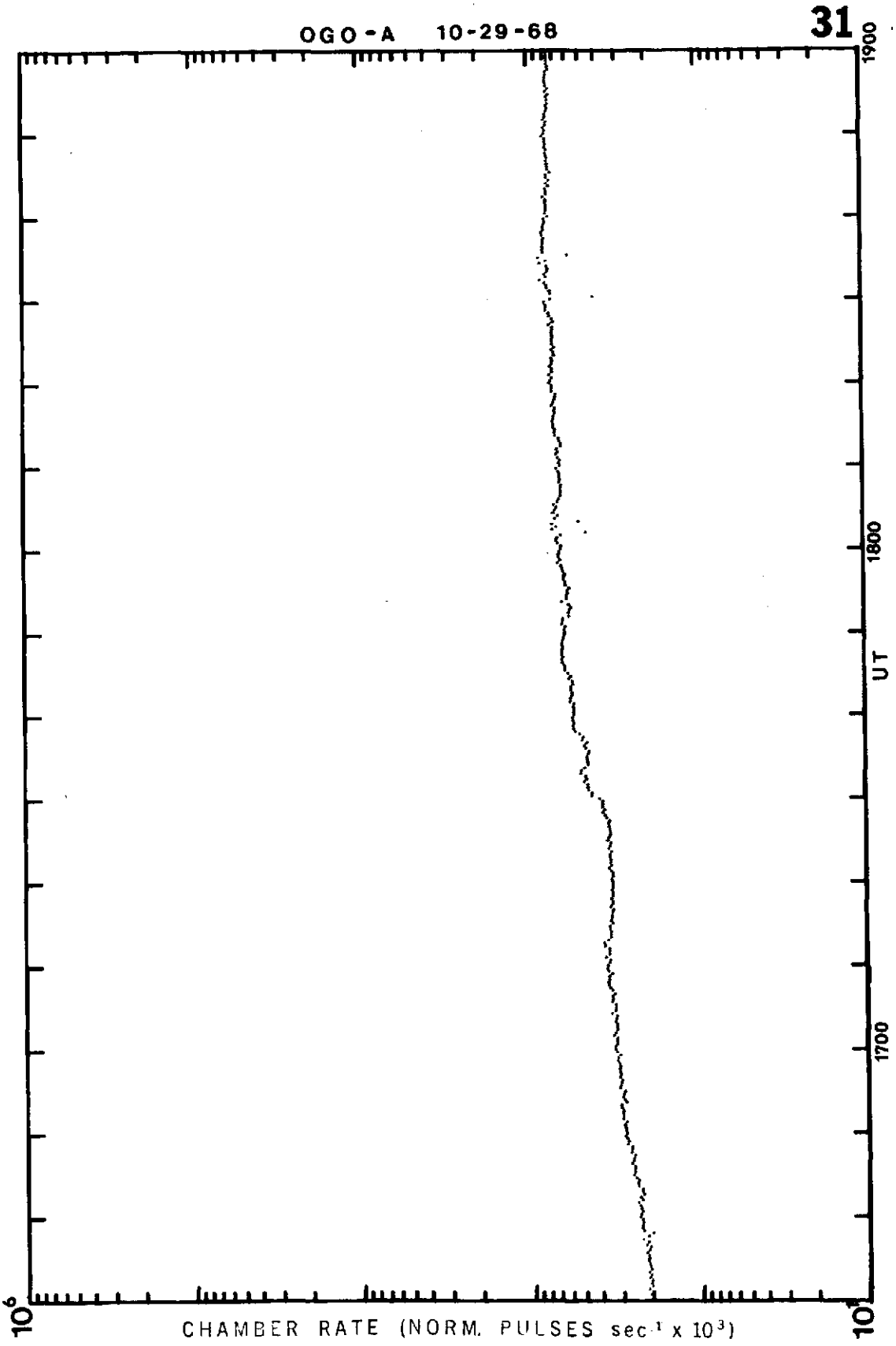
OGO-A 10-29-68
1900
1800
UT
1700
10^6
10^5
CHAMBER RATE (NORM. PULSES $sec^{-1} \times 10^3$)

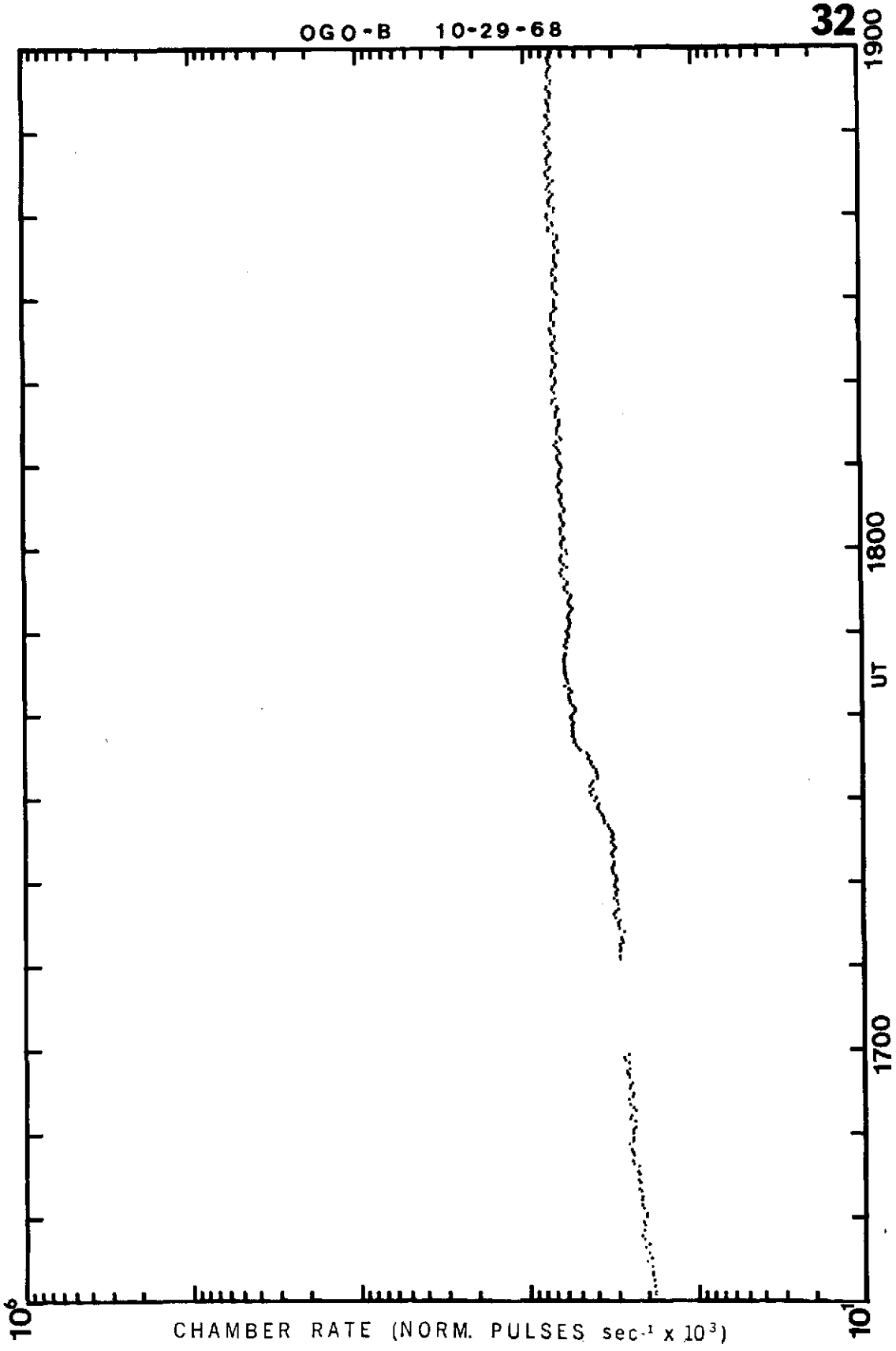
OGO-B 10-29-68
32
1900
1800
1700
UT
10^0
10^1
CHAMBER RATE (NORM. PULSES sec^{-1} x 10^3)

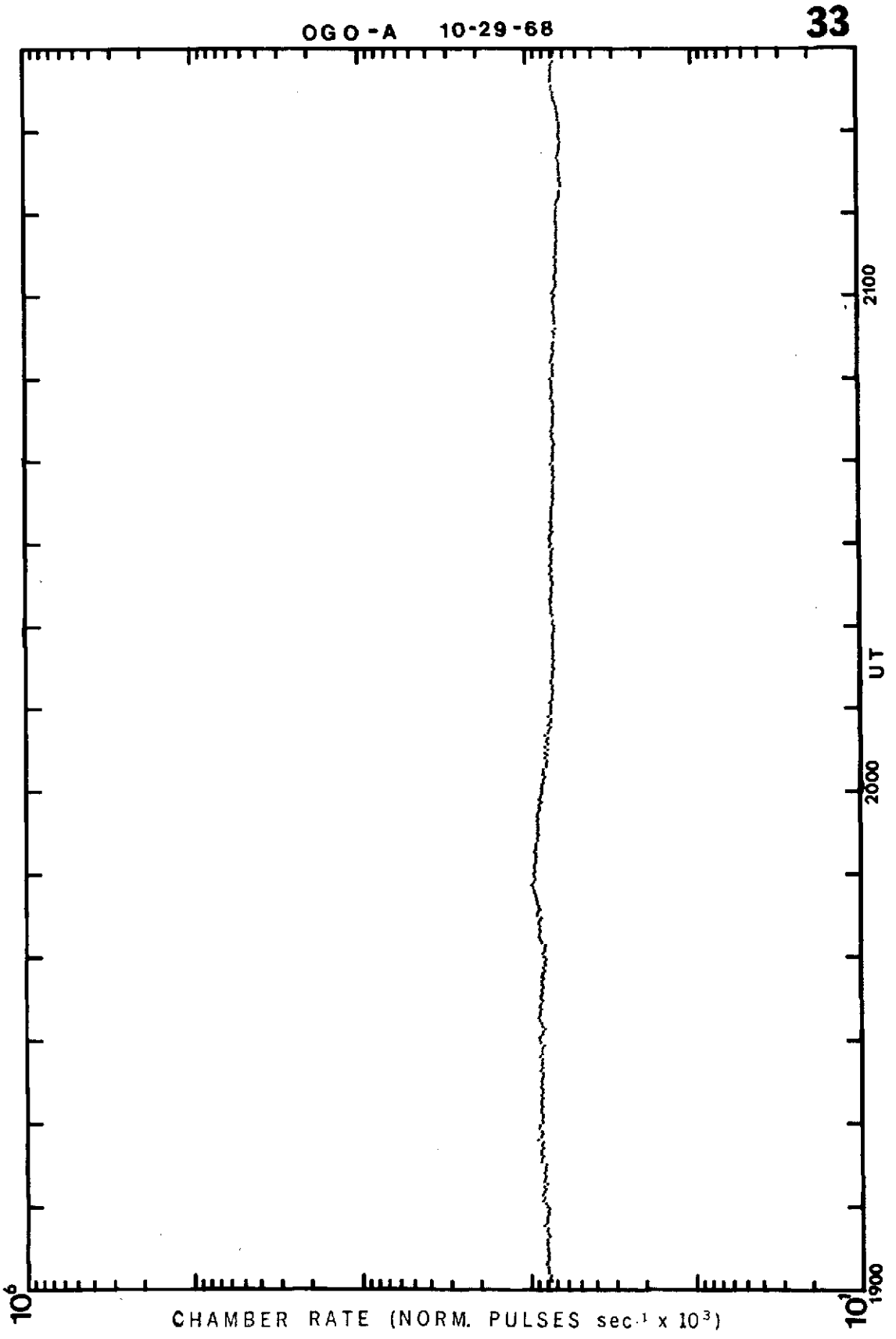
OGO-A 10-29-68
33
2100
2000
1900
UT
10^6
10^1
CHAMBER RATE (NORM. PULSES $sec^{-1} \times 10^3$)

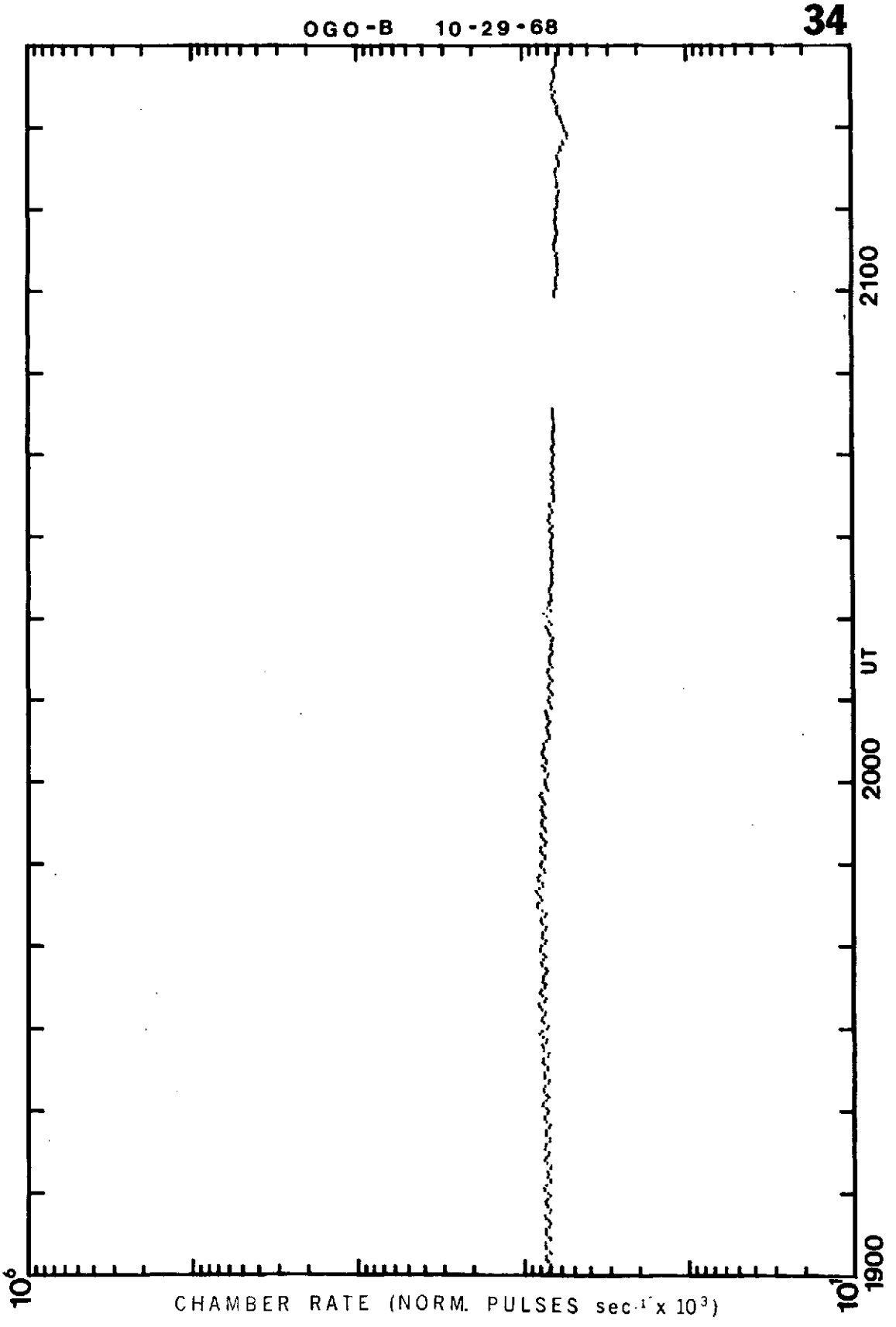
OGO-B 10-29-68
34
2100
2000
1900
UT
10^6
10^1
CHAMBER RATE (NORM. PULSES sec^{-1} x 10^3)

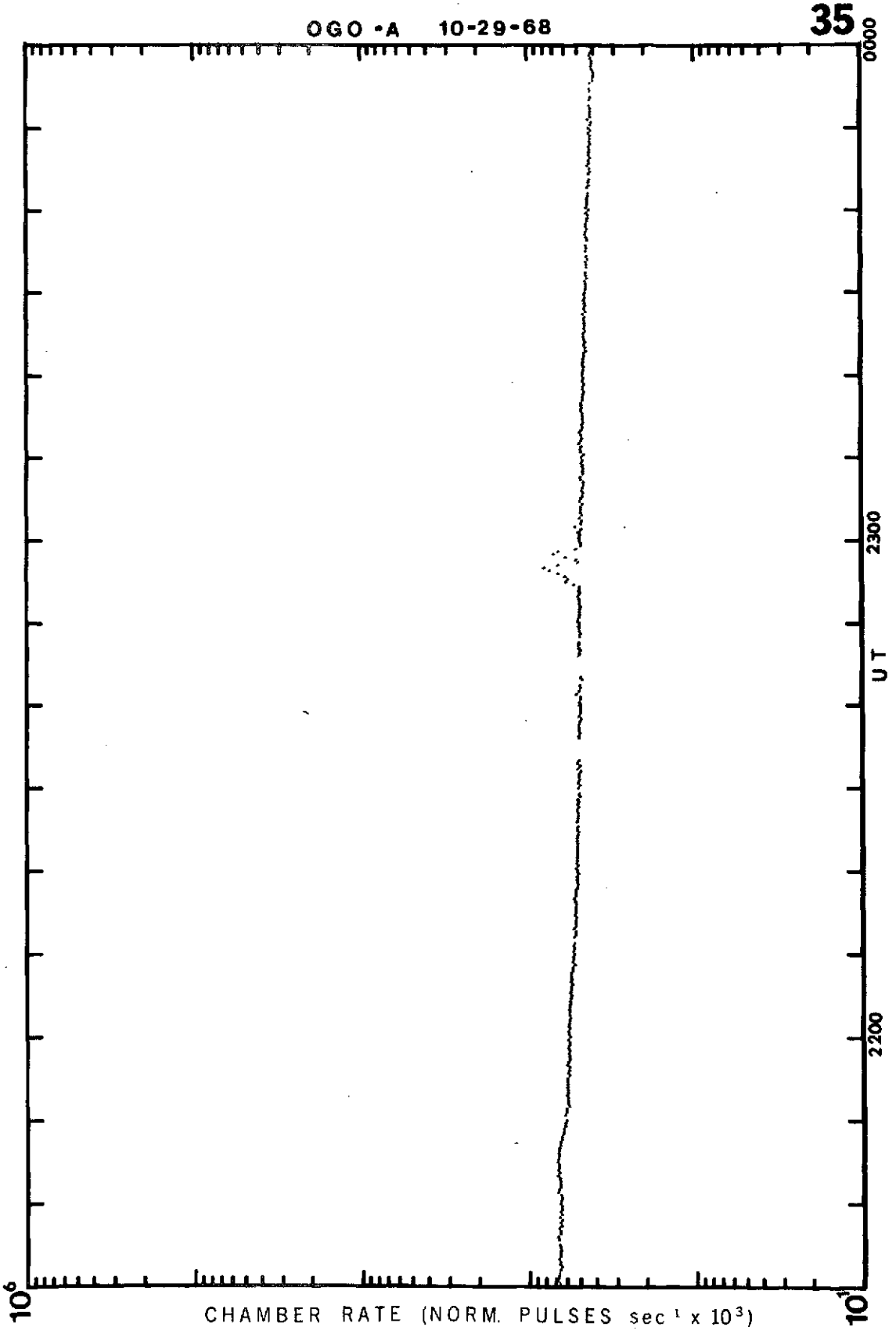
OGO -A 10-29-68
35
0000
2300
2200
UT
10^6
10^5
CHAMBER RATE (NORM. PULSES sec^{-1} x 10^3)

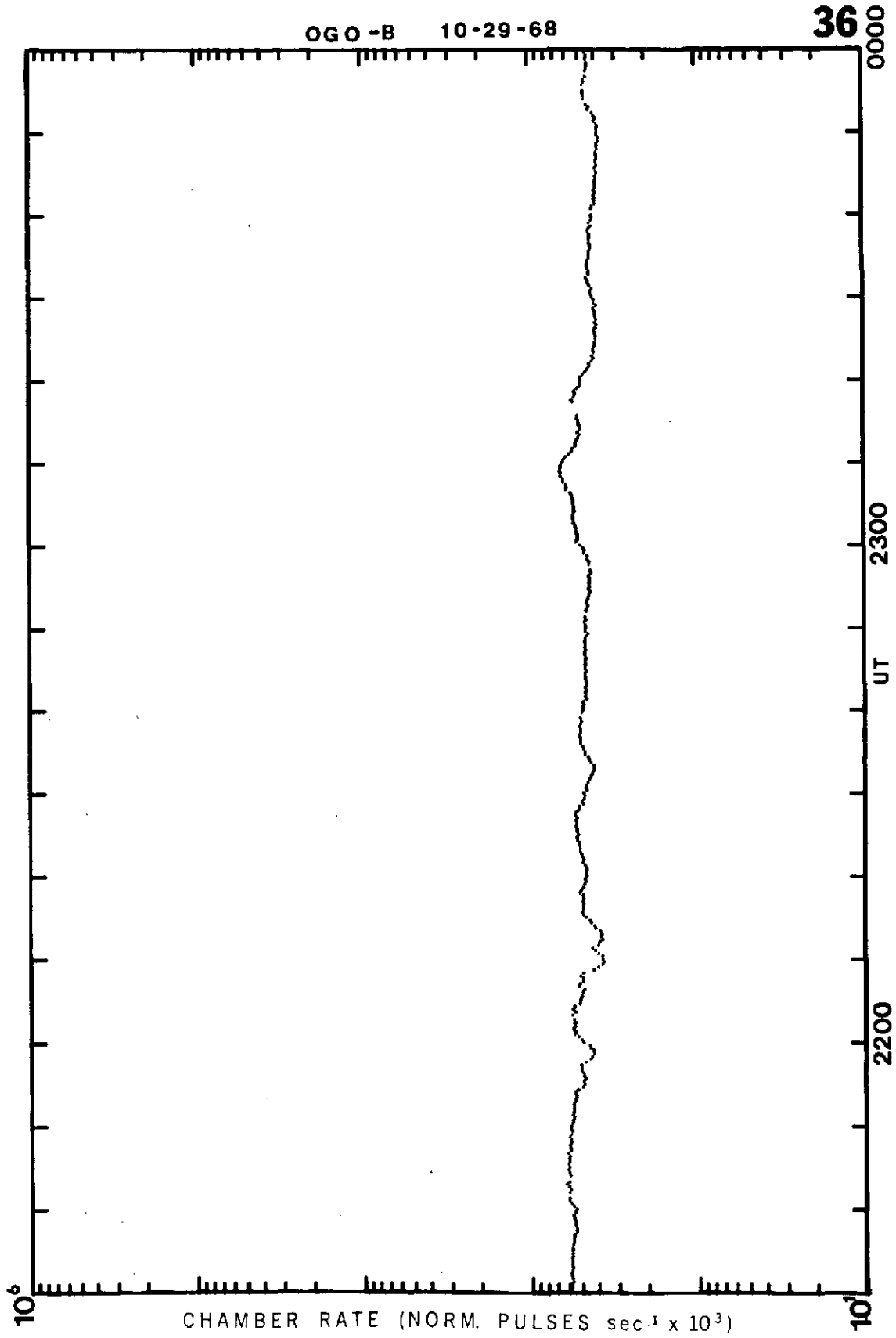
OGO-B 10-29-68
36
0000
2300
UT
2200
10^0
10^1
CHAMBER RATE (NORM. PULSES sec^{-1} x 10^3)

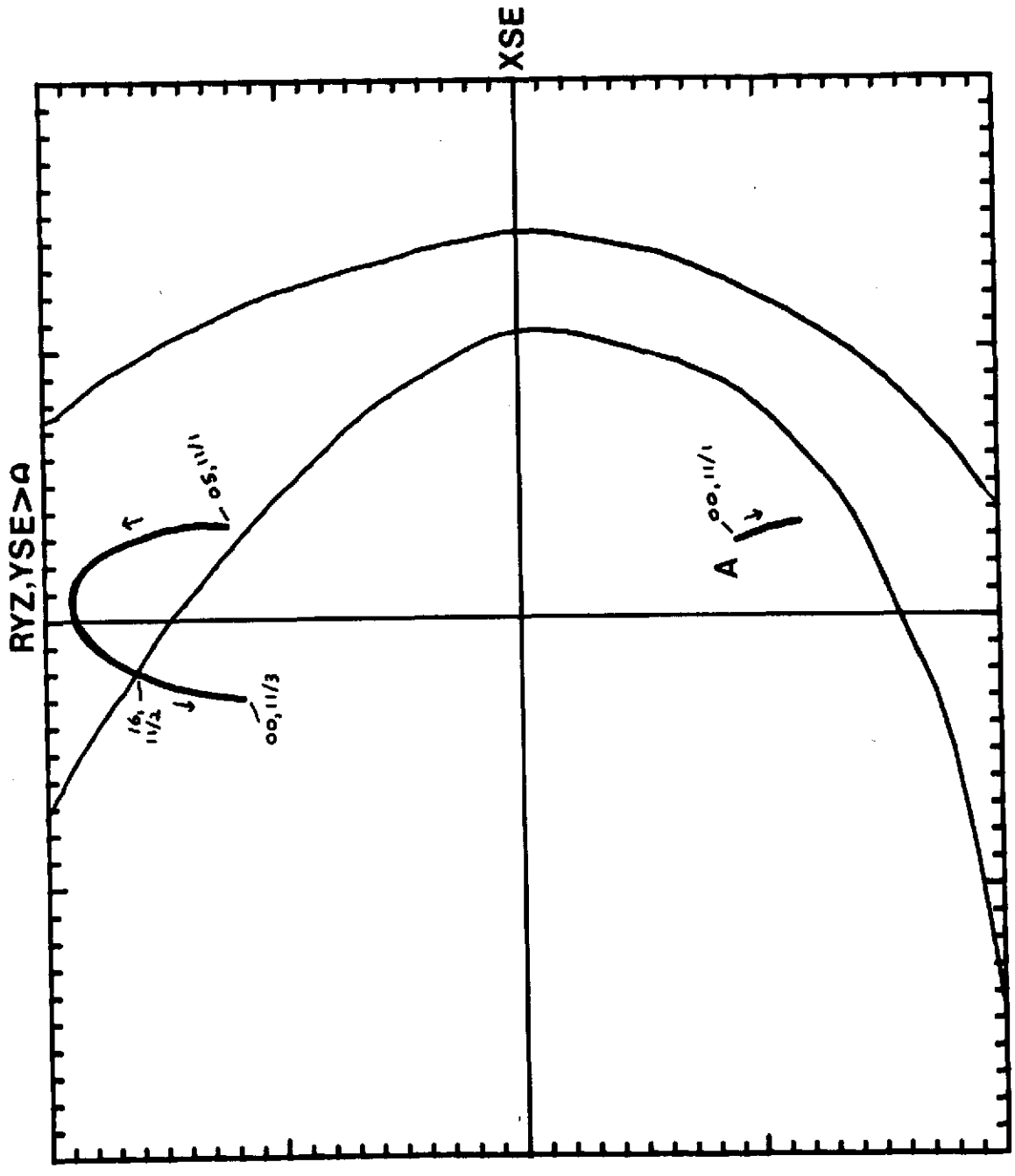
XSE
RYZ,YSE>0
00,11/1
A
00,11/2
16,
11/2
00,11/3

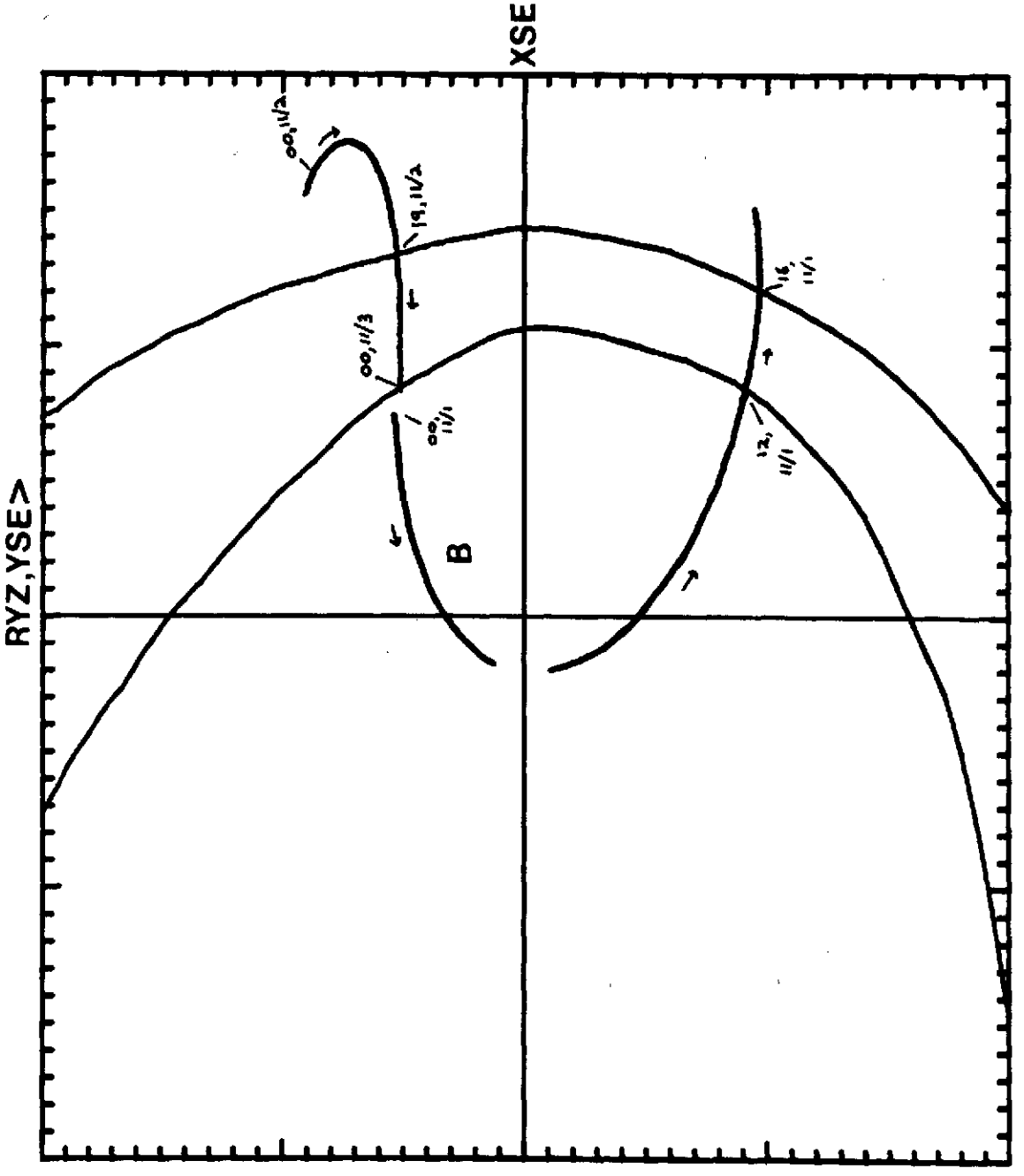
XSE
RYZ,YSE>
B

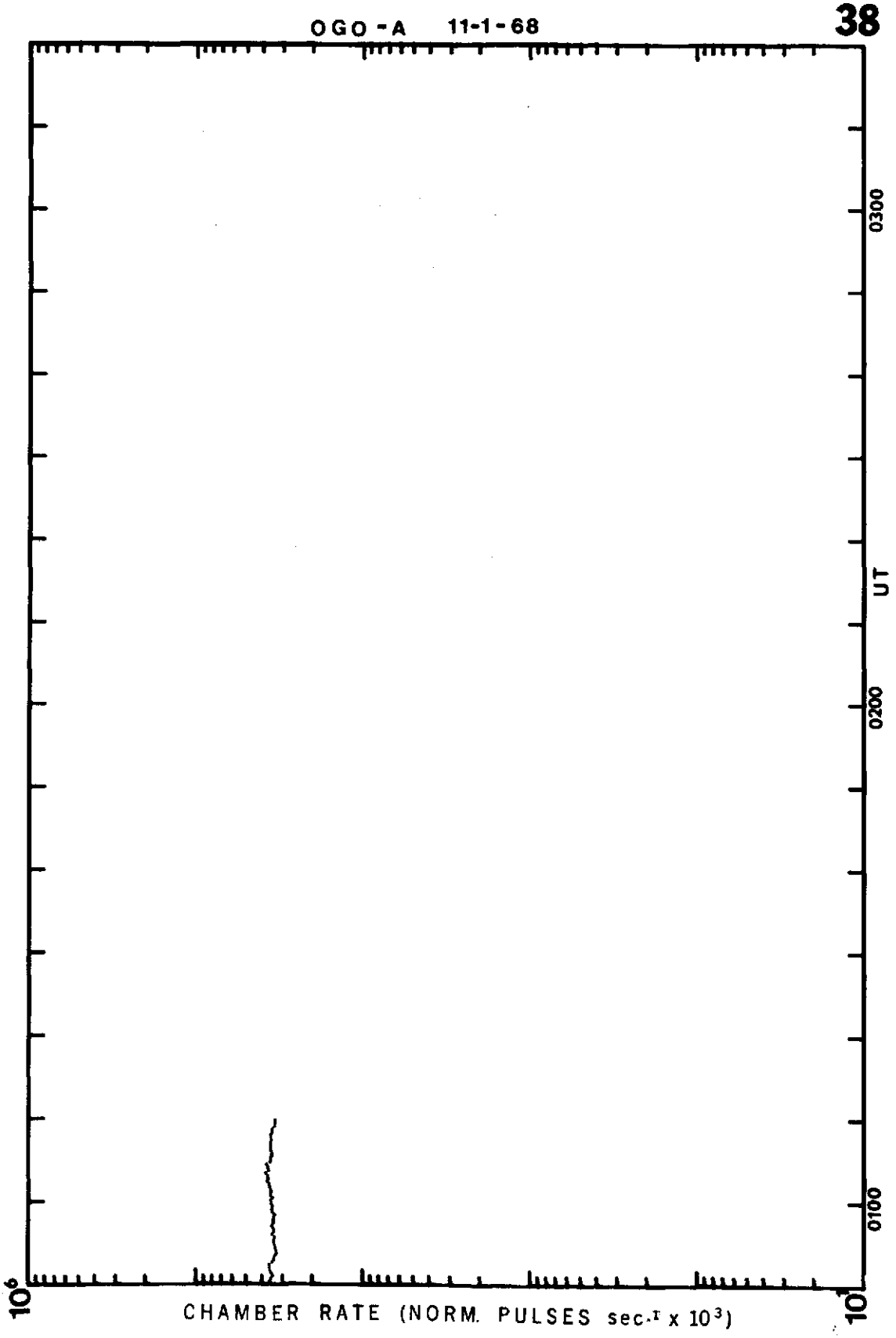
OGO - A 11-1-68
0300
UT
0200
0100
10^6
10^5
CHAMBER RATE (NORM. PULSES sec.$^{-1}$ x 10^3)

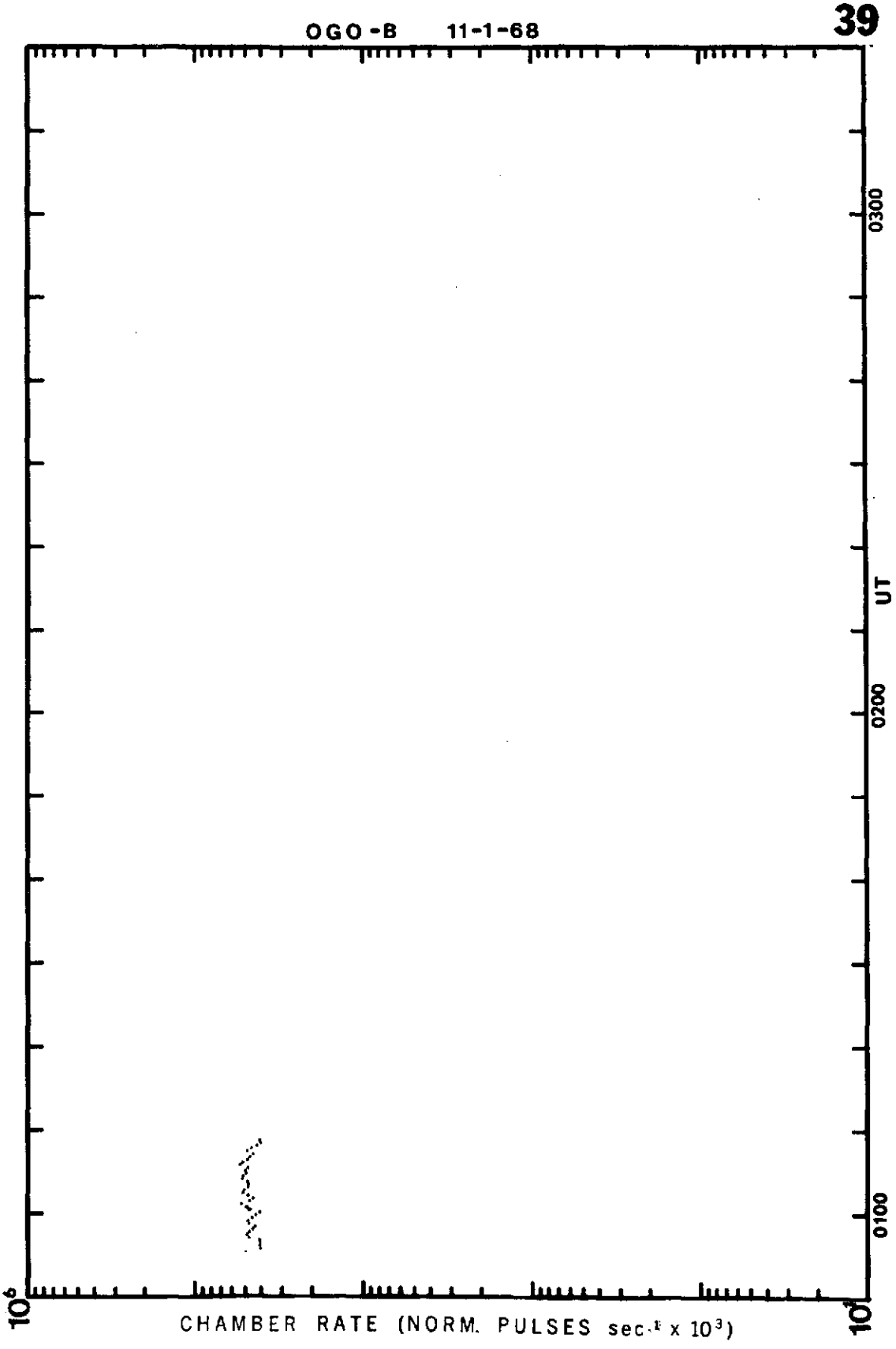
OGO-B 11-1-68
0300
UT
0200
0100
10^6
10^4
CHAMBER RATE (NORM. PULSES sec^{-1} x 10^3)

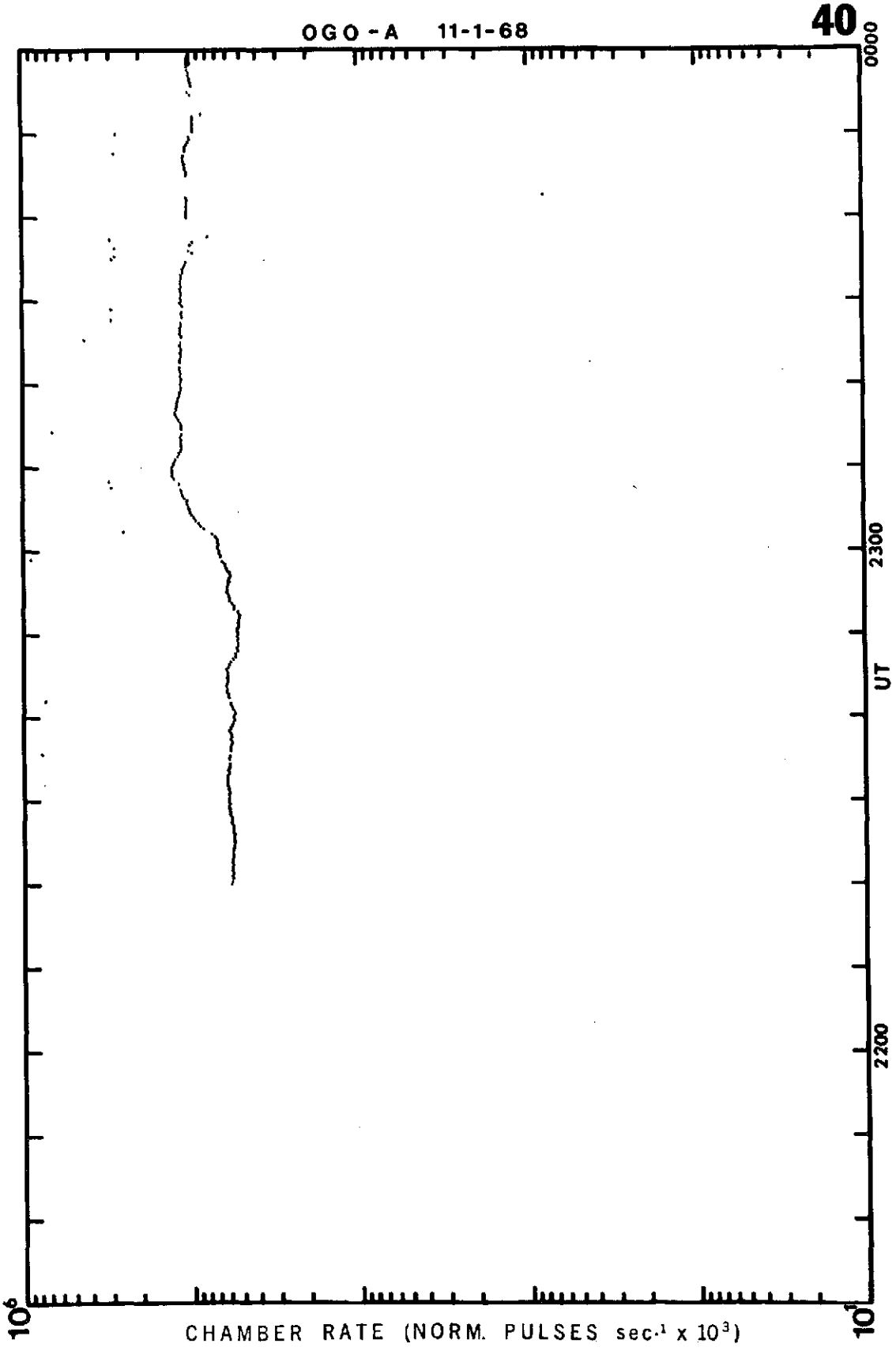
OGO-A 11-1-68
40
0000
2300
UT
2200
10^6
10^1
CHAMBER RATE (NORM. PULSES sec^{-1} x 10^3)

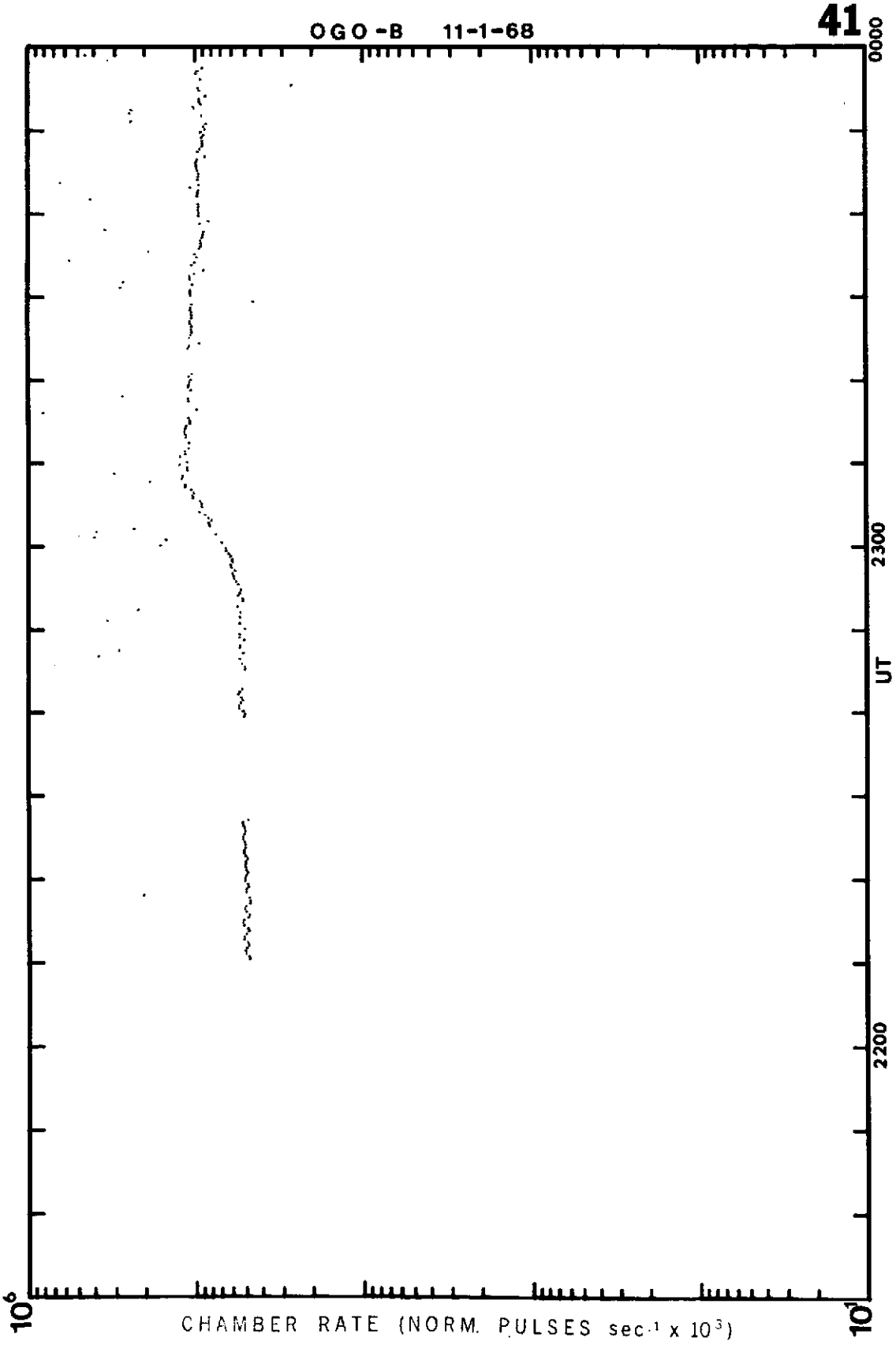
OGO-B 11-1-68
41
0000
2300
2200
UT
10^6
10^1
CHAMBER RATE (NORM. PULSES sec^{-1} x 10^3)

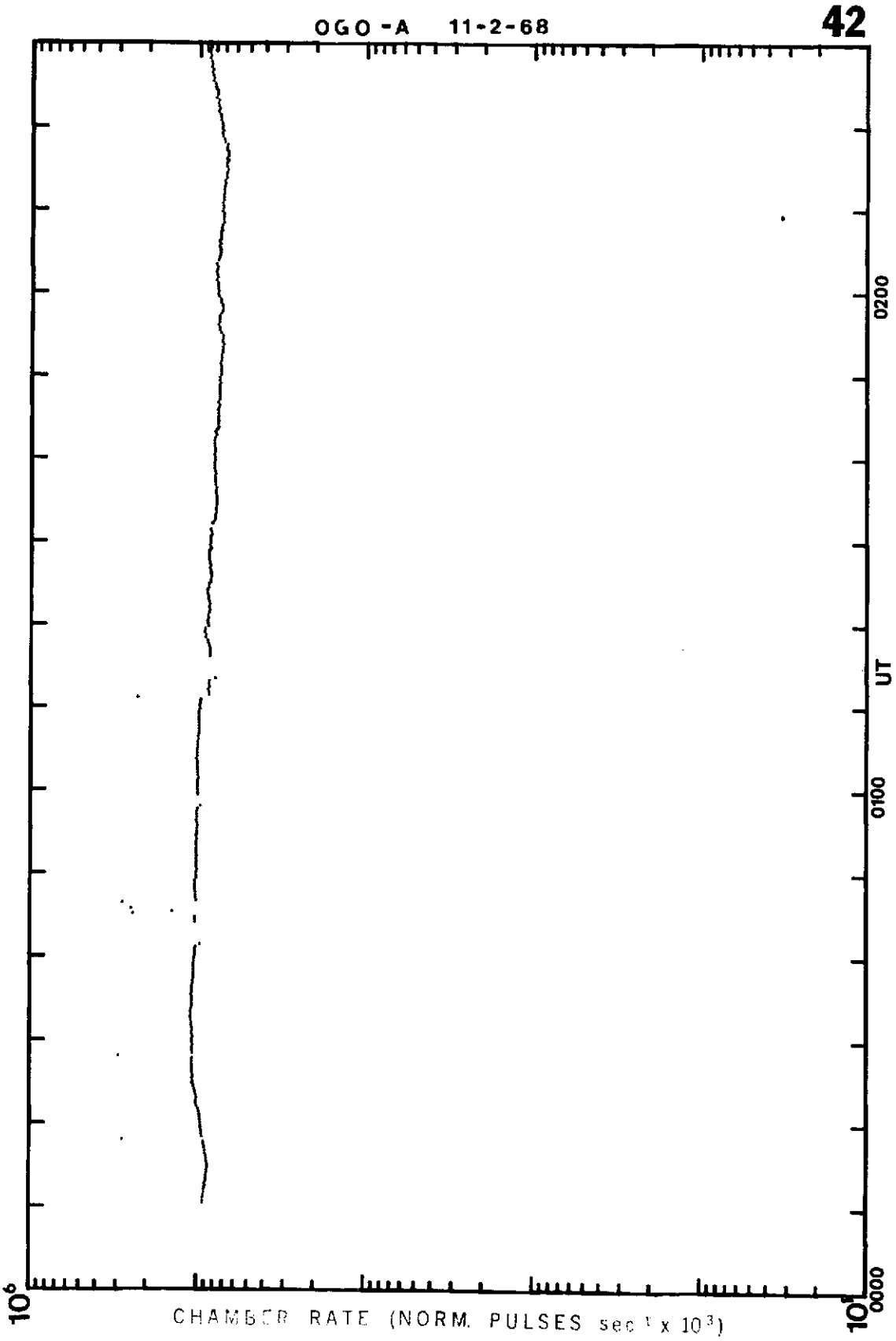
OGO-A 11-2-68
0200
UT
0100
0000
10^6
10^5
CHAMBER RATE (NORM. PULSES sec^{-1} x 10^3)

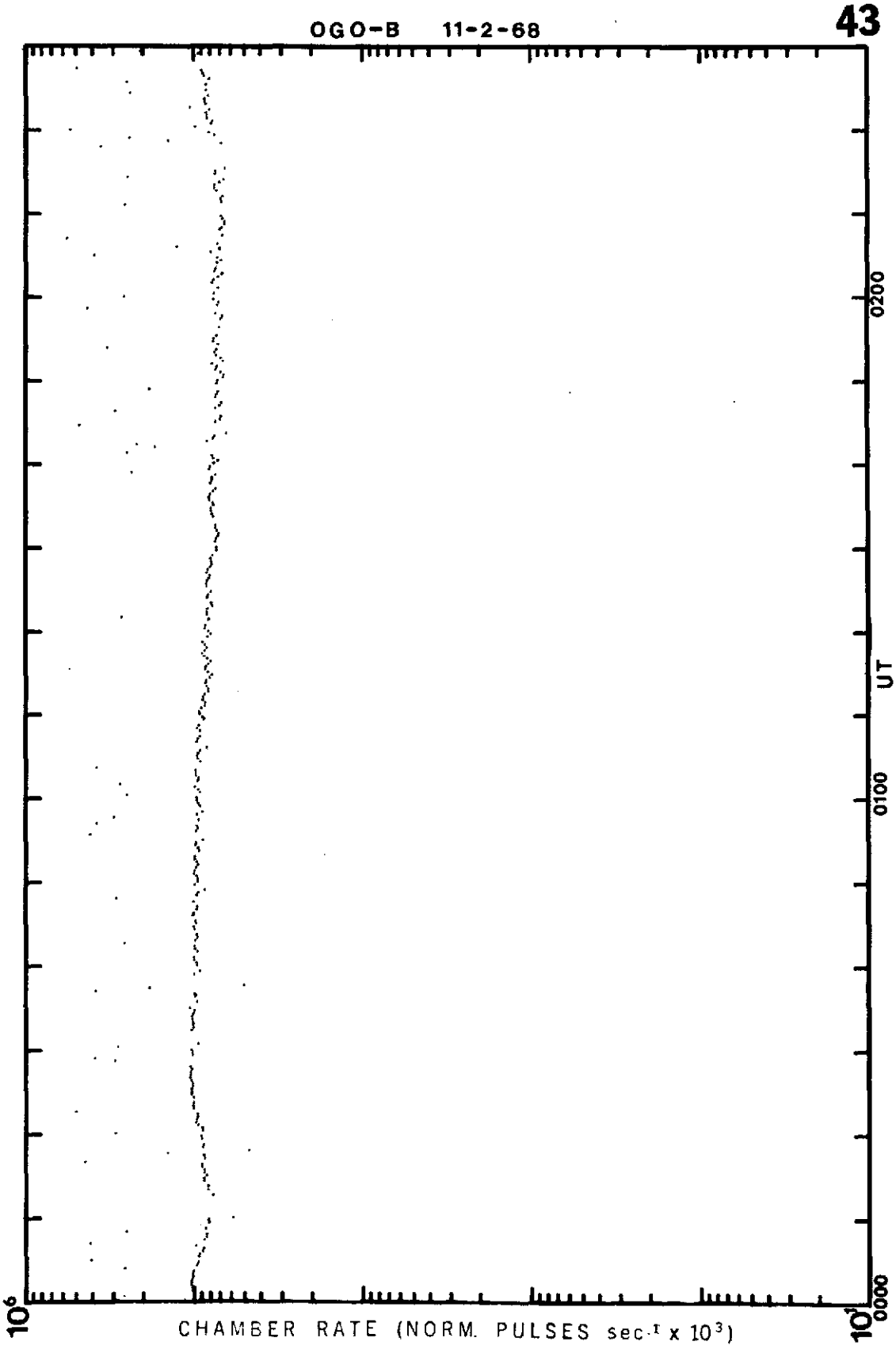
OGO-B 11-2-68
0200
0100
0000
UT
10^6
10^5
CHAMBER RATE (NORM. PULSES $sec^{-1} \times 10^3$)

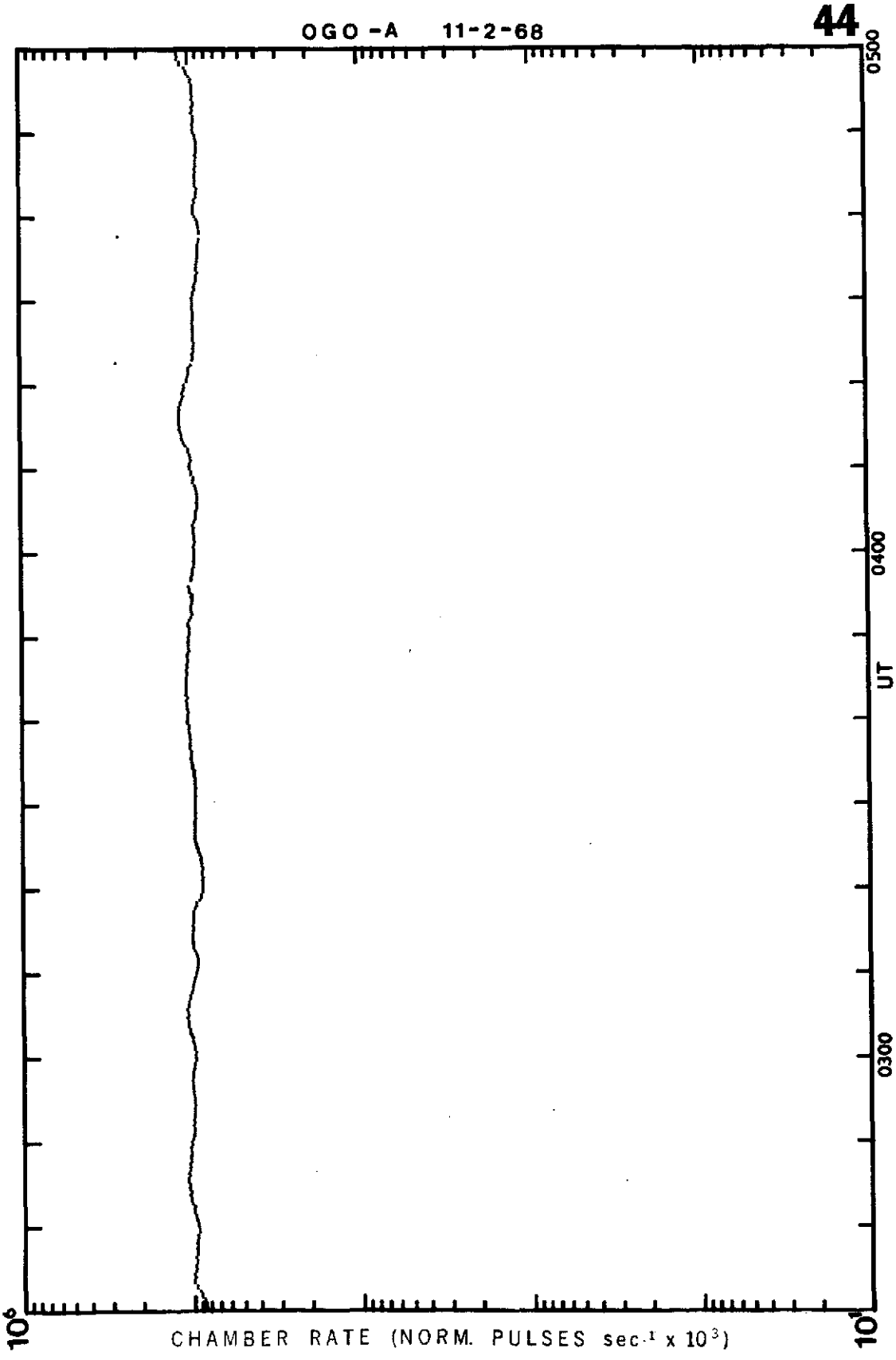
OGO -A 11-2-68
44
0500
0400
0300
UT
10^0
10^1
CHAMBER RATE (NORM. PULSES sec^{-1} x 10^3)

C-2

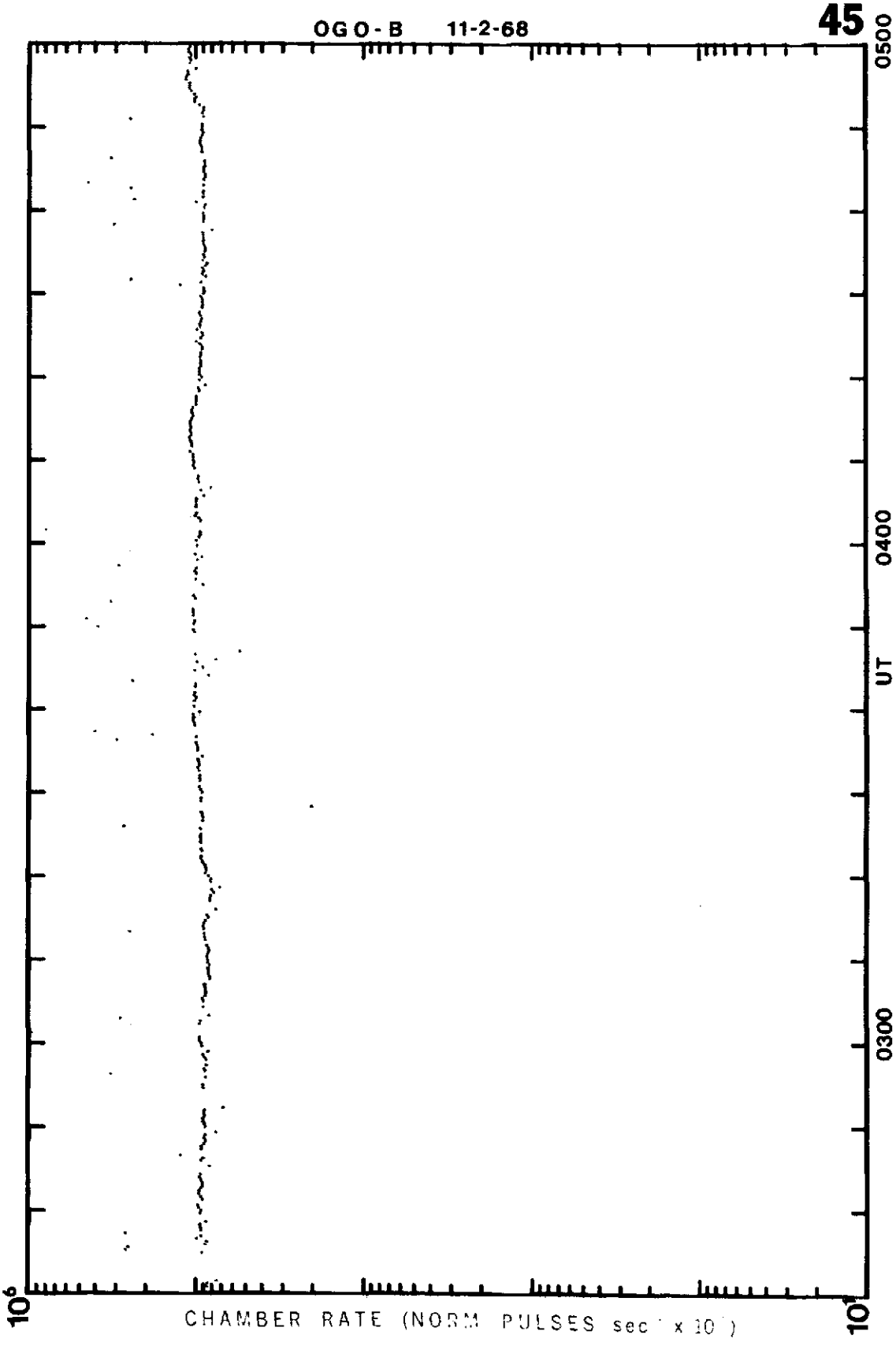
OGO-B 11-2-68
45
0500
0400
0300
UT
10^6
10^5
CHAMBER RATE (NORM PULSES sec^{-1} x 10^{-1})

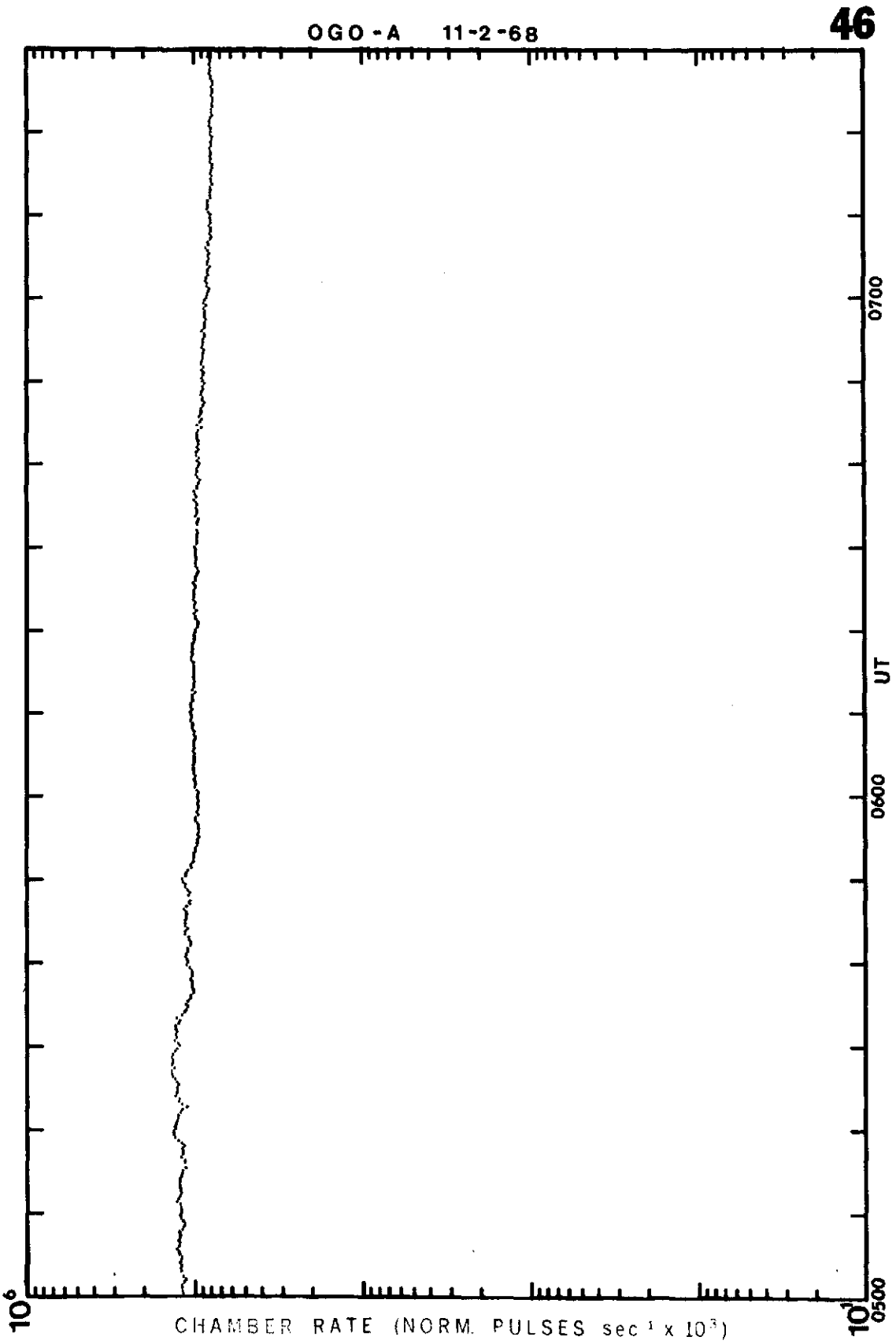
OGO-A 11-2-68
0700
UT
0600
0500
10^6
10^1
CHAMBER RATE (NORM. PULSES sec^{-1} x 10^3)

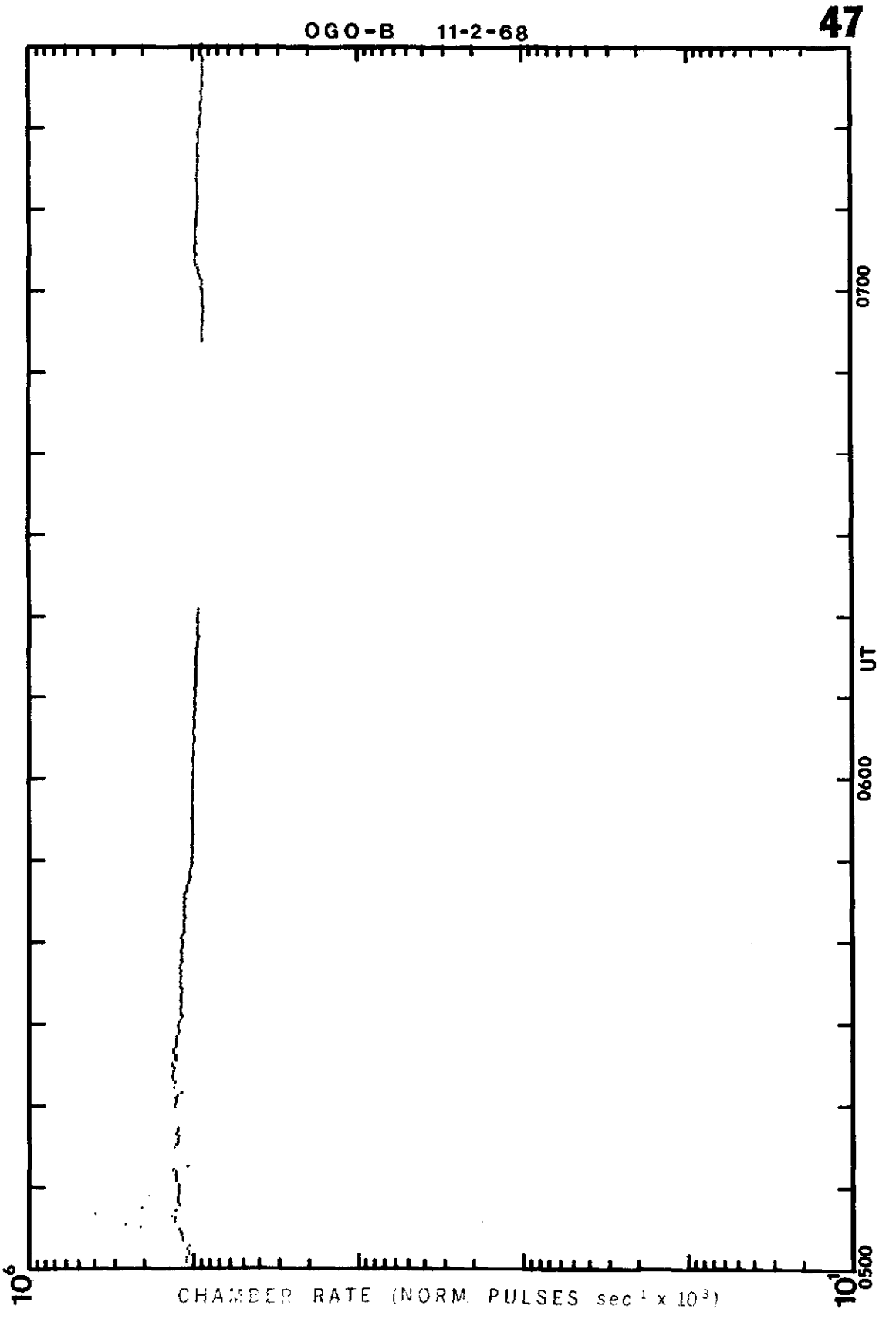
OGO-B 11-2-68
0700
UT
0600
0500
10^6
10^1
CHAMBER RATE (NORM. PULSES $sec^{-1} \times 10^3$)

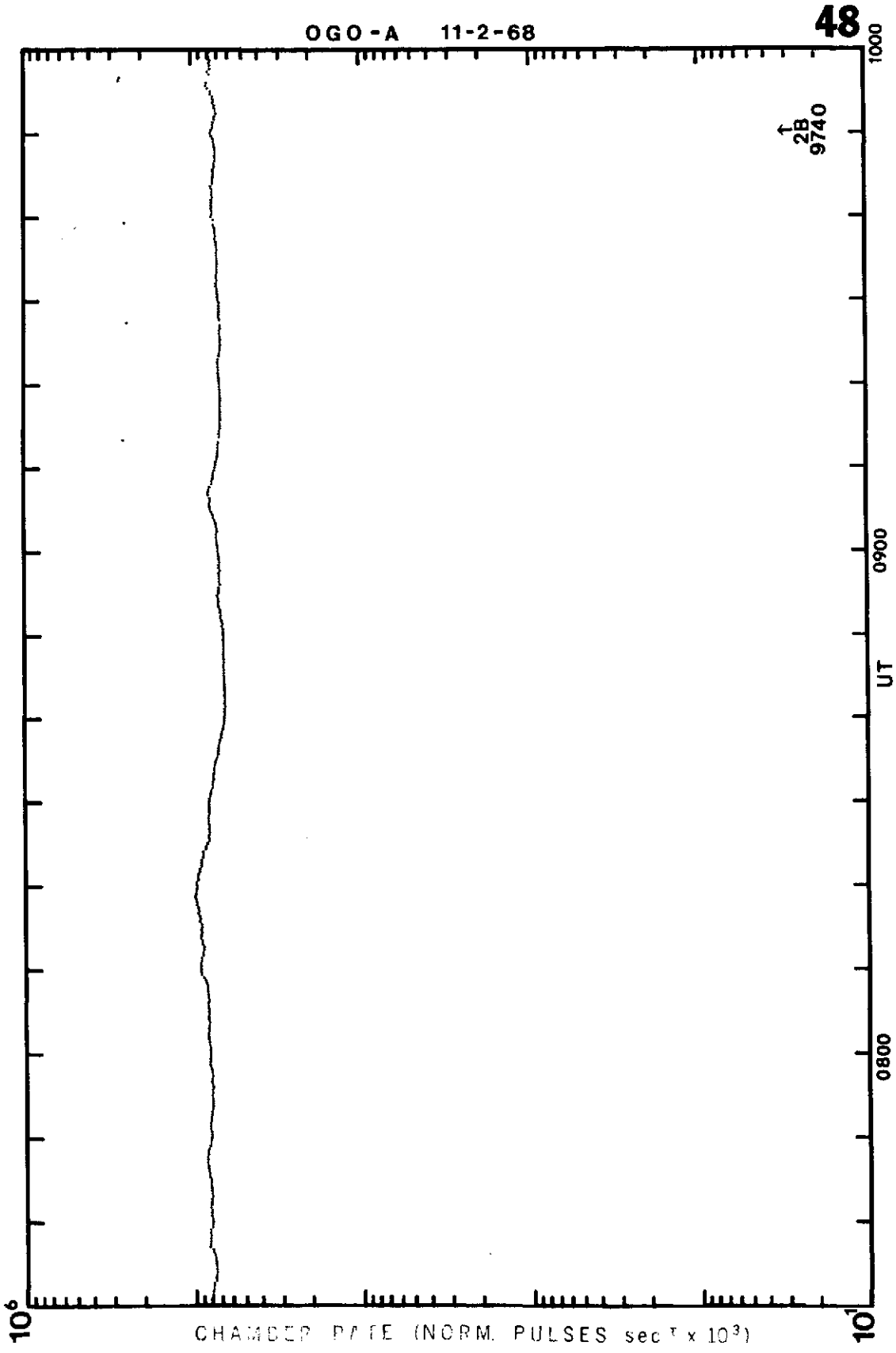
OGO-A 11-2-68
48
1000
0900
0800
UT
2B
9740
10^6
10^1
CHAMBER RATE (NORM. PULSES sec^{-1} x 10^3)

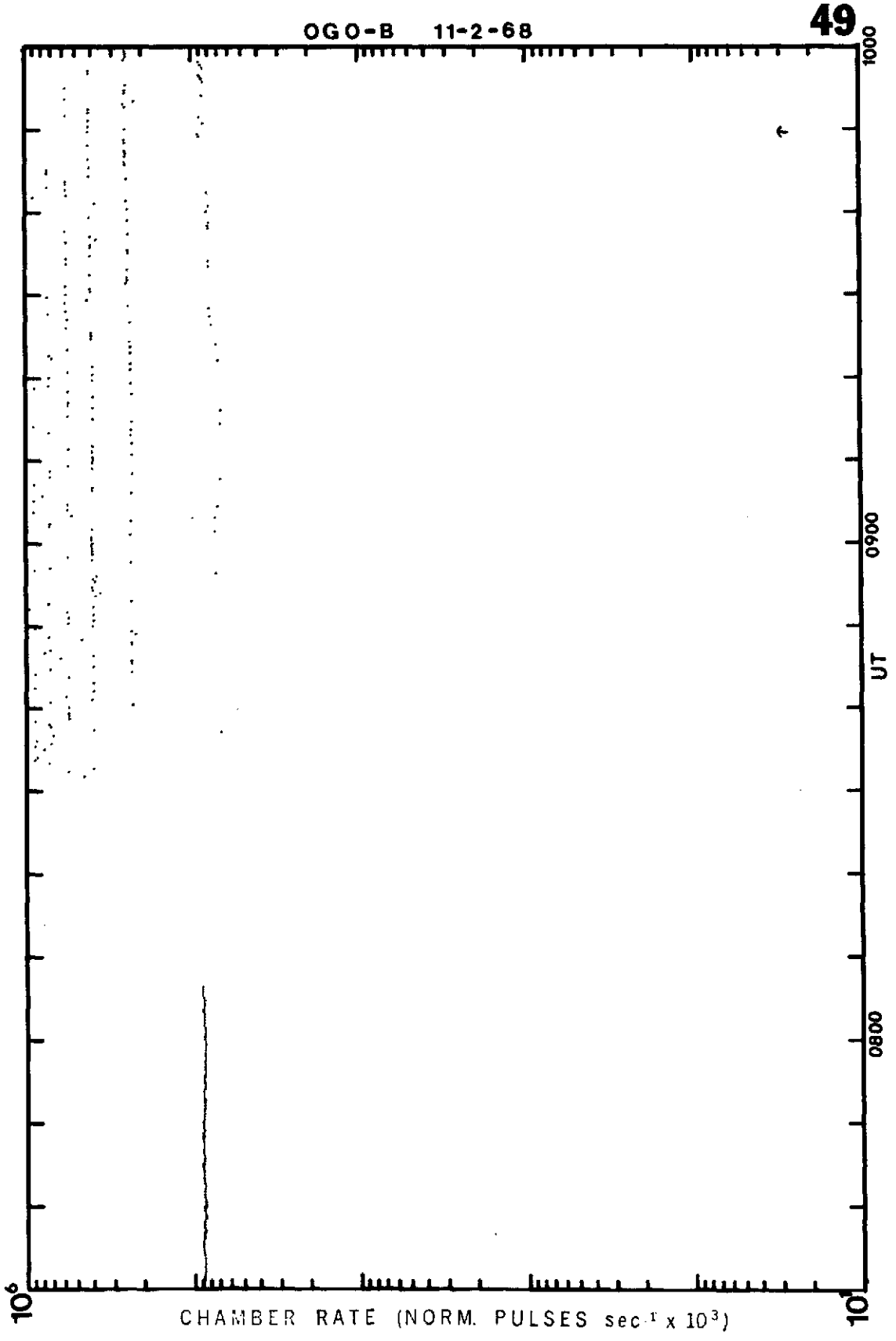
OGO-B 11-2-68
49
1000
0900
0800
UT
10^6
10^5
CHAMBER RATE (NORM. PULSES $sec^{-1} \times 10^3$)

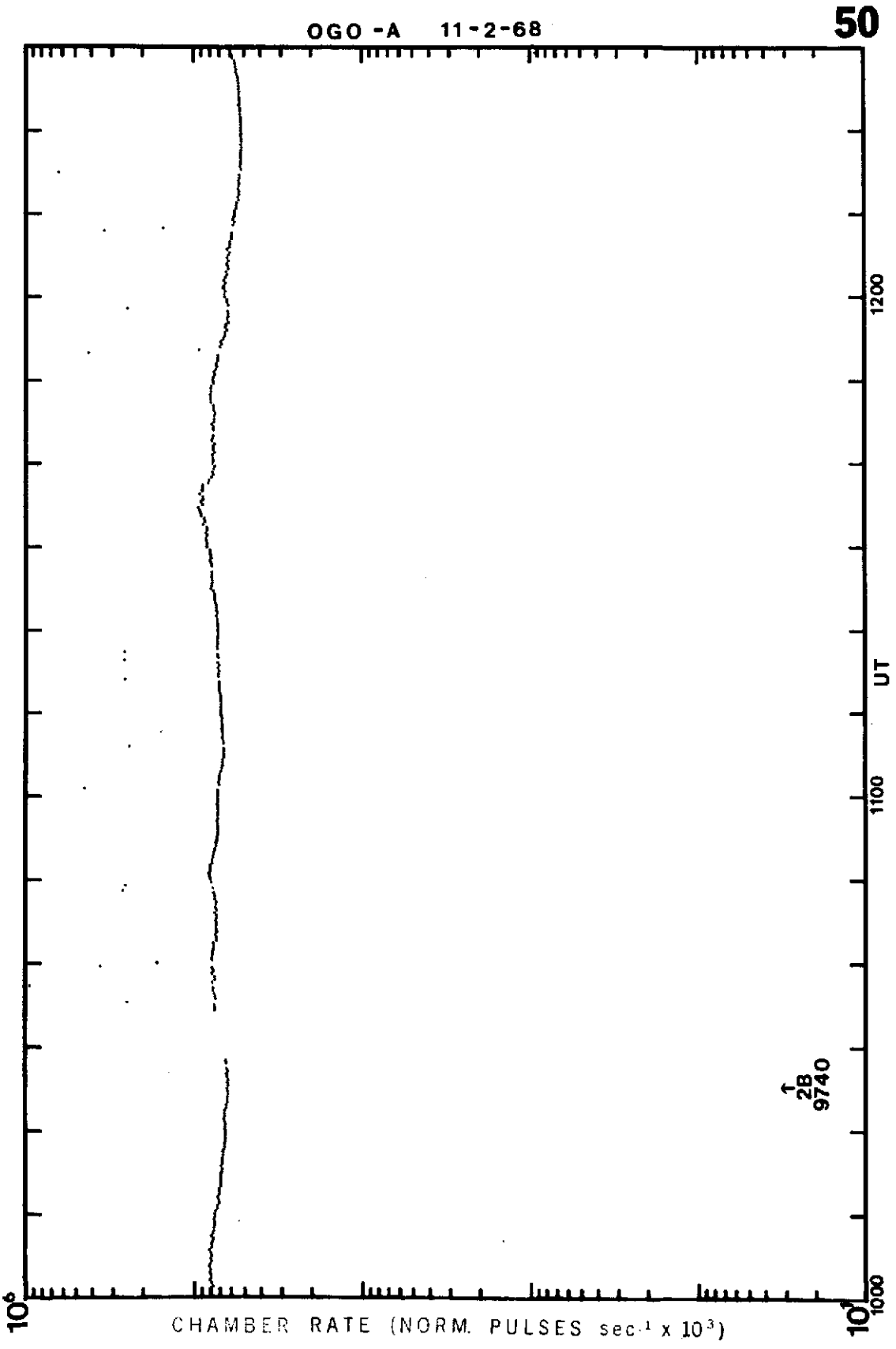
OGO -A 11-2-68
50
1200
UT
1100
1000
2B
9740
10^6
10^5
CHAMBER RATE (NORM. PULSES sec^{-1} x 10^3)

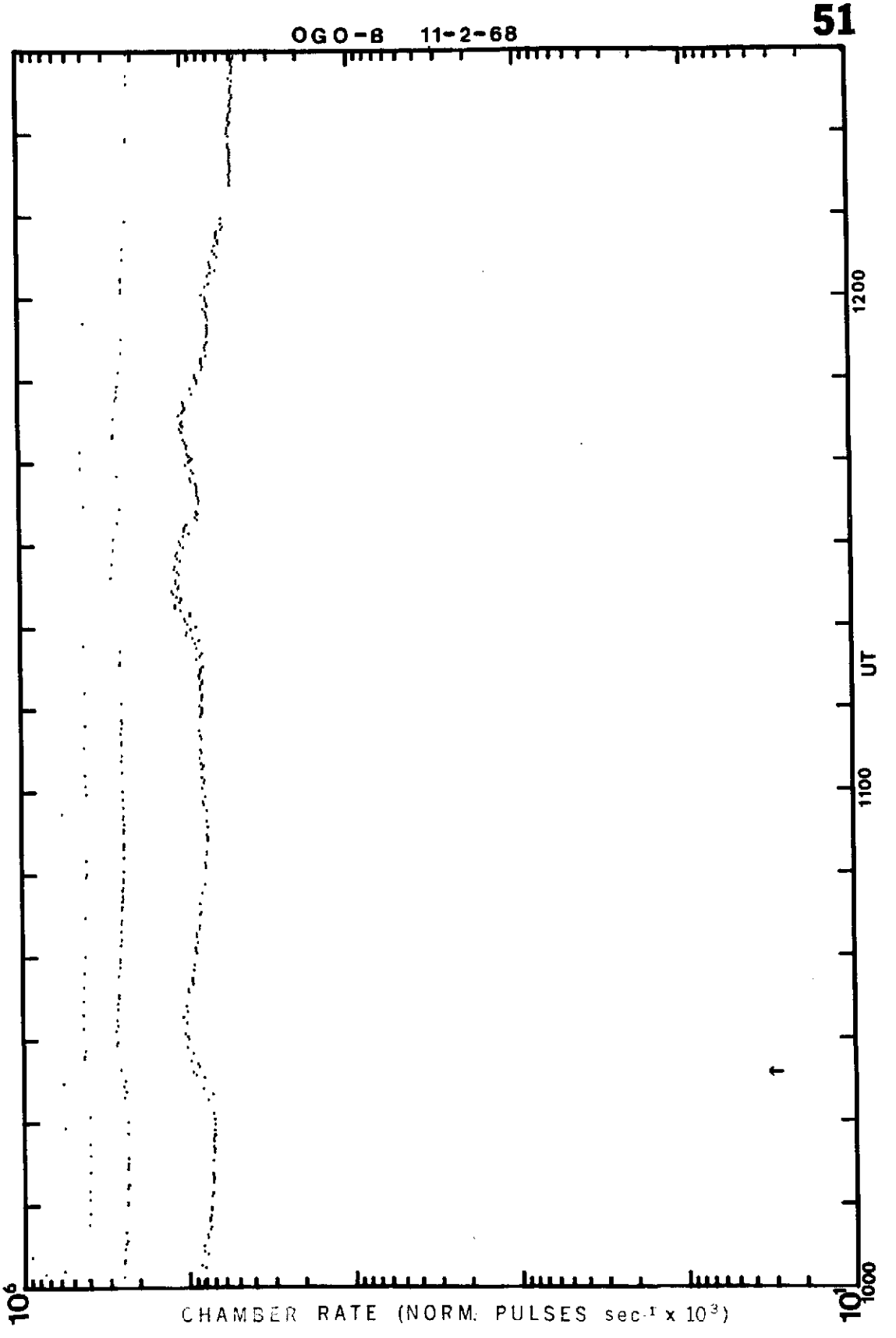
OGO-B 11-2-68
1200
UT
1100
1000
10^6
10^1
CHAMBER RATE (NORM. PULSES $sec^{-1} \times 10^3$)

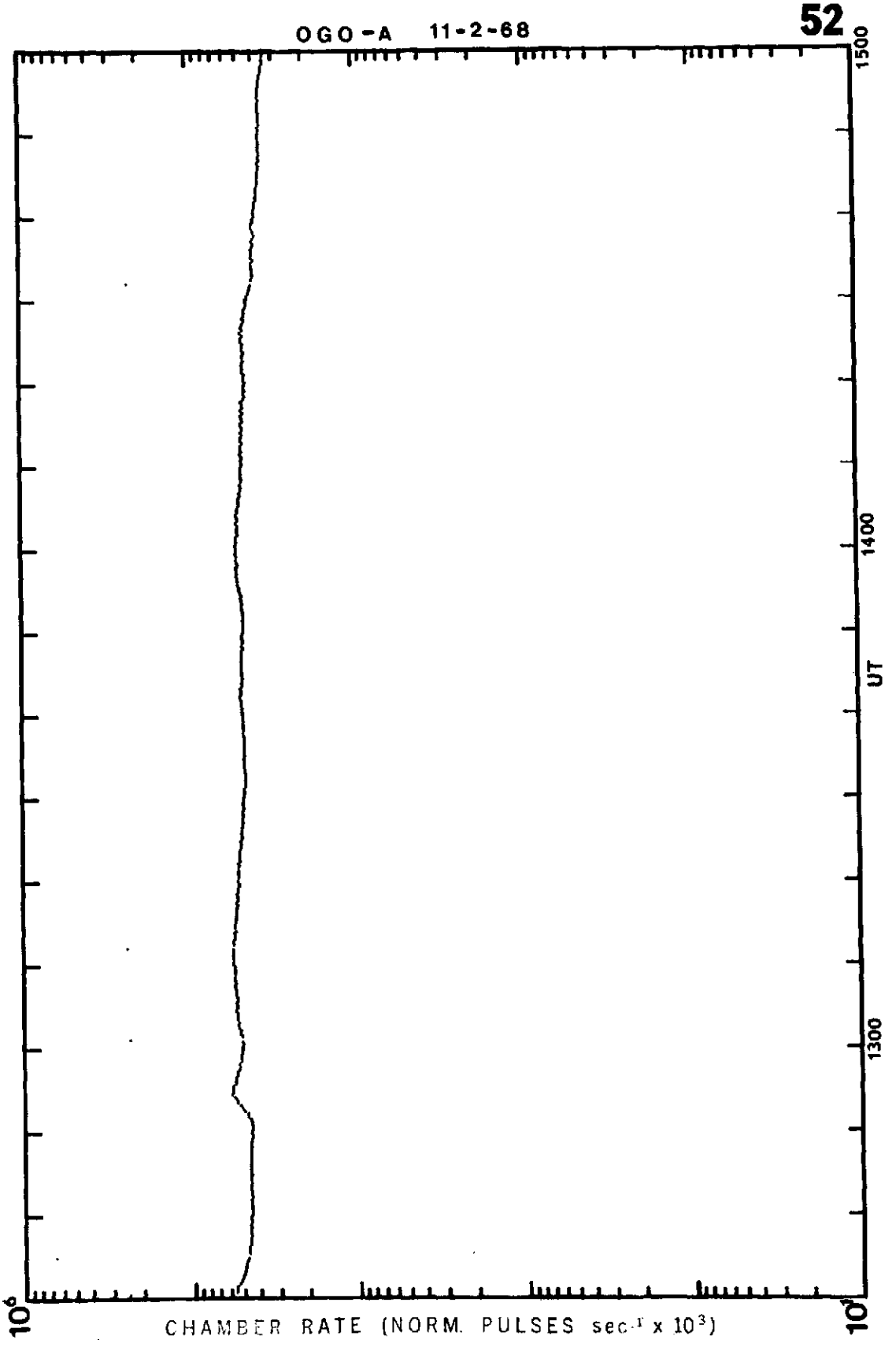
OGO-A 11-2-68
52
1500
1400
1300
UT
10^6
10^1
CHAMBER RATE (NORM. PULSES $sec^{-1} \times 10^3$)

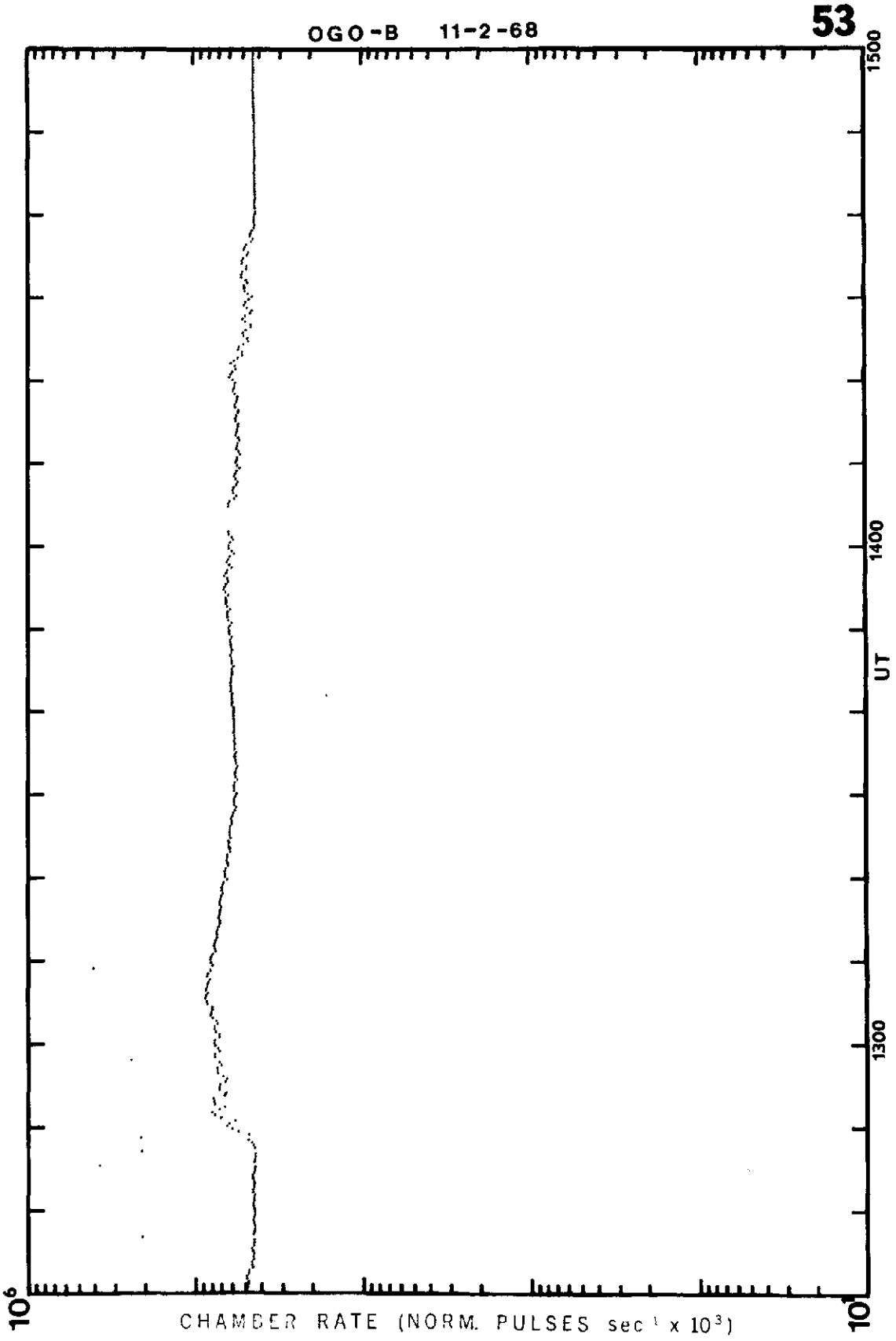
OGO-B 11-2-68
53
1500
1400
1300
UT
10^6
10^1
CHAMBER RATE (NORM. PULSES sec^{-1} x 10^3)

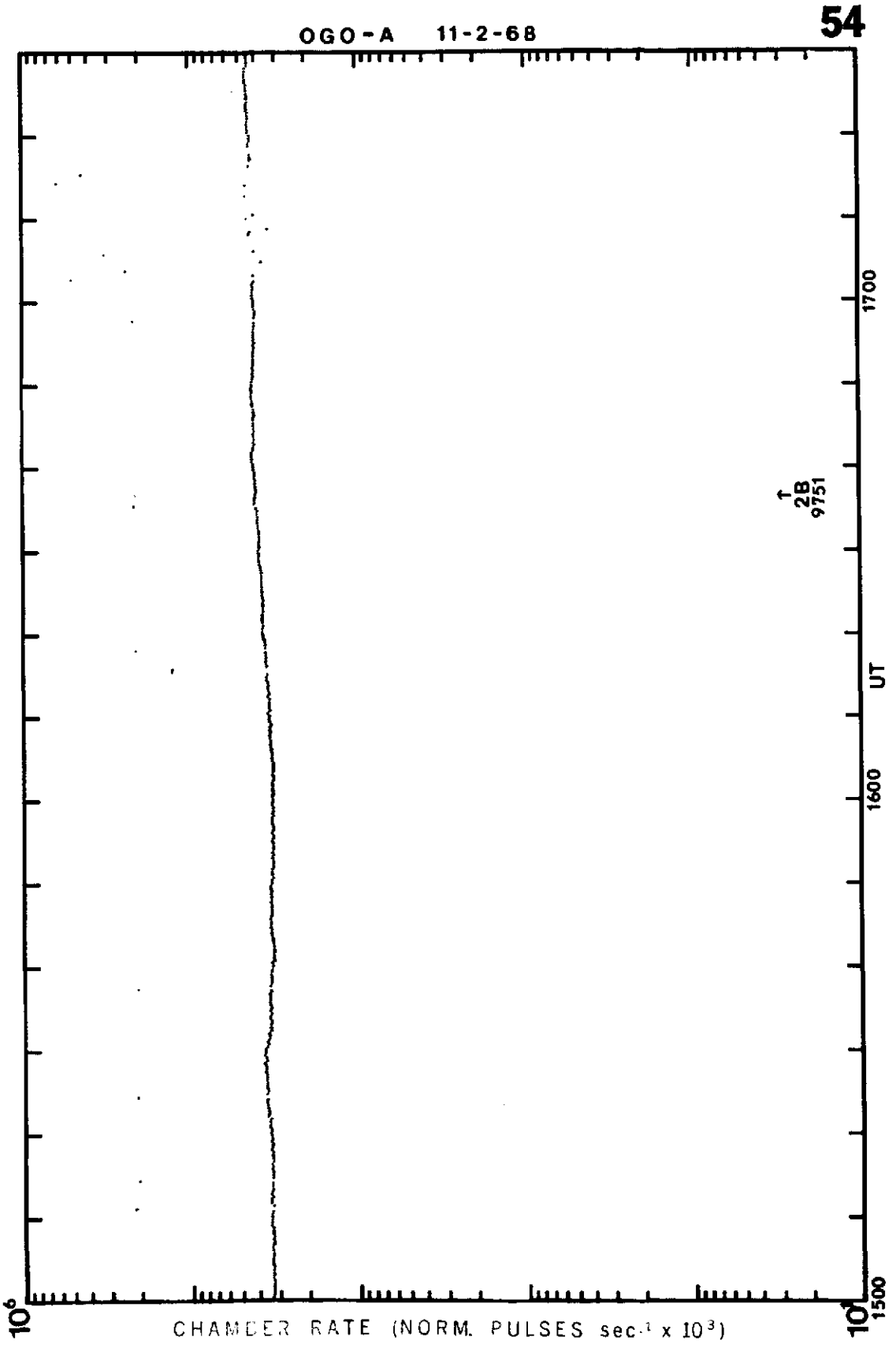
54
OGO-A 11-2-68
1700
1600
1500
UT
2B
9751
10^6
10^4
CHAMBER RATE (NORM. PULSES sec^{-1} x 10^3)

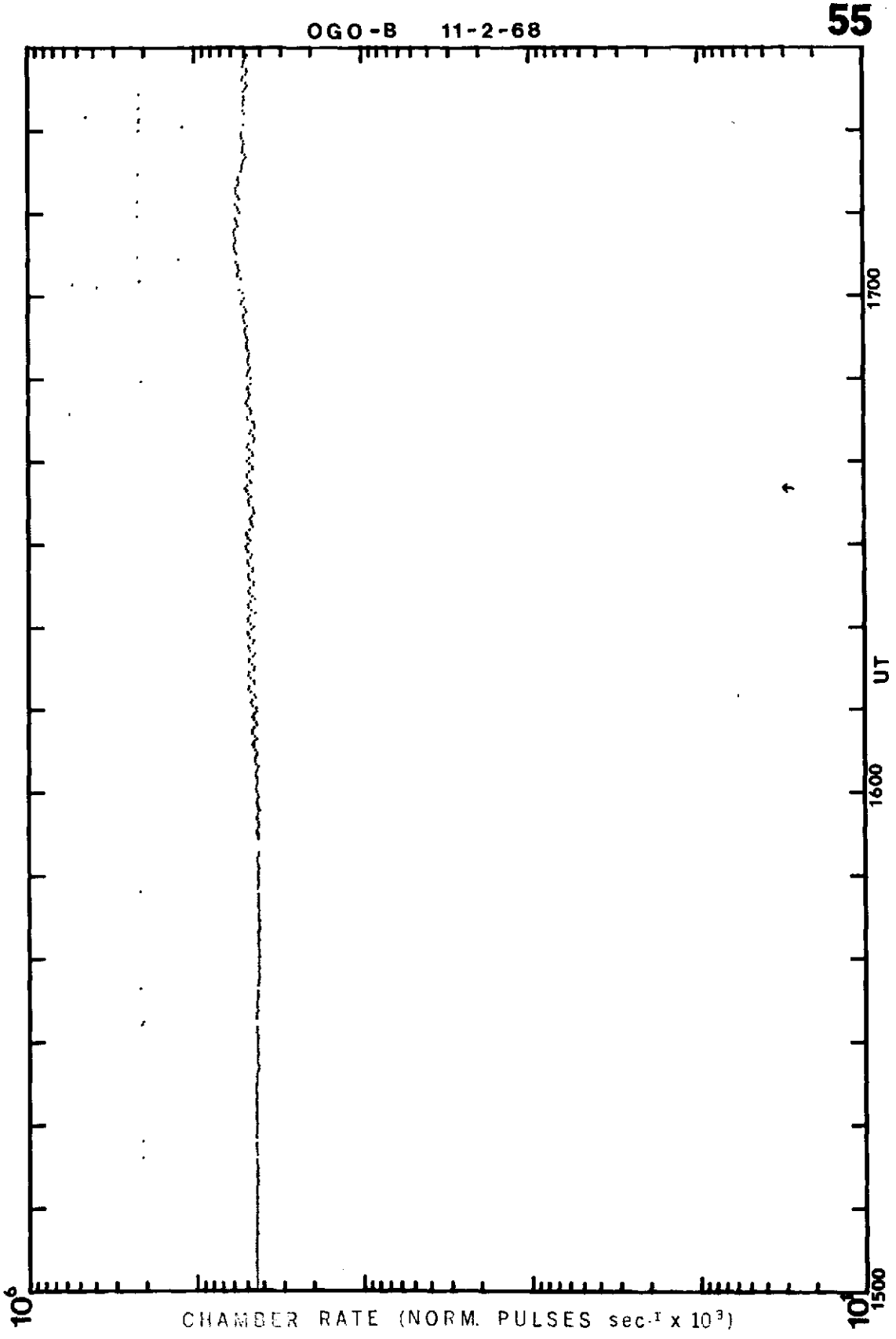
OGO-B 11-2-68
1700
1600
1500
UT
10^6
10^1
CHAMBER RATE (NORM. PULSES $sec^{-1} \times 10^3$)

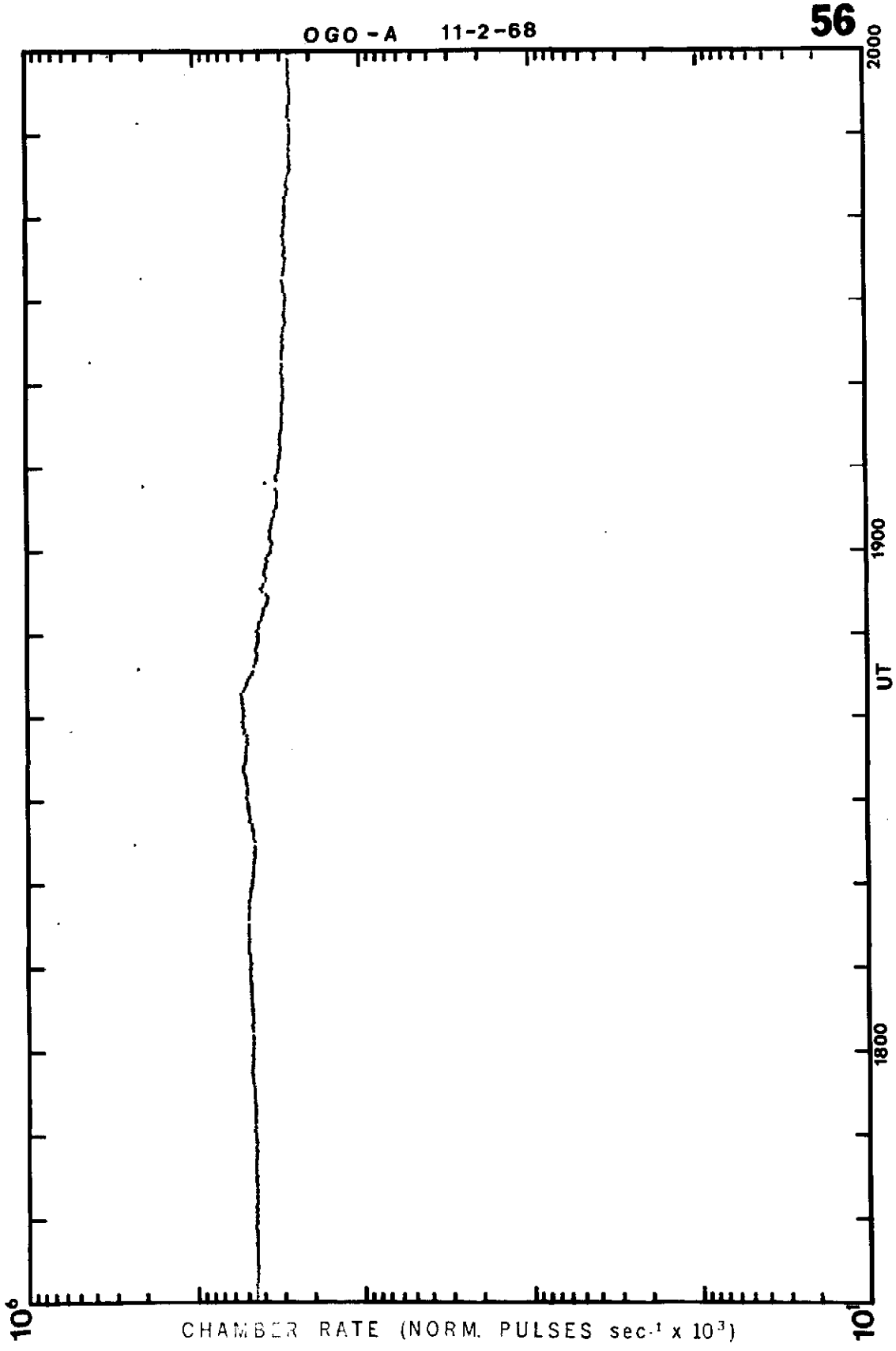
OGO - A 11-2-68
56
2000
1900
1800
UT
10^0
10^1
CHAMBER RATE (NORM. PULSES sec^{-1} x 10^3)

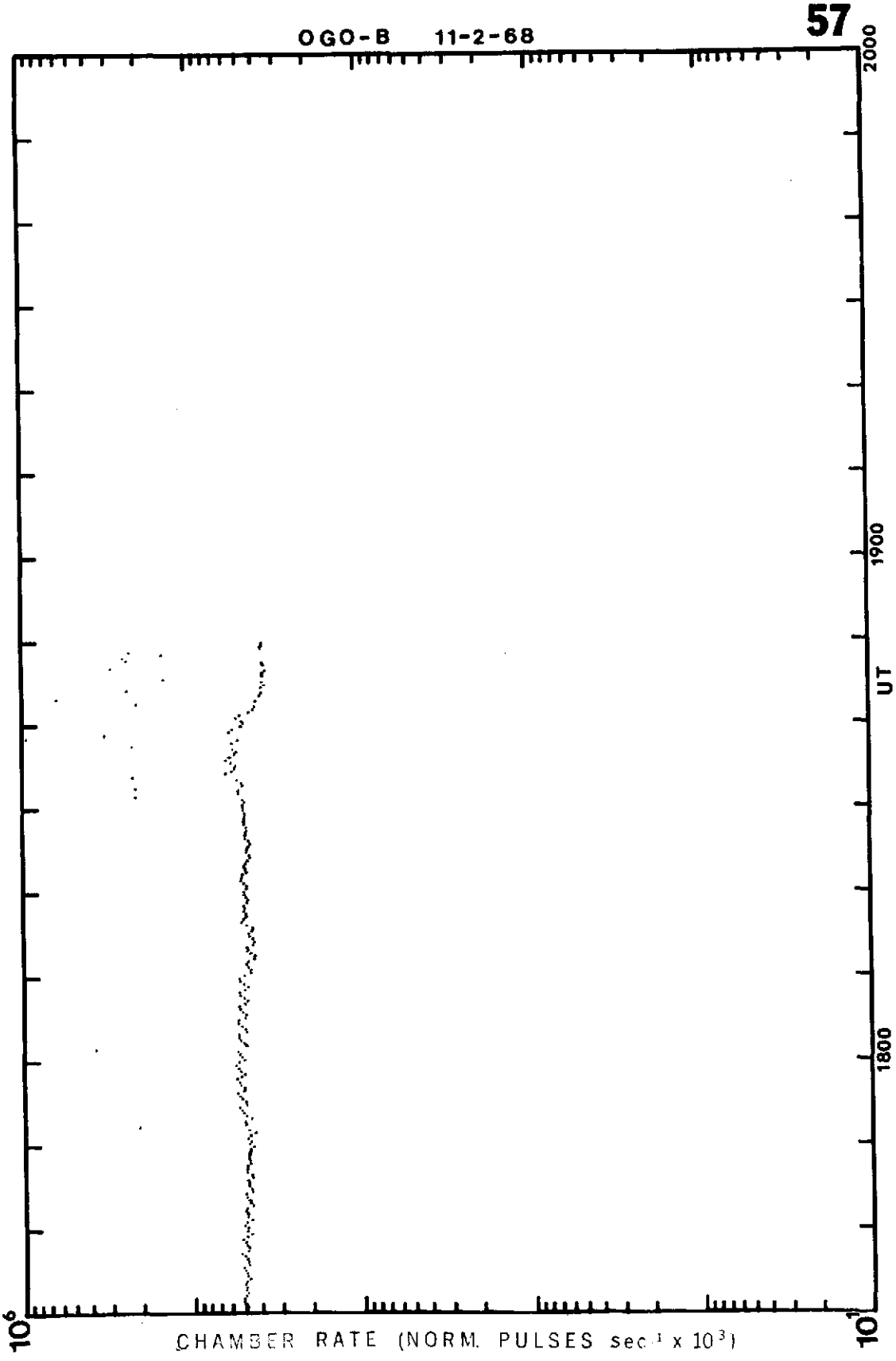
OGO-B 11-2-68
2000
1900
1800
UT
10^6
10^1
CHAMBER RATE (NORM. PULSES $sec^{-1} \times 10^3$)

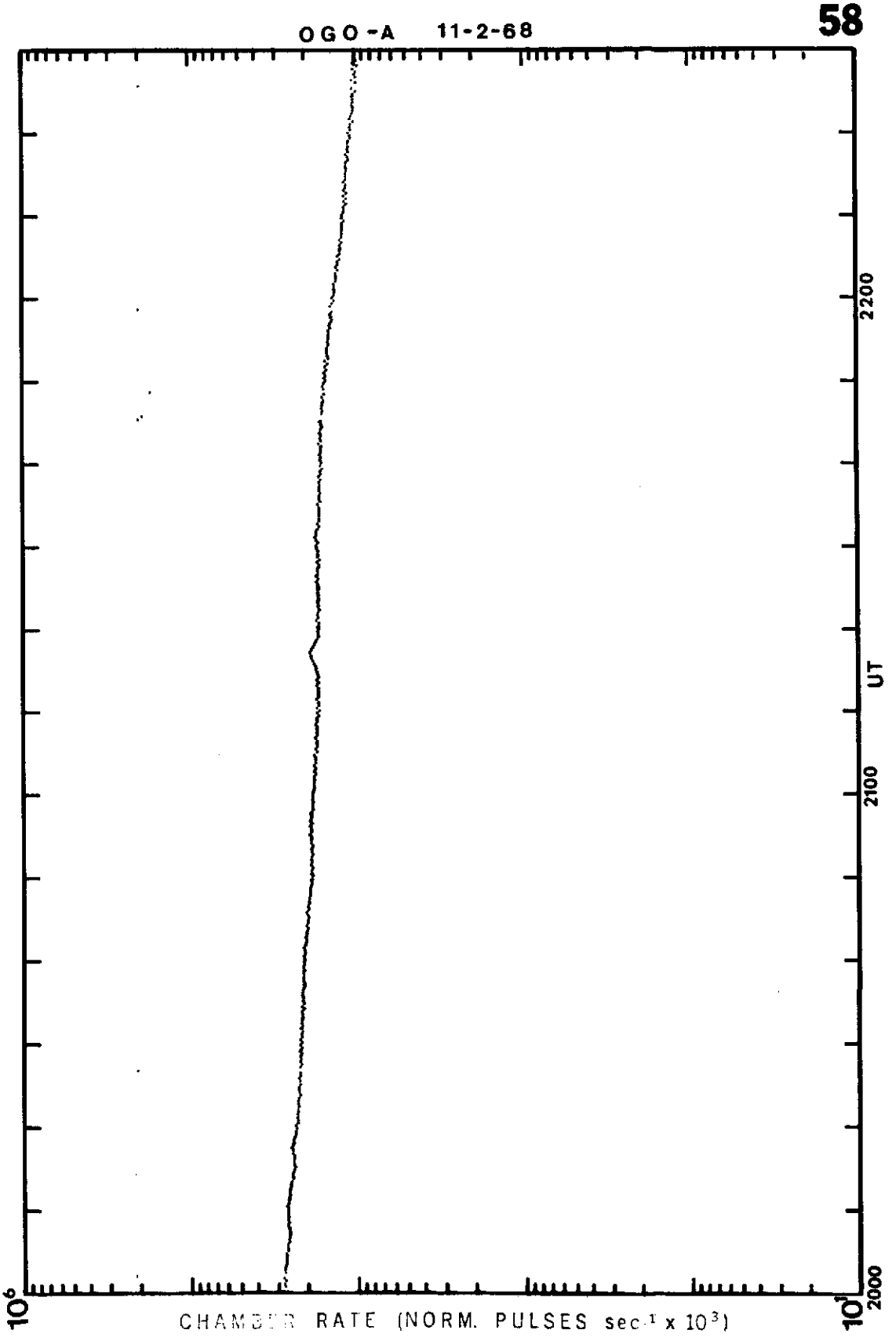
OGO-A 11-2-68
2200
2100
2000
UT
10^0
10^1
CHAMBER RATE (NORM. PULSES $sec^{-1} \times 10^3$)

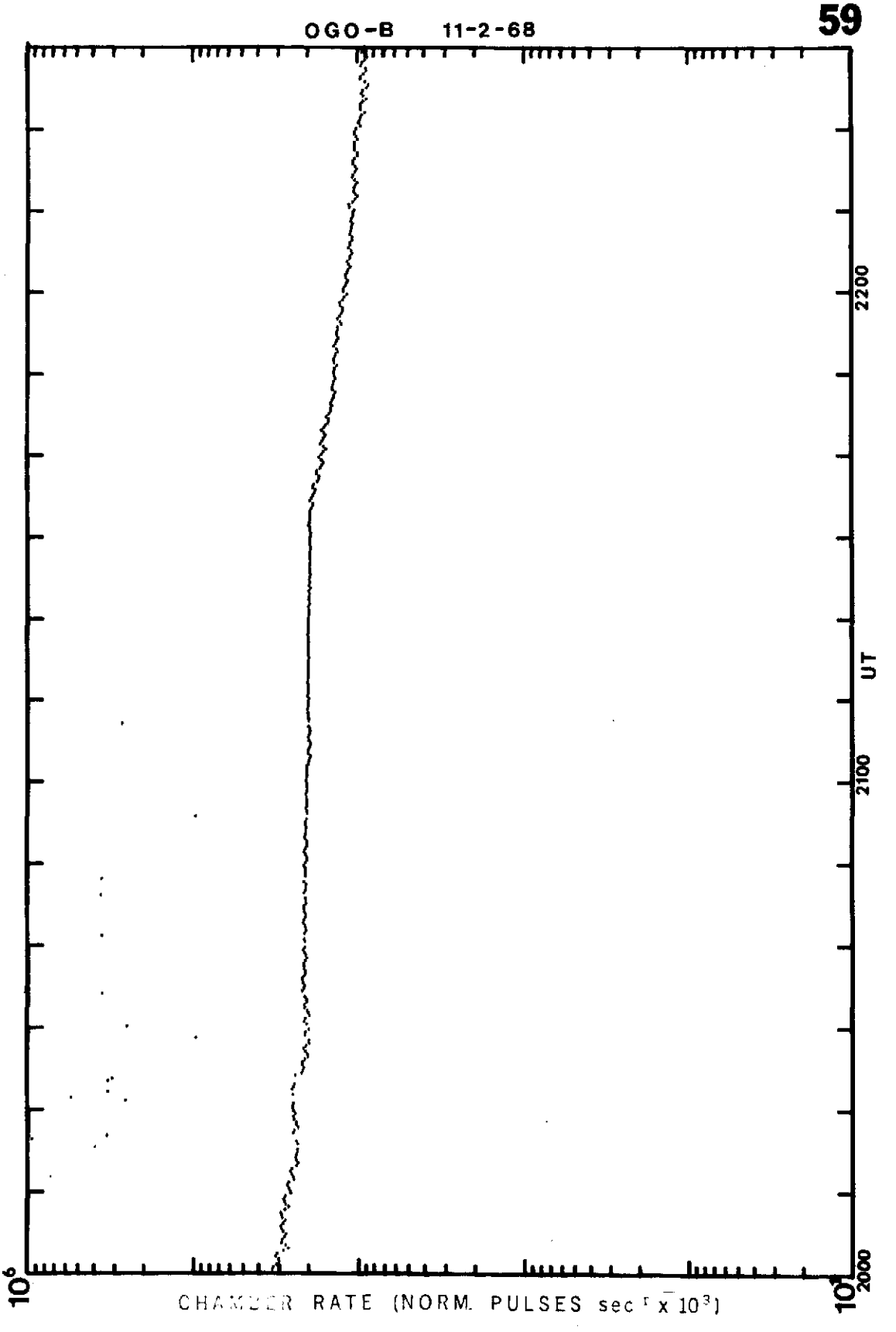
OGO-B 11-2-68
2200
2100
2000
UT
10^6
10^4
CHAMBER RATE (NORM. PULSES sec^{-1} x 10^3)

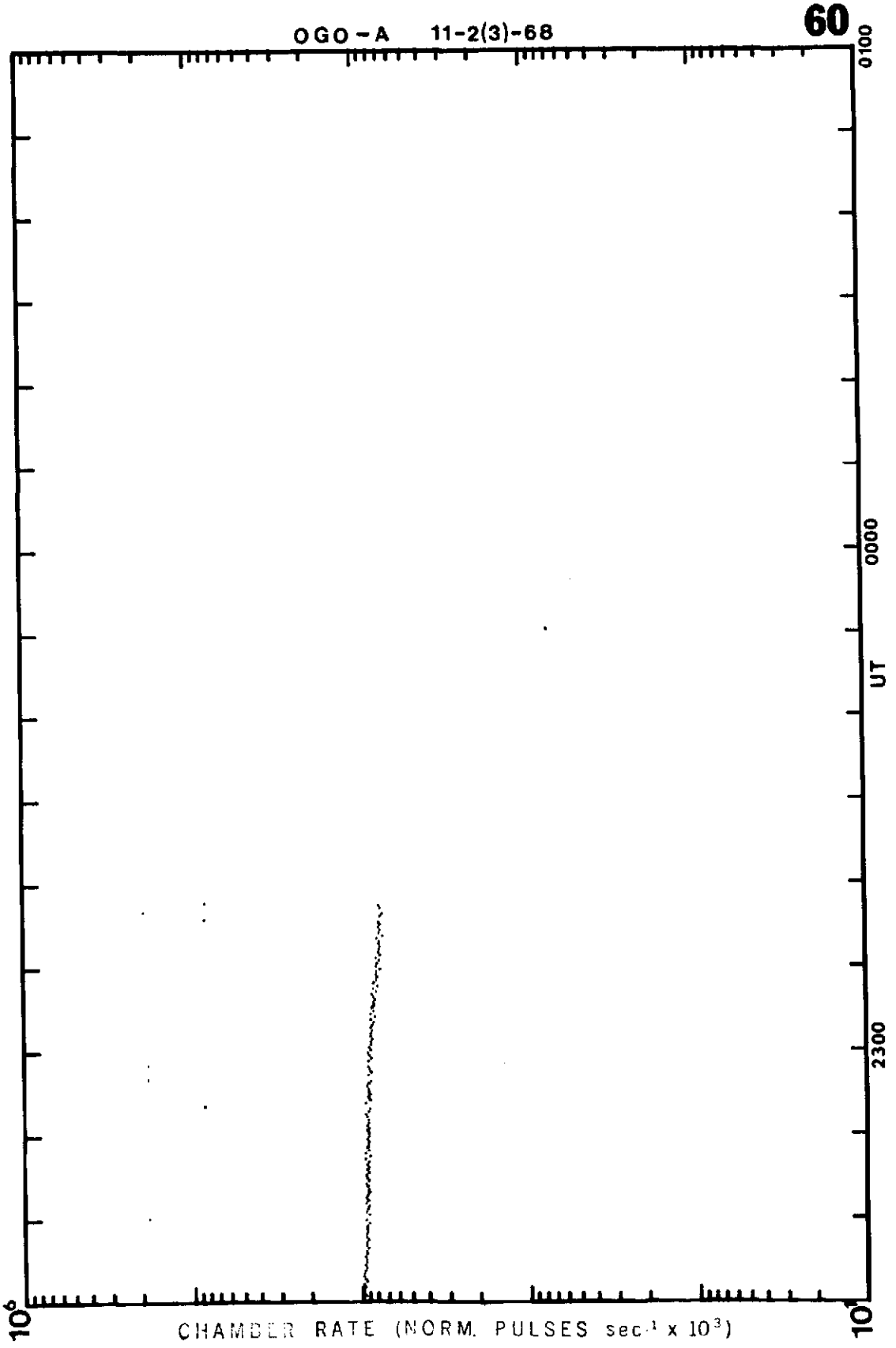
OGO - A 11-2(3)-68
60
0100
0000
UT
2300
10^6
10^5
CHAMBER RATE (NORM. PULSES $sec^{-1} \times 10^3$)

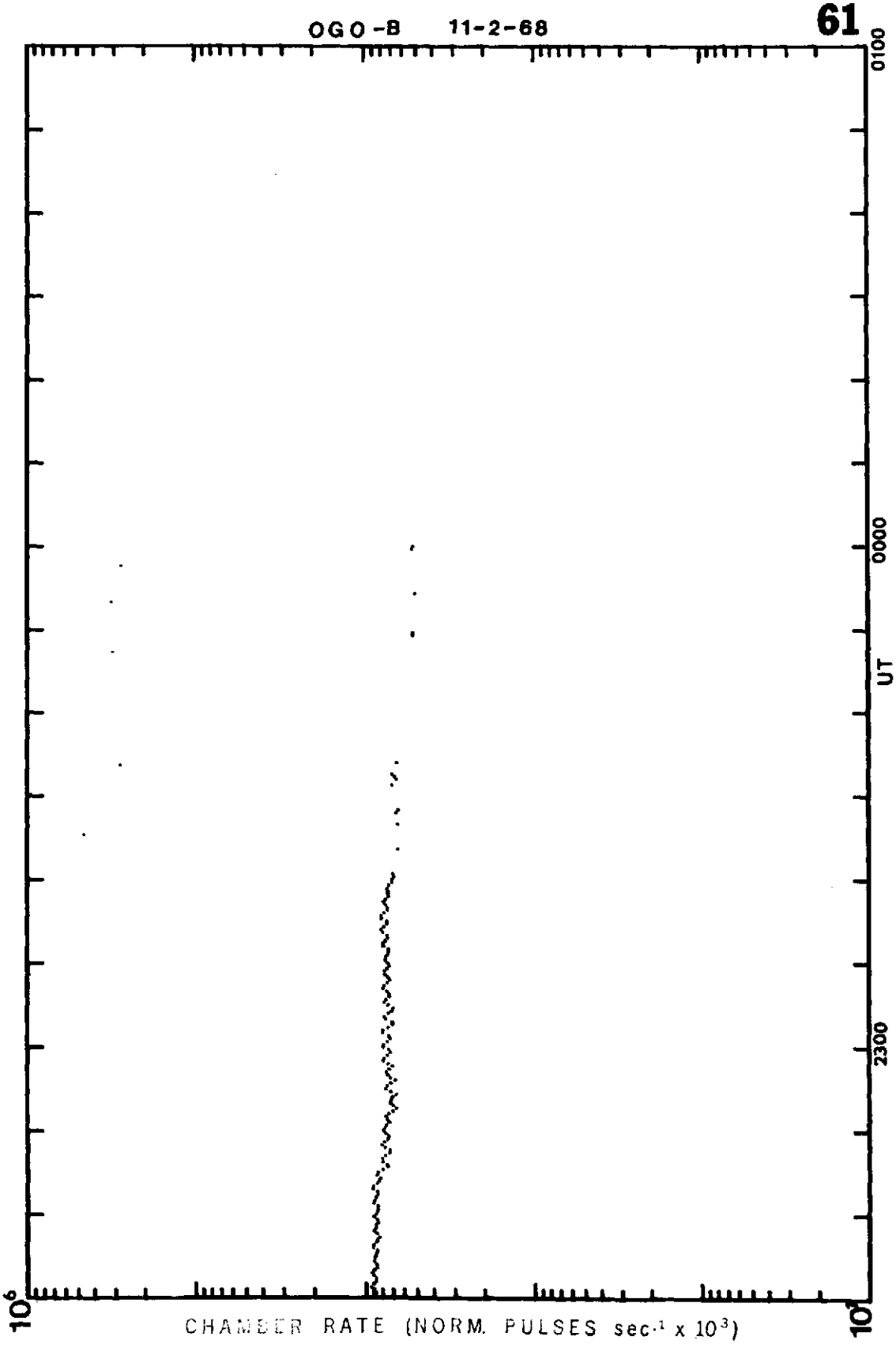
OGO-B 11-2-68
0100
0000
2300
UT
10^6
10^1
CHAMBER RATE (NORM. PULSES $sec^{-1} \times 10^3$)

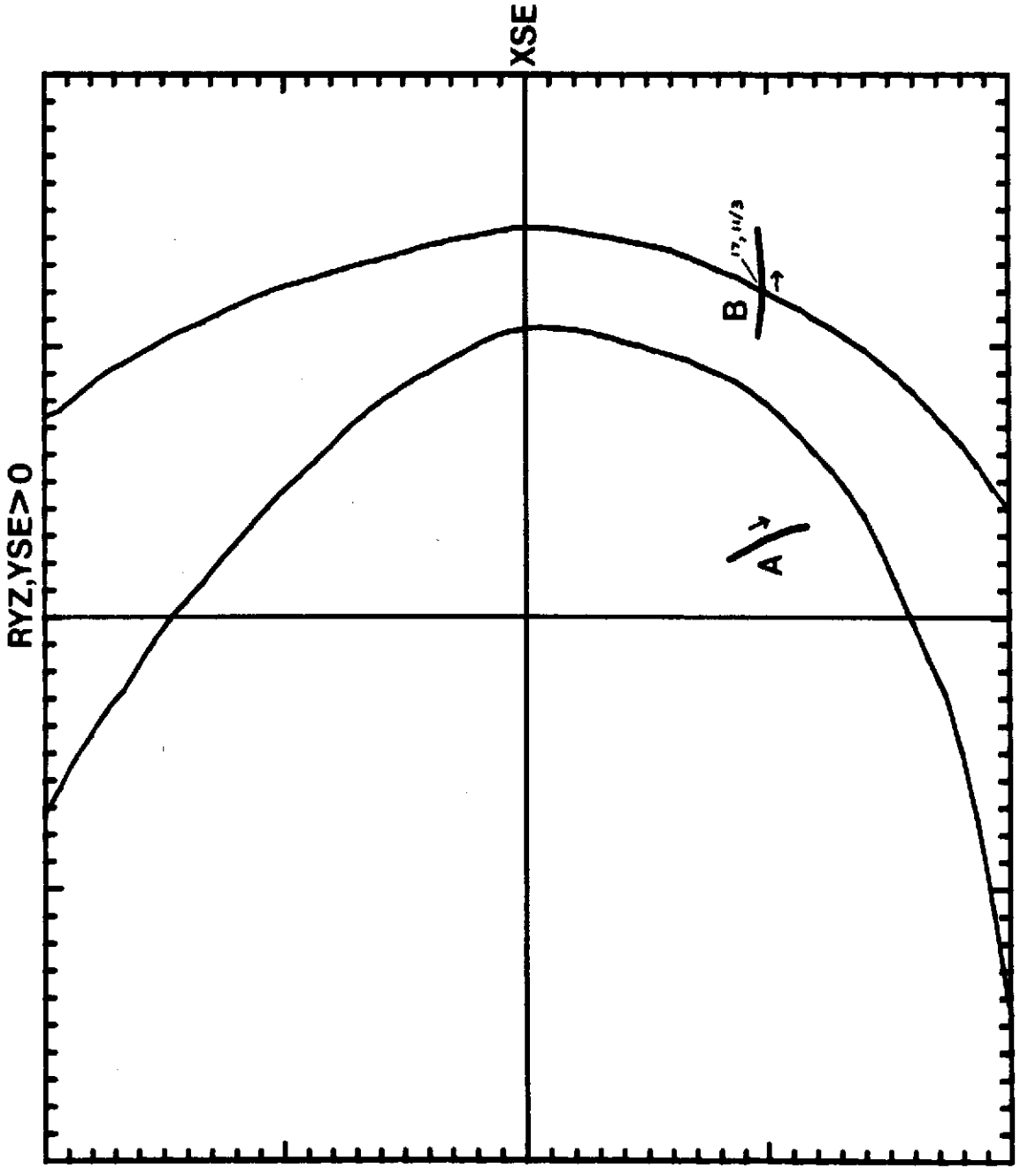
XSE
RYZ,YSE>0
B
A

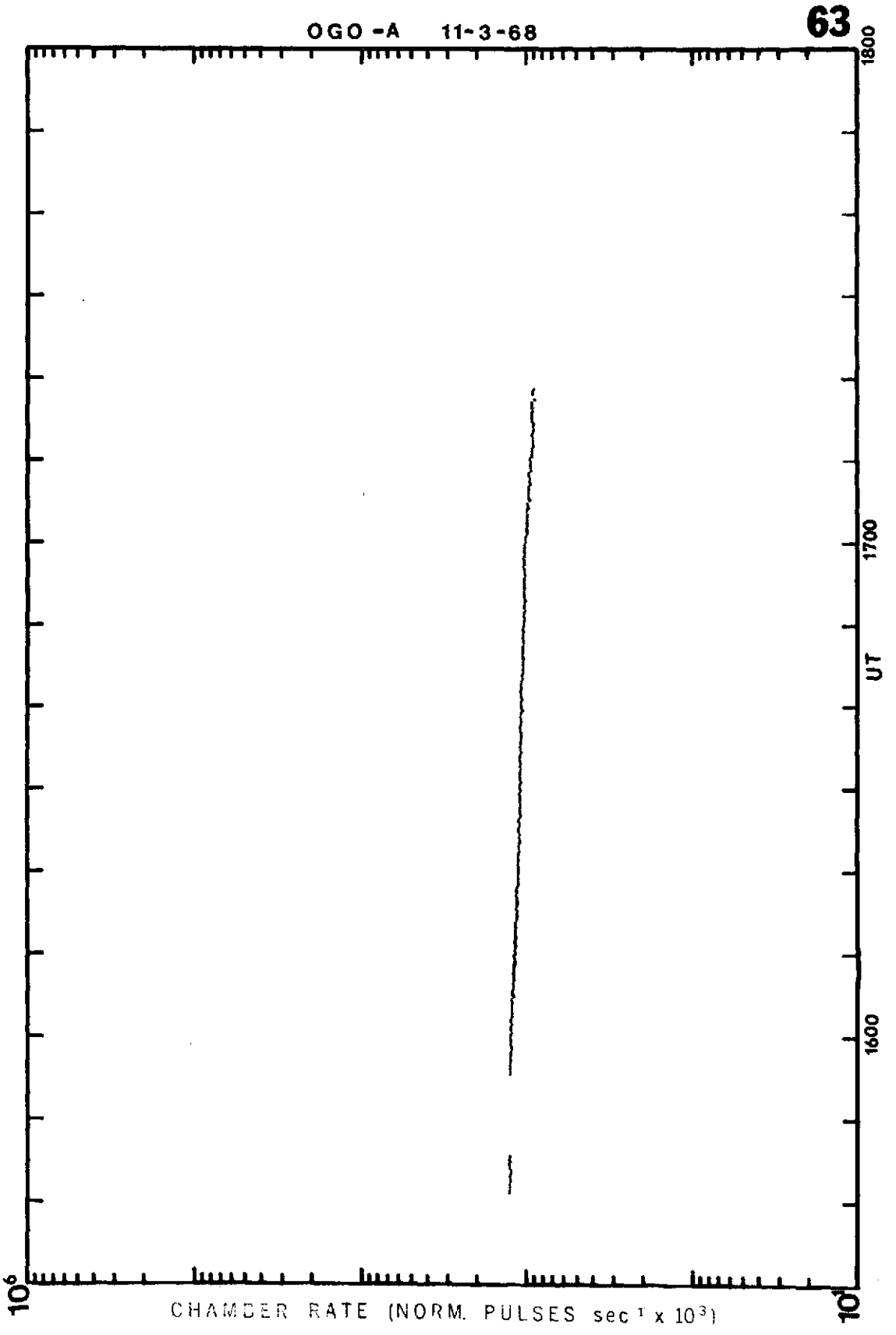
OGO -A 11-3-68
63
1800
1700
1600
UT
10^6
10^5
CHAMBER RATE (NORM. PULSES $sec^{-1} \times 10^3$)

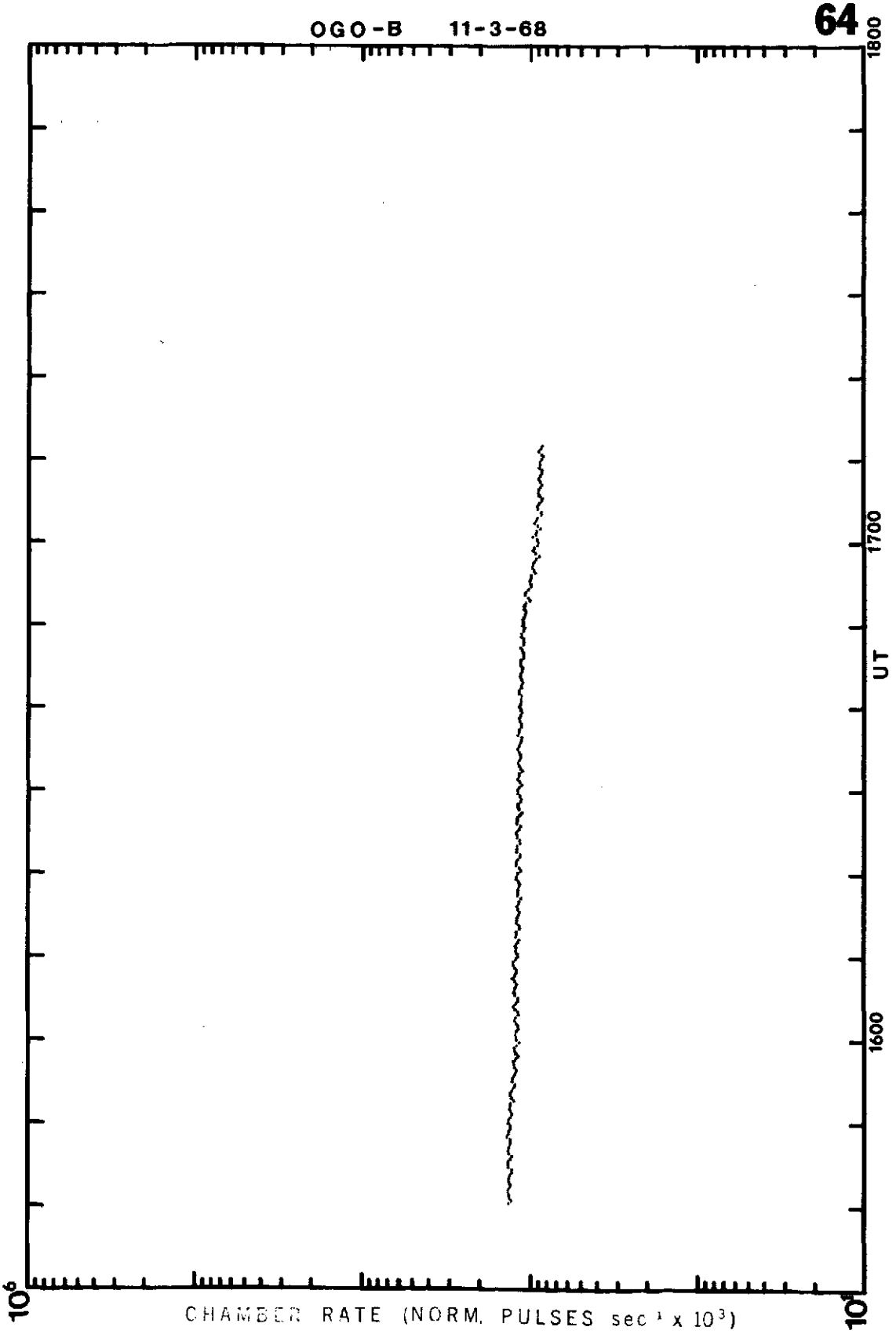
OGO-B 11-3-68
64
1800
1700
1600
UT
10^6
10^5
CHAMBER RATE (NORM. PULSES sec^{-1} x 10^3)

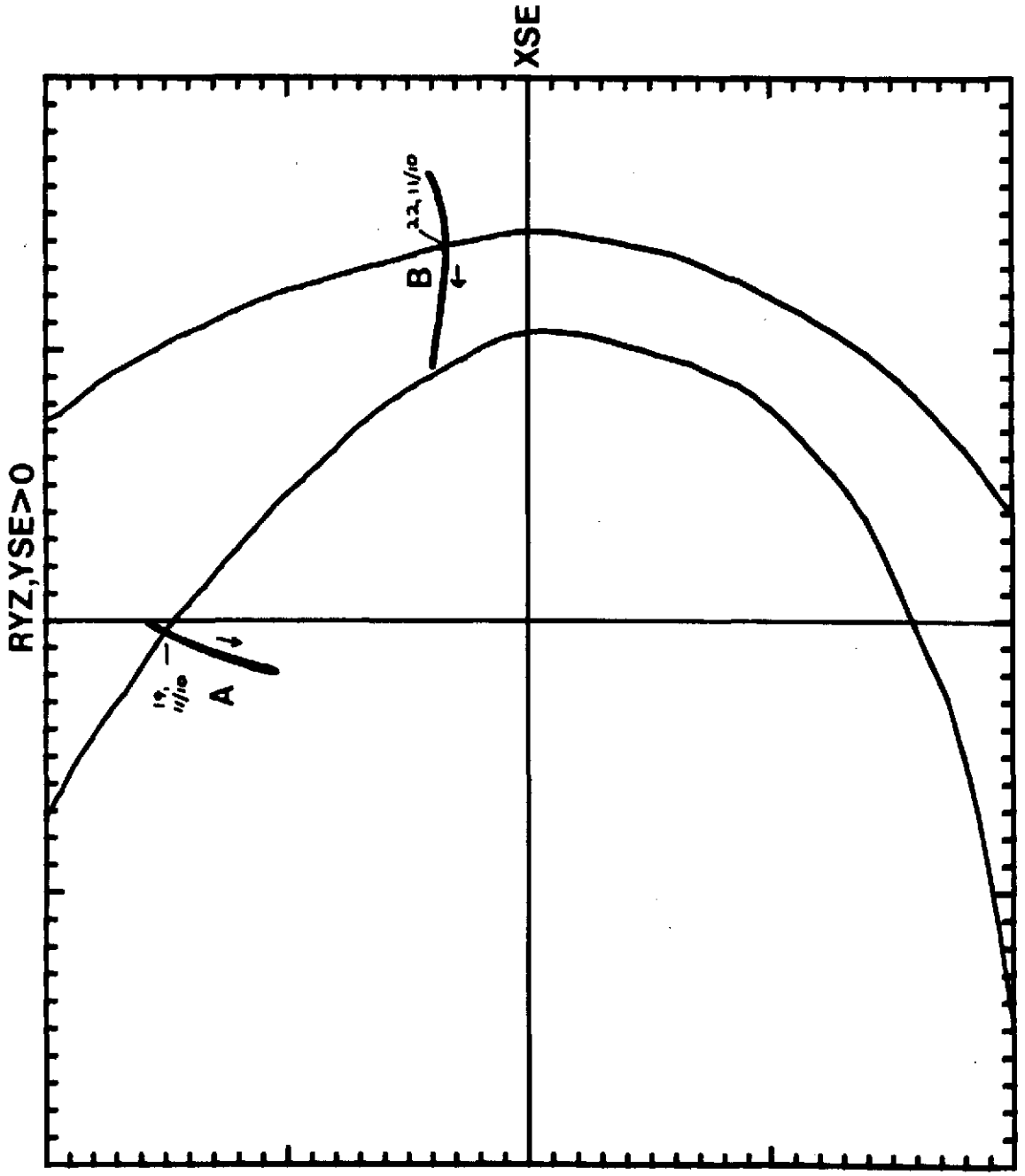
XSE
RYZ,YSE>0
B
A

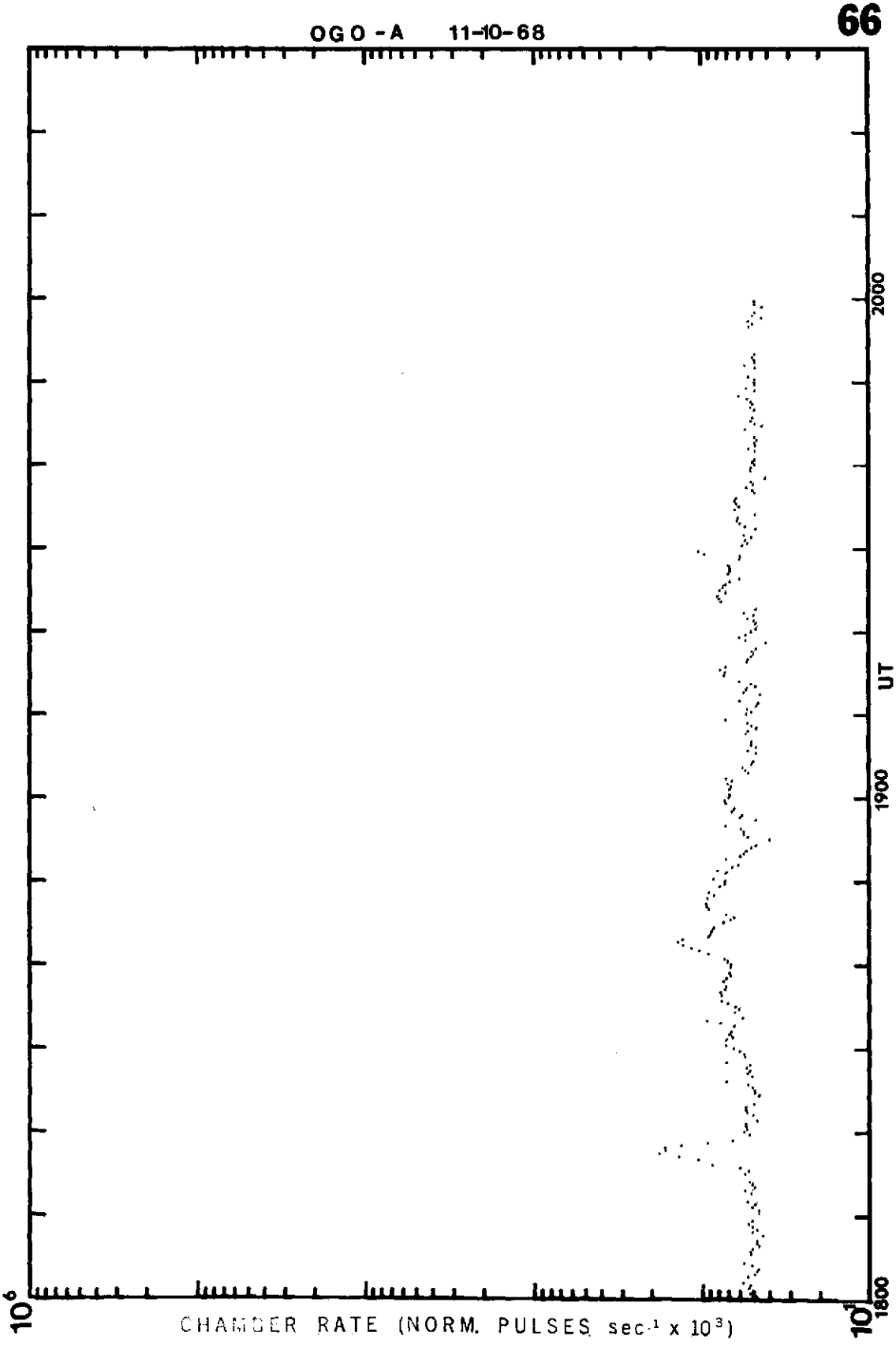
OGO - A 11-10-68
2000
1900
1800
UT
10^6
10^5
CHAMBER RATE (NORM. PULSES $sec^{-1} \times 10^3$)

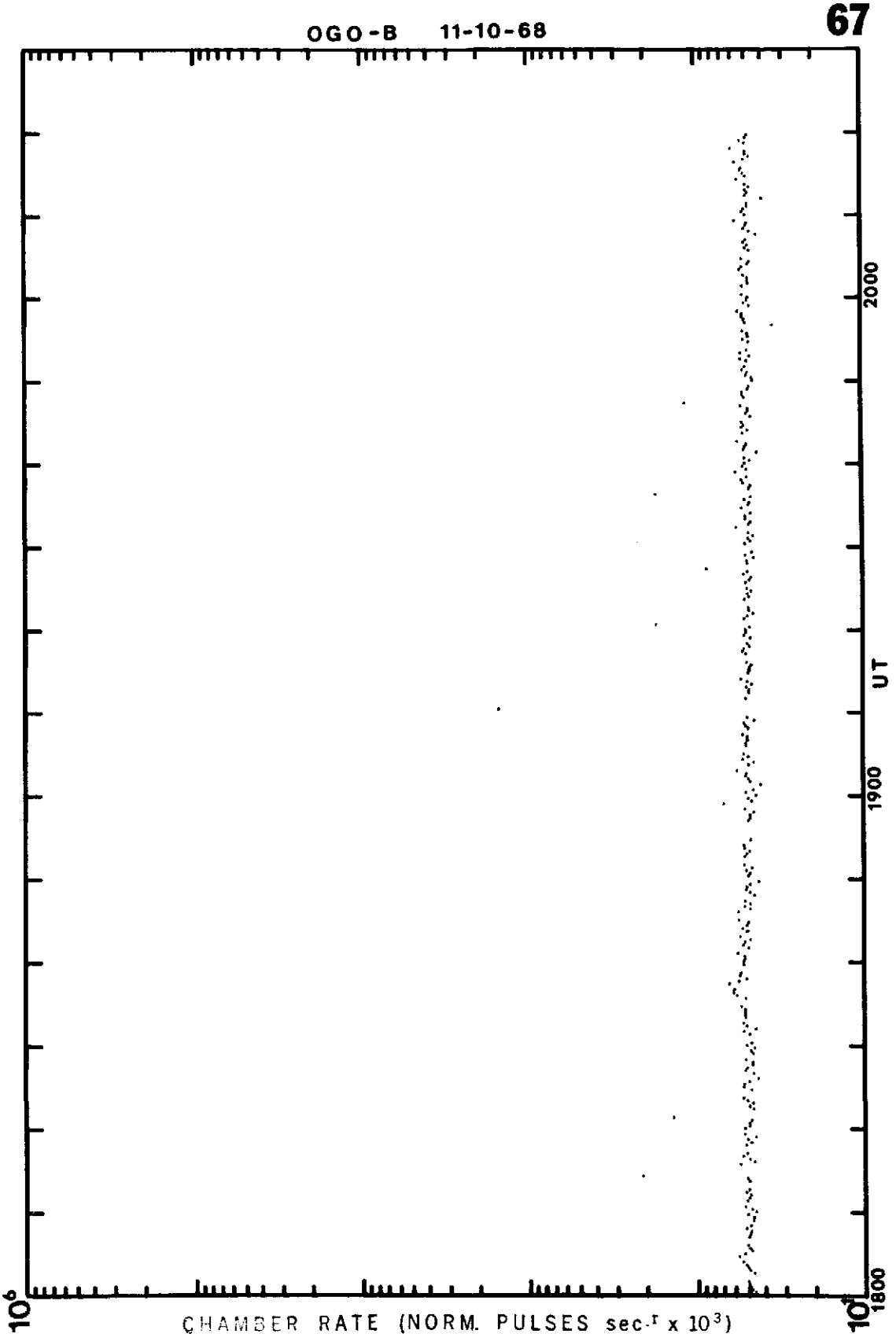
OGO-B 11-10-68
2000
1900
1800
UT
10^6
10^4
CHAMBER RATE (NORM. PULSES sec^{-1} x 10^3)

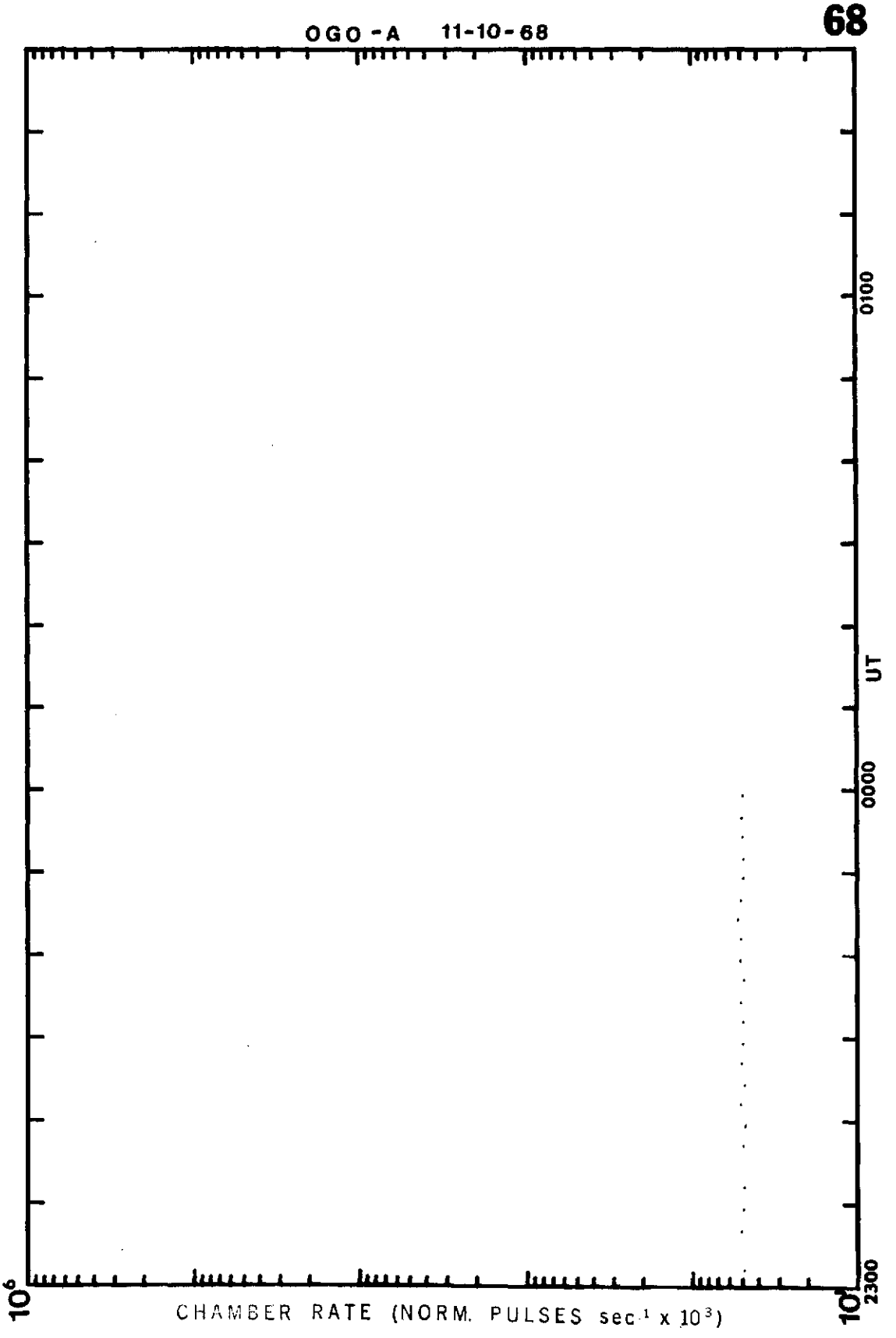
OGO-A 11-10-68
0100
UT
0000
2300
10^6
10^5
CHAMBER RATE (NORM. PULSES $sec^{-1} \times 10^3$)

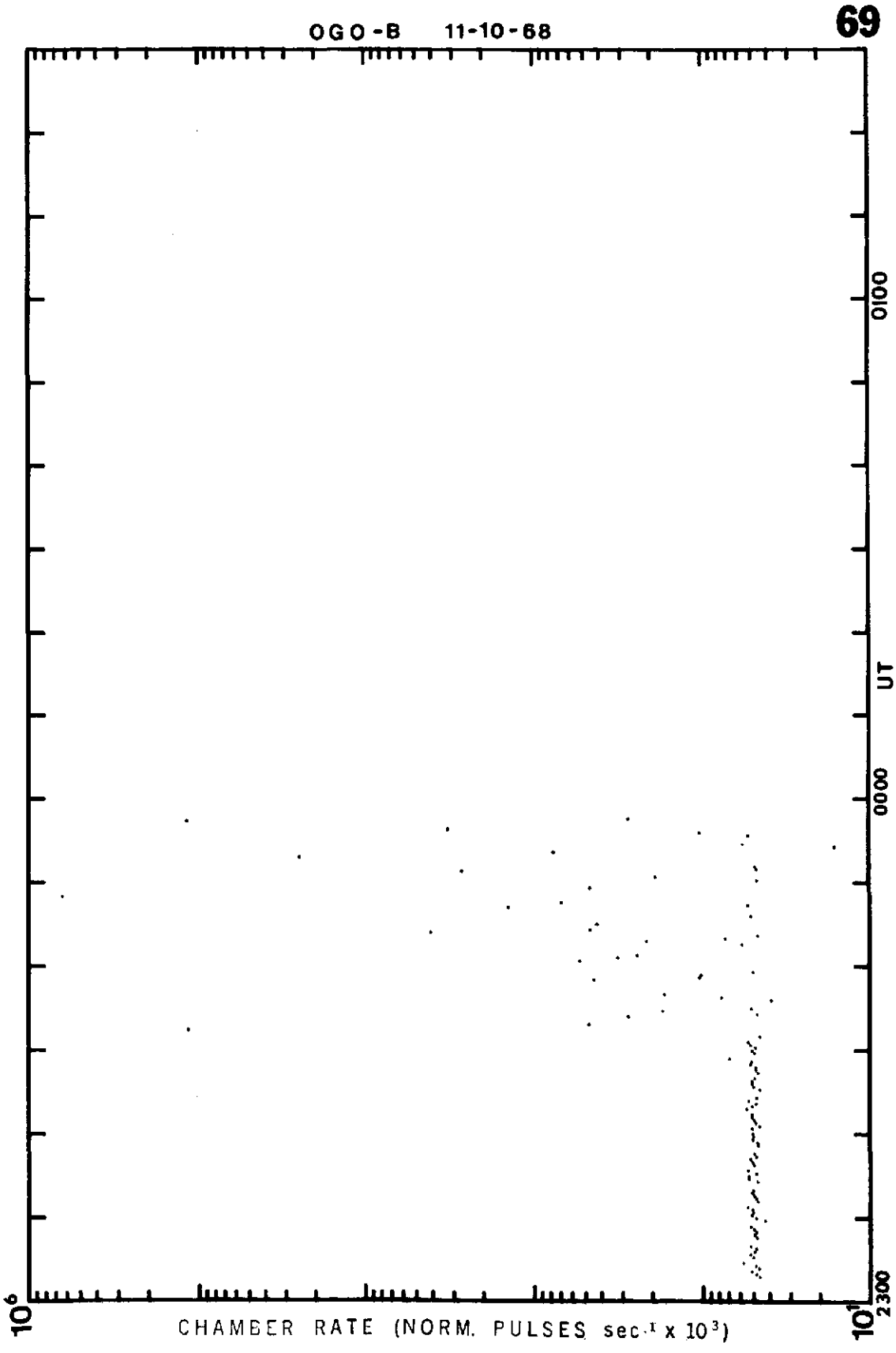
OGO-B 11-10-68
0100
UT
0000
2300
10^0
10^1
CHAMBER RATE (NORM. PULSES $sec^{-1} \times 10^3$)

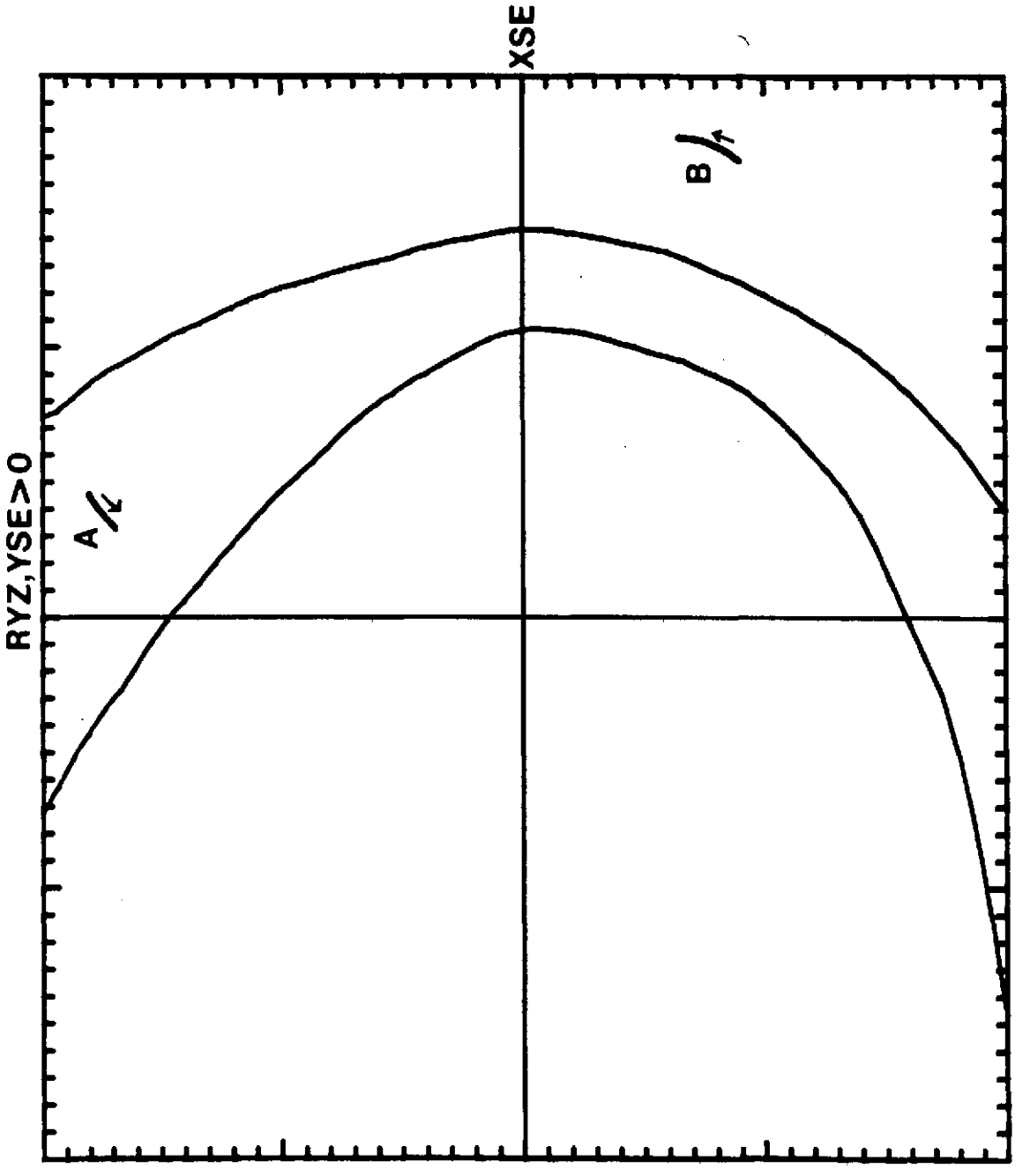
XSE
RYZ, YSE>0
A//
B//

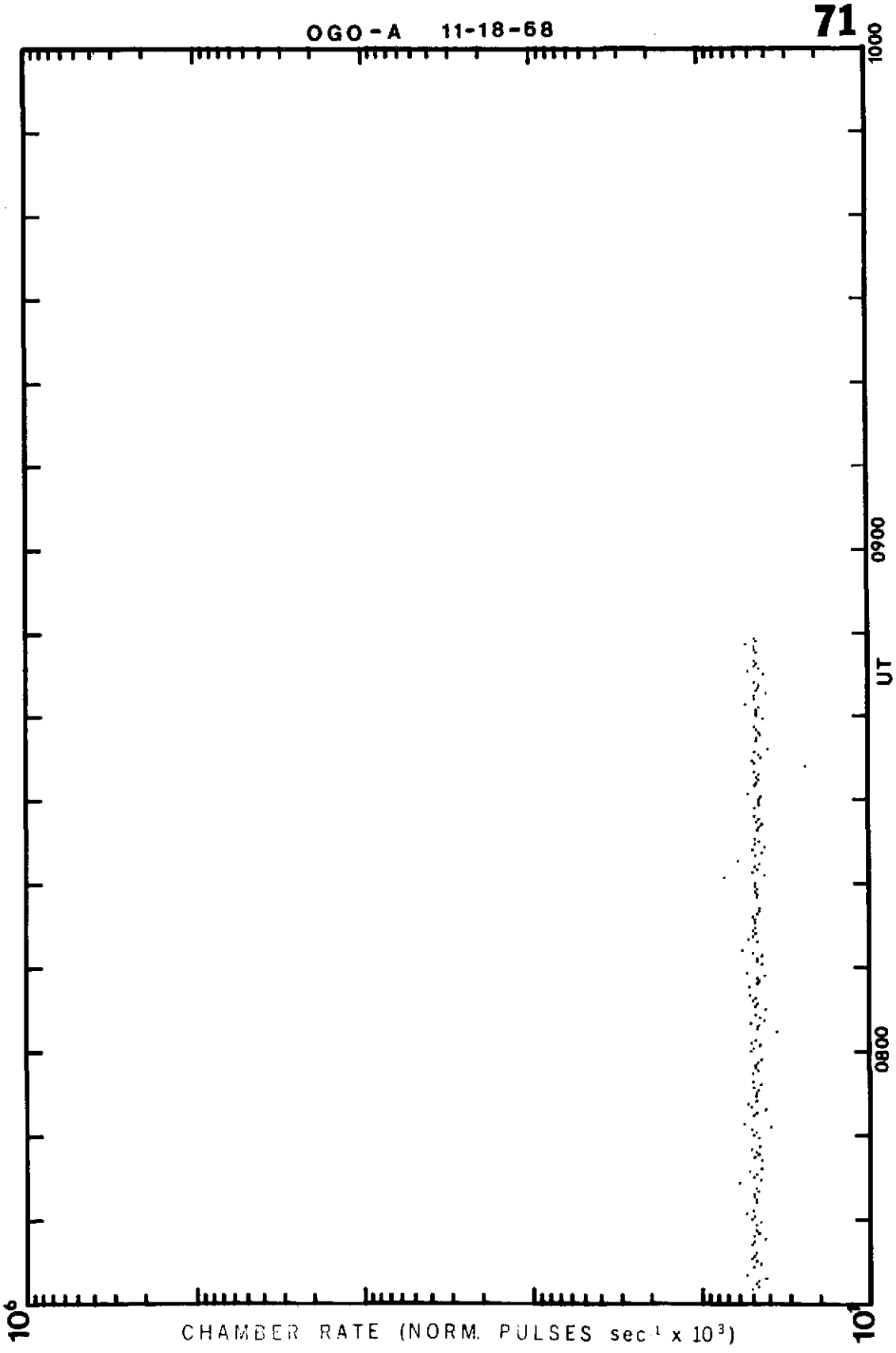
OGO-A 11-18-68
1000
0900
UT
0800
10^6
10^4
CHAMBER RATE (NORM. PULSES $sec^{-1} \times 10^3$)

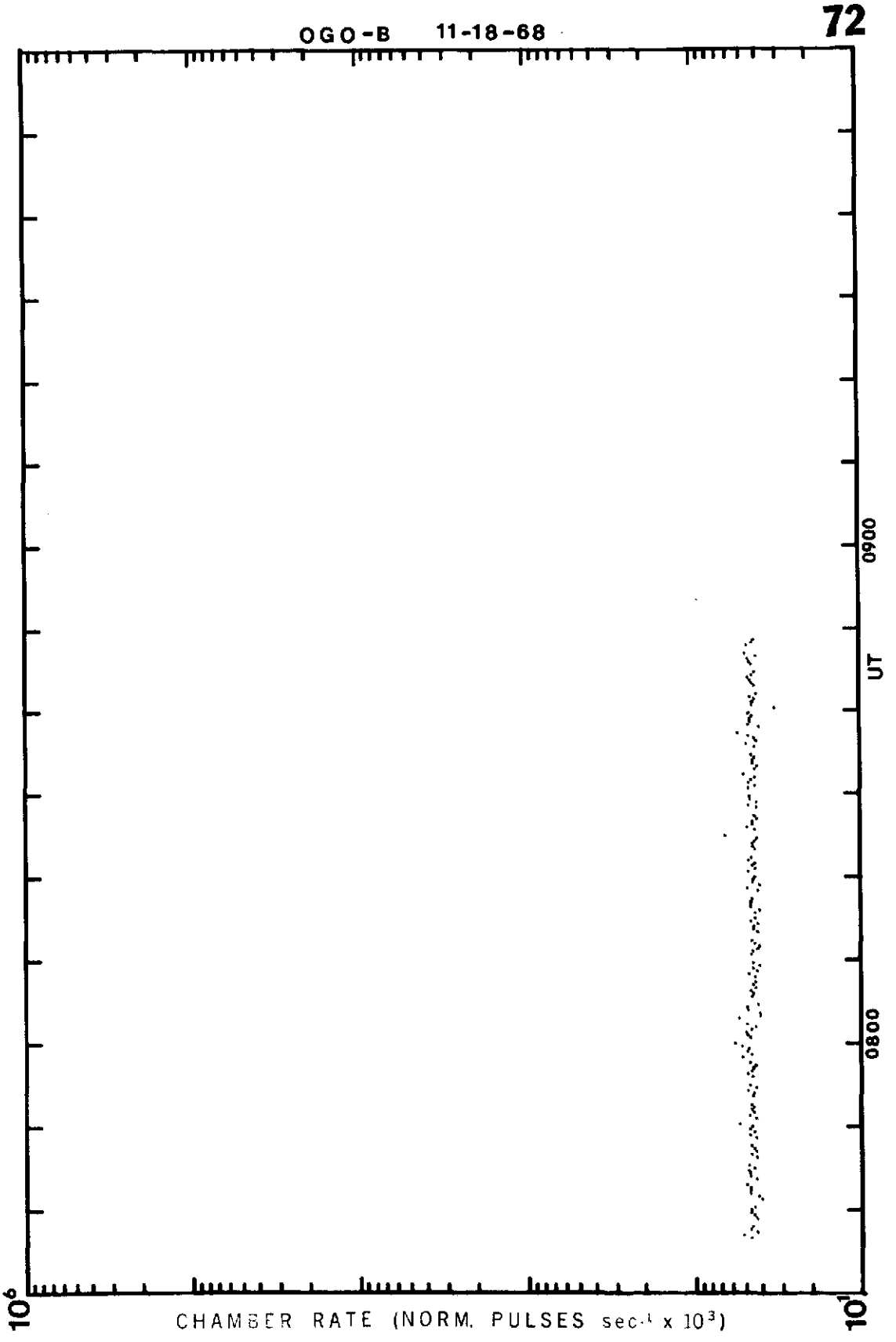
OGO-B 11-18-68
0900
UT
0800
10^6
10^1
CHAMBER RATE (NORM. PULSES sec^{-1} x 10^3)

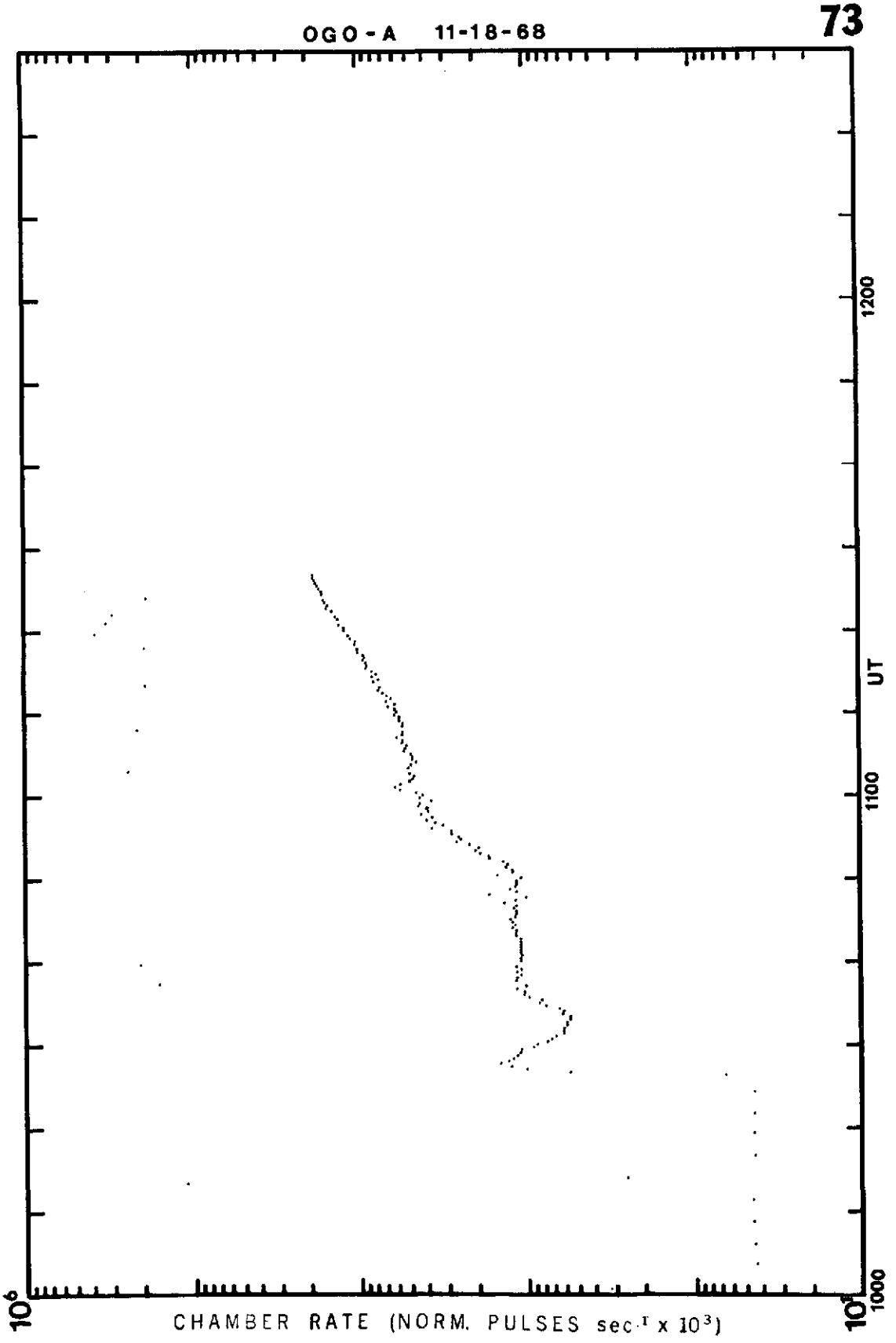
OGO-A 11-18-68
1200
UT
1100
1000
10^6
10^5
CHAMBER RATE (NORM. PULSES $sec^{-1} \times 10^3$)

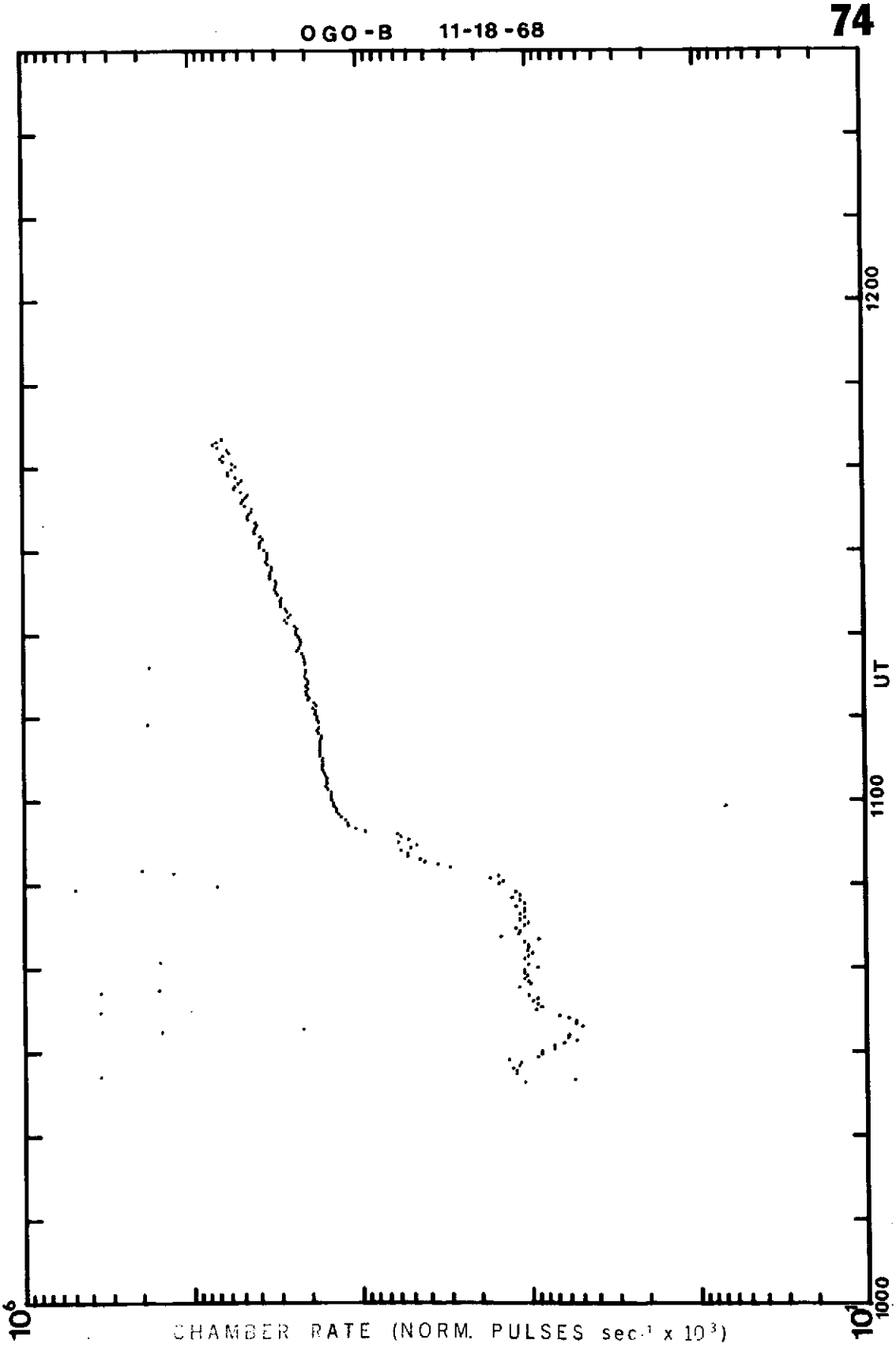
OGO-B 11-18-68
1200
1100
1000
UT
10^6
10^1
CHAMBER RATE (NORM. PULSES sec^{-1} x 10^3)

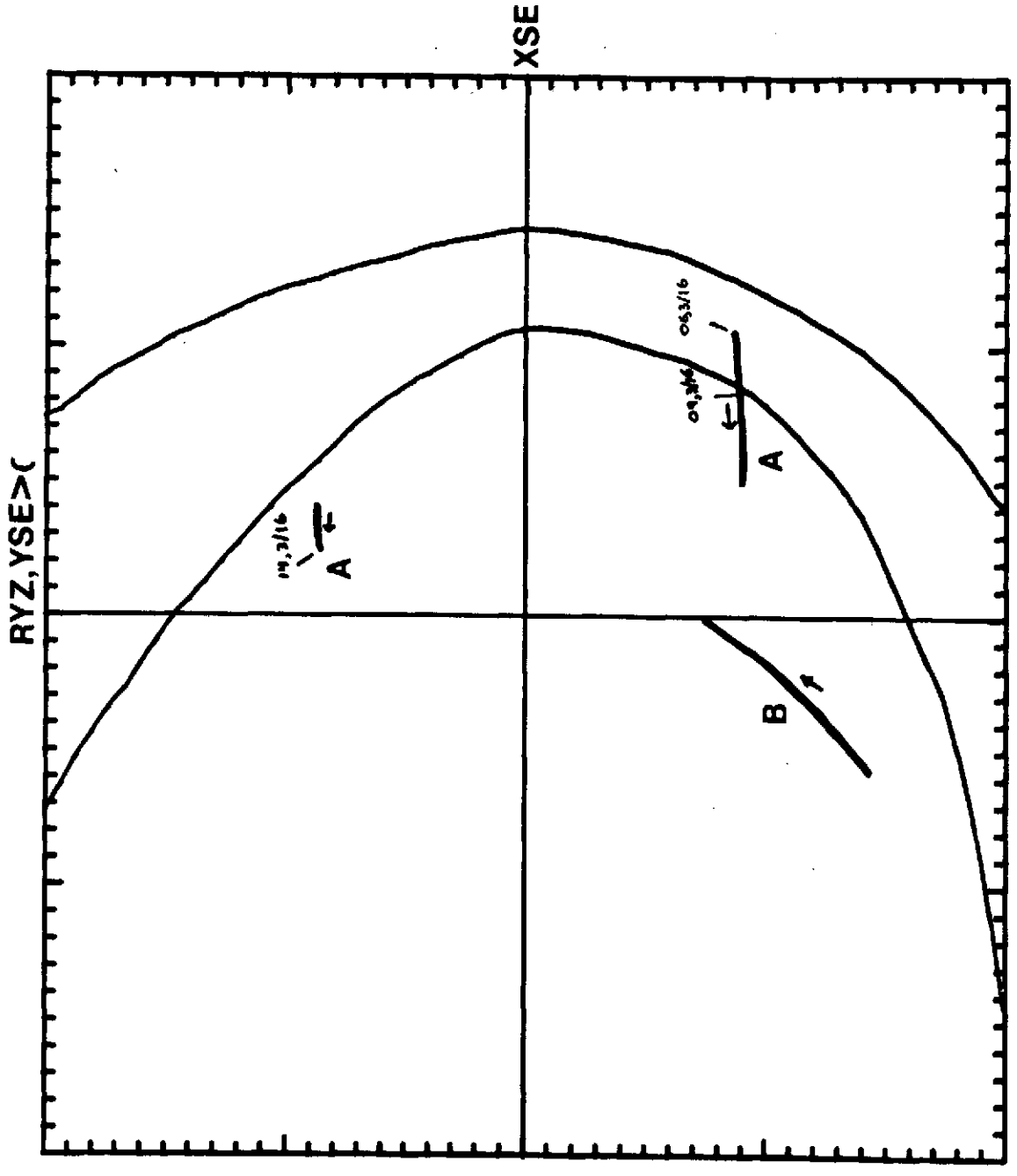
XSE
RYZ,YSE>(
A
A
B

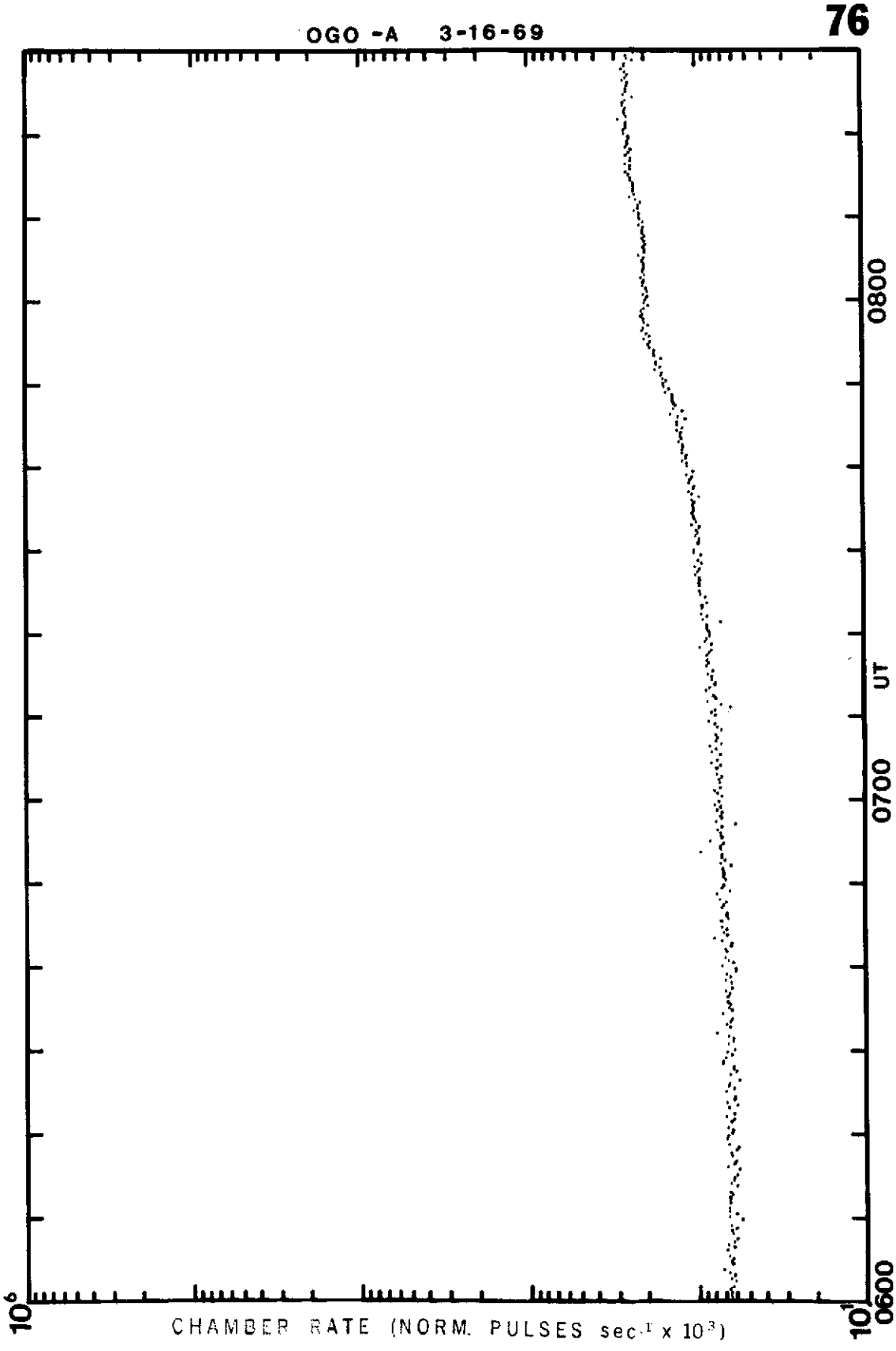
OGO -A 3-16-69
0800
0700
0600
UT
10^6
10^1
CHAMBER RATE (NORM. PULSES $sec^{-1} \times 10^3$)

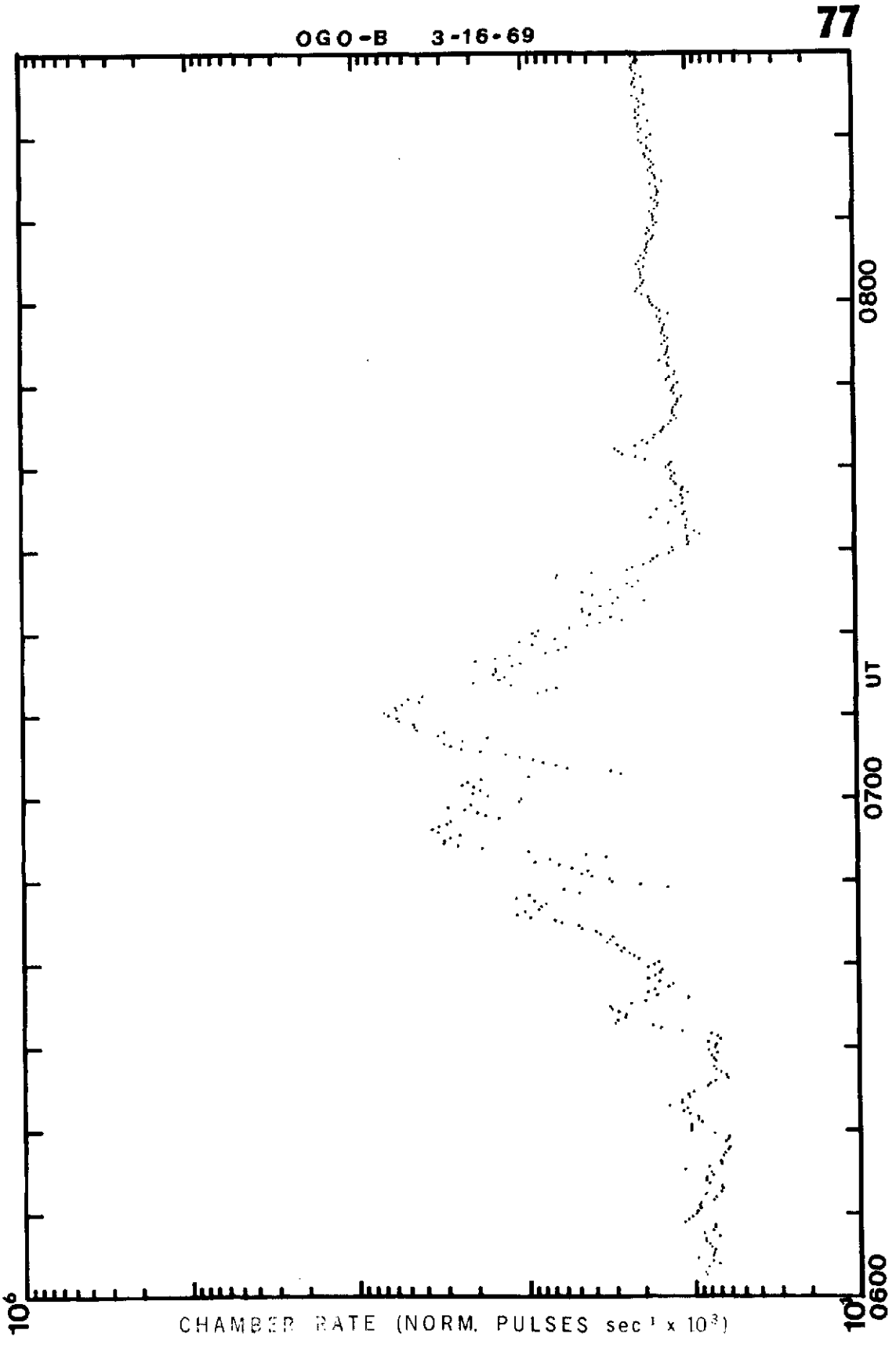
OGO-B 3-16-69
0800
UT
0700
0600
10^6
10^5
CHAMBER RATE (NORM. PULSES $sec^{-1} \times 10^3$)

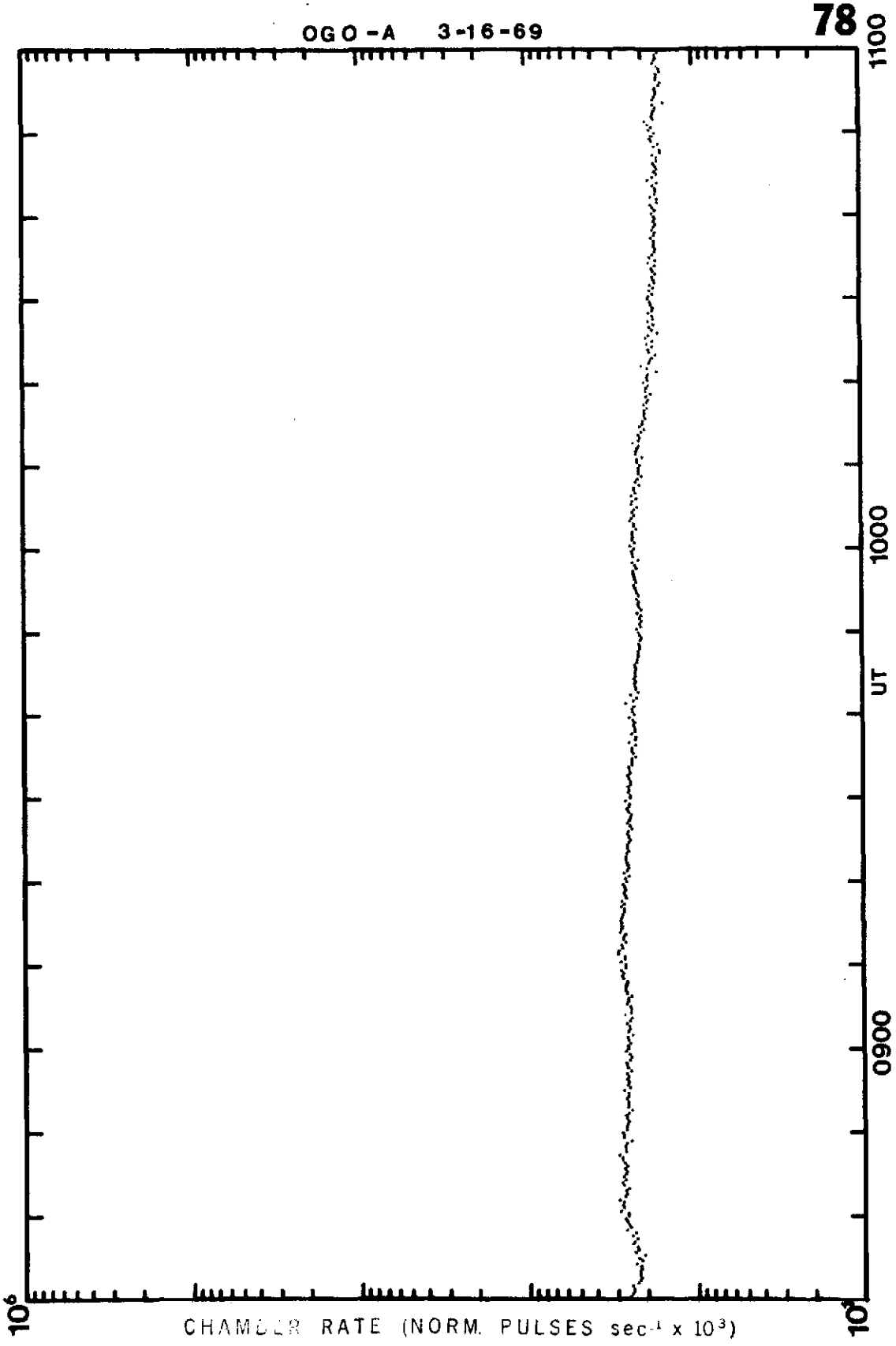
OGO-A 3-16-69
78
1100
1000
0900
UT
10^6
10^5
CHAMBER RATE (NORM. PULSES $sec^{-1} \times 10^3$)

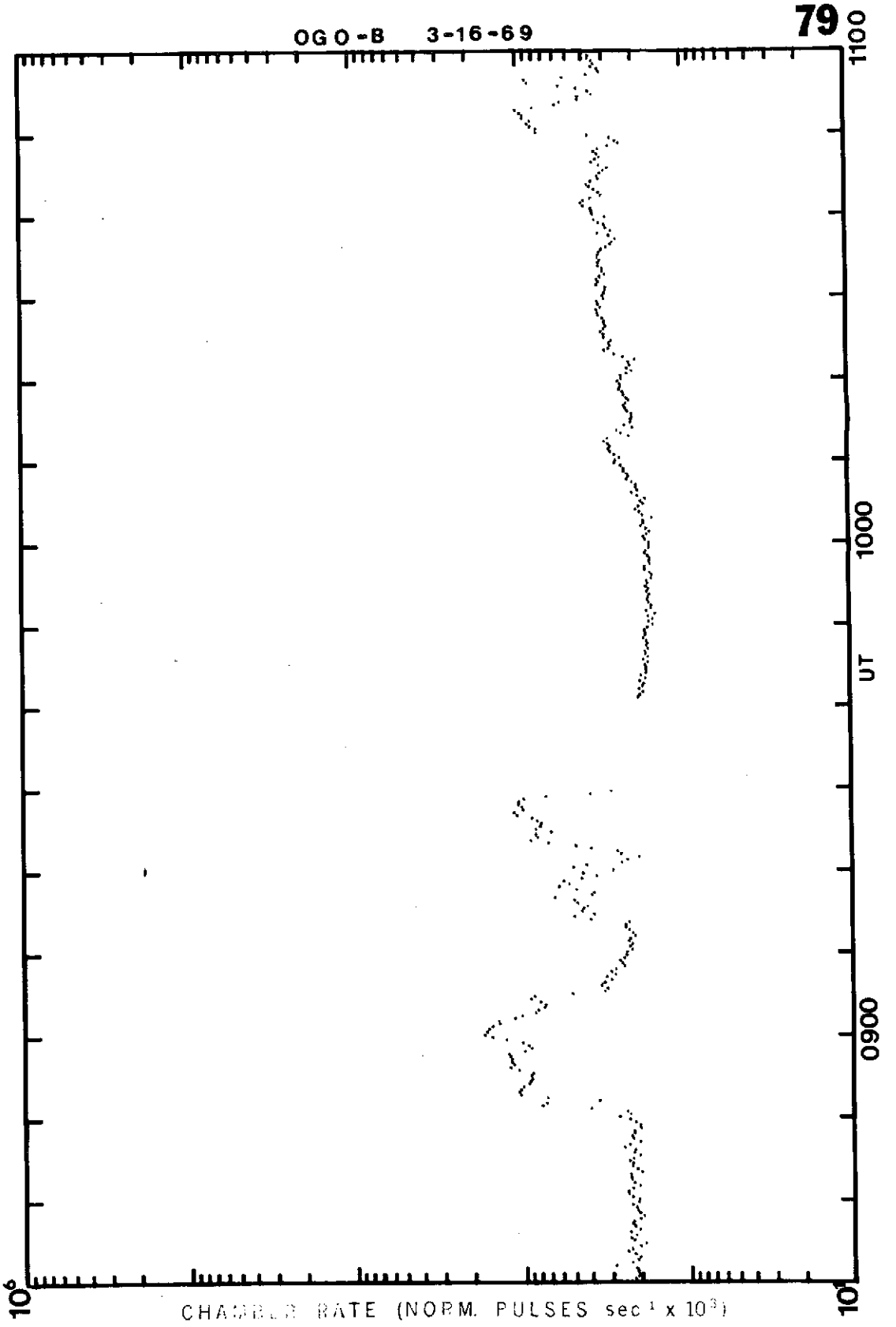
OGO-B 3-16-69
79
1100
1000
0900
UT
10^6
10^5
CHANNEL RATE (NORM. PULSES $sec^{-1} \times 10^3$)

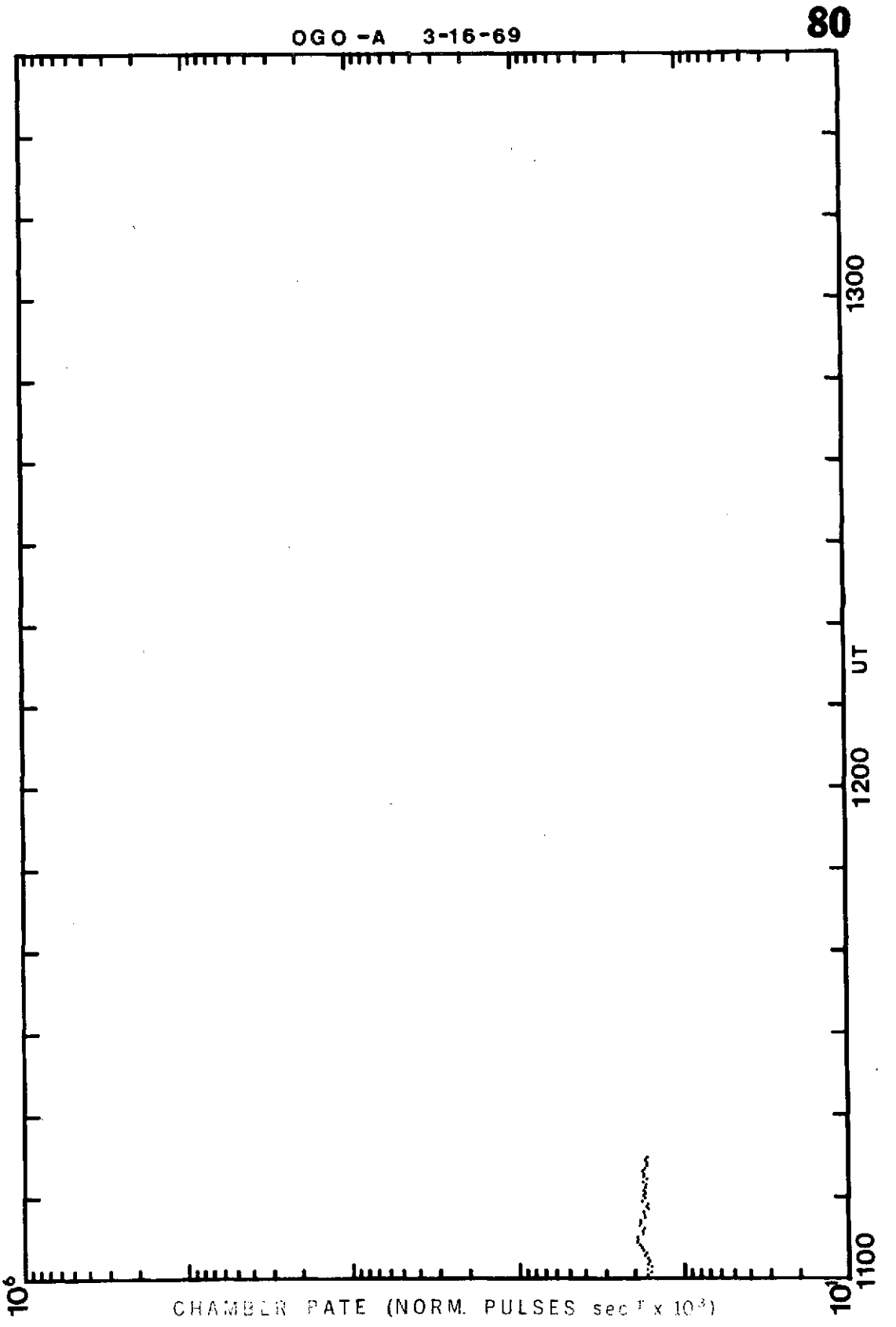
80
OGO -A 3-16-69
1300
1200
UT
1100
10^6
10^1
CHAMBER RATE (NORM. PULSES sec^{-1} x 10^3)

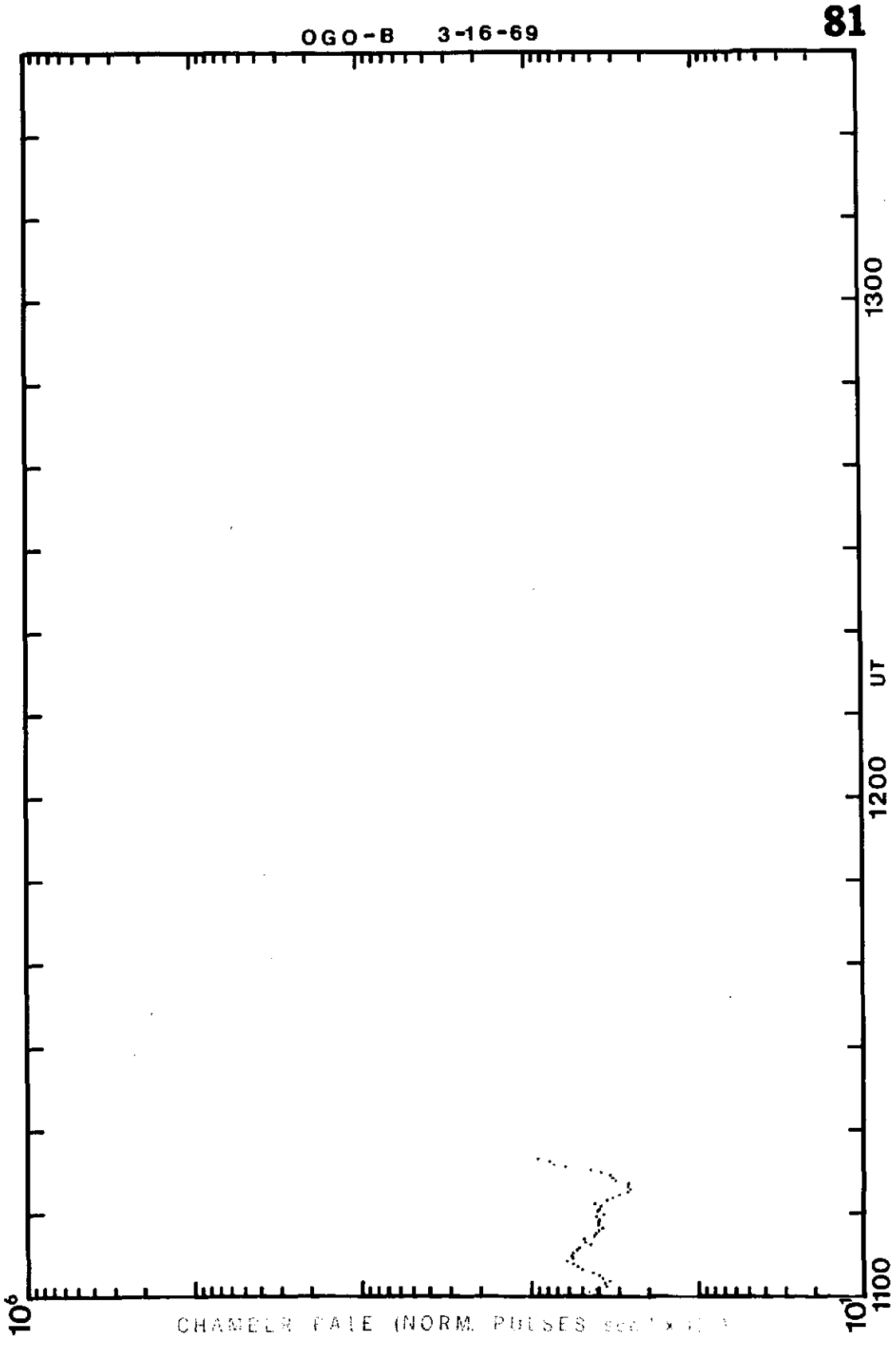
OGO-B 3-16-69
1300
1200
UT
1100
10^6
10^1
CHAMELEON FALE (NORM. PULSES

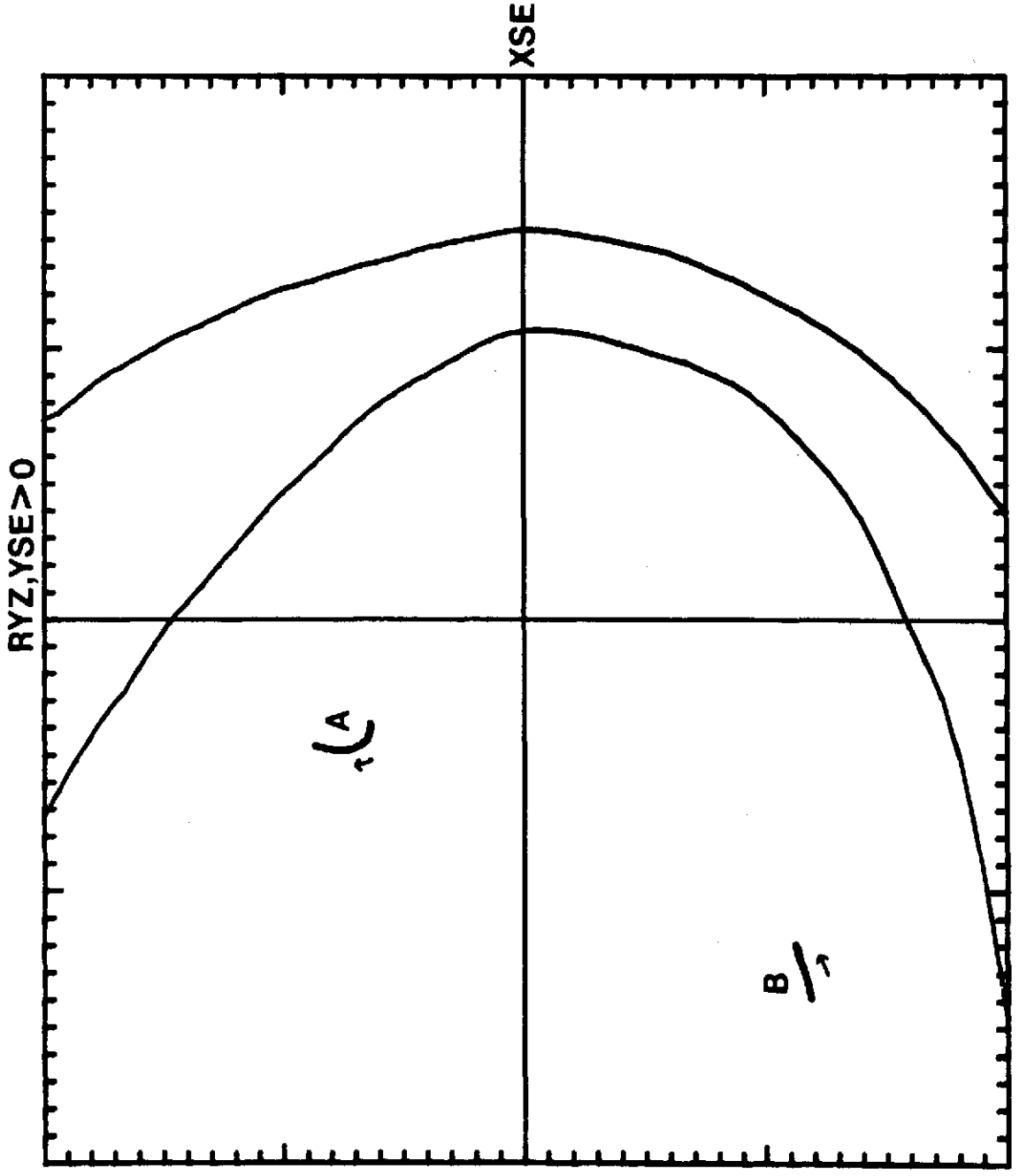
XSE
RYZ,YSE>0
A
B

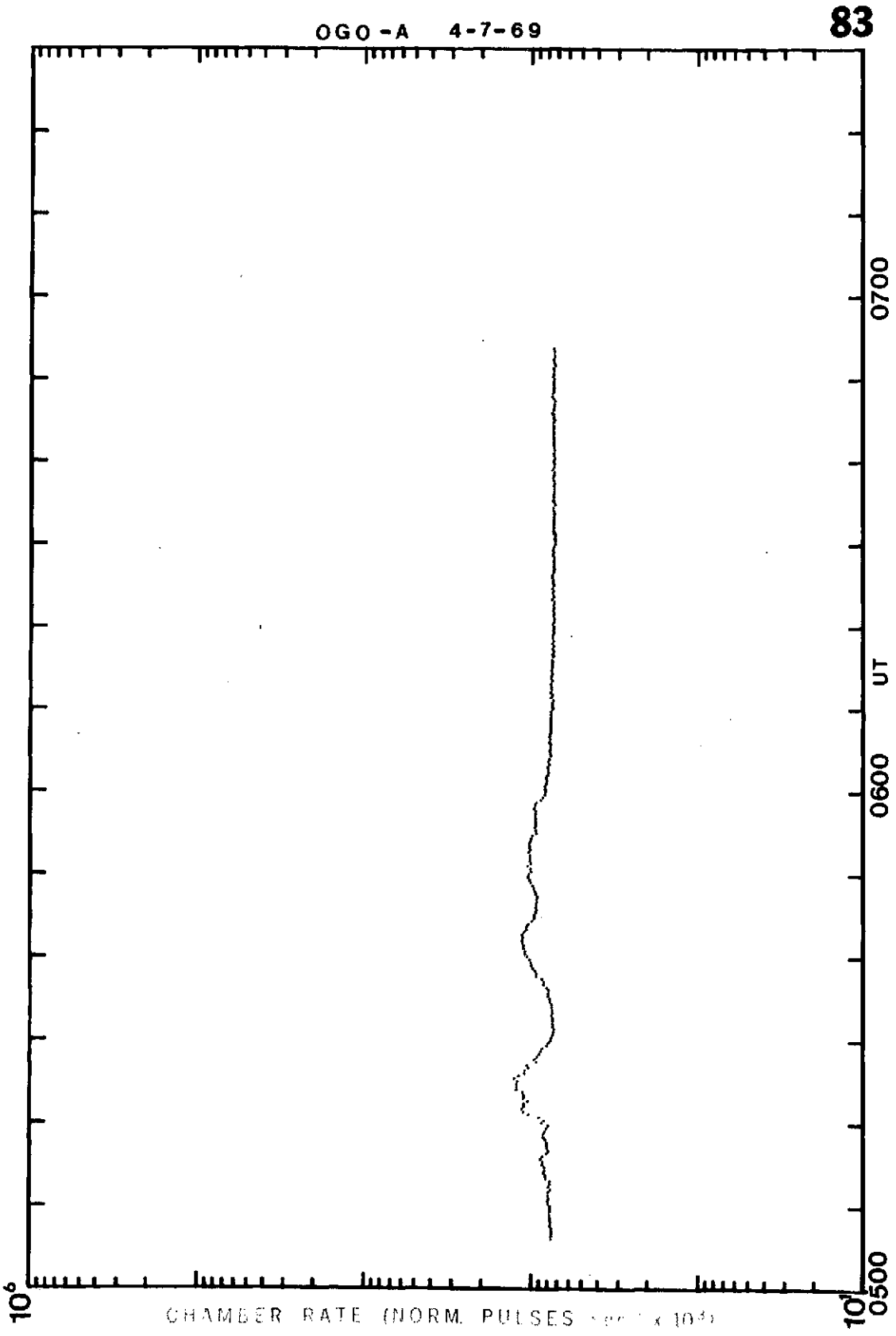
OGO-A 4-7-69
0700
0600
0500
UT
10^6
10^1
CHAMBER RATE (NORM. PULSES

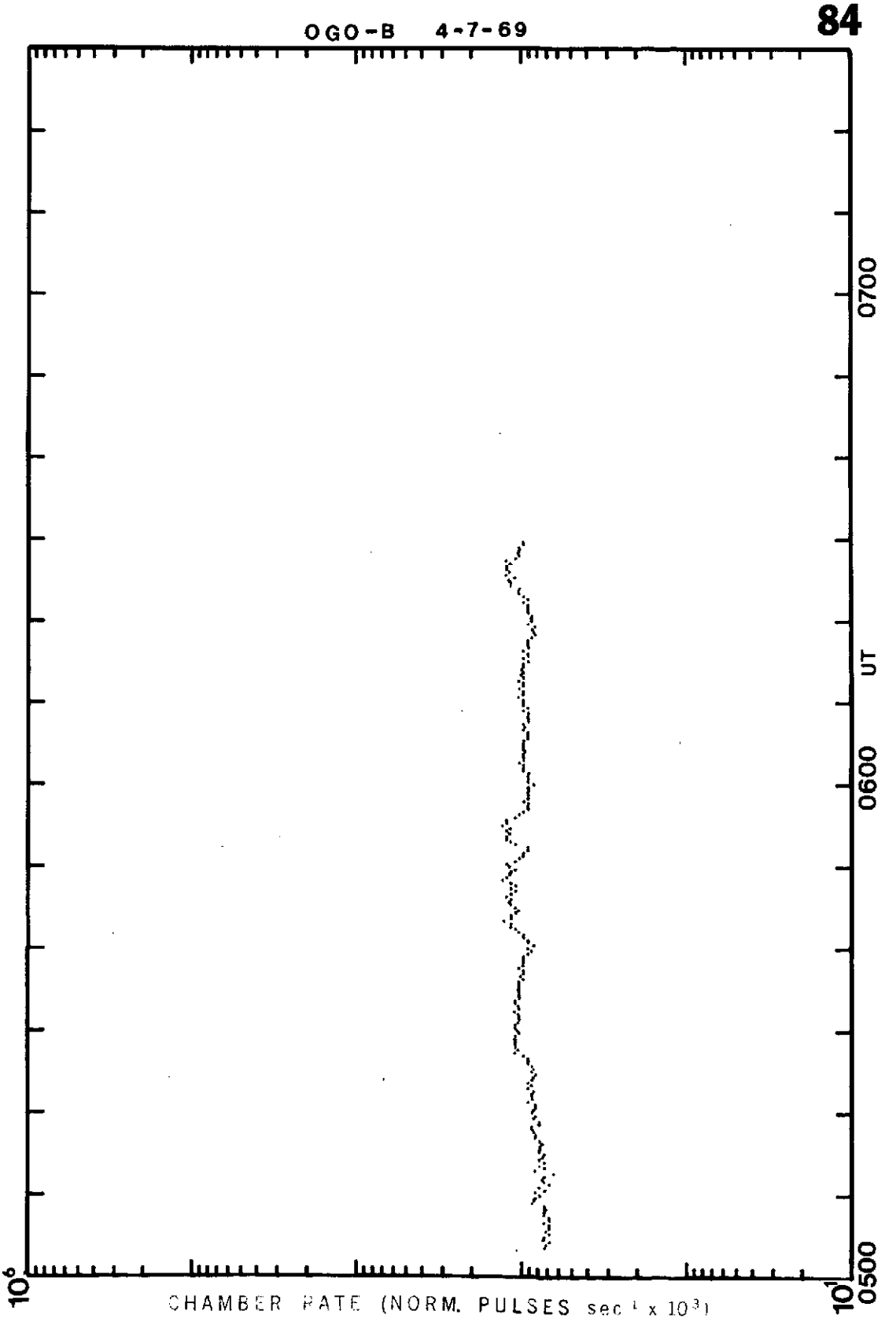
OGO-B 4-7-69
0700
0600
UT
0500
10^6
10^1
CHAMBER RATE (NORM. PULSES sec^{-1} x 10^3)

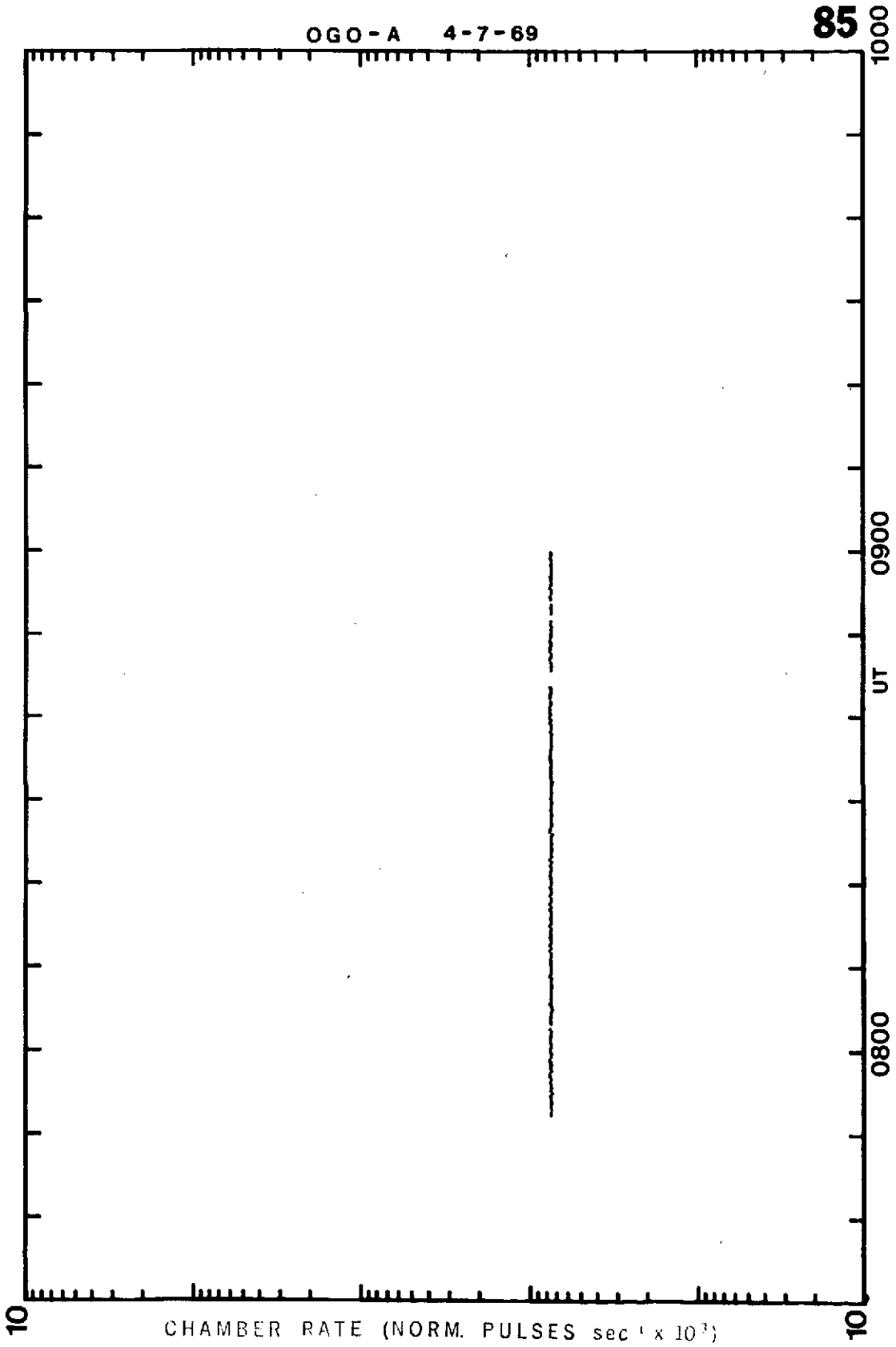
OGO-A 4-7-69
85
1000
0900
UT
0800
10
10
CHAMBER RATE (NORM. PULSES sec⁻¹ x 10³)

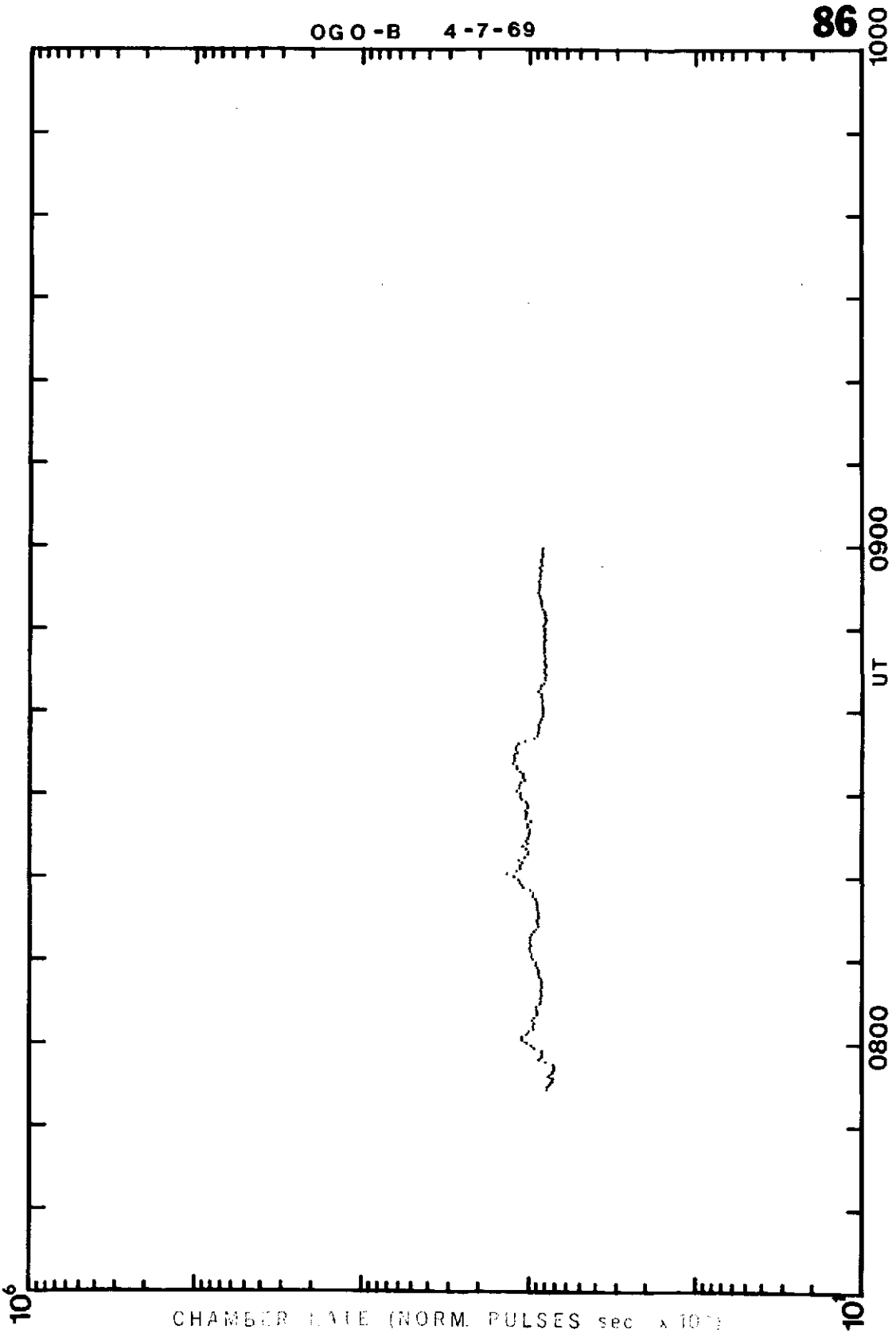
OGO-B 4-7-69
86
1000
0900
0800
UT
10^6
10^5
CHAMBER RATE (NORM. PULSES sec x 10⁻¹)

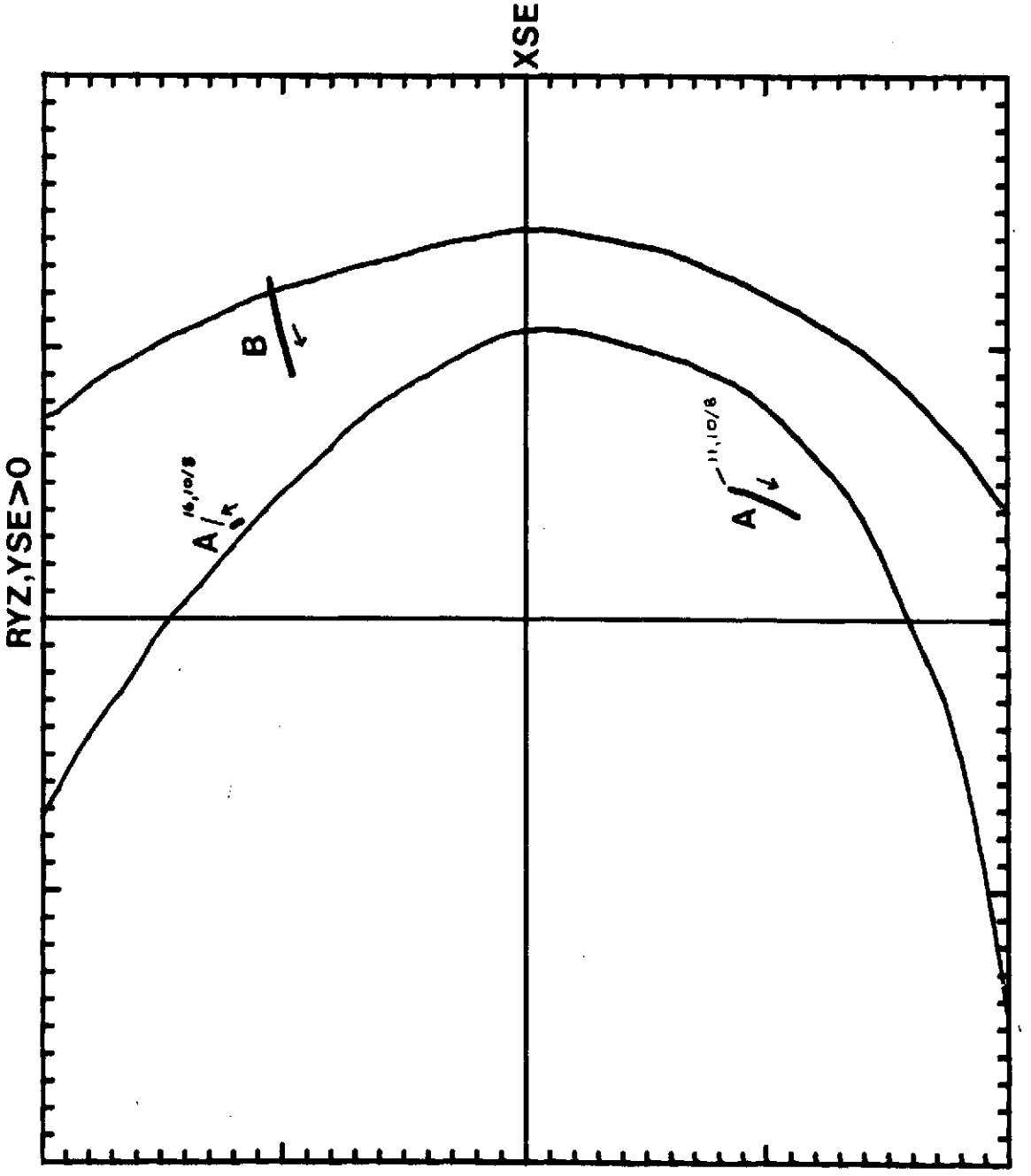
XSE
RYZ,YSE>0
B
A
A

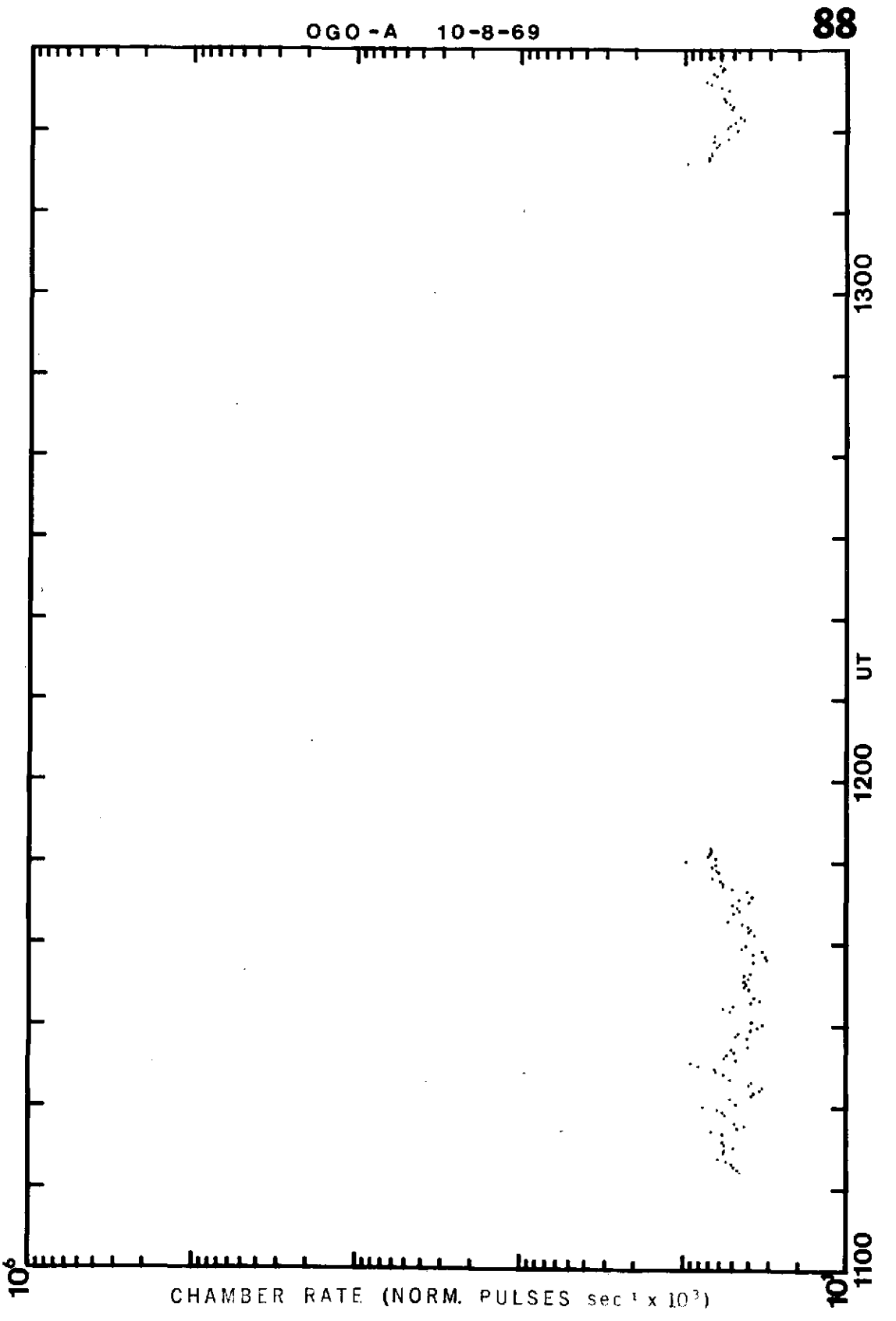
OGO-A 10-8-69
1300
1200
UT
1100
10^6
10^1
CHAMBER RATE (NORM. PULSES sec^{-1} x 10^3)

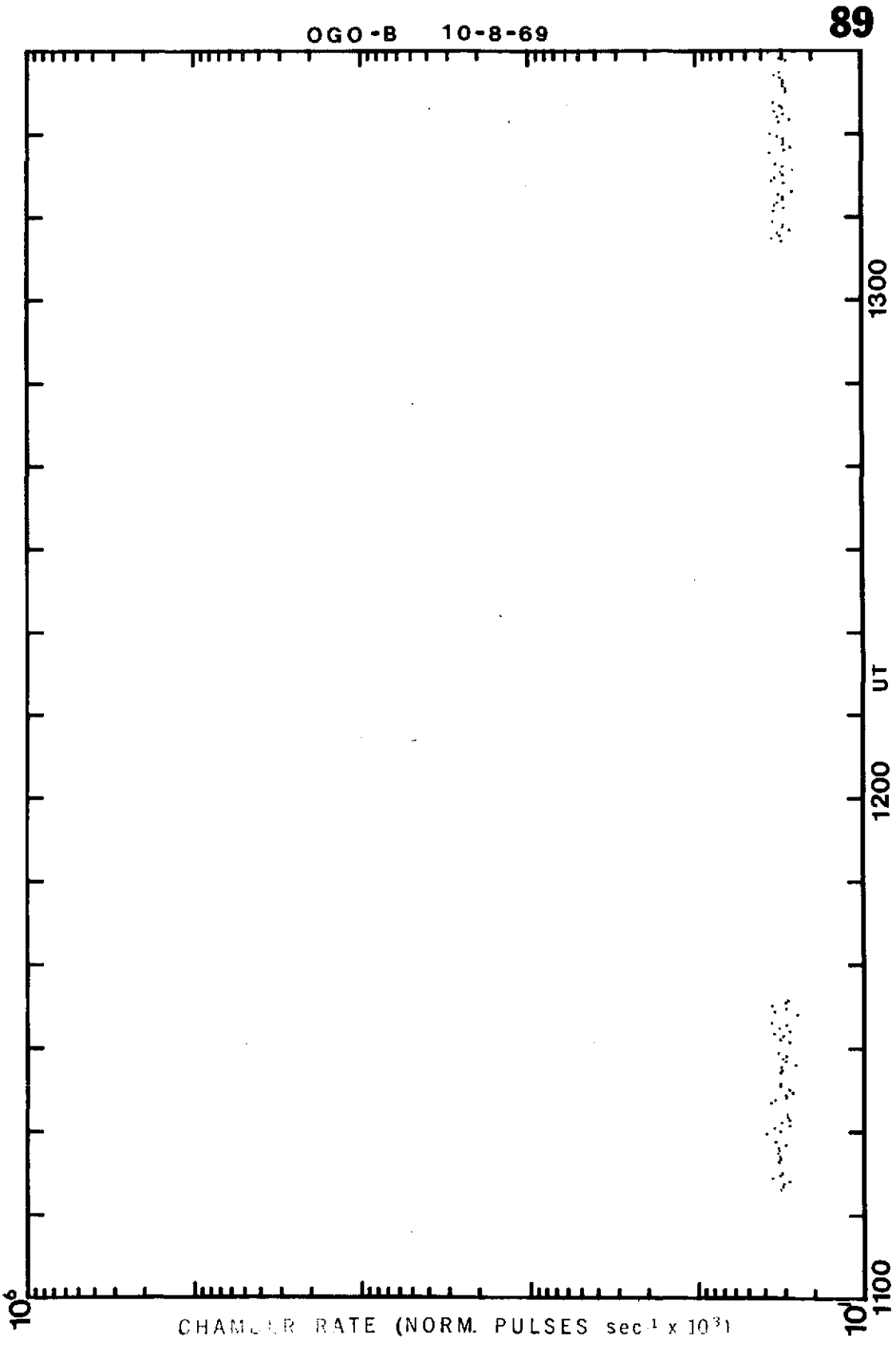
OGO-B 10-8-69
1300
1200
UT
1100
10^6
10^1
CHAMBER RATE (NORM. PULSES $sec^{-1} \times 10^3$)

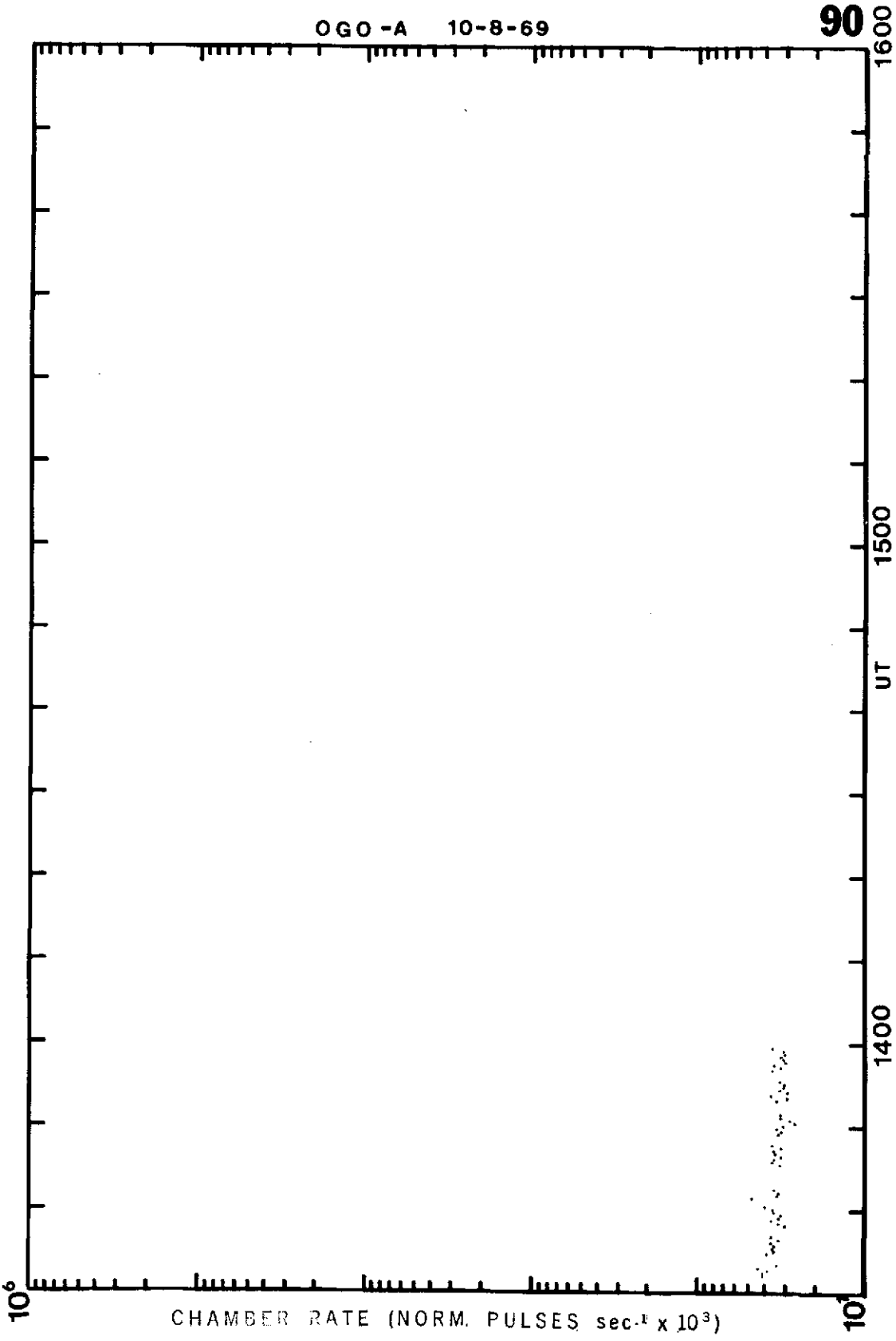
OGO-A 10-8-69
90
1600
1500
UT
1400
10^6
10^1
CHAMBER RATE (NORM. PULSES $sec^{-1} \times 10^3$)

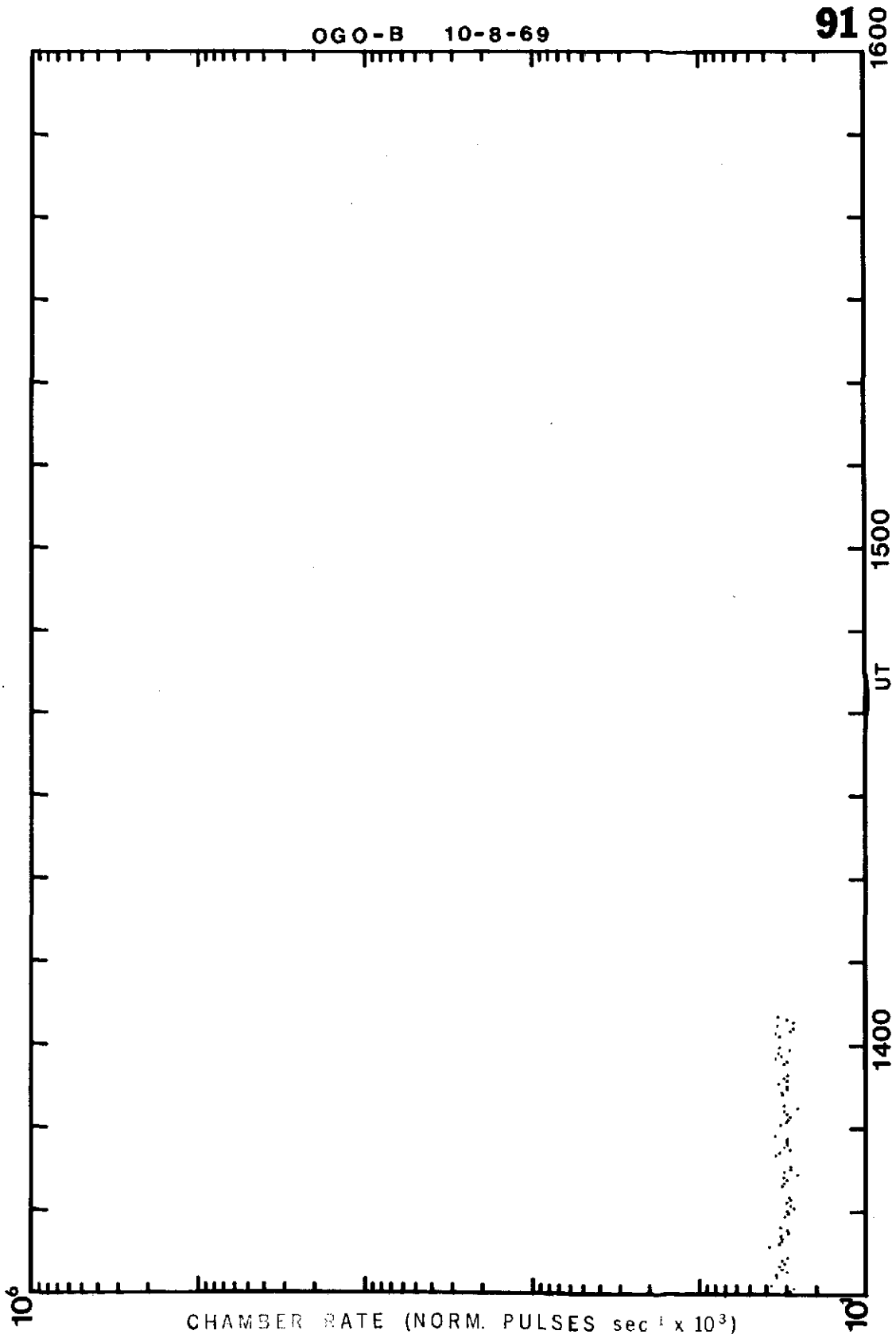
OGO-B 10-8-69
91
1600
1500
1400
UT
10^6
10^1
CHAMBER RATE (NORM. PULSES sec^{-1} x 10^3)

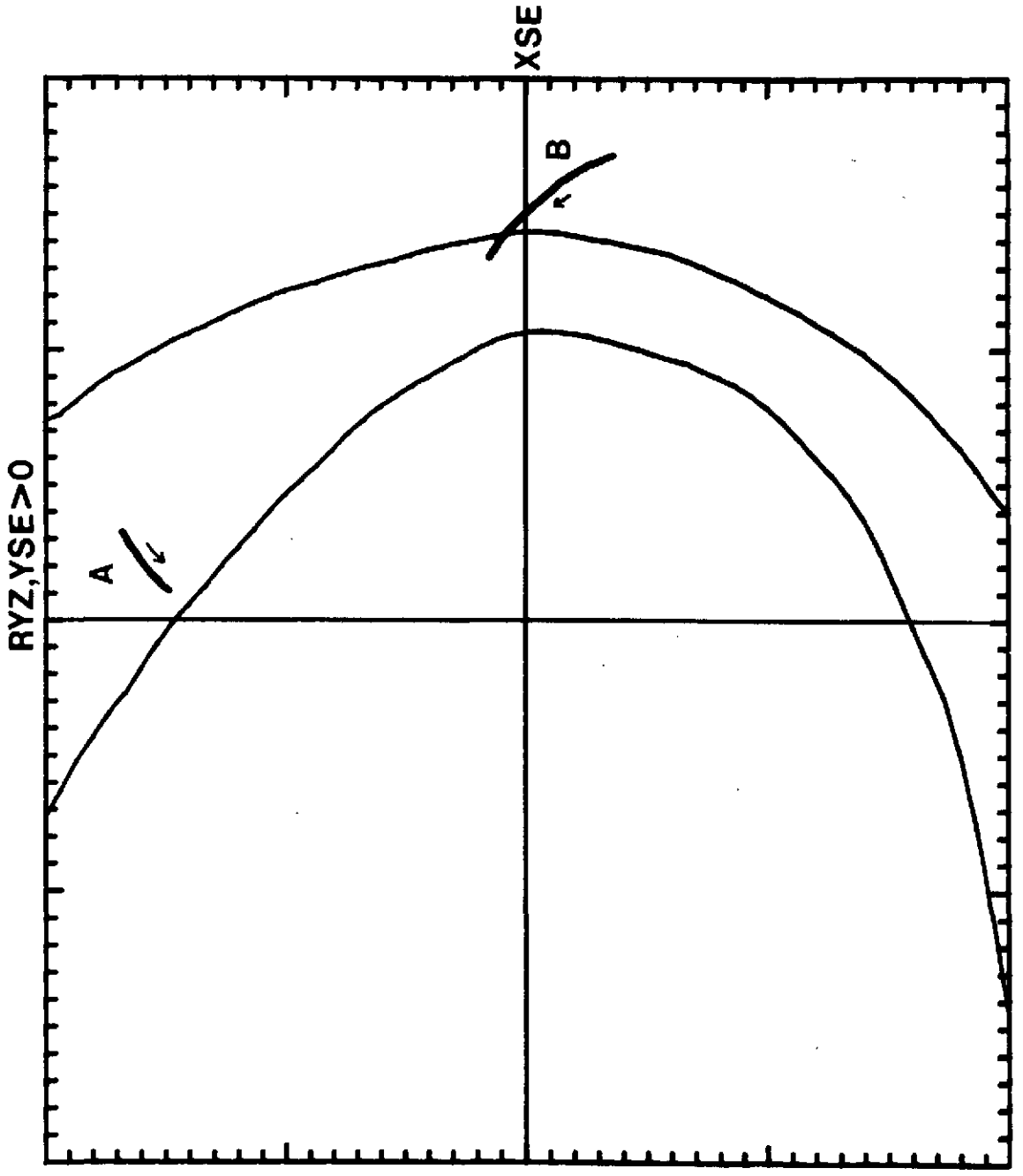
XSE
RYZ,YSE>0
A
B

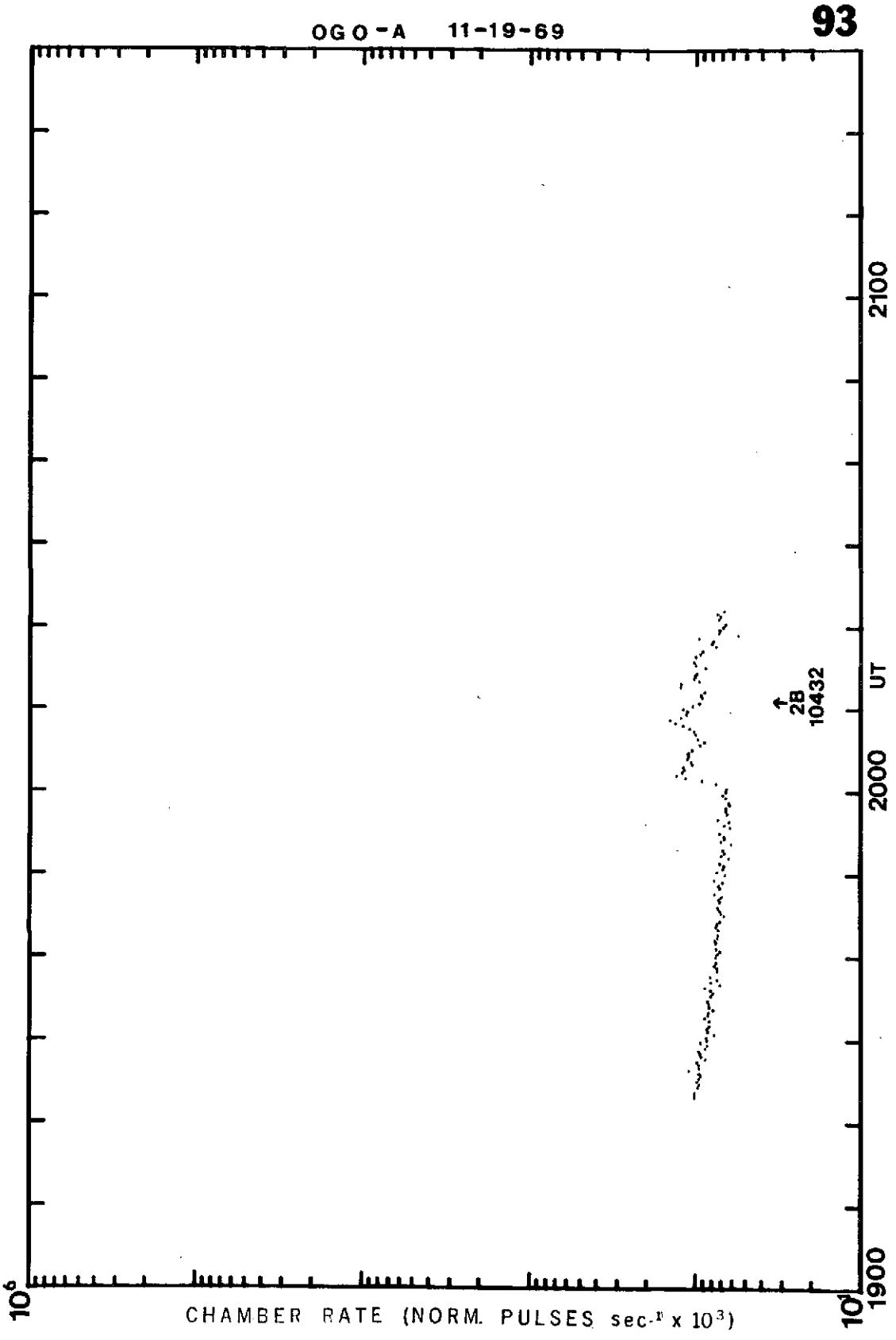
OGO-A 11-19-69
2100
2000
1900
UT
28
10432
10^6
10^1
CHAMBER RATE (NORM. PULSES sec^{-1} x 10^3)

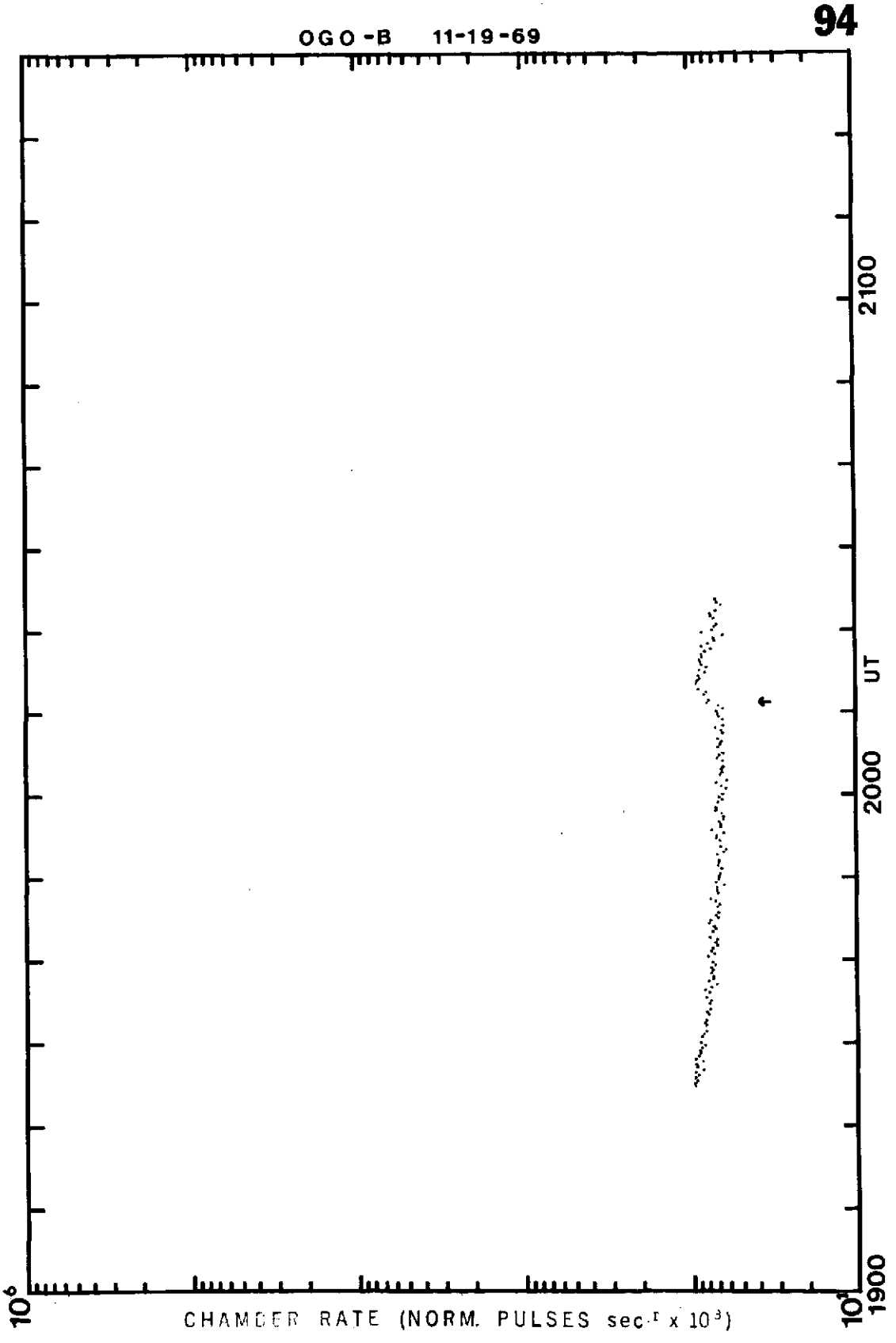
OGO-B 11-19-69
2100
2000
1900
UT
10^6
10^3
CHAMBER RATE (NORM. PULSES $sec^{-1} \times 10^3$)

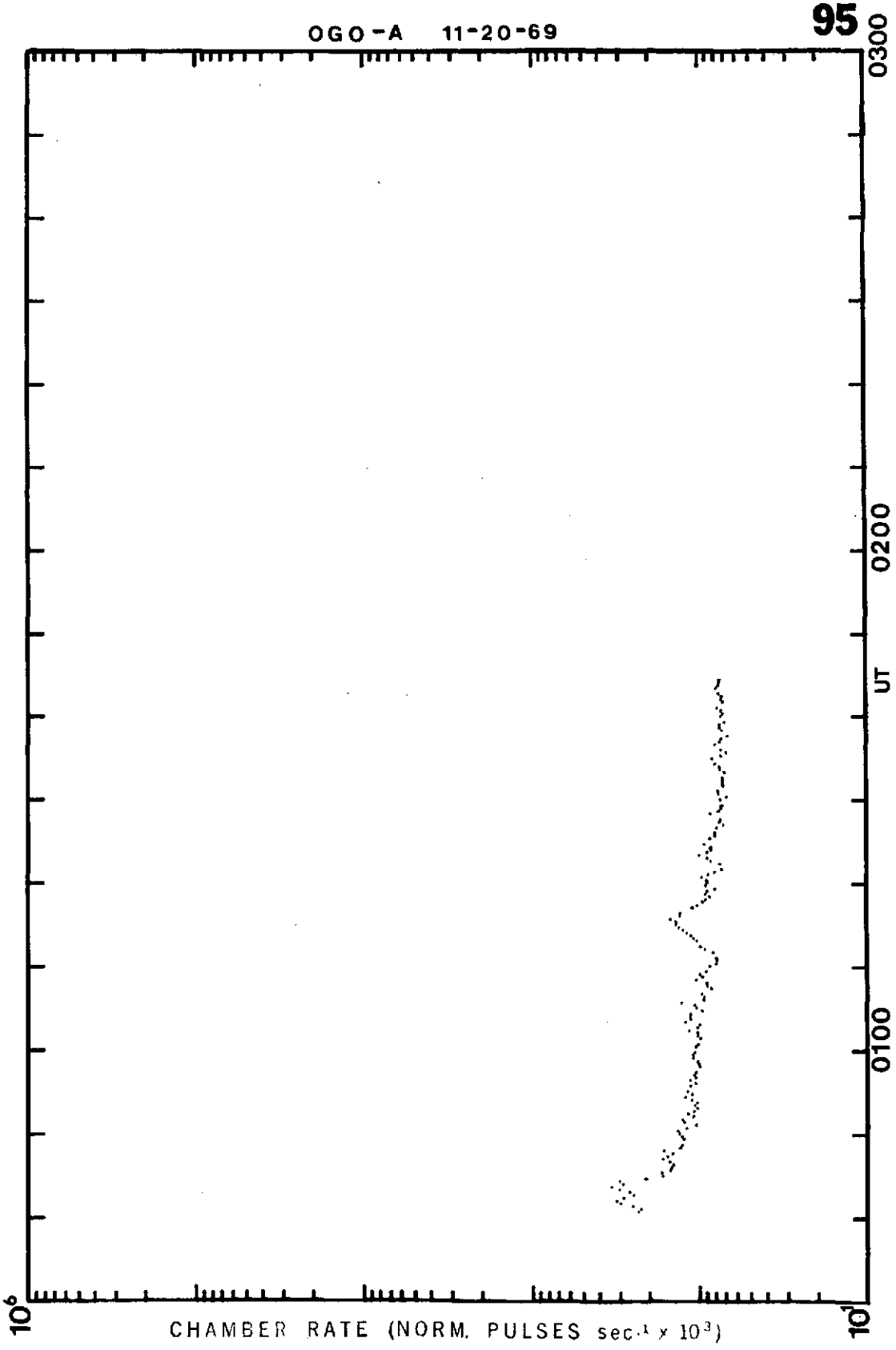
OGO-A 11-20-69
95
0300
0200
0100
UT
10^6
10^1
CHAMBER RATE (NORM. PULSES $sec^{-1} \times 10^3$)

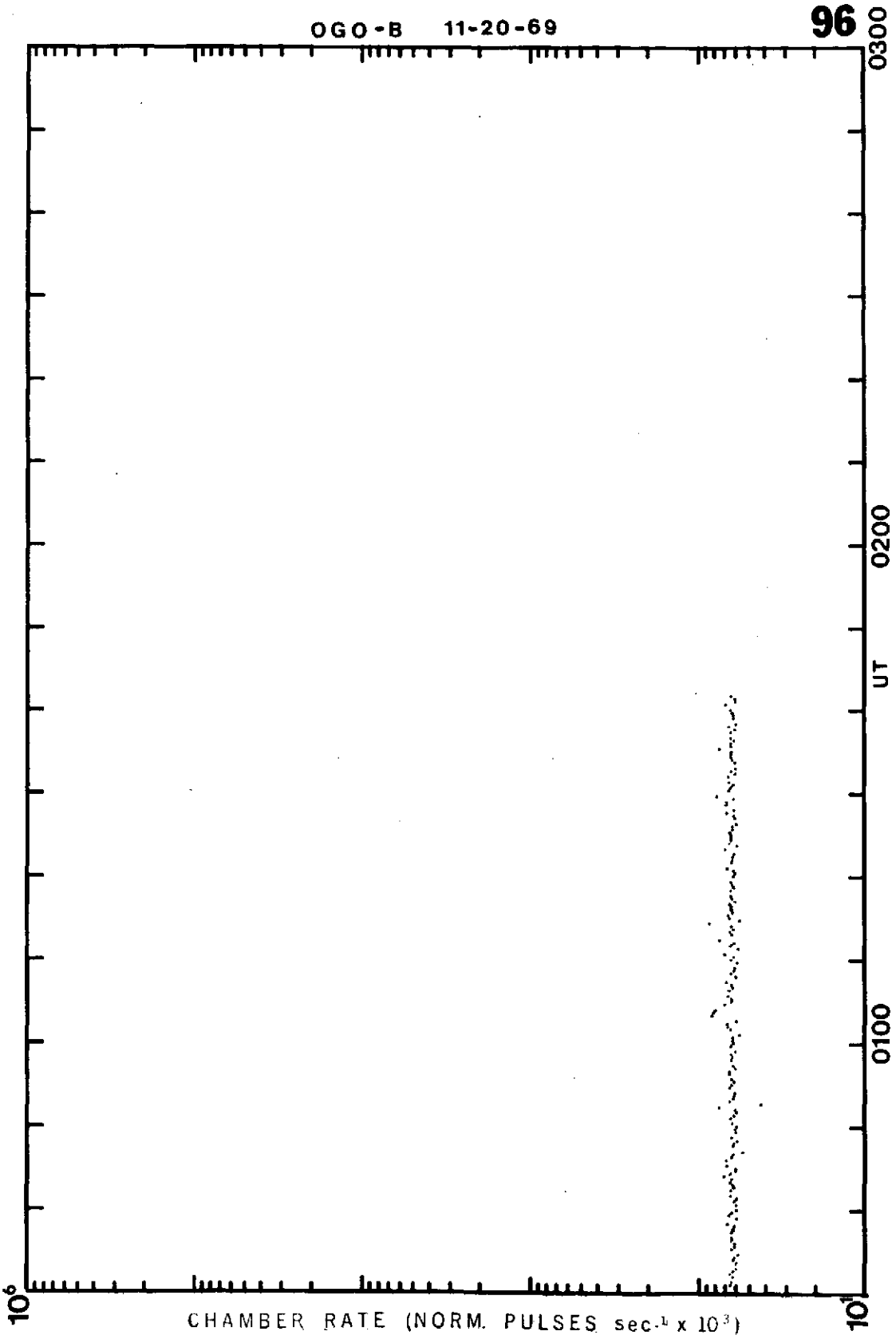
OGO-B 11-20-69
96
0300
0200
0100
UT
10^0
10^1
CHAMBER RATE (NORM. PULSES $sec^{-1} \times 10^3$)